NON-NEWTONIAN ANNULAR FLOW

AND

CUTTINGS TRANSPORT THROUGH DRILLING ANNULI AT VARIOUS ANGLES

YUEJIN LUO

This thesis is submitted for the degree of
Doctor of Philosophy

Department of Petroleum Engineering
Heriot-Watt University
Edinburgh, U.K.

October 1988

Dedicated to my wife, Zhenhua Wei,

and my son, Jiesi Luo

The boundary of one's knowledge is like
an ever increasing circle:

The more one has known,
The more unknowns one faces.

TABLE OF CONTENTS

PART TWO

DRILLED CUTTINGS TRANSPORT THROUGH DRILLING ANNULI AT VARIOUS ANGLES

LIST OF APPENDICES

LIST OF TABLES

Table No.:

LIST OF FIGURES

Figure No.:

ACKNOWLEDGEMENTS

I am deeply grateful to my supervisor, professor J.M. Peden, for his guidance and help during the course of my study in the Department of Petroleum Engineering at Heriot-Watt University. Also I would like to take this opportunity to express my appreciation to professor J.M. Peden for his continuous encouragement and support during my participation in the Student Paper Contest in SPE European Region in 1986, 1987 and 1988, from which I won not only the awards but also more importantly, the confidence.

Thanks should be extended to all the staff in the Department of Petroleum Engineering, particularly to the workshop staff for their help and cooperation during my experimental work.

I should also thank Mr. John Ford for his tremendous effort to read through this thesis and make corrections.

Special thanks should be given to the Department of Petroleum Engineering at Heriot-Watt University for offering me the scholarship.

Finally, I would like to express my appreciation to the Chinese government for providing me the opportunity of studying in U.K.

ABSTRACT

This thesis presents the results of the investigations in two areas, i.e. non-Newtonian annular flow and cuttings transport in drilling annuli at various angles.

In the first part of the thesis, a review of the fundamentals and the previous studies on laminar concentric annular flow of non-Newtonian fluids is given at first. Then two parallel theoretical studies are performed, respectively, on:

a. Laminar eccentric annular flow of power-law and Bingham plastic fluids. In this analysis, a new method is used which treats an eccentric annulus as infinite number of concentric annuli with variable outer radius. The analytical solutions of the shear stress, shear rate, velocity and the volumetric flowrate/pressure gradient are obtained over the entire eccentric annulus. This analysis is useful in design of any engineering operations related to eccentric annular flow such as oil drilling operations.

b. Laminar helical flow of power-law fluids through concentric annuli. A group of dimensionless equations are derived in this analysis for the profiles of the apparent viscosity, angular and axial velocities, and for the volumetric flowrate. These equations are essential when one needs to simulate the helical flow conditions in various engineering operations. In addition, another group of dimensionless equations are also derived for pressure gradient calculations which can be used directly by drilling engineers to predict the reduction of the annular friction pressure drop caused by drillpipe rotation during drilling operations.

The second part of the thesis is dedicated to the investigations into the problems directly related to cuttings transport through drilling annuli at various angles. First, both theoretical and experimental studies on settling velocities of drilled cuttings in drilling fluids are conducted using new approaches to account for the non-Newtonian nature of drilling fluids and for the shape irregularity of drilled cuttings. Based on experimental results, a generalised model is developed for calculating settling velocities of variously shaped particles in power-law fluids. Then, the effects of various parameters on cuttings transport during drilling operations are analysed based on the previous and the present studies. After that, an extensive theoretical analysis for the previous studies on the minimum transport velocity (MTV) in solid-liquid mixture flow through pipelines, on initiation of sediment transport in open channels and on MTV for cuttings transport in deviated wells is presented. At last, theoretical studies on the minimum transport velocity for cuttings transport in drilling annuli at various angles are conducted and two parallel general correlations are developed. When these correlations are experimentally verified and numerically established in the future, they can be served as general criteria for evaluating and correlating the effects of various parameters on cuttings transport, and as a guideline for cuttings transport programme design during directional drilling.

NOMENCLATURE

(In consistent units)

PART ONE

a	A constant in the bipolar coordinate system
d	Diameter of a circular pipe
d_1	Diameter of the drillpipe
d_2	Diameter of the casing or wellbore
e	Distance between the axes of the inner and outer tubes
E	$= e/r_2$, Dimensionless eccentricity
E_f	$= e/(r_2-r_1)$, Fractional eccentricity
F_p	Ratio of the annular friction pressure drop when the inner tube is rotated to that when it is stationary
g_i, where the subscript i = r, θ, z	i-component of the gravitational constant
g_p	Axial pressure gradient defined by Eq.(2-6)
h	Distance between two flat parallel plates
h_e	Equivalent height of slot-equivalents of eccentric annuli
K	Consistency index of power-law fluids
L	Lenth of the fluid element considered or well depth
n	Flow behaviour index of power-law fluids
N_{Re}	Reynolds number of fluid flow
P_1 , P_2	Axial fluid pressure at point 1 and point 2, respectively
P_f	Fluid pressure drop
P_o	Annular friction pressure drop when the drillpipe is not rotated

P_ω Annular friction pressure drop under the rotating drillpipe condition

ΔP $= P_o - P_\omega$

q Volumetric flowrate

Q $= x + iy$, a complex number defined in Eq.(A3-2b)

r Radial coordinate of the cylindrical coordinate system

r_o Radius of the point of zero shear stress and maximum velocity in annular flow of power-law fluids

r_1 Radius of the inner tube

r_2 Radius of the outer tube

r_- Inner radius of the unsheared plug ring in concentric annular flow of Bingham plastic fluids

r_+ Outer radius of the unsheared plug ring in concentric annular flow of Bingham plastic fluids

s $=1/n$

T Stress tensor

v_f Mean fluid velocity

v_i, where the subscript $i = r, \theta, z$

i-component of the velocity vector in fluid flow

w Width of flat plates

w_p Width of the unsheared plug ring in concentric annular flow of Bingham plastic fluids

x, y Rectangular coordinates

z Axial coordinate of the cylindrical coordinate system

β A constant of integration in Eq.(4-4a)

γ Shear rate in fluid flow

Δ Rate of deformation tensor

θ Angular coordinate of the cylindrical coordinate system

λ $= r/r_2$

λ_o = r_o/r_2

λ_1 = $r_1/r_2 = d_1/d_2$

λ_- = r_-/r_2

λ_+ = r_+/r_2

λ_p = $\lambda_+ - \lambda_- = w_p/r_2$

μ Viscosity of Newtonian fluids

μ_a Apparent viscosity of non-Newtonian fluids defined by Eq.(1-6)

μ_e Effective viscosity of non-Newtonian fluids

μ_p Plastic viscosity of Bingham plastic fluids

ξ, η Bipolar coordinates defined in Fig.(A3-1)

π = 3.14159 .....

π_p Dimensionless axial pressure gradient in annular helical flow

π_q Dimensionless volumetric flowrate

π_v Dimensionless axial velocity in annular helical flow

π_μ Dimensionless apparent viscosity in annular helical flow

$\pi_{\tau z}$ Dimensionless axial shear stress in annular helical flow

$\pi_{\tau\theta}$ Dimensionless tangential shear stress in annular helical flow

π_ω Dimensionless angular velocity in annular helical flow

$\pi_{\omega 1}$ Dimensionless angular velocity of the inner tube

$\pi_{\omega 1}'$ Modified dimensionless angular velocity of the inner tube or drillpipe for pressure gradient calculations

ρ Density of fluids

σ Ratio of the tangential shear stress on the outer tube to the equivalent axial pressure stress

σ_{ii}, where the subscripts i = r, θ, z

Normal stress, the first subscript indicates the acting direction and the second subscript indicates the acting surface

τ_{ii}, where the subscripts i = r, θ, z or i = x, y, z

Shear stress, the first subscript indicates the acting direction and the second subscript indicates the acting surface

τ_y Yield stress of Bingham plastic fluids

Ψ $= \xi + i\eta$, a complex number defined in Eq.(A3-2a)

ω Angular velocity of fluids

ω_1 Angular velocity of the inner tube or drillpipe

Superscript:

e Eccentric

PART TWO

a Coefficient defined in Eq.(7-35)

A_a Cross-section area of an annulus

A_e Projected area of the exposed portion of particles, defined in Eq.(10-2)

A_L Projected area of a particle in the direction normal to the flowstream, defined in Eq.(10-3)

A_p Characteristic area of particles, defined in Eq.(7-2)

A_{se} Edge-area of plate-like particles

A_{sf} Face-area of plate-like particles

A_{sp} Projected area of particles in the direction of settling

b Coefficient defined in Eq.(7-35)

b_{ea} Distance between the inner and the outer wall of an inclined annulus at the lowest position

b_{s1} Width of rectangular plate particles

b_{s2} Length of rectangular plate particles

b_{eq} Equivalent width of rectangular plate particles

$$b_{eq} = (b_{s1} \cdot b_{s2})^{1/2}$$

C_D Drag coefficient of spherical particles defined in Eq.(7-2)

C_D' Drag coefficient of non-spherical particles, defined in Eq.(7-38)

C_L Coefficient of the lift force, defined in Eq.(10-3)

C_s Concentration of solid particles in liquid by volume

d Inside diameter of pipes

d_1 Outside diameter of drillpipes

d_2 Wellbore diameter

d_{eq} Equivalent diameter of an annulus

d_s Diameter of spherical particles

d_{sd} Diameter of disk particles

d_{sde} , d_{si} Characteristic diameters of particles defined in reference (20)

d_{sh} Hydraulic diameter of non-spherical particles, defined by Eq.(7-31)

d_{sv} Volume equivalent diameter of non-spherical particles, defined by Eq.(7-30)

f Friction factor for fluid flow in pipes or annuli

f_s Friction coefficient between cuttings and the annular wall under the "wet" condition

$f(\cdots\cdots)$ Function of $\cdots\cdots$

F_D Fluid drag force, defined by Eq.(7-2)

F_g Effective gravitational force on settling particles, defined by Eq.(7-1)

F_{hb} Ratio of the thickness and the width of a plate-like particle

F_L Fluid lift force defined by Eq.(10-3)

F_{mt} Dimensionless constant for MTV correlations

F_{Re} Ratio of the fluid flow Reynolds number to the particle Reynolds number, defined by Eq.(7-47)

F_s Shape correction factor for drag coefficient of non-spherical particles

F_T Cuttings transport ratio, defined by Eq.(6-2a)

F_w Correction factor for the wall-effect on the particle settling velocity

g Gravitational constant

h_s Thickness of a plate-like particle

I A function of λ_1 defined in Eq.(7-21)

K Consistency index of power-law fluids

L_{sp} Particle perimeter around its projected area A_{sp}

m $= \rho_s/\rho_f$

m_1 , m_2 , m_3 Coefficients defined in Eq.(10-17)

n Flow behaviour index of power-law fluids

n_1 , n_2 , n_3 Coefficients defined in Eq.(10-18)

N_{Re} Reynolds number of fluid flow

$N_{Re}(n,\lambda_1)$ Reynolds number for annular fluid flow, defined by Eq.(7-21)

N_{Reb} Particle-boundary layer Reynolds number, defined by Eq.(10-14)

N_{Ren} Particle Reynolds number for Newtonian fluids, defined by Eq.(7-5)

N_{Rep}	Generalised particle Reynolds number for power-law fluids, defined by Eq.(7-33)
q_f	Volumetric flowrate of drilling fluids
q_s	Volume of drilled cuttings generated in unit time
s	= 1/n
v_d	Penetration rate of drilling
v_f	Mean velocity of fluid flow
v_m	Mean flow velocity of solid-liquid mixture
s	
v_{mt}	Minimum transport velocity (MTV) of solid-liquid mixtures, which is defined as the mean mixture velocity when the critical condition for MTV is achieved
v_p	Representative velocity of the fluid in the vicinity of the particles
v_s	Particle settling velocity
v_t	Cuttings transport velocity, defined by Eq.(6-1)
$v*$	$= (\tau_w/\rho_f)^{1/2}$, friction velocity of fluid flow
$v*_{mt}$	$= (\tau_{wmt}/\rho_f)^{1/2}$, minimum transport friction velocity
V_s	Volume of a solid particle
X	A constant in Eq.(7-34)
y	Distance between a point in the flow stream and the solid boundary
β	Shields' Beta, defined in Eq.(9-29)
γ	Shear rate of fluids in uni-directional shear flows
γ_{eq}	Equivalent shear rate for particle settling
γ_s	Shear rate on settling particles, defined by Eq.(7-29)
γ_w	Wall shear rate in annular or pipe flow
δ	Thickness of the viscous sublayer or buffer layer in turbulent pipe flow

κ_1 = d_1/d_2

μ Viscosity of Newtonian fluids

μ_a Apparent viscosity of non-Newtonian fluids, defined by Eq.(7-14)

μ_e Effective viscosity of non-Newtonian fluids, defined in reference (13b)

μ_{eq} Equivalent viscosity of non-Newtonian fluids for particle settling

μ_m Viscosity of solid-liquid mixtures

μ_p Plastic viscosity of Bingham plastic fluids

π = 3.14159·····

Π_i i = 1, 2, 3... Dimensionless groups

ρ_f Density of fluids

ρ_m Density of solid-liquid mixtures

ρ_s Density of solid particles

τ Shear stress of fluids in uni-directional shear flows

τ_c Critical shear stress for initiation of sediment transport

τ_s Shear stress on settling particles, defined by Eq.(7-28)

τ_w Wall shear stress in annular or pipe flow

τ_{wmt} Minimum transport wall shear stress

τ_y Yield stress of Bingham plastic fluids

Φ Inclination of drilling annuli or hole angle

Φ_c Critical angle for cuttings sliding-down when circulation is stopped

ψ Sphericity of non-spherical particles, defined by Eq.(7-32)

PART ONE

LAMINAR FLOW OF NON-NEWTONIAN FLUIDS THROUGH ANNULAR SPACE

INTRODUCTION

Annular flow refers to the flow of fluids through an annular space between two infinitely long circular tubes. Like fluid flow through a circular pipe or in an open channel, the annular flow may be laminar or turbulent in terms of flow regime and the fluids may be Newtonian or non-Newtonian in terms of rheological behaviour. However the most interesting characteristic which makes the annular flow unique is the diversity in configuration and dynamic condition of the flow channel: the two tubes forming the annulus may be coaxial or non-coaxial; one of or both the tubes may be stationary or in (rotary/translational) motion. Therefore, in addition to "laminar" or "turbulent" and "Newtonian" or "non-Newtonian", many more words like "concentric" or "eccentric" and "axial" or "tangential" or "helical", etc. must be supplemented to the word "annular flow" in order to distinguish its different cases. In fact, the annular flow is so "versatile" that many of its different cases have been hardly mentioned yet in spite of all the effort made by numerous investigators since early this century[1a].

Although the present author was fascinated from the beginning by the "versatility" of annular flow, the following studies were really motivated by the plain fact that there is considerable lack of understanding for some simple and yet important cases of annular flow which must be dealt with in many industrial and engineering designs.

In petroleum drilling operations, the drilling fluids, which are generally non-Newtonian in rheological behaviour, flow through the

annular space between the drillpipe and the casing or wellbore under the action of an axial pressure gradient. So the calculations relevant to non-Newtonian annular flow are often required in the drilling hydraulics design, the cuttings transport design, cementing design, and the well control operations, etc. However, because of our lack of understanding of the non-Newtonian annular flow, these calculations are generally made based on two unrealistic assumptions:

1) the drillpipe is placed concentrically in the casing or wellbore;

2) the drillpipe is not rotated.

This part of the thesis presents the theoretical studies conducted by the present author on laminar non-Newtonian annular flow. In the first chapter, some basic assumptions are made and some fundamental concepts are introduced for the subsequent analyses. Then laminar flow of non-Newtonian fluids through a concentric annulus is reviewed in the second chapter based on the principles used by previous investigators and some approximations are made to some of the solutions. In Chapter 3, theoretical studies on laminar flow of non-Newtonian fluids through an eccentric annulus is presented in which a new method is used to describe the eccentric annular geometry. Chapter 4 is devoted to theoretical studies on laminar helical flow of power-law fluids. In the last chapter of the first part of the thesis, some additional discussions on the present studies are given and recommendations are made for future studies.

CHAPTER 1.

FUNDAMENTALS

1.1. Basic assumptions

Like the cases of fluid flow through circular pipes and other shaped channels, some assumptions are required in the derivation of the equations for non-Newtonian annular flow in the present analyses. In terms of the fluids we will deal with, it is assumed that:

a. The fluids are incompressible, i.e. they have a constant density;

b. The fluids are inelastic, i.e. the fluids, on removal of the shearing force, do not recover from any deformation they have undergone under its action;

c. The fluids are time-independent in rheological behaviour, i.e. the rate of shear at a given point is solely dependent upon the instantaneous shear stress at that point;

In terms of the flow system we will deal with, it is assumed that:

d. The flow is in steady state, i.e. the fluid velocities at different points in space are independent of time;

e. The flow system is isothermal, i.e. the heat generated or absorbed internally does not cause appreciable temperature change;

f. The non-slip condition is satisfied at all solid boundaries.

1.2. Rheological models

Based on the assumptions made in the preceding section, the fluids we are dealing with are those which are incompressible, inelastic and

time independent. The characteristics of any given fluid within the above category can be described, under a given pressure and temperature, by the relationship:

shear stress = f(shear rate)

This relationship is generally called the constitutive or rheological equation for the fluid.

The simplest form of the above relationship describes the rheological behaviour of so called "Newtonian fluids". If the cylindrical coordinate system is used, the flow is z-directional and the fluid velocity varies only in the r-direction, the rheological equation for a Newtonian fluid, usually called "Newtonian model", may be written as[2a]:

$$\tau_{zr} = - \mu \frac{dv_z}{dr} \qquad (1-1)$$

where the quantity "μ" is a property of the fluid and it is a measure of its viscosity. Under a given pressure and temperature, μ is a constant and thus the shear stress is proportional to the shear rate. If a flow curve is drawn for the shear stress vs shear rate, then the flow curve is a straight line through the origin of the coordinates. Eq.(1-1) is also known as Newton's law of friction and it may be regarded as the definition of viscosity.

Non-Newtonian fluids, on the contrary, refer to all those fluids for which the flow curve of the shear stress vs shear rate is not linear through the origin at a given pressure and temperature. These non-Newtonian fluids are generally subdivided into two different types. The first type is the fluids without a yield stress. A fluid of this

type responds to the smallest applied shear stress and there is no "yield" strength required to be overcome before flow commences. The flow curves of this type of fluids pass through the origin but they are not linear. The second type of non-Newtonian fluids is the fluids with a yield stress. For this type of fluids, a finite shear stress is required before flow commences and thus the flow curve does not pass through the origin but intercepts the shear stress coordinate at a finite value known as the "yield stress".

Numerous rheological models are available for describing the rheological behaviours of the above two different types of non-Newtonian fluids. However the most commonly used models are the power-law model and the Bingham plastic model because these two models are simple, as they contain only two rheological parameters, and can describe adequately the rheological behaviours of the majority of the commonly seen non-Newtonian fluids.

The power-law model, which is used for non-Newtonian fluids without a yield stress, is generally expressed as:

$$\tau_{zr} = - K \left| \frac{dv_z}{dr} \right|^{n-1} \frac{dv_z}{dr} \qquad (1\text{-}2)$$

where the quantity 'K' is called the consistency index and 'n' is called the flow behaviour index. The non-Newtonian fluids which can be described by the power-law model are generally called the "power-law fluids". Strictly speaking, any non-Newtonian fluid does not possess a property which may be called the viscosity. However it is often convenient to refer to a viscosity, usually called "apparent viscosity", of a non-Newtonian fluid under many circumstances. According to Newton's law of friction, i.e. Eq.(1-1), the apparent viscosity of power-law fluids may be defined as:

$$\mu_a = K \left| \frac{dv_z}{dr} \right|^{n-1} \qquad (1\text{-}3)$$

As it may be seen, the apparent viscosity μ_a is not a constant but shear dependent. If $n < 1$, μ_a decreases as shear rate increases and so the fluid is called a "pseudoplastic fluid". If $n > 1$, then μ_a increases as shear rate increases and the fluid is called a "dilatant fluid".

Another most commonly used non-Newtonian model, the Bingham plastic model, is generally expressed as:

$$\tau_{zr} = \mp \tau_y - \mu_p \frac{dv_z}{dr} \qquad (|\tau_{zr}| \geq \tau_y) \qquad (1\text{-}4)$$

where "-" is used for $\frac{dv_z}{dr} > 0$ and "+" for $\frac{dv_z}{dr} < 0$. In the above equation, μ_p is called the plastic viscosity and τ_y is called the yield stress. The characteristic of the Bingham plastic fluid is that the fluid does not shear unless the shear stress has exceeded its yield stress τ_y. The flow curve of the fluid is linear but it dose not pass through the origin. The apparent viscosity for Bingham plastic fluids may be defined as:

$$\mu_a = \mu_p + \frac{\tau_y}{\left| \frac{dv_z}{dr} \right|} \qquad (1\text{-}5)$$

As it may be seen, the apparent viscosity for Bingham plastic fluids also decreases as shear rate increases, and vice versa.

Obviously, Newtonian fluids may be treated as the special case of either power-law fluids when $n = 1$ or Bingham plastic fluids when $\tau_y = 0$. In this case, the apparent viscosity obtained from Eq.(1-3) or Eq.(1-5) becomes a constant. Fig.(1-1) shows the flow curves for

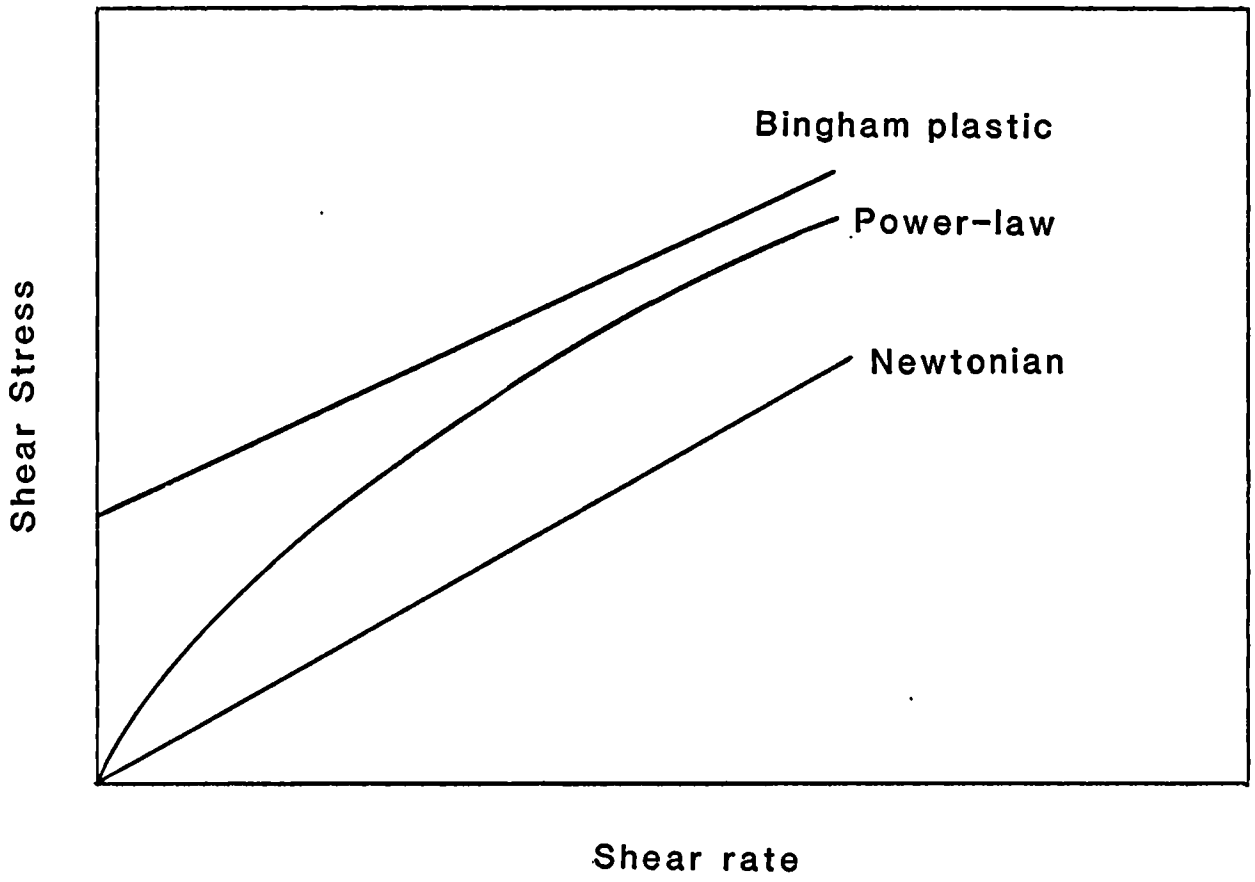

Fig.1-1 Flow curves on arithmetic coordinates for Newtonian, power-law and Bingham plastic fluids

Newtonian, power-law and Bingham plastic fluids.

The rheological models discussed above are only used for uni-directional shear flow, i.e. for the flow where the fluid velocity varies only in one direction. For the multi-directional shear flow, as in some cases of annular flow, the rheological models must be expressed in the tensor form. A general form of the rheological model for incompressible, inelastic and time-independent fluids may be expressed as[3a]:

$$T = -\mu_a \cdot \Delta \tag{1-6}$$

where T is the stress tensor and Δ is the rate of deformation tensor. In the cylindrical coordinate system, the stress tensor T may be expressed as:

$$T = \begin{pmatrix} \sigma_{rr} & \tau_{r\theta} & \tau_{rz} \\ \tau_{\theta r} & \sigma_{\theta\theta} & \tau_{\theta z} \\ \tau_{zr} & \tau_{z\theta} & \sigma_{zz} \end{pmatrix} \tag{1-7}$$

where the normal stress is denoted by 'σ' and the shear stress is denoted by 'τ'. In the above expression, the first subscript indicates the direction to which the stress is parallel and the second subscript indicates the axis to which the surface corresponding to the stress is perpendicular. The rate of deformation tensor may be written as:

$$\Delta = \begin{pmatrix} 2\frac{\partial v_r}{\partial r} & \frac{1}{r}\frac{\partial v_r}{\partial \theta} + r\frac{\partial}{\partial r}\left(\frac{v_\theta}{r}\right) & \frac{\partial v_r}{\partial z} + \frac{\partial v_z}{\partial r} \\ r\frac{\partial}{\partial r}\left(\frac{v_\theta}{r}\right) + \frac{1}{r}\frac{\partial v_r}{\partial \theta} & 2\cdot\left(\frac{1}{r}\frac{\partial v_\theta}{\partial \theta} + \frac{v_r}{r}\right) & \frac{\partial v_\theta}{\partial z} + \frac{1}{r}\frac{\partial v_z}{\partial \theta} \\ \frac{\partial v_z}{\partial r} + \frac{\partial v_r}{\partial z} & \frac{1}{r}\frac{\partial v_z}{\partial \theta} + \frac{\partial v_\theta}{\partial z} & 2\frac{\partial v_z}{\partial z} \end{pmatrix} \tag{1-8}$$

For a given Newtonian fluid, the apparent viscosity μ_a in Eq.(1-6) is a constant and for a given kind of non-Newtonian fluids, it is a function of Δ. For power-law fluids, μ_a takes the form of:

$$\mu_a = K \left| \left[\frac{1}{2} (\bar{\Delta}:\Delta) \right]^{0.5} \right|^{n-1} \tag{1-9}$$

For Bingham plastic fluids, μ_a may be written as:

$$\mu_a = \mu_p + \frac{\tau_y}{\left| \left[\frac{1}{2} (\bar{\Delta}:\Delta) \right]^{1/2} \right|} \qquad \left[\frac{1}{2} (T:T) \geq \tau_y^2 \right] \tag{1-10}$$

where the term $\frac{1}{2} (\bar{\Delta}:\Delta)$ represents a scalar product of the rate of deformation tensors and it may be expressed as:

$$\frac{1}{2} (\bar{\Delta}:\Delta) = \frac{1}{2} \sum_i \sum_j \Delta_{ij} \Delta_{ji} \tag{1-11}$$

In cylindrical coordinates, the above expression becomes:

$$\frac{1}{2} (\bar{\Delta}:\Delta) = \frac{1}{2} \left\{ \left(2 \frac{\partial v_r}{\partial r}\right)^2 + \left[2 \cdot \left(\frac{1}{r} \frac{\partial v_\theta}{\partial \theta} + \frac{v_r}{r}\right)\right]^2 + \left(2 \frac{\partial v_z}{\partial z}\right)^2 \right\} +$$

$$+ \left[\frac{1}{r} \frac{\partial v_r}{\partial \theta} + r \frac{\partial}{\partial r}\left(\frac{v_\theta}{r}\right)\right]^2 + \left(\frac{\partial v_\theta}{\partial z} + \frac{1}{r} \frac{\partial v_z}{\partial \theta}\right)^2 + \left(\frac{\partial v_z}{\partial r} + \frac{\partial v_r}{\partial z}\right)^2 \tag{1-12}$$

If the flow is z-directional and the fluid velocity varies only in r-direction, then the only non-zero component of the velocity vector in Eqs.(1-8) and (1-12) is $\frac{\partial v_z}{\partial r}$. In this case, based on Eqs.(1-7) through (1-12), Eq.(1-6) returns to Eq.(1-2) for power-law fluids and to Eq.(1-4) for Bingham plastic fluids. Therefore, Eqs.(1-2) and (1-4) are only special forms of Eq.(1-6) for uni-directional flow of power-law and Bingham plastic fluids, respectively.

CHAPTER 2.

A REVIEW ON LAMINAR AXIAL FLOW OF NON-NEWTONIAN FLUIDS THROUGH CONCENTRIC ANNULI

The term: "annular axial flow" refers to the flow of fluids through an annular space between two infinitely long circular tubes and the fluid elements move only in the z-direction while other components of the fluid velocity are zero. It is often simply called the 'annular flow'. This situation occurs when both the inner tube and the outer tube are stationary and the fluid flows through the annulus under the action of a constant pressure gradient in the z-direction. If the annular space is concentric, i.e. the axes of the inner and outer tubes coincide with each other, then the flow is called the 'concentric annular flow'.

2.1. Previous studies

The investigations into concentric annular flow of power-law fluids were started thirty years ago. Fredrickson and Bird[4] in 1958 first reported their comprehensive theoretical studies and presented the solutions in the dimensionless form. Their theoretical solutions were substantiated by the expremental data reported by Tui and Bhattacharyya [5]. Hanks and Larsen[6] later improved the Fredrickson and Bird's expression for the volumetric flowrate/pressure gradient. However, because the radial position for the zero shear stress point can not be calculated directly, any of the flow calculations for the concentric annular flow of power-law fluids must involve some iterative calculations and/or numerical integrations.

Laird[7] was the first to present the theoretical analysis on concentric annular flow of Bingham plastic fluids. Later Fredrickson and Bird[4] also reported the results of their studies and presented the solutions for Bingham plastic fluids in the dimensionless form. Using their expressions, once the radial positions for the central unsheared plug boundaries have been obtained by using iterative calculation methods, other flow calculations can be made directly.

In the following review of concentric annular flow of power-law and Bingham plastic fluids, the equations for the shear stress, shear rate, velocity and volumetric flowrate/pressure gradient will be developed based on the principles used by the above investigators. In addition, some approximations will be made based on the present new analysis.

With the theoretical analysis performed in this chapter as a foundation, we will proceed to investigate laminar eccentric annular flow in Chapter 3 and laminar helical flow in Chapter 4.

2.2. Derivation of the governing equation

2.2.1. From equations of motion

In this section, the governing equation for concentric annular flow will be derived based on the fundamental equations of fluid mechanics, i.e. the equation of continuity and the equations of motion.

In the cylindrical coordinate system, the equation of continuity is expressed as[8a]:

$$\frac{\partial v_r}{\partial r} + \frac{1}{r}\frac{\partial v_\theta}{\partial \theta} + \frac{\partial v_z}{\partial z} + \frac{v_r}{r} = 0 \qquad (2\text{-}1)$$

and the equations of motion may be expressed as[8b]:

$$r: \quad \rho \left(\frac{\partial v_r}{\partial t} + v_r \frac{\partial v_r}{\partial r} + \frac{v_\theta}{r} \frac{\partial v_r}{\partial \theta} - \frac{v_\theta^2}{r} + v_z \frac{\partial v_r}{\partial z} \right) =$$

$$= \rho \cdot g_r - \frac{\partial P_f}{\partial r} - \left[\frac{1}{r} \frac{\partial}{\partial r}(r \cdot \sigma_{rr}) + \frac{1}{r} \frac{\partial \tau_{r\theta}}{\partial \theta} - \frac{\sigma_{\theta\theta}}{r} + \frac{\partial \tau_{rz}}{\partial z} \right] \quad (2\text{-}2a)$$

$$\theta: \quad \rho \cdot \left(\frac{\partial v_\theta}{\partial t} + v_r \frac{\partial v_\theta}{\partial r} + \frac{v_\theta}{r} \frac{\partial v_\theta}{\partial \theta} + \frac{v_r \cdot v_\theta}{r} + v_z \frac{\partial v_\theta}{\partial z} \right) =$$

$$= \rho \cdot g_\theta - \frac{1}{r} \frac{\partial P_f}{\partial \theta} - \left[\frac{1}{r^2} \frac{\partial}{\partial r}(r^2 \cdot \tau_{\theta r}) + \frac{1}{r} \frac{\partial \sigma_{\theta\theta}}{\partial \theta} + \frac{\partial \tau_{\theta z}}{\partial z} \right] \quad (2\text{-}2b)$$

$$z: \quad \rho \cdot \left(\frac{\partial v_z}{\partial t} + v_r \frac{\partial v_z}{\partial r} + \frac{v_\theta}{r} \frac{\partial v_z}{\partial \theta} + v_z \frac{\partial v_z}{\partial z} \right) =$$

$$= \rho \cdot g_z - \frac{\partial P_f}{\partial z} - \left[\frac{1}{r} \frac{\partial}{\partial r}(r \cdot \tau_{zr}) + \frac{1}{r} \frac{\partial \tau_{z\theta}}{\partial \theta} + \frac{\partial \sigma_{zz}}{\partial z} \right] \quad (2\text{-}2c)$$

Based on the assumptions made in the preceding chapter, for the present case of annular axial flow through concentric annuli, the following characteristics of the flow may be identified:

(i) the flow is in steady state, i.e. it is independent of time. Then:

$$\frac{\partial v_i}{\partial t} = 0 \qquad i = r, \theta, z$$

(ii) both the inner tube and the outer tube are stationary and the fluid flows under the action of a constant pressure gradient in z-direction, so the flow is purely axial. Thus the only non-zero velocity component is v_z and the radial and the tangential velocity components are all zero, i.e.

$$v_r = 0$$

$$v_\theta = 0$$

(iii) the annualr space is concentric or axisymmetric, so the fluid velocity is independpent of θ, i.e.

$$\frac{\partial v_z}{\partial \theta} = 0$$

(iv) the cross section of the annulus is uniform in z-direction. Based on the equation of continuity, the flow is independent of z, i.e.

$$\frac{\partial v_z}{\partial z} = 0$$

Based on the above characteristics, the only non-zero component of the fluid velocity is the axial component v_z and this component is a function of the radial position r only, i.e.

$$v_z = v(r) \qquad (2\text{-}3)$$

Examining Eqs.(1-6) through (1-8) and noting that T is a symmetric tensor, it may be revealed that the only non-zero component of the stress tensor is the shear stress τ_{zr} which is also a function of r only, i.e.

$$\tau_{zr} = \tau(r) \qquad (2\text{-}4)$$

Then, based on the above two equations, the equations of motion, i.e. Eqs.(2-2), may be simplified to a single equation which may be written as:

$$g_p - \frac{1}{r}\frac{\partial}{\partial r}(r \cdot \tau_{zr}) = 0$$

Integrating the above equation yields:

$$\frac{g_p}{2} r^2 - r \cdot \tau_{zr} = C \qquad (2\text{-}5)$$

where C is a constant of integration and g_p is the pressure gradient which is defined by:

$$g_p = \rho \cdot g_z - \frac{\partial P_f}{\partial z} \qquad (2\text{-}6)$$

Eq.(2-5) is the governing equation for concentric annular flow. Because no specific rheological model was assumed during the derivation of this equation, it is valid for both Newtonian and non-Newtonian fluids.

2.2.2. Using shell balance method

The governing equation of concentric annular flow, i.e. Eq.(2-5), may be also derived by considering Newton's law of motion for a shell of fluid at radius r in the flow. Shown in Fig.(2-1) is a free-body diagram of a shell of fluid of length L and of thickness dr. When the fluid element is moving at a constant velocity, the sum of the forces acting on the element must equal to zero, i.e.

$$\pi \cdot [(r+dr)^2 - r^2] \cdot (P_1 - P_2) + \pi \cdot [(r+dr)^2 - r^2] \cdot L \cdot \rho \cdot g_z +$$

$$+ 2\pi \cdot r \cdot L \cdot \tau_{zr} - 2\pi \cdot (r+dr) \cdot L \cdot (\tau_{zr} + d\tau_{zr}) = 0$$

Simplifying and omitting the higher order differentials, i.e. $(dr)^2 = 0$

and $dr \cdot d\tau_{zr} \simeq 0$, we have:

$$r \cdot dr \cdot \left(\frac{P_1 - P_2}{L} + \rho \cdot g_z \right) - \left(r \cdot d\tau_{zr} + \tau_{zr} \cdot dr \right) = 0$$

Integrating the above equation gives:

$$\frac{g_p}{2} r^2 - r \cdot \tau_{zr} = C$$

where $g_p = \rho \cdot g_z - \frac{\partial P_f}{\partial z}$ and $\frac{\partial P_f}{\partial z} = \frac{P_2 - P_1}{L} = -\frac{P_1 - P_2}{L}$.

The above equation is the same as Eq.(2-5) derived in the preceding section from the equations of motion. Again, the above equation has been derived solely based on the force balance principle and no specific rheological model was used, so Eq.(2-5) is valid for both Newtonian and non-Newtonian fluids.

In the following sections, the expressions for the shear stress, shear rate and velocity profiles and for the volumetric flowrate /pressure gradient will be developed consecutively based on the governing equation.

2.3. Concentric annular flow of power-Law fluids

A nomenclature for the symbols which will be used in this section has been provided in Fig.(2-1). In addition, the following dimensionless variables will also be used:

$$\hat{r} = \frac{r}{r_2} \qquad \hat{r}_1 = \frac{r_1}{r_2} \qquad \hat{r}_o = \frac{r_o}{r_2}$$

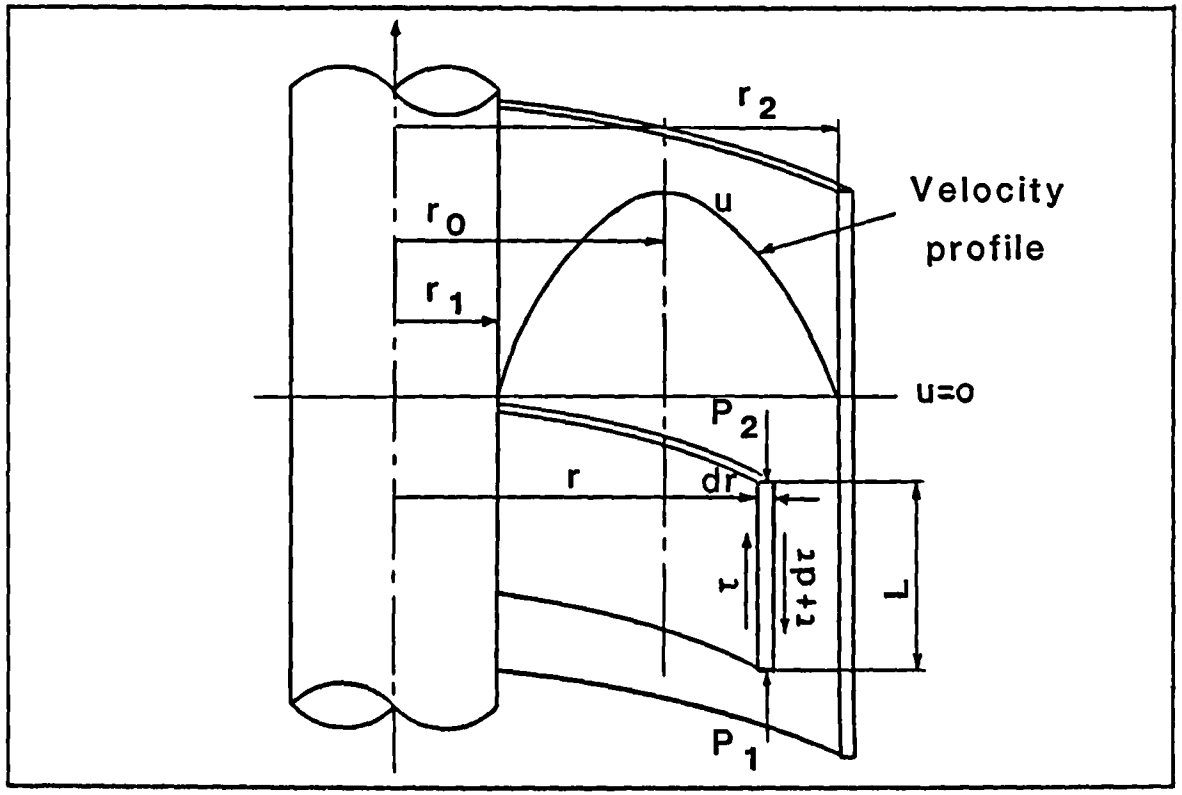

Fig.2-1 Free body diagram for a fluid element in concentric annular flow

Shear stress profile

For power-law fluids, applying the boundary condition to Eq.(2-5) that $\tau_{zr} = 0$ at $r = r_o$, the expression for the shear stress profile may be established as:

$$\tau_{zr} = \frac{g_p \cdot r_2}{2} \left(\dot{\gamma} - \frac{\dot{\gamma}_o^2}{\dot{\gamma}} \right) \qquad (2\text{-}7)$$

It should be noticed that, unlike the case in pipe flow, the shear stress profile in annular flow is not linear. The shear stresses on the inner and outer tubes are of particular interest. From Eq.(2-7) it may be obtained that:

$$\tau_{zr}\big|_{\dot{\gamma}=\dot{\gamma}_1} = \frac{g_p \cdot r_2}{2} \left(\dot{\gamma}_1 - \frac{\dot{\gamma}_o^2}{\dot{\gamma}_1} \right) \qquad (2\text{-}7a)$$

$$\tau_{zr}\big|_{\dot{\gamma}=1} = \frac{g_p \cdot r_2}{2} \left(1 - \dot{\gamma}_o^2 \right) \qquad (2\text{-}7b)$$

It can be easily shown from the above equations that $\tau_{zr}|_{\dot{\gamma}=\dot{\gamma}_1}$ is not equal to $\tau_{zr}|_{\dot{\gamma}=1}$ in magnitude.

Shear rate profile

From Eq.(1-2) we have:

$$\frac{dv_z}{dr} = \pm \left| \frac{\tau_{zr}}{K} \right|^s$$

where "+" is used for $r < r_o$ and "-" for $r > r_o$, and $s = 1/n$. The expression for the shear rate profile may be found by substituting

Eq.(2-7) into the above equation:

$$\frac{dv_z}{dr} = \gamma = \pm \left(\frac{g_p \cdot r_2}{2 \cdot K} \right)^s \left| \lambda - \frac{\lambda_o^2}{\lambda} \right|^s \qquad (2\text{-}8)$$

Velocity profile

The velocity profile can be obtained by integrating Eq.(2-8):

$$v = \left(\frac{g_p \cdot r_2}{2 \cdot K} \right)^s r_2 \int_{\lambda_1}^{\lambda} \left(\frac{\lambda_o^2}{\lambda} - \lambda \right)^s d\lambda \qquad (\lambda_1 \leq \lambda \leq \lambda_o) \qquad (2\text{-}9a)$$

$$v = \left(\frac{g_p \cdot r_2}{2 \cdot K} \right)^s r_2 \int_{\lambda}^{1} \left(\lambda - \frac{\lambda_o^2}{\lambda} \right)^s d\lambda \qquad (r_o \leq r \leq r_2) \qquad (2\text{-}9b)$$

Determining equation for λ_o

The term λ_o in Eqs.(2-7) through (2-9) is the dimensionless radius at which the shear stress τ_{zr} is zero and the fluid velocity v_z is maximum. When $\lambda = \lambda_o$, both Eqs.(2-9a) and (2-9b) must give the same value of the maximum velocity. So λ_o may be found by solving the following equation:

$$\int_{\lambda_1}^{\lambda_o} \left(\frac{\lambda_o^2}{\lambda} - \lambda \right)^s d\lambda = \int_{\lambda_o}^{1} \left(\lambda - \frac{\lambda_o^2}{\lambda} \right)^s d\lambda \qquad (2\text{-}10a)$$

The above equation can not be integrated and solved for λ_o directly, so the numerical integration must be utilised when λ_o is to be found. However, the calculations have been made for λ_o by using Eq.(2-10a) and the results are shown in Fig.(2-2). It can be seen that λ_o is rather insensitive to the variation of the flow behaviour index 'n'. In fact it can be shown that, within an error of about ±3%, Eq.(2-10a) may be

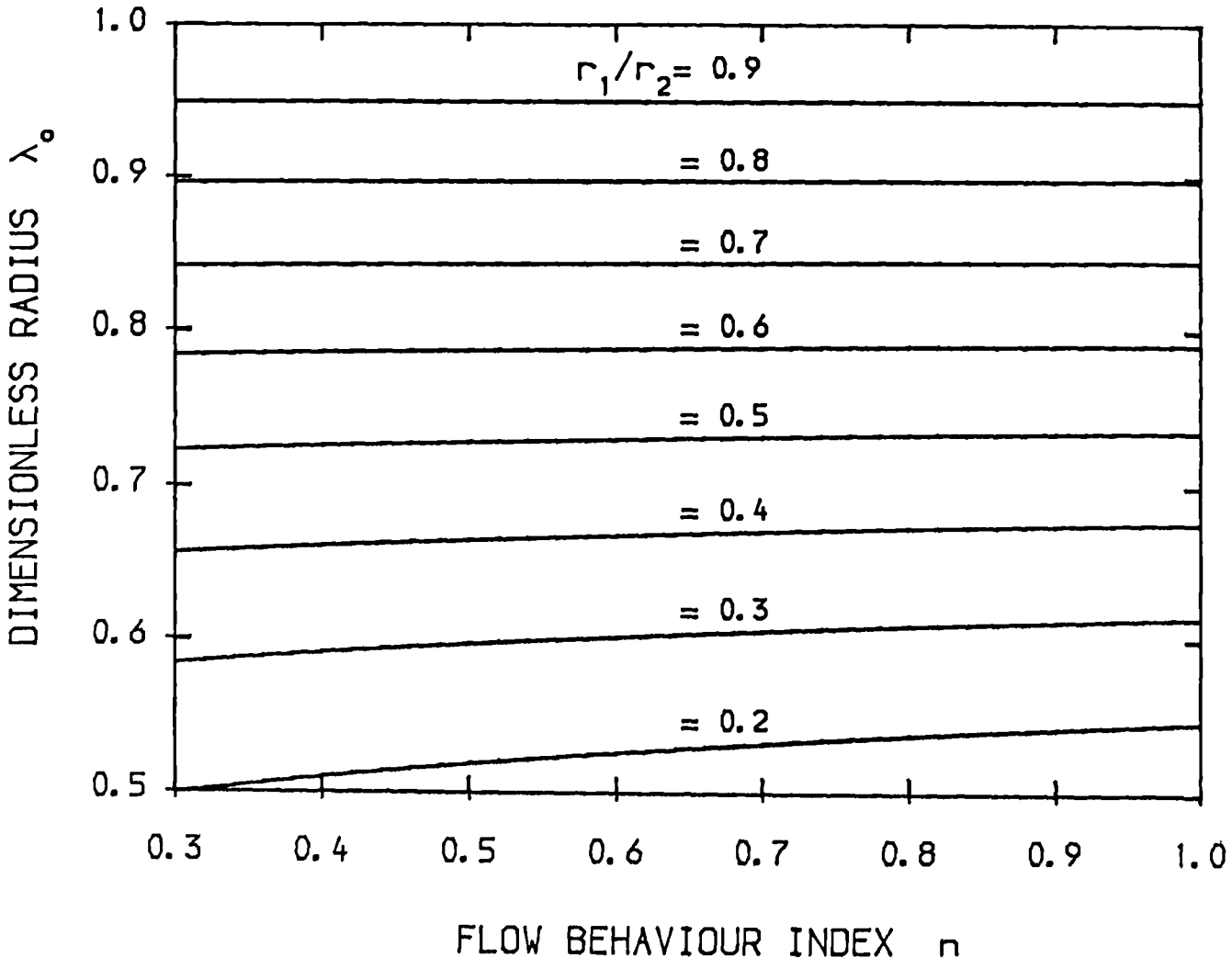

Fig.2-2 Dimensionless radius λ_o for concentric annular flow of power-law fluids

approximated by setting $n = 1$, i.e. assuming Newtonian fluids, for the cases where $n \geq 0.5$ and $\dot{\kappa}_1 \geq 0.3$. Then integrating Eq.(2-10a) and solving for $\dot{\kappa}_o$ yields:

$$\dot{\kappa}_o = \left[\frac{1 - \dot{\kappa}_1^2}{2 \cdot \ell n(\frac{1}{\dot{\kappa}_1})} \right]^{1/2} \qquad (2\text{-}10b)$$

Volumetric flowrate/pressure gradient

By definition, the volumetric flowrate may be expressed as:

$$q = r_2^2 \int_{\dot{\kappa}_1}^{1} 2\pi \cdot \dot{\kappa} \cdot v_z \cdot d\dot{\kappa} \qquad (2\text{-}11a)$$

Substituting Eqs.(2-9) into the above equation, it may be obtained that:

$$q = 2\pi \cdot r_2^3 \cdot (\frac{g_p \cdot r_2}{2 \cdot K})^s \left[\int_{\dot{\kappa}_1}^{\dot{\kappa}_o} \dot{\kappa} \cdot d\dot{\kappa} \cdot \int_{\dot{\kappa}_1}^{\dot{\kappa}} \left(\frac{\dot{\kappa}_o^2}{\dot{\kappa}} - \dot{\kappa} \right)^s d\dot{\kappa} + \right.$$

$$\left. + \int_{\dot{\kappa}_o}^{1} \dot{\kappa} \cdot d\dot{\kappa} \cdot \int_{\dot{\kappa}}^{1} \left(\dot{\kappa} - \frac{\dot{\kappa}_o^2}{\dot{\kappa}} \right)^s d\dot{\kappa} \right] \qquad (2\text{-}11b)$$

The above equation was integrated by Hanks and Larsen[6] and they obtained that:

$$q = r_2^3 \cdot (\frac{g_p \cdot r_2}{K})^s \cdot \pi_q \qquad (2\text{-}11c)$$

where 'π_q' is defined as the dimensionless volumetric flowrate by the present author:

$$\pi_q = \frac{n \cdot \pi}{1+3 \cdot n} (\frac{1}{2})^s \left[\left(1 - \dot{\kappa}_o^2 \right)^{1+s} - \dot{\kappa}_1^{1-s} \cdot \left(\dot{\kappa}_o^2 - \dot{\kappa}_1^2 \right)^{1+s} \right] \qquad (2\text{-}12)$$

The expression for the pressure gradient may be found by reversing Eq.(2-11c):

$$g_p = \left(\frac{q}{\pi_q \cdot r_2^3}\right)^n \frac{K}{r_2} \qquad (2\text{-}13)$$

2.4. Concentric annular flow of Bingham plastic fluids

For Bingham plastic fluids, a finite shear stress is required to start a flow, i.e. the fluid does not shear unless the shear stress exceeds the yield stress τ_y. So in Bingham plastic flow through various shaped ducts, there is always a volume of the fluid within which the fluid does not shear and the fluid elements move at the same velocity like a "plug". So this unsheared volume of fluid is often called the "unsheared plug" as shown in Fig.(2-3).

In concentric annular axial flow, because the flow is independent of 'θ' and is a function of 'r' only, as shown in the section 2.2.1, it may be easily deduced that the unsheared plug should be in the shape of a circular cylinder with a constant thickness and its cross section is a circular ring with a constant width. If we use r_- and r_+ to denote the inner and outer radii of the plug cylinder, then the thickness of the plug cylinder or the width of the plug ring may be found by considering the balance between the shear force and the pressure force, i.e. the shear force acting on the inner and outer surfaces of the plug cylinder, which is equal to τ_y times the total area of the surfaces, should be balanced with the pressure force acting on the cross section area of the plug cylinder:

$$2\pi \cdot (r_+ + r_-) \cdot L \cdot \tau_y = \pi \cdot (r_+^2 - r_-^2) \cdot g_p \cdot L$$

Simplifying the above equation gives the width of the plug ring as:

$$w_p = r_+ - r_- = \frac{2 \cdot \tau_y}{g_p} \qquad (2\text{-}14)$$

It should be noted that the thickness of the plug cylinder or the width of the plug ring depends only on the yield stress and the pressure gradient and is independent of the annular size. If the width of the plug ring, w_p, is equal or greater than the annular gap, (r_2-r_1), then the plug cylinder will occupy the entire annular space and the fluid will become stagnant. Therefore there is a minimum pressure gradient which is required to start a concentric annular flow of Bingham plastic fluids. Based on Eq.(2-14), this minimum pressure gradient may be calculated by:

$$(g_p)_{min} = \frac{2 \cdot \tau_y}{r_2 - r_1} \qquad (2\text{-}15)$$

In the following analysis, it is always assumed that:

$$g_p > (g_p)_{min}$$

$$w_p < (r_2 - r_1)$$

A nomenclature has been provided in Fig.(2-3) for the following analysis of the concentric annular flow of Bingham plastic fluids. The dimensionless parameters are defined as follows:

$$\kappa = \frac{r}{r_2} \qquad \kappa_1 = \frac{r_1}{r_2} \qquad \kappa_- = \frac{r_-}{r_2} \qquad \kappa_+ = \frac{r_+}{r_2}$$

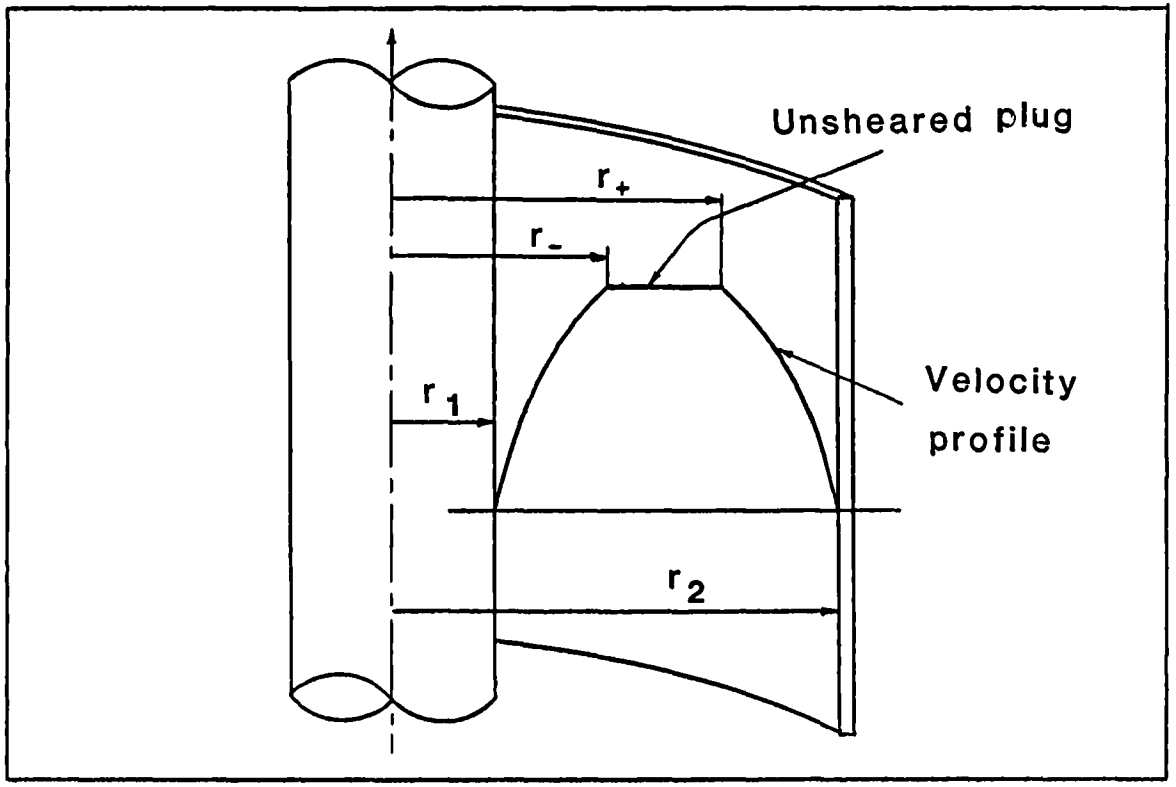

Fig.2-3 Nomenclature for concentric annular flow of Bingham plastic fluids

In addition, the dimensionless width of the unsheared plug ring is defined as:

$$\kappa_p = w_p/r_2 = \kappa_+ - \kappa_- \qquad (2\text{-}16)$$

Based on the above definition and Eq.(2-14), the following relationship exists:

$$\kappa_p = \frac{2 \cdot \tau_y}{g_p \cdot r_2} \qquad (2\text{-}16)$$

Shear stress profile

In the region of $\kappa_1 \leq \kappa \leq \kappa_-$, the fluid velocity increases with increase of κ, so $dv_z/dr \geq 0$. Based on Eq.(1-4) and applying the boundary condition to Eq.(2-5) that $\tau_{zr} = -\tau_y$ at $\kappa = \kappa_-$, the shear stress profile in this region may be found as:

$$\tau_{zr} = -\frac{g_p \cdot r_2}{2} \left[\left(\frac{\kappa_-^2}{\kappa} - \kappa \right) + \frac{\kappa_-}{\kappa} \kappa_p \right] \quad (\kappa_1 \leq \kappa \leq \kappa_-) \qquad (2\text{-}17a)$$

Similarly, from $\tau_{zr} = \tau_y$ at $\kappa = \kappa_+$, Eq.(2-5) becomes:

$$\tau_{zr} = \frac{g_p \cdot r_2}{2} \left[\left(\kappa - \frac{\kappa_+^2}{\kappa} \right) + \frac{\kappa_+}{\kappa} \kappa_p \right] \quad (\kappa_+ \leq \kappa \leq 1) \qquad (2\text{-}17b)$$

Like the case for power-law fluids, it may be seen from Eqs.(2-17) that the shear stress profile is not linear for the present case of the concentric annular flow of Bingham plastic fluids. The shear stresses on the inner and the outer tubes may be obtained from the above equations as:

$$\tau_{zr}\Big|_{\kappa=\kappa_1} = -\frac{g_p \cdot r_2}{2}\left[\left(\frac{\kappa_-^2}{\kappa_1} - \kappa_1\right) + \frac{\kappa_-}{\kappa_1}\kappa_p\right] \qquad (2\text{-}17c)$$

$$\tau_{zr}\Big|_{\kappa=1} = \frac{g_p \cdot r_2}{2}\left[(1 - \kappa_+^2) + \kappa_+ \cdot \kappa_p\right] \qquad (2\text{-}17d)$$

Shear rate profile

From Eq.(1-4) it may be found that:

$$-\frac{dv_z}{dr} = \frac{\tau_{zr} \pm \tau_y}{\mu_p}$$

where "+" is used when $r_1 \le r \le r_-$ or $\tau_{zr} < 0$ and "-" is used when $r_+ \le r \le r_2$ or $\tau_{zr} > 0$. Substituting Eqs.(2-17a) and (2-17b) into the above equation, respectively, we may obtain:

$$\frac{dv_z}{dr} = \gamma = \frac{g_p \cdot r_2}{2 \cdot \mu_p}\left[\left(\frac{\kappa_-^2}{\kappa} - \kappa\right) + \kappa_p \cdot \left(\frac{\kappa_-}{\kappa} - 1\right)\right]$$

$$(\kappa_1 \le \kappa \le \kappa_-) \qquad (2\text{-}18a)$$

$$\frac{dv_z}{dr} = \gamma = -\frac{g_p \cdot r_2}{2 \cdot \mu_p}\left[\left(\kappa - \frac{\kappa_+^2}{\kappa}\right) + \kappa_p \cdot \left(\frac{\kappa_+}{\kappa} - 1\right)\right]$$

$$(\kappa_+ \le \kappa \le 1) \qquad (2\text{-}18b)$$

Velocity profile

The velocity profile may be found by integrating Eqs.(2-18):

$$v_z = \frac{g_p \cdot r_2^2}{2 \cdot \mu_p} \{ [\kappa_-^2 \cdot \ell n(\frac{\kappa}{\kappa_1}) - \frac{\kappa^2 - \kappa_1^2}{2}] + \kappa_p \cdot [\kappa_- \cdot \ell n(\frac{\kappa}{\kappa_1}) - (\kappa - \kappa_1)] \}$$

$$(\kappa_1 \leq \kappa \leq \kappa_-) \qquad (2\text{-}19a)$$

$$v_z = \frac{g_p \cdot r_2^2}{2 \cdot \mu_p} \{ [\frac{1 - \kappa^2}{2} - \kappa_+^2 \cdot \ell n(\frac{1}{\kappa})] + \kappa_p \cdot [\kappa_+ \cdot \ell n(\frac{1}{\kappa}) - (1 - \kappa)] \}$$

$$(\kappa_+ \leq \kappa \leq 1) \qquad (2\text{-}19b)$$

Determining equations for plug boundaries

The dimensionless inner and outer radii of the plug ring may be determined by the fowllowing two equations:

1) The force balance equation developed previously, i.e. Eq.(2-14), in the dimensionless form:

$$\kappa_p = \kappa_+ - \kappa_- = \frac{2 \cdot \tau_y}{g_p \cdot r_2} \qquad (2\text{-}14')$$

2) Substituting $\kappa = \kappa_-$ into Eq.(2-19a) and $\kappa = \kappa_+$ into Eq.(2-19b), respectively, the two equations must give the same maximum velocity. So it may be obtained that:

$$\frac{1}{\kappa_p} [\frac{(1 - \kappa_1^2) - (\kappa_+^2 - \kappa_-^2)}{2} - \kappa_+^2 \cdot \ell n(\frac{1}{\kappa_+}) - \kappa_-^2 \cdot \ell n(\frac{\kappa_-}{\kappa_1})] +$$

$$+ [(\kappa_+ + \kappa_-) - (1 + \kappa_1) + \kappa_+ \cdot \ell n(\frac{1}{\kappa_+}) - \kappa_- \cdot \ell n(\frac{\kappa_-}{\kappa_1})] = 0 \qquad (2\text{-}20a)$$

However, it can be shown that, within an error of about ±0.2%,

Eq.(2-20a) may be replaced by the following explicit equation for $\kappa_1 \geq 0.3$ and $\kappa_p/(1-\kappa_1) \leq 0.5$:

$$\kappa_+ \simeq \left[\frac{1 - \kappa_1^2}{2 \cdot \ell n \left(\frac{1}{\kappa_1}\right)} \right]^{1/2} + \frac{\kappa_p}{2} \qquad (2\text{-}20b)$$

Now the unsheared plug boundaries κ_- and κ_+ can be calculated easily from Eqs.(2-14') and (2-20b).

Volumetric flowrate/pressure gradient

For the volumetric flowrate, Fredrickson and Bird[4] obtained that:

$$q = \frac{g_p \cdot r_2^4}{\mu_p} \pi_q \qquad (2\text{-}21)$$

where the dimensionless volumetric flowrate is expressed as:

$$\pi_q = \frac{\pi}{8} \left[(1 - \kappa_1^4) - 2 \kappa_+ \cdot (\kappa_+ - \kappa_p) \cdot (1 - \kappa_1^2) \right.$$

$$\left. - \frac{4}{3} \kappa_p \cdot (1 + \kappa_1^3) + \frac{1}{3} \kappa_p \cdot (2 \cdot \kappa_+ - \kappa_p)^3 \right] \qquad (2\text{-}22)$$

From Eq.(2-21), the pressure gradient may be calculated by:

$$g_p = \frac{q \cdot \mu_p}{\pi_q \cdot r_2^4} \qquad (2\text{-}23)$$

CHAPTER 3.

THEORETICAL STUDIES ON LAMINAR AXIAL FLOW OF NON-NEWTONIAN FLUIDS THROUGH ECCENTRIC ANNULI

In Chapter 2, we have discussed the laminar flow of non-Newtonian fluids through an annular space where the axes of the inner tube and the outer tube coincide with each other. Under many circumstances however, the realistic situation is that the axis of the inner tube offsets some distance from the axis of the outer tube and thus the annulus is "eccentric". During oilwell drilling operations, for example, the drillpipe is often positioned eccentrically in the casing or wellbore, especially in the inclined section of a directional well where the drillpipe has a strong tendency to offset towards the low-side of the wellbore.

In this chapter, we will investigate the laminar flow of non-Newtonian fluids through an eccentric annulus. Again, the solutions will be developed based on the power-law model and the Bingham plastic model which have been most commonly used to describe the rheological behaviour of two different kinds of non-Newtonian fluids, i.e. the fluids which exhibit a yield stress and the fluids which do not.

3.1. Previous studies

3.1.1. Fluids without a yield stress

The eccentric annular flow of fluids without a yield stress has been under investigation for many decades. Two alternative methods have been used in the previous studies. The first mehtod uses the bi-polar

coordinates to describe the eccentric annular geometry; the second one treats an eccentric annulus as a slot of variable height.

a. Bipolar coordinate method

The flow of Newtonian fluids through an eccentric annulus had been tackled for a long time as a methematical and hydrodynamic problem by mathematicians using the bipolar coordinate system[9,10]. In 1962, Redberger and Charles[11] reported their numerical evaluations of the velocity profile and the volumetric flowrate for the Newtonian eccentric annular flow and showed two significant results: 1) the fluid velocity is higher in the enlarged region than in the reduced region of an eccentric annulus; 2) the volumetric flowrate increases with increase of offset of the inner tube for a given pressure gradient. Mitsuishi and Aoyagi[12] extended the bipolar coordinate method to the eccentric annular flow of non-Newtonian fluids using the Sutterby model and similar conclusions as those obtained by Redberger and Charles were reached. They also conducted the experiments and reported that the calculated velocities and the volumetric flowrates were in good agreement with their experimental data. Guckes[13] presented a systematic procedure for calculating the volumetric flowrate by using the bipolar coordinate approach and developed a series of dimensionless curves for the laminar eccentric annular flow of power-law fluids.

There are also some other investigators[14,15] using the bipolar coordinate method to solve the eccentric annular flow problem.

Examining the above reported investigations it may be seen that, although the bipolar coordinate method may theoretically gives accurate solutions for eccentric annular flow, the procedures are extremely tedious, and laborious iterative computations are required. The

procedures of the bipolar coordinate method have been summarized in Appendix (A3-1).

b. Slot model method

Because of the complexity of the bipolar coordinate method, some investigators tryed to find an approximate method to solve the problems of eccentric annular flow. Tao and Donovan[16] probably first treated a fine clearance eccentric annulus as a slot with variable height. They used an approximate model to calculate the slot height and developed the analytical solutions of the velocity profile and the volumetric flowrate for Newtonian fluids. Later, Vaughn[17] extended this approach to the eccentric annular flow of power-law fluids. Iyoho and Azar[18] derived the exact model for calculating the slot height and developed the solution of the velocity profile for power-law fluids. They claimed that their model should be valid for all the cases where $\kappa_1 \geq 0.3$. Tosun[19] and Uner, et.al.[20] recently extended Iyoho and Azar's model to approximate the volumetric flowrate in eccentric annular flow of Newtonian and power-law fluids, respectively.

It should be pointed out that the slot model is in reality a modified model for flow between two parallel flat plates. The only difference is that the slot model treats the distance between the plates as a variable instead of a constant. As a result, the shear stress profile obtained from the slot model is linear and velocity profile is symmetric about the mid-point across the annular space. It is known, as shown in the preceding chapter, that the shear stress profile is not linear and the velocity profile is not symmetric about the midpoint in a concentric annulus, so there is no reason to assume that this situation would occur in an eccentric annulus. Although a concentric annulus

can be modelled accurately under some circumstances by a constant-height slot for volumetric flowrate/pressure gradient calculations[2b,21a], similar treatment may result in erroneous results for the problems pertaining to the shear stress and velocity profiles. For example, in a concentric annulus with the radii ratio of $\kappa_1 = 0.3$, the shear stress on the inner tube is about 54% higher in magnitude than that on the outer tube for Newtonian fluids, and 38% higher for power-law fluids with $n = 0.5$. Obviously the shear stress profile can not be treated as linear and the shear stresses on the inner and the outer tubes can not be treated as equal in magnitude.

A summary of derivation of the slot model for eccentric annular flow of power-law fluids is given in Appendix (A3-2).

3.1.2. Fluids with a yield stress

The only investigation, in the knowledge of the present author, into eccentric annular flow of fluids with a yield stress was reported in Guckes' paper[13] in which the procedures for calculating the volumetric flowrate for Bingham plastic fluids using the bipolar coordinate approach were presented. However, Guckes failed to impose the boundary condition for the central unsheared plug to the solutions and thus the effect of the central unsheared plug on volumetric flowrate was neglected. So Guckes' procedures are but complicated approximations. Guckes conducted experiments and the results showed a large discrepancy between the experimentally measured and the predicted volumetric flowrates. This was 'unexplainable', according to the author.

3.2. Proposed representation of eccentric annular geometry

In the present analysis of eccentric annular flow, an eccentric annulus is assumed to be replaced by an infinite number of concentric annuli with variable outer radii. Fig.(3-1) depicts an eccentric annulus with an eccentricity 'e'. The point O is the centre of the inner tube which is taken as the centre of the eccentric annulus. O' is the centre of the outer tube. 'θ' is a characteristic angle as defined in Fig.(3-1). If the cylindrical coordinate system is used and the z-coordinate is assumed to coincide with the axis of the inner tube, then 'θ' will be the angular coordinate of the coordinate system. The outer radius of the eccentric annulus is defined as 'r_2^e'. Applying the cosine rule to the triangle OAO' and simplifying, we find:

$$r_2^e = e\cdot\cos(\theta) + \{ r_2^2 - [e\cdot\sin(\theta)]^2 \}^{1/2} \qquad (3\text{-}1)$$

It is assumed that the eccentric annulus at position OA may be replaced by a concentric annulus with the inner radius 'r_1' and the outer radius 'r_2^e', instead of 'r_2'. With variation of 'θ', 'r_2^e' varies while 'r_1' remains constant. Then the whole eccentric annulus may be replaced by an infinite number of concentric annuli with variable outer radius 'r_2^e' defined by Eq.(3-1). When $e = 0$, $r_2^e = r_2$ and the present case reduces to that of a concentric annulus.

By using the above method, the equations developed for the concentric annular flow in the preceding chapter can be modified easily for the analysis of the eccentric annular flow. In the following sections, we will show how to use the present method to analyse the eccentric annular flow of power-law and Bingham plastic fluids, respectively.

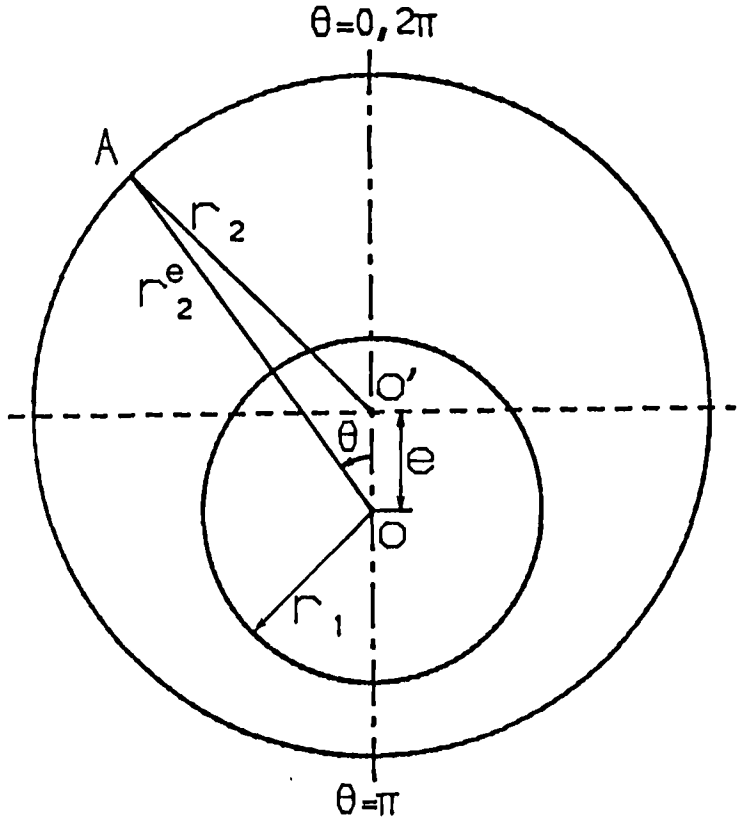

Fig.3-1 Nomenclature for an eccentric annulus

In the following analysis, the symbols used in the preceding chapter for the concentric annular flow will be modified by simply adding the superscript 'e' to represent the corresponding parameters for eccentric annular flow.

3.3. Eccentric annular flow of power-law fluids

For the present analysis of the eccentric annular flow of power-law fluids, the following dimensionless parameters are defined:

$$\lambda = \frac{r^e}{r_2^e} \qquad \lambda_1^e = \frac{r_1}{r_2^e} \qquad \lambda_o^e = \frac{r_o^e}{r_2^e} \qquad \lambda_2^e = \frac{r_2^e}{r_2}$$

To use the method described in the preceding section for the analysis of various profiles in eccentric annular flow of power-law fluids, the following procedures may be followed:

(i) calculate the equivalent outer radius, r_2^e, of the eccentric annulus at θ using Eq.(3-1);

(ii) calculate the local ratio of the radii, λ_1^e, according to its definition;

(iii) replacing λ_1 with λ_1^e in Eq.(2-10a) or Eq.(2-10b), the local zero shear stress point, λ_o^e, may be obtained:

$$\int_{\lambda_1^e}^{\lambda_o^e} \left[\frac{(\lambda_o^e)^2}{\lambda} - \lambda \right]^s d\lambda = \int_{\lambda_o^e}^{1} \left[\lambda - \frac{(\lambda_o^e)^2}{\lambda} \right]^s d\lambda \qquad (3\text{-}2a)$$

$$\lambda_o^e = \left[\frac{1 - (\lambda_1^e)^2}{2 \cdot \ln(\frac{1}{\lambda_1^e})} \right]^{1/2} \qquad (3\text{-}2b)$$

Similarly with Eqs.(2-10b) and (2-10a), Eq.(3-2b) may be used to

approximate Eq.(3-2a) for the cases where $n \geq 0.5$ and $\lambda_1^e \geq 0.3$.

(iv) replacing r_2 with r_2^e, λ_1 with λ_1^e and λ_0 with λ_0^e in Eq.(2-7) through Eqs.(2-9), the profiles of the shear stress, shear rate and the velocity may be obtained, respectively,

$$\tau_{zr}^e = \frac{g_p}{2} r_2^e \left[\lambda - \frac{(\lambda_o^e)^2}{\lambda} \right] \tag{3-3}$$

$$\gamma^e = \pm \left(\frac{g_p \cdot r_2^e}{2 \cdot K} \right)^s \left| \lambda - \frac{(\lambda_o^e)^2}{\lambda} \right|^s \tag{3-4}$$

where '+' is used for $\lambda < \lambda_o^e$ and '-' for $\lambda > \lambda_o^e$, and

$$v_z^e = \left(\frac{g_p \cdot r_2^e}{2 \cdot K} \right)^s \cdot r_2^e \int_{\lambda_1^e}^{\lambda} \left[\frac{(\lambda_o^e)^2}{\lambda} - \lambda \right]^s d\lambda$$

$$(\lambda_1^e \leq \lambda \leq \lambda_o^e) \tag{3-5a}$$

$$v_z^e = \left(\frac{g_p \cdot r_2^e}{2 \cdot K} \right)^s \cdot r_2^e \int_{\lambda}^{1} \left[\lambda - \frac{(\lambda_o^e)^2}{\lambda} \right]^s d\lambda$$

$$(\lambda_o^e \leq \lambda \leq 1) \tag{3-5b}$$

For the volumetric flowrate, based on Eq.(2-11a), the general formula may be expressed for the present eccentric annular flow as:

$$q = r_2^2 \int_0^{2\pi} \int_{\lambda_1^e}^{1} (\lambda_2^e)^2 \cdot v_z^e \cdot \lambda \, d\lambda \, d\theta \tag{3-6}$$

Based on Eq.(2-12) and considering the symmetry of the two halves of the eccentric annulus, the dimensionless volumetric flowrate may be obtained as:

$$\pi_q^e = \frac{n}{1+3\cdot n}\left(\frac{1}{2}\right)^s \int_0^{\pi} (\dot{\kappa}_2^e)^{3+s}\left\{\left[1-(\dot{\kappa}_o^e)^2\right]^{1+s} - (\dot{\kappa}_1^e)^{1-s}\left[(\dot{\kappa}_o^e)^2 - (\dot{\kappa}_1^e)^2\right]^{1+s}\right\} d\theta \qquad (3\text{-}7)$$

Then the volumetric flowrate and the pressure gradient expressions may be obtained as, respectively:

$$q = r_2^3\cdot\left(\frac{g_p\cdot r_2}{K}\right)^s\cdot\pi_q^e \qquad (3\text{-}8)$$

$$g_p = \left(\frac{q}{\pi_q^e\cdot r_2^3}\right)^n \frac{K}{r_2} \qquad (3\text{-}9)$$

3.4. Eccentric annular flow of Bingham plastic fluids

For the present analysis of the eccentric annular flow of Bingham plastic fluids, it is necessary to define the following dimensionless parameters:

$$\dot{\kappa} = \frac{r^e}{r_2^e} \qquad \dot{\kappa}_1^e = \frac{r_1}{r_2^e} \qquad \dot{\kappa}_-^e = \frac{r_-^e}{r_2^e} \qquad \dot{\kappa}_+^e = \frac{r_+^e}{r_2^e} \qquad \dot{\kappa}_2^e = \frac{r_2^e}{r_2}$$

and the dimentionless plug width at θ is defined as:

$$\dot{\kappa}_p^e = \dot{\kappa}_+^e - \dot{\kappa}_-^e = \frac{r_+^e - r_-^e}{r_2^e}$$

The following procedures may be followed for the analysis of the profiles of the shear stress, shear rate and the velocity in the eccentric annular flow of Bingham plastic fluids:

(i) calculate the equivalent outer radius, r_2^e, of the eccentric annulus at θ using Eq.(3-1);

(ii) calculate the local radii ratio, κ_1^e, according to its definition;

(iii) replacing r_2 with r_2^e in Eq.(2-14') and κ_1 with κ_1^e in Eq.(2-20a), the equations for the plug boundary radii at θ, i.e. κ_-^e and κ_+^e, can be obtained by solving the following simultaneous equations:

$$\kappa_p^e = \kappa_+^e - \kappa_-^e = \frac{2 \cdot \tau_y}{g_p \cdot r_2^e} \tag{3-10}$$

$$\frac{1}{\kappa_p^e} \{ \frac{[\,1 - (\kappa_1^e)^2\,] - [(\kappa_+^e)^2 - (\kappa_-^e)^2]}{2} - (\kappa_+^e)^2 \cdot \ln(\frac{1}{\kappa_+^e}) - (\kappa_-^e)^2 \cdot \ln(\frac{\kappa_-^e}{\kappa_1^e}) \} +$$

$$+ \{ (\kappa_+^e + \kappa_-^e) - (1 + \kappa_1^e) + \kappa_+^e \cdot \ln(\frac{1}{\kappa_+^e}) - \kappa_-^e \cdot \ln(\frac{\kappa_-^e}{\kappa_1^e}) \} = 0 \tag{3-11a}$$

Based on Eq.(2-20b), Eq.(3-11a) can be approximated by the following equation for the cases where $\kappa_1^e \geq 0.3$ and $\kappa_p^e/(1-\kappa_1^e) \leq 0.5$:

$$\kappa_+^e = [\, \frac{1 - (\kappa_1^e)^2}{2 \cdot \ln(\frac{1}{\kappa_1^e})} \,]^{1/2} + \frac{\kappa_p^e}{2} \tag{3-11b}$$

(iv) replacing κ_1 , κ_- , κ_+ and r_2 with κ_1^e , κ_-^e , κ_+^e and r_2^e , respectively, in Eqs.(2-17) through Eqs.(2-19), the profiles of the shear stress, shear rate and the velocity may be obtained as follows:

$$\tau_{zr}^e = -\frac{g_p \cdot r_2^e}{2} \{ [\, \frac{(\kappa_-^e)^2}{\kappa} - \kappa \,] + \frac{\kappa_-^e}{\kappa} \kappa_p^e \} \quad (\kappa_1^e \leq \kappa \leq \kappa_-^e) \tag{3-12a}$$

$$\tau_{zr}^{e} = -\frac{g_p \cdot r_2^e}{2}\left\{\left[\lambda - \frac{(\lambda_+^e)^2}{\lambda}\right] + \frac{\lambda_+^e}{\lambda}\lambda_p^e\right\} \quad (\lambda_+^e \leq \lambda \leq 1) \qquad (3\text{-}12b)$$

$$\gamma^e = \frac{g_p \cdot r_2^e}{2 \cdot \mu_p}\left\{\left[\frac{(\lambda_-^e)^2}{\lambda} - \lambda\right] + \lambda_p^e \cdot \left[\frac{\lambda_-^e}{\lambda} - 1\right]\right\}$$

$$(\lambda_1^e \leq \lambda \leq \lambda_-^e) \qquad (3\text{-}13a)$$

$$\gamma^e = -\frac{g_p \cdot r_2^e}{2 \cdot \mu_p}\left\{\left[\lambda - \frac{(\lambda_+^e)^2}{\lambda}\right] + \lambda_p^e \cdot \left[\frac{\lambda_+^e}{\lambda} - 1\right]\right\}$$

$$(\lambda_+^e \leq \lambda \leq 1) \qquad (3\text{-}13b)$$

$$v_z^e = \frac{g_p \cdot r_2^e}{2 \cdot \mu_p}\left\{\left[(\lambda_-^e)^2 \cdot \ln\left(\frac{\lambda}{\lambda_1^e}\right) - \frac{\lambda^2 - (\lambda_1^e)^2}{2}\right] + \right.$$

$$\left. + \lambda_p^e\left[\lambda_-^e \ln\left(\frac{\lambda}{\lambda_1^e}\right) - (\lambda - \lambda_1^e)\right]\right\} \qquad (\lambda_1^e \leq \lambda \leq \lambda_-^e) \qquad (3\text{-}14a)$$

$$v_z^e = \frac{g_p \cdot r_2^e}{2 \cdot \mu_p}\left\{\left[\frac{1 - \lambda^2}{2} - (\lambda_+^e)^2 \cdot \ln\left(\frac{1}{\lambda}\right)\right] + \lambda_p^e \cdot \left[\lambda_+^e \ln\left(\frac{1}{\lambda}\right) - (1 - \lambda)\right]\right\}$$

$$(\lambda_+^e \leq \lambda \leq 1) \qquad (3\text{-}14b)$$

For the dimensionless volumetric flowrate, based on Eq.(2-22) and considering that λ_1^e , λ_+^e and λ_p^e are functions of θ in the eccentric annular flow, it may be obtained that:

$$\pi_q^e = \frac{1}{8}\int_0^{\pi} (\lambda_2^e)^4 \cdot \left\{\left[1 - (\lambda_1^e)^4\right] - 2 \cdot (\lambda_+^e) \cdot \left[\lambda_+^e - \lambda_p^e\right] \cdot \left[1 - (\lambda_1^e)^2\right]\right.$$

$$\left. - \frac{4}{3}(\lambda_p^e) \cdot \left[1 + (\lambda_1^e)^3\right] + \frac{1}{3}\lambda_p^e \cdot \left[2 \cdot \lambda_+^e - \lambda_p^e\right]^3\right\} d\theta \qquad (3\text{-}15)$$

Then the volumatric flowrate and the pressure gradient can be calculated by:

$$q = \frac{g_p \cdot r_2^4}{\mu_p} \pi_q^e \qquad (3\text{-}16)$$

$$g_p = \frac{q \cdot \mu_p}{r_2^4 \cdot \pi_q^e} \qquad (2\text{-}17)$$

In addition, a special feature of the eccentric annular flow of Bingham plastic fluids should be mentioned. Unlike the case in a concentric annulus, a Bingham plastic fluid may not start to flow over an entire eccentric annulus at the same time, i.e. the fluid may be flowing in one area but stagnant in the other, depending on the imposed pressure gradient and the eccentricity. Theoretically, if the pressure gradient is gradually increased from zero, at some point the flow will start first in the area of $\theta = 0$ where the flowing area has the maximum dimension, then the flow will spread gradually towards the other areas with smaller dimensions. Based on Eq.(3-10), if the width of the unsheared plug ring, $\bar{\kappa}_p^e$ equals or exceeds the value of $(1 - \bar{\kappa}_1^e)$ at 'θ', the fluid will be stagnant in the areas with the characteristic angles greater than θ. Because r_2^e equals $r_2 + e$ at the maximum dimension position, i.e. at $\theta = 0$, the minimum pressure gradient required to start the flow may be obtained as:

$$(g_p)_{min}\Big|_{\theta=0} = \frac{2 \cdot \tau_y}{r_2 + e - r_1} \qquad (3\text{-}18a)$$

Similarly, the minimum pressure gradient required to start the flow over the entire eccentric annulus is:

$$(g_p)_{min}\Big|_{\theta=\pi} = \frac{2\cdot\tau_y}{r_2 - e - r_1} \qquad (3\text{-}18b)$$

3.5. Analysis and discussions

By using the method described above, the shear stress, shear rate and velocity profiles corresponding to different values of 'θ' in the eccentric annular flow of power-law and Bingham plastic fluids have been calculated and shown in Fig.(3-2) through Fig.(3-7).

Shown in Fig.(3-2) and Fig.(3-3) are the shear stress profiles and it may be seen that the profiles are not straight lines and therefore the magnitudes of the shear stress are not symmetric about the zero shear stress points. Because a smaller angle θ corresponds to a larger $r_2{}^e$, the shear stress is higher in magnitude in the enlarged area than in the reduced area of the eccentric annulus. The similar conclusions may also be drawn for the shear rate and velocity profiles which are shown from Fig.(3-4) to Fig.(3-7). Particular attention should be drawn to the velocity profiles of the Bingham plastic fluid shown in Fig.(3-7) where it may be seen that the unsheared plug is relatively wider in the reduced area than in the enlarged area of the eccentric annulus. Therefore the situation may happen that the unsheared plug may cover the entire space across the annulus in the reduced area and thus the fluid becomes stagnant in this region while at the same time the fluid is still flowing in the enlarged area of the annulus, as mentioned in the preceding section.

The present solution of the volumetric flowrate for power-law fluids have been numerically compared to those by using the bipolar coordinate method and by using the slot model method. The procedures of using the slot model method is quite straight forward and has been shown in Appendix (A3-2). The procedures of using the bipolar coordinate

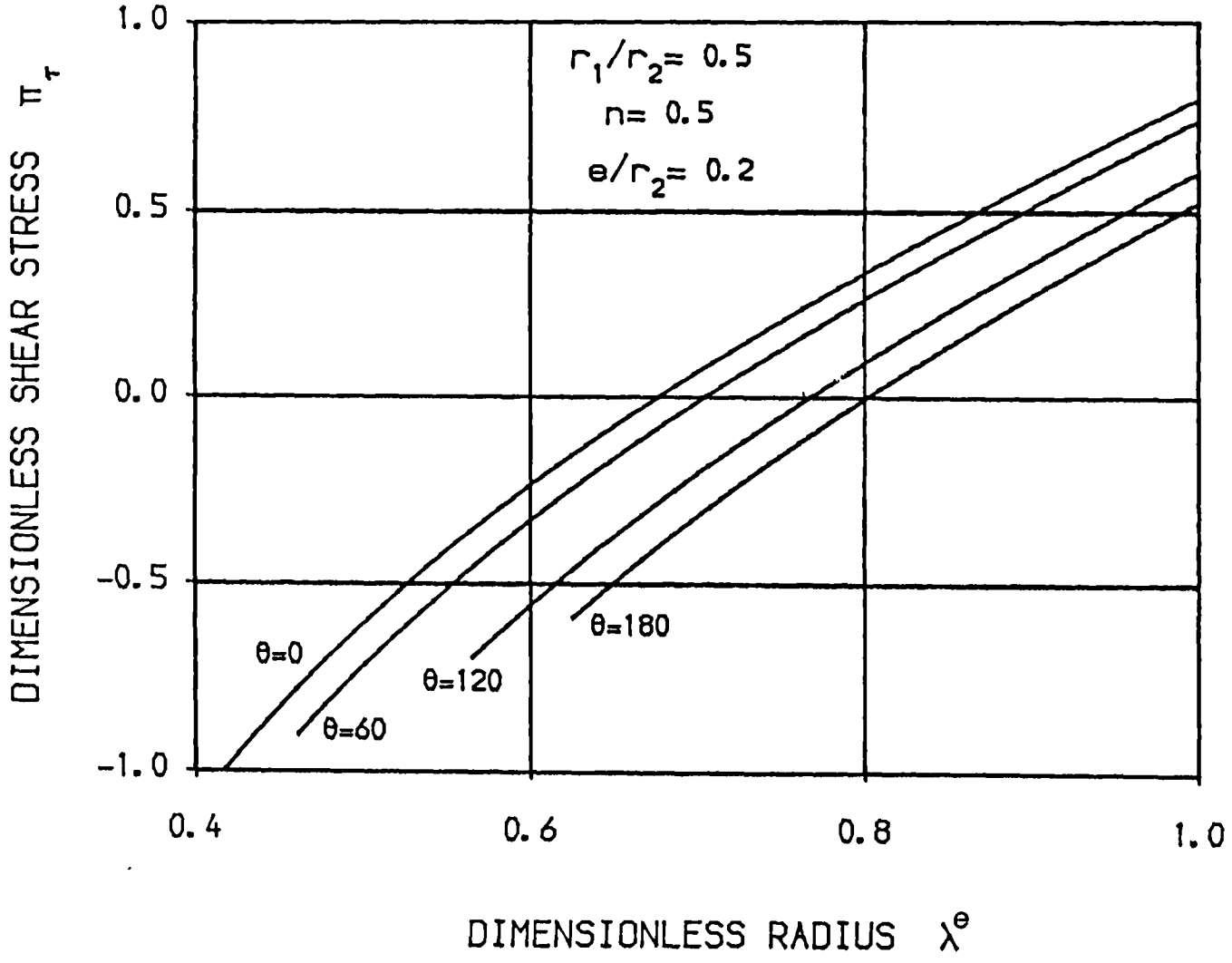

Fig.3-2 Shear stress profiles in eccentric annular flow of power-law fluids

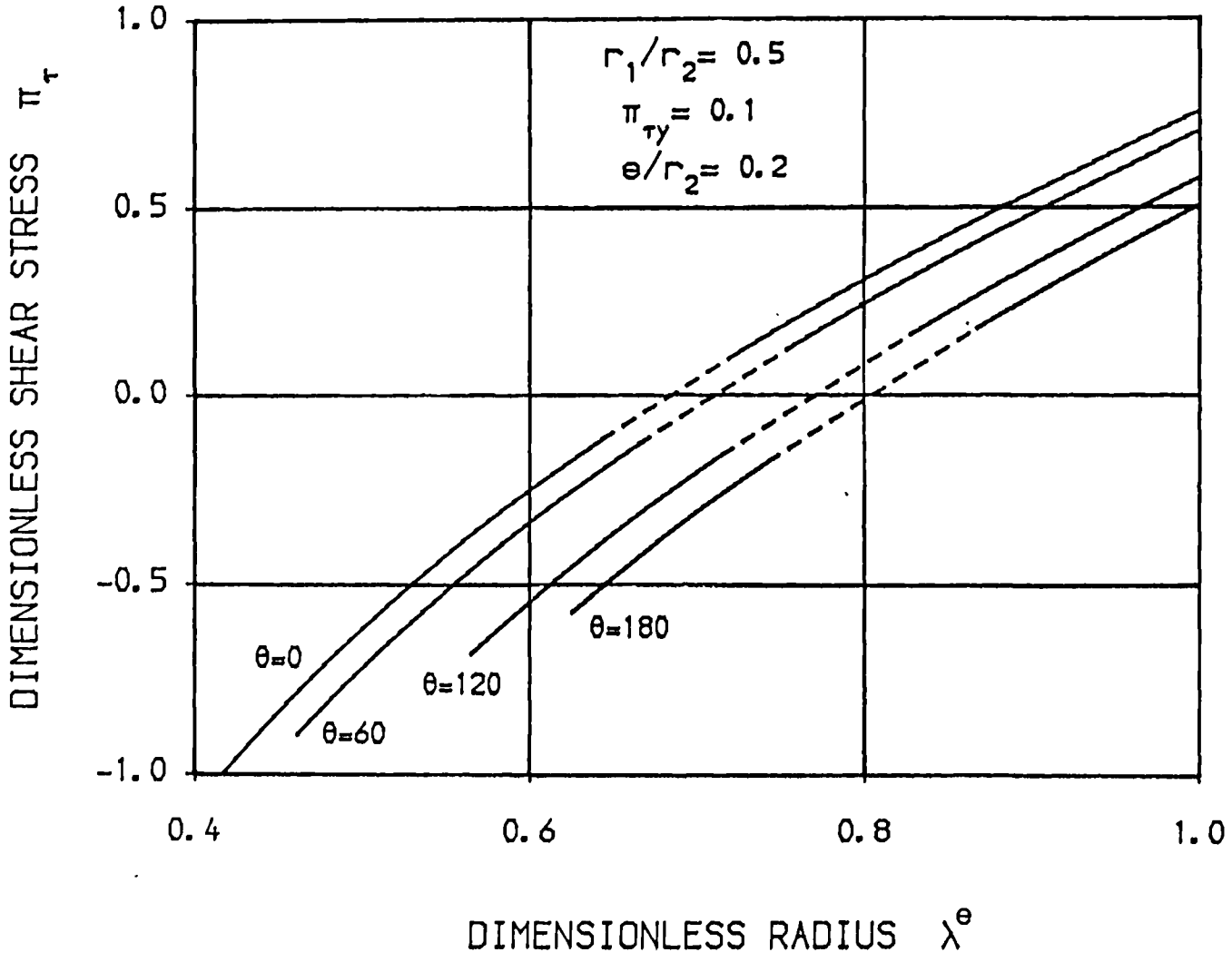

Fig.3-3 Shear stress profiles in eccentric annular flow of Bingham plastic fluids

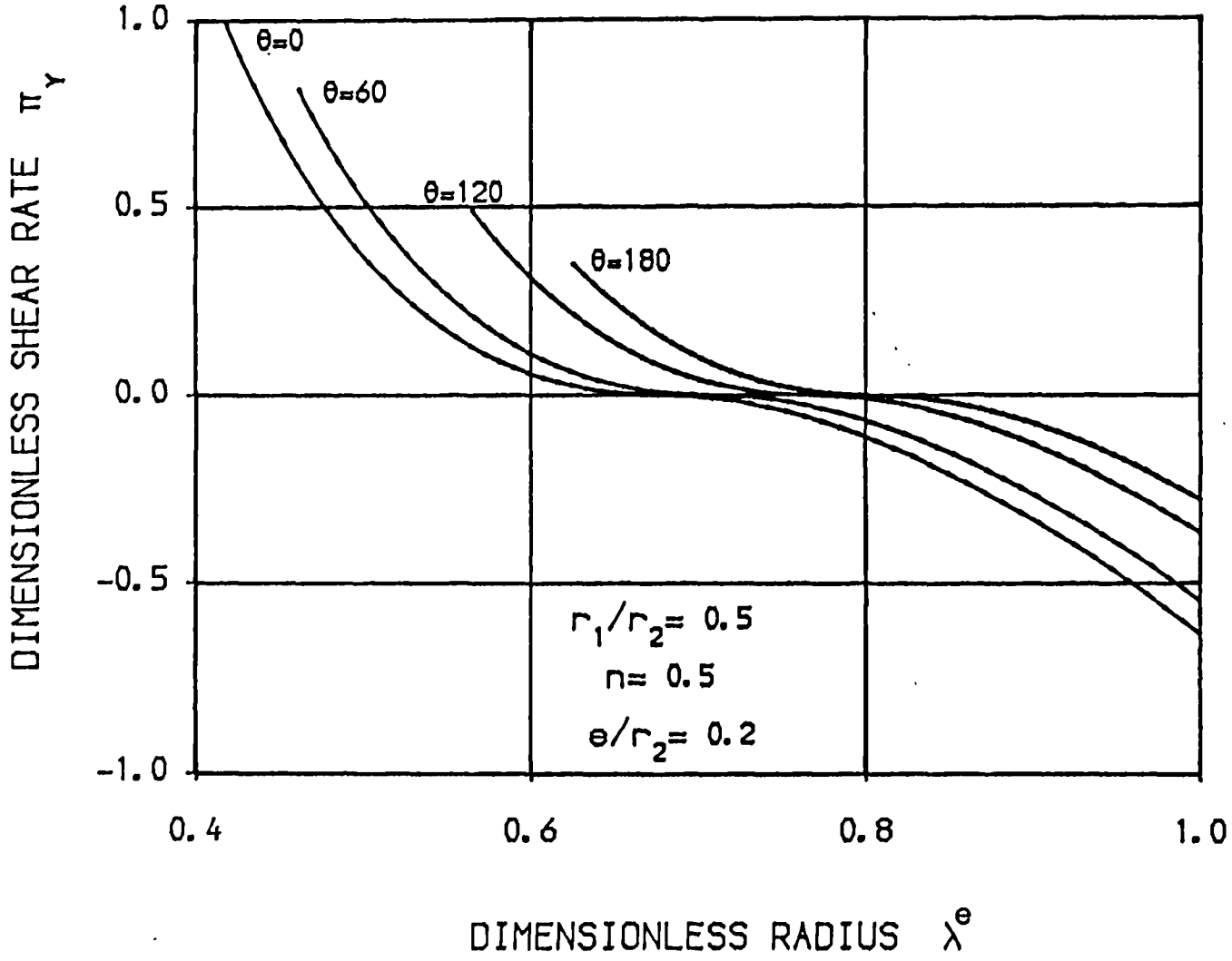

Fig.3-4 Shear rate profiles in eccentric annular flow of power-law fluids

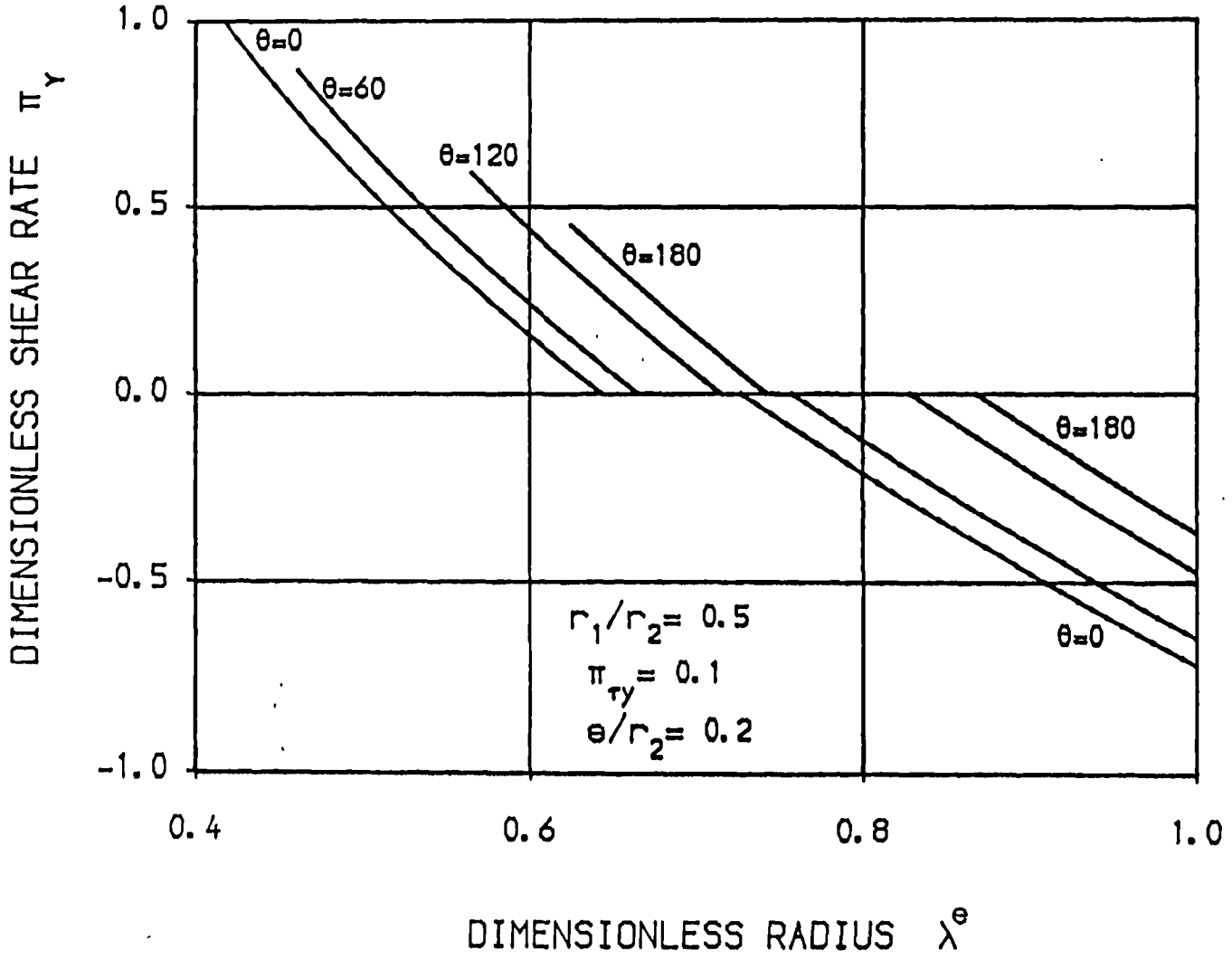

Fig.3-5 Shear rate profiles in eccentric annular flow of Bingham plastic fluids

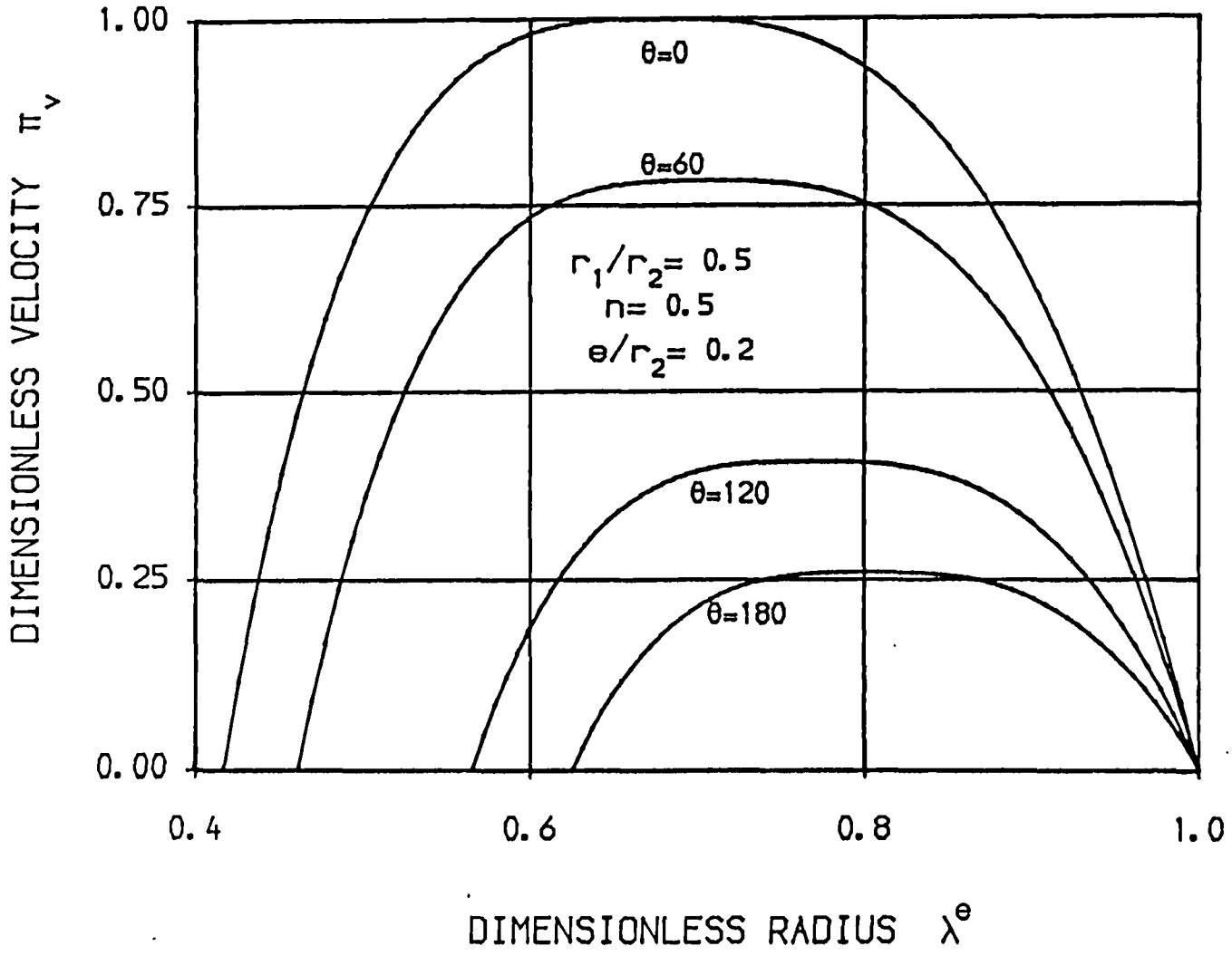

Fig.3-6 Velocity profiles in eccentric annular flow of power-law fluids

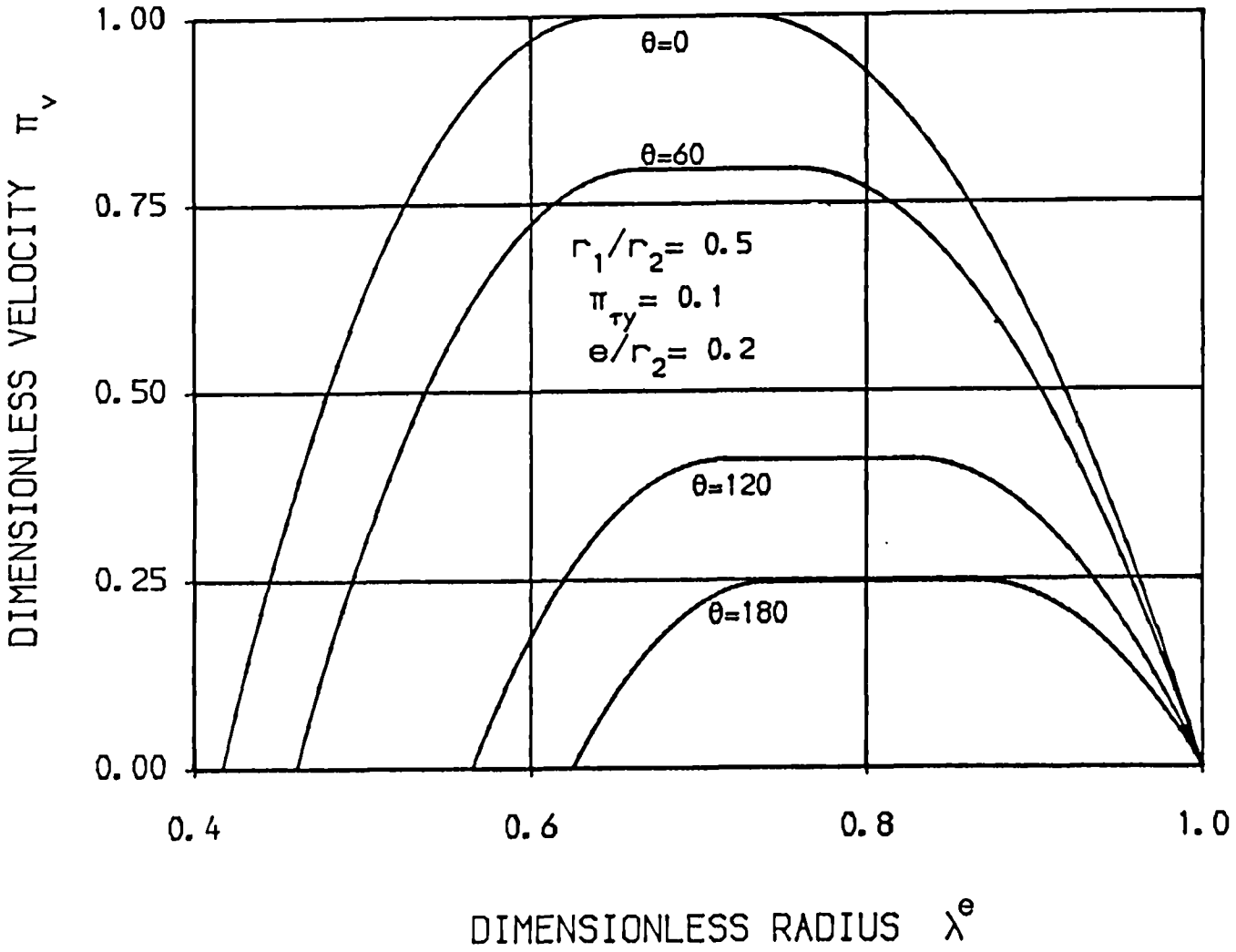

Fig.3-7 Velocity profiles in eccentric annular flow of Bingham plastic fluids

method has also been summarized in Appendix (A3-1). Because the apparent viscosity μ_a in Eq.(A3-10) is a function of velocity gradient itself, solving the differential equation of Eq.(A3-10) becomes extremely tedious and requires laborious computations. In the present analysis, the finite difference form of Eq.(A3-10) in Appendix (A3-1) is derived and a computer programme is developed on the MicroVAX system. The succesive-over-relaxation (SOR) method is applied in the programme to solve the resulting matrix by using 50 row times 50 column grid on the rectangular region corresponding to the eccentric annulus. To cope with the velocity-dependent viscosity problem, an iterative solution scheme is used in the computer programme.

The numerical comparison shows that the proposed method gives good approximations of the volumetric flowrate for the cases where the eccentricity is not high. As the eccentricity increases, the error increases. The slot model method also gives good approximations for the cases where the eccentricity is not high and the ratio of κ_1 is not too small. As the eccentricity increases or the ratio of κ_1 decreases, the error increases. Comparison between the present and the slot model method shows that for the low eccentricity cases, the present method gives better approximations while for the middle and higher eccentricity cases, the slot model method gives better approximations. The volumetric flowrates predicted by using different methods for the cases of $\kappa_1 = 0.7$ and $n = 1.0$ and 0.6, respectively, are shown in Fig.(3-8) and Fig.(3-9) in which the horizontal coordinate is the fractional eccentricity which is defined as:

$$E_f = \frac{e}{r_2 - r_1} \qquad (3\text{-}19)$$

As the values of the ratio κ_1 and the flow behaviour index 'n'

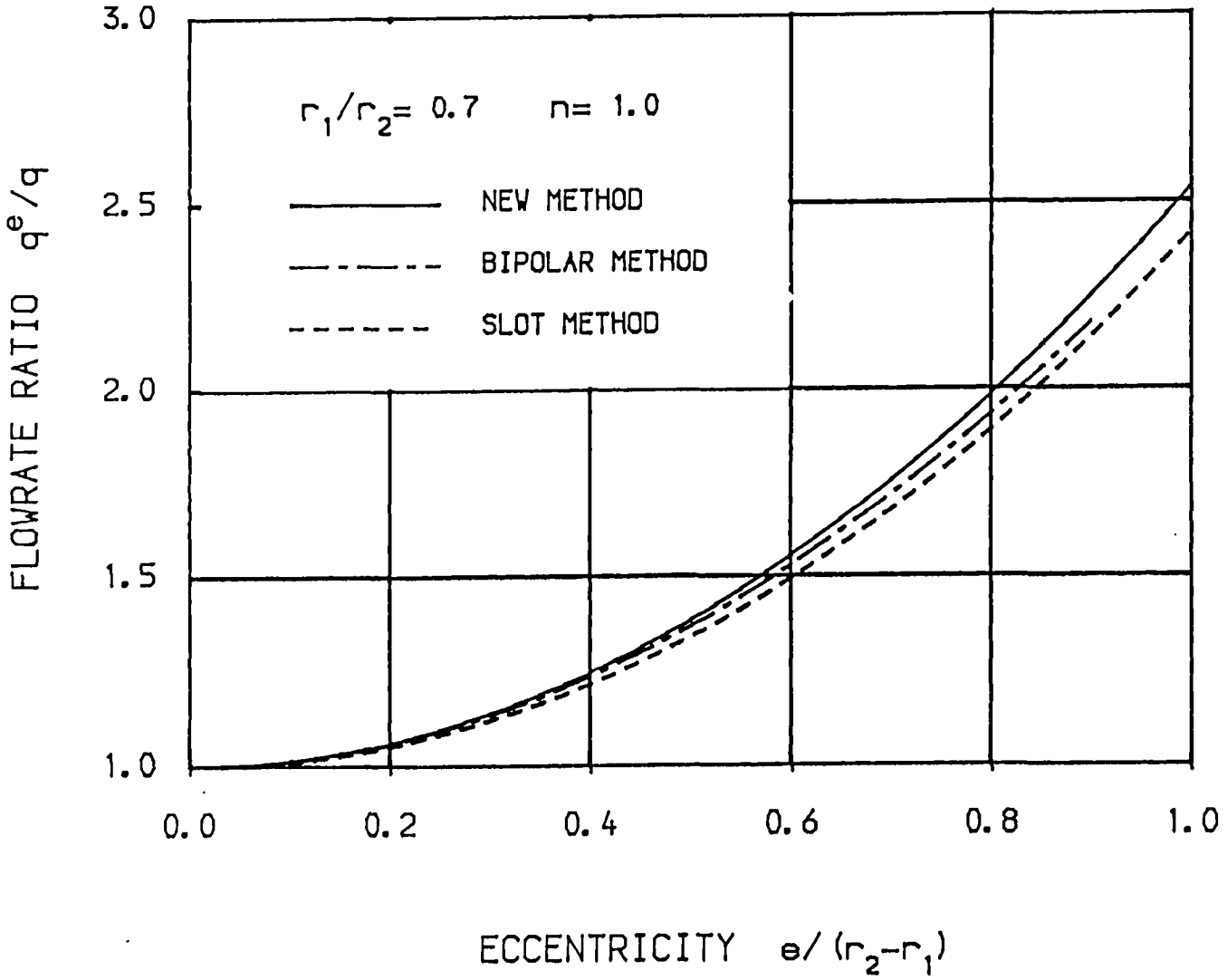

Fig.3-8 Comparison of volumetric flowrates by using diffenrent methods in eccentric annular flow of Newtonian fluids

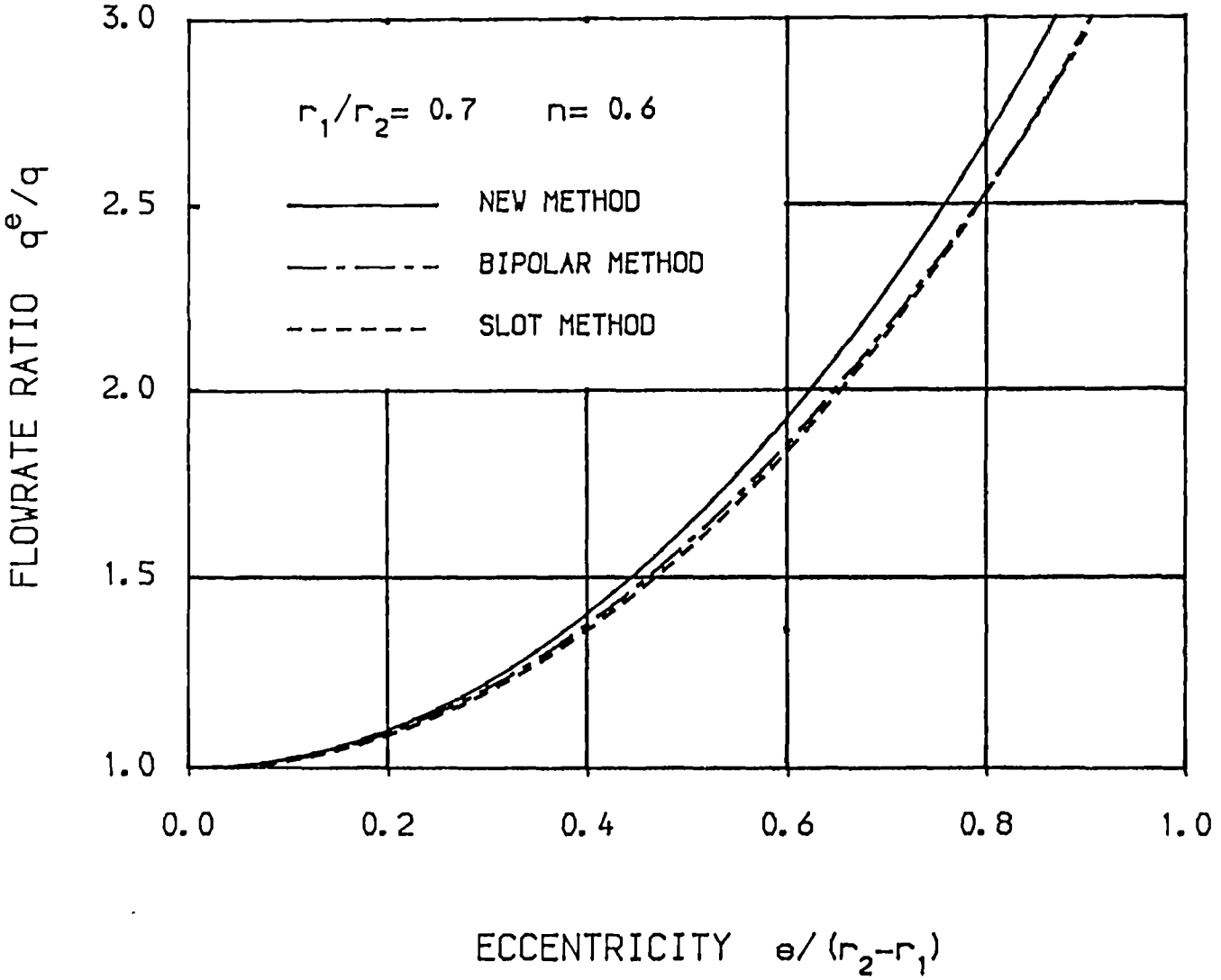

Fig.3-9 Comparison of volumetric flowrates by using different methods in eccentric annular flow of power-law fluids

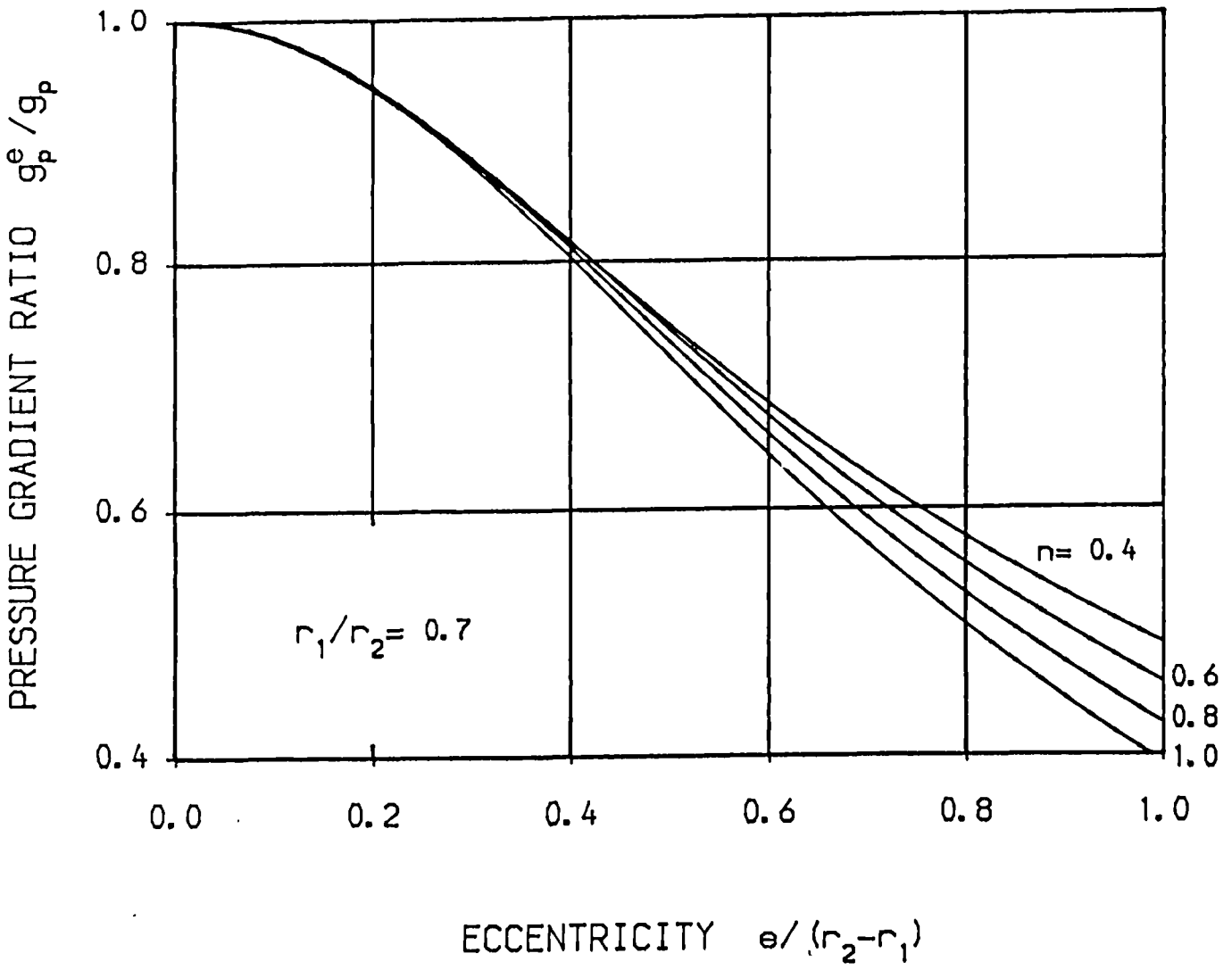

Fig.3-10 Reduction of pressure gradient with increasing eccentricity in eccentric annular flow of power-law fluids

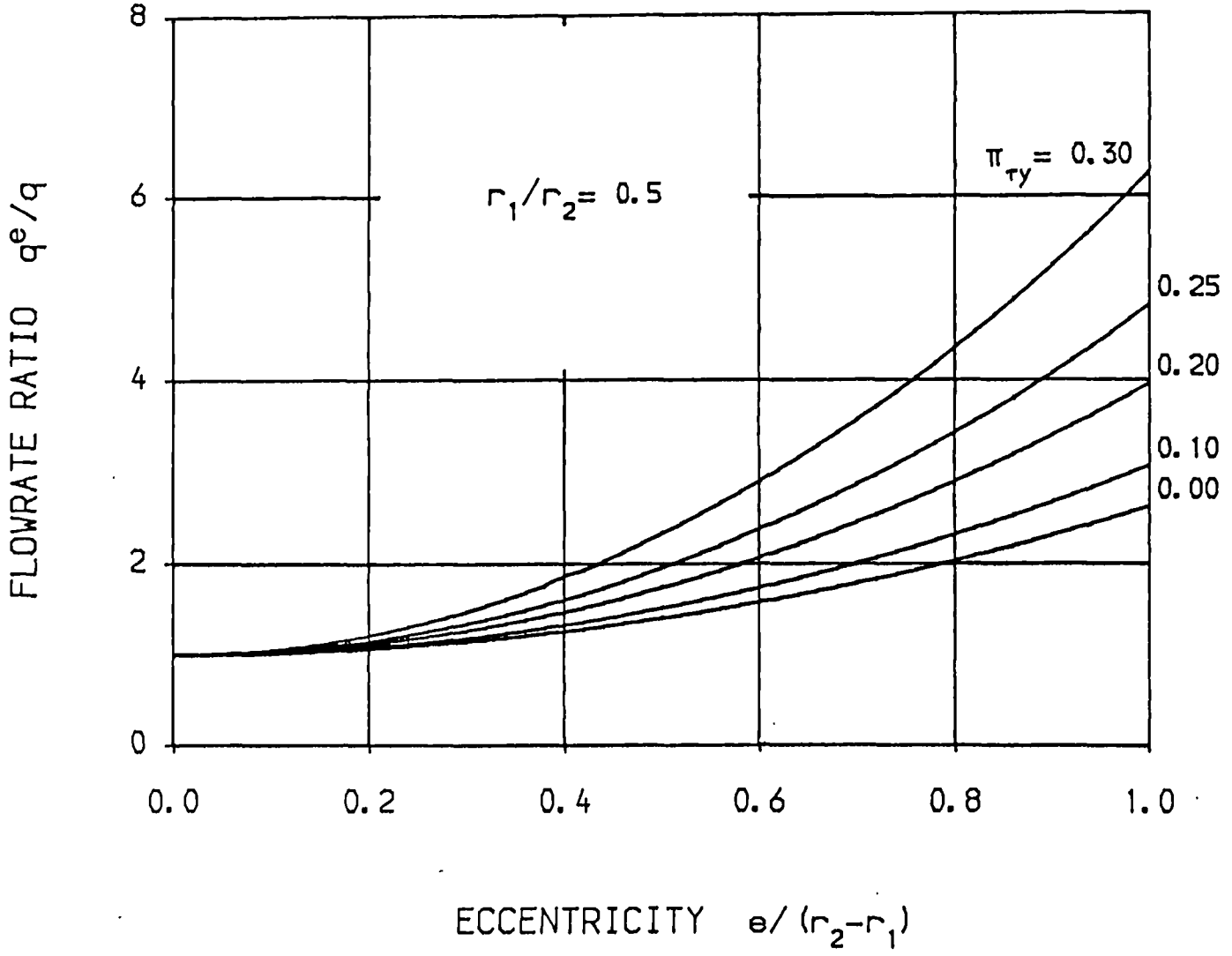

Fig.3-11 Increasing of volumetric flowrates with increasing eccentricity in eccentric annular flow of Bingham plastic fluids

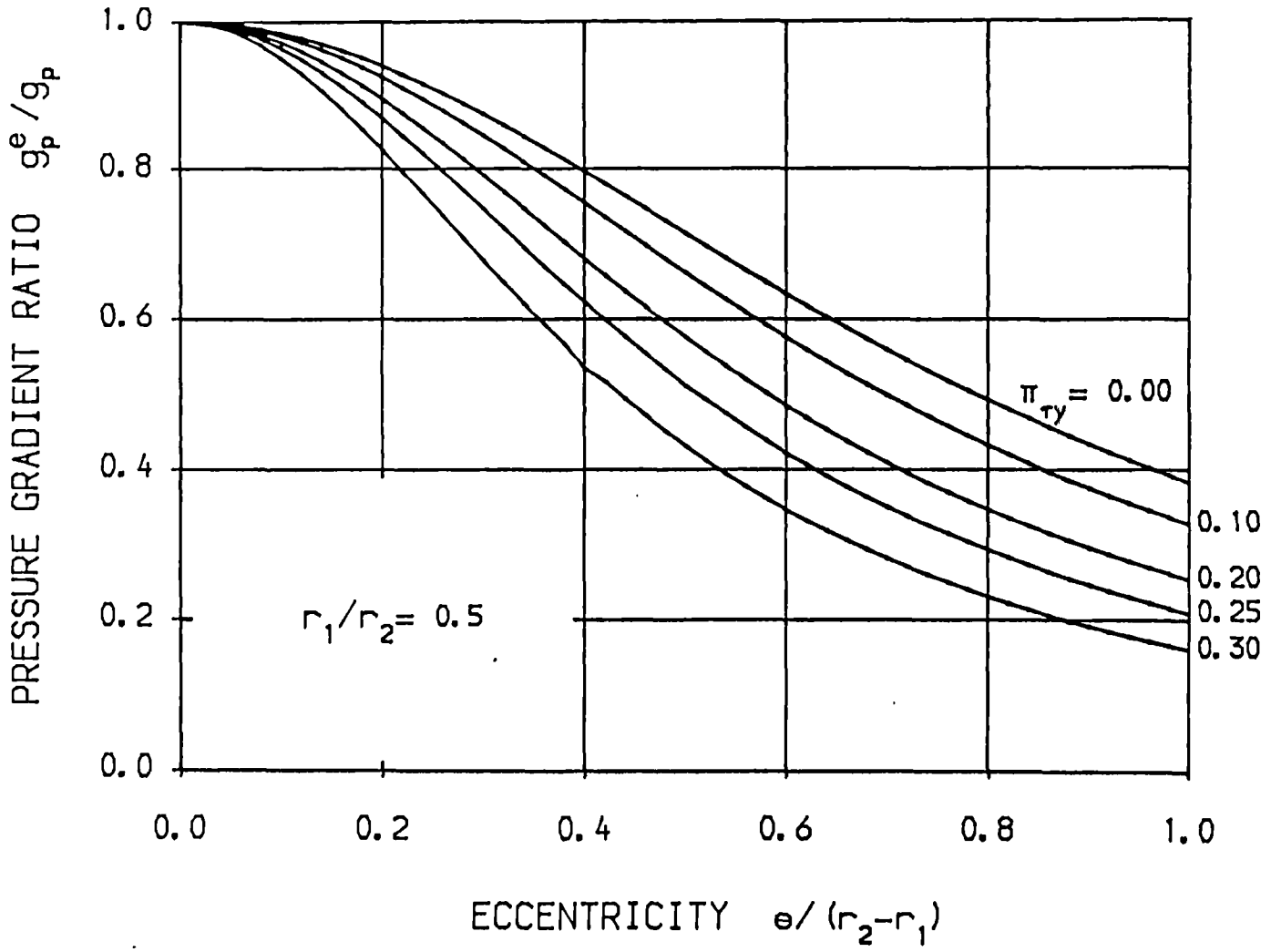

Fig.3-12 Reduction of pressure gradient with increasing eccentricity in eccentric annular flow of Bingham plastic fluids

increase, the results by using both the proposed and the slot model methods become closer to those by using the bipolar coordinate method. The pressure gradients obtained by using the present method for power-law fluids are shown in Fig.(3-10).

As mentioned in Section 3.1.1, the slot model gives unrealistic profiles of the shear stress, shear rate and the velocity. In some cases however, it may provide good approximations of the average magnitudes of the shear stresses on the inner and outer walls of the annulus. This is why the slot model may approximate the volumetric flowrate/pressure gradient well in some cases of both the concentric [2b,21] and the eccentric annular flow.

Although in Guckes' paper[13], the procedures for Bingham plastic fluids were also presented, he did not impose the boundary condition for the central unsheared plug to Eq.(A3-10) and thus the results given by Guckes are at most approximations. Therefore, no effort is made in the present analysis to compare the present solutions of the volumetric flowrate/pressure gradient with those using the bipolar method for Bingham plastic fluids. Figs.(3-11) and (3-12) show the volumetric flowrate and the pressure gradient, respectively, for the eccentric annular flow of Bingham plastic fluids by using the proposed method.

3.6. Conclusions

Based on the above analysis, several conclusions may be drawn on the laminar eccentric annular flow of non-Newtonian fluids:

(i) the magnitudes of the shear stress, shear rate and velocity are higher in the enlarged region than in the reduced region of the eccentric annulus;

(ii) increasing the eccentricity will increase the volumetric flowrate if the pressure gradient is held constant, or will decrease the pressure gradient if the volumetric flowrate is held constant.

About the present new method for analysis of the eccentric annular flow, it may be concluded that:

(i) a new method has been introduced for the analysis of the eccentric annular flow, in which an eccentric annulus is treated as an infinite number of concentric annuli with variable outer radii. The advantages of the present method are that it is simple and may provide more accurate results;

(ii) using the present method, the analytical solutions of the shear stress, shear rate, velocity and the volumetric flowrate/pressure gradient have been obtained for both power-law and Bingham plastic fluids;

(iii) the volumetric flowrates predicted by using the present method for power-law fluids have been numerically compared with those using the previously published methods and the results show that the present method may provide good approximations for the cases where the fractional eccentricity is below about 40%.

CHAPTER 4.

THEORETICAL STUDIES ON LAMINAR HELICAL FLOW OF POWER-LAW FLUIDS THROUGH CONCENTRIC ANNULI

In Chapter 2, we have discussed laminar axial flow of non-Newtonian fluids through a concentric annulus where both the inner and the outer tubes are stationary and thus the flow is purely axial. If one of or both the tubes are rotated, however, a tangential component of the fluid velocity, or say, rotating flow, will be imposed upon the annular flow, in addition to the axial velocity component. In this situation, each fluid particle will follow a spiral or a helical path about the axis of the tubes with an angular velocity ω and an axial velocity v_z. This is the so called 'annular helical flow' or simply 'helical flow'. A perfect practical example of the helical flow is the flow of drilling fluids through the drilling annulus when the drillpipe is rotated.

For a Newtonian fluid, its viscosity is a constant and thus not shear-dependent. So the axial and the tangential components of a helical flow are independent of each other. Therefore they can be dealt with separately and the solutions for the helical flow can be obtained by a simple superposition of the two flow components. These separate treatments may be seen in many standard textbooks of fluid mechanics[8b,1b].

For non-Newtonian fluids, i.e. the fluids with a shear-dependent viscosity function, the axial and the tangential components will be interdependent and the resulting helical flow will not be a simple superposition of the axial flow and the tangential flow. Therefore the tangential and the axial components of the flow must be dealt with simultaneously in this situation. This chapter presents a theoretical

analysis of laminar helical flow of power-law non-Newtonian fluids through a concentric annulus.

4.1. Previous studies

Numerous studies have been reported on the modelling of laminar helical flow of non-Newtonian fluids. Rivlin's study[23] contained a treatment of helical flow for incompressible fluids and he developed two simultaneous, first-order, non-linear differential equations for determining the angular and the axial velocity components. Coleman and Noll[24] solved the problem for general fluids by making no special constitutive assumptions other than fluid incompressibility and showed that it is necessary to know only one material function which relates shear stress and shear rate in simple shear flow in order to calculate the volumetric flowrate. Fredrickson[25] presented equations for the helical flow of viscoelastic fluids which contains an arbitrary apparent viscosity function.

Following the above treatments, a number of other studies have also been reported. Savins and Wallick[26] showed how the axial volumetric flowrate and angular velocity become interdependent in helical flow of Oldroyd-type fluids. With a single set of data obtained from their experiment, Dierckes and Schowalter[27] claimed that excellent agreement had been obtained between the experimentally measured and the theoretically calculated volumetric flowrate for polyisobutylene (PIB) solution based on the power-law model. Later their result was further confirmed by Rea and Schowalter[28] who experimentally measured both velocity profiles and volumetric flowrates and obtained substantial agreement between the predicted and the experimental data.

Walker and Al-Rawi[29] presented a paper in 1970 in which an

iterative solution method was proposed for calculating the pressure gradient in non-Newtonian helical flow based on the equations developed by Fredrickson[25]. Walker and Al-Rawi's work, in the knowledge of the present author, is the only study reported so far in terms of the pressure gradient calculation in annular helical flow of non-Newtonian fluids.

There are some other studies which have been reported on the annular helical flow of non-Newtonian fluids[30,31].

In the present analysis, analytical dimensionless equations for the apparent viscosity, shear stress, velocities and the axial volumetric flowrate in the laminar annular helical flow of power-law fluids will be developed for the first time. Based on these equations, a comprehensive analysis will be performed to study the characteristics of annular helical flow of power-law fluids. In addition, an analytical solution for the pressure gradient will also be derived and by using the proposed solution, the pressure gradient can be obtained directly and no iterative solution is necessary.

For convenience of derivation in the following analysis, the dimensional equations will be developed first, then the dimensionless parameters will be defined and finally the dimensionless equations will be derived.

4.2. Derivation of the governing equations

In order to simulate the situation in oilwell drilling annuli, it is assumed throughout the following analysis that the inner tube is rotated at an angular velocity ω_1 while the outer tube is held stationary and the fluid flows under the action of a constant pressure gradient in the axial direction. For other cases, e.g. where the inner tube is held

stationary while the outer tube is rotated or both the tubes are rotated with different speeds, solutions can be obtained easily based on the present analysis by modifying the corresponding boundary conditions. Therefore, the present analysis does not lose its generality for the helical flow because of the assumption that the inner tube is rotated while the outer tube in held stationary. Fig.(4-1) illustrates the helical flow system.

In Section 2.2.1 of Chapter 2, we discussed several characteristics of laminar axial flow of fluids through a concentric annulus. It was found that the only non-zero velocity component, the axial velocity 'v_z', is a function of 'r' only. Based on this characteristic, the governing equation for the flow was derived from the equations of motion.

It can be shown that the characteristics identified for the concentric annular axial flow will also exist in the present case of the annular helical flow through a concentric annulus except that the tangential component of the fluid velocity is not zero. Considering that a concentric annulus is axisymmetric and its cross-section is uniform in z-direction, it can be easily deduced that the tangential component of the fluid velocity 'v_θ' is independent of 'θ' and 'z' and thus it is also a function of r only. Thus the two velocity components in the considered helical flow may be expressed as:

$$v_z = v_z(r) \qquad (4\text{-}1a)$$

$$v_\theta = v_\theta(r) \qquad (4\text{-}1b)$$

Therefore, based on Eq.(1-6) through Eq.(1-8), the non-zero components of the stress tensor are the shear stress τ_{zr} and $\tau_{\theta r}$ which are also functions of r only, i.e.

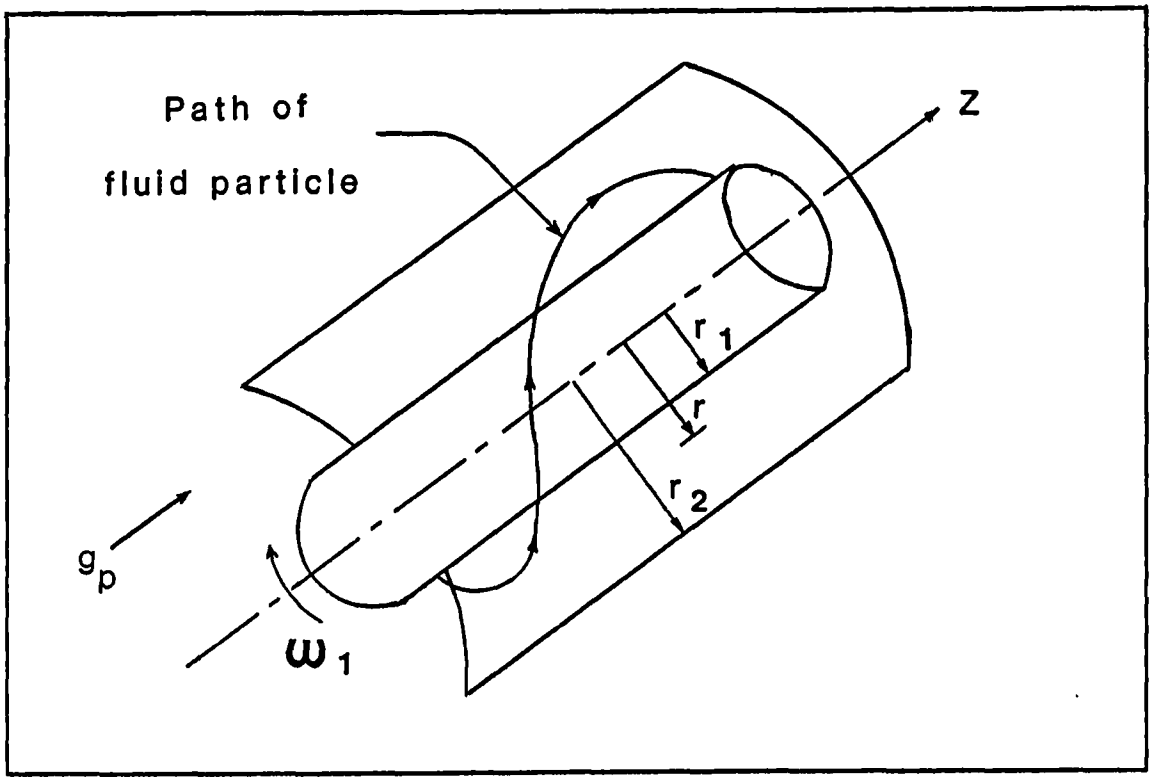

Fig.4-1 Illustration of a helical flow system

$$\tau_{zr} = \tau_{zr}(r) \qquad (4\text{-}2a)$$

$$\tau_{\theta r} = \tau_{\theta r}(r) \qquad (4\text{-}2b)$$

Then, the equations of motion, i.e. Eqs.(2-2), may be simplified for the present case to the following three equations:

$$-\rho \frac{v_\theta^2}{r} = \rho \cdot g_r - \frac{\partial P_f}{\partial r} \qquad (4\text{-}3a)$$

$$\frac{\partial}{\partial r}(r^2 \cdot \tau_{\theta r}) = 0 \qquad (4\text{-}3b)$$

$$g_p - \frac{1}{r}\frac{\partial}{\partial r}(r \cdot \tau_{zr}) = 0 \qquad (4\text{-}3c)$$

where g_p is defined by Eq.(2-6) in Chapter 2. Eq.(4-3a) states that the centrifugal force developed by the rotational motion of the fluid is balanced by the pressure force and the gravitational force. This equation determines the radial pressure distribution. However, since it contributes nothing to the fluid motion, it can be dropped out in the present analysis. Integrating Eqs.(4-3b) and (4-3c) yields:

$$\tau_{\theta r} = \frac{\beta}{r^2} \qquad (4\text{-}4a)$$

$$\frac{g_p}{2} r^2 - r \cdot \tau_{zr} = C \qquad (4\text{-}4b)$$

where β and C are constants of integration. The above equations are the governing equations for annular helical flow through concentric annuli. Like Eq.(2-5) for annular axial flow, Eqs.(4-4) are developed without any assumption regarding the rheological behaviour of the fluid, so it is valid for both Newtonian and non-Newtonian fluids.

4.3. Derivation of the dimensional equations

Shear stress profiles

In Eq.(4-4a) we have obtained the expression for shear stress $\tau_{\theta r}$. The shear stress τ_{zr} may be found by applying the boundary condition to Eq.(4-4b) that $\tau_{zr} = 0$ at $r = r_o$:

$$\tau_{\theta r} = \frac{\beta}{r^2} \tag{4-5a}$$

$$\tau_{zr} = \frac{g_p}{2} \left(r - \frac{r_o^2}{r} \right) \tag{4-5b}$$

Apparent viscosity profile

According to Eq.(1-6) through (1-8) and Eqs.(4-1), the shear stress $\tau_{\theta r}$ and τ_{zr} may be expressed in terms of velocity gradients as:

$$\tau_{\theta r} = - \mu_a \left(r \frac{\partial \omega}{\partial r} \right) \tag{4-6a}$$

$$\tau_{zr} = - \mu_a \frac{\partial v_z}{\partial r} \tag{4-6b}$$

where the angular velocity ω may be also expressed as:

$$\omega = \frac{v_\theta}{r} \tag{4-7}$$

For the present annular helical flow, based on Eq.(1-12), the scalar product of the rate of deformation tensor may be simplified as:

$$\frac{1}{2}(\Delta:\Delta) = \left(r\frac{\partial \omega}{\partial r} \right)^2 + \left(\frac{\partial v_z}{\partial r} \right)^2 \qquad (4\text{-}8)$$

Then, according to Eq.(1-9), the apparent viscosity for the annular helical flow of power-law fluids becomes:

$$\mu_a = K \left[\left(r\frac{\partial \omega}{\partial r} \right)^2 + \left(\frac{\partial v_z}{\partial r} \right)^2 \right]^{\frac{n-1}{2}} \qquad (4\text{-}9)$$

Combining the above equation with Eqs.(4-5) and (4-6), the expression of the apparent viscosity profile for the annular helical flow of power-law fluids may be obtained as:

$$\mu_a = K^s \left[\frac{\beta^2}{r^4} + \frac{g_p^2}{4} \left(r - \frac{r_o^2}{r} \right)^2 \right]^{\frac{n-1}{2n}} \qquad (4\text{-}10)$$

where $s = 1/n$.

Velocity profiles

The profile of the angular velocity may be obtained by combining Eq.(4-5a) with (4-6a):

$$-\mu_a \cdot r\frac{\partial \omega}{\partial r} = \frac{\beta}{r^2}$$

Integrating the above equation and applying the boundary condition that $\omega = \omega_1$ at $r = r_1$, we find:

$$\omega = \omega_1 - \beta \cdot \int_{r_1}^{r} \frac{dr}{\mu_a \cdot r^3} \qquad (4\text{-}11a)$$

The expression for the axial velocity may be found by combining

Eq.(4-5b) with Eq.(4-6b):

$$-\mu_a \frac{\partial v_z}{\partial r} = \frac{g_p}{2}\left(r - \frac{r_o^2}{r}\right)$$

Integrating the above equation and applying the boundary condition that $v_z = 0$ at $r = r_1$, we have:

$$v_z = \frac{g_p}{2}\int_{r_1}^{r} \frac{1}{\mu_a}\left(\frac{r_o^2}{r} - r\right) dr \qquad (4\text{-}11b)$$

Determining equations for β and r_o

Because the outer tube is held stationary, the constant β can be determined by applying the boundary condition to Eq.(4-11a) that $\omega = 0$ at $r = r_2$, whereupon, we have:

$$\beta = \frac{\omega_1}{\int_{r_1}^{r_2} \frac{dr}{\mu_a \cdot r^3}} \qquad (4\text{-}12a)$$

Similarly, the constant r_o is determined by applying the boundary condition to Eq.(4-11b) that $v_z = 0$ at $r = r_2$, then:

$$r_o = \left(\frac{\int_{r_1}^{r_2} \frac{r}{\mu_a} dr}{\int_{r_1}^{r_2} \frac{dr}{\mu_a \cdot r}}\right)^{1/2} \qquad (4\text{-}12b)$$

It should be reminded that Eq.(4-12a) and Eq.(4-12b) are not the explicit expressions for β and r_o, respectively, because both the terms 'β' and 'r_o' are contained in the term 'μ_a' of the Eqs.(4-12). Therefore, Eqs.(4-12) together with Eq.(4-10) must be solved

simultaneously in order to obtain the constants β and r_o.

Volumetric flowrates

The general formula for the axial volumetric flowrate may be expressed as:

$$q = 2\pi \int_{r_1}^{r_2} r \cdot v_z \cdot dr \qquad (4\text{-}13a)$$

Integrating the above equation by parts and noting that $v_z = 0$ at $r = r_1$ and $r = r_2$, we may find that:

$$q = -2\pi \int_{r_1}^{r_2} \frac{r^2}{2} \frac{\partial v_z}{\partial r} dr \qquad (4\text{-}13b)$$

Substituting the derivative of Eq.(4-11b) into the above equation, it may be obtained that:

$$q = \frac{\pi \cdot g_p}{2} \int_{r_1}^{r_2} \frac{r \cdot (r^2 - r_o^2)}{\mu_a} dr \qquad (4\text{-}13c)$$

4.4. Derivation of the dimensionless equations

In Section 2.3 of Chapter 2, the following three dimensionless variables have been defined:

$$\lambda = \frac{r}{r_2} \qquad \lambda_1 = \frac{r_1}{r_2} \qquad \lambda_o = \frac{r_o}{r_2}$$

For the present case of annular helical flow, some additional dimensionless parameters are required. Examining Eqs.(4-4) through

Eqs.(4-13), we may find that the following dimensionless parameters may be defined:

$$\sigma = \frac{\beta}{g_p \cdot r_2^{\,3}} \qquad \pi_{\omega_1} = \frac{\omega_1}{\left(\frac{g_p \cdot r_2}{K}\right)^s}$$

The physical significance of the above dimensionless parameters can be identified as follows:

(i) from Eq.(4-4a) it may be found that $\beta/r_2^{\,2}$ represents the shear stress on the outer tube. The term $g_p \cdot r_2$ represents the axial pressure stress. So according to its defination above, σ may be considered as a ratio of the tangential shear stress on the outer tube to an equivalent axial pressure stress;

(ii) because the term:

$$\left(\frac{g_p \cdot r_2}{K}\right)^s$$

has the dimensions of shear rate, it may be taken as an equivalent axial shear rate while ω_1 is the tangential shear rate on the inner tube. So the dimensionless parameter $\pi_{\omega 1}$ may be considered as the ratio of the tangential shear rate on the inner tube to an equivalent axial shear rate. Hereafter we call $\pi_{\omega 1}$ the dimensionless angular velocity of the inner tube.

By using the above dimensionless parameters, the dimensionless equations for the laminar helical flow of power-law fluids may be derived from the corresponding dimensional equations developed in the preceding section.

From Eq.(4-10), the dimensionless apparent viscosity may be found:

$$\pi_\mu = \frac{\mu_a \cdot \left(\frac{g_p \cdot r_2}{K} \right)^s}{g_p \cdot r_2} = \left[\frac{\sigma^2}{\lambda^4} + \frac{(\lambda^2 - \lambda_o^2)^2}{4 \cdot \lambda^2} \right]^{\frac{n-1}{2n}} \qquad (4\text{-}14)$$

Corresponding to β and r_o, the determining equations for the dimensionless constants σ and λ_o may be found, respectively, as:

$$\sigma = \frac{\pi_{\omega 1}}{\int_{\lambda_1}^{1} \frac{d\lambda}{\pi_\mu \cdot \lambda^3}} \qquad (4\text{-}15a)$$

$$\lambda_o = \left(\frac{\int_{\lambda_1}^{1} \frac{\lambda}{\pi_\mu} d\lambda}{\int_{\lambda_1}^{1} \frac{d\lambda}{\pi_\mu \cdot \lambda}} \right)^{1/2} \qquad (4\text{-}15b)$$

Because the term π_μ in Eqs.(15) contain both σ and λ_o, the dimensionless constants σ and λ_o must be determined by combining Eq.(4-14) and solving Eq.(4-15a) and Eq.(4-15b) simultaneously.

The dimensionless tangential and axial shear stresses may be obtained from Eqs.(4-5), respectively, as:

$$\pi_{\tau\theta} = \frac{\tau_{\theta r}}{g_p \cdot r_2} = \frac{\sigma}{\lambda^2} \qquad (4\text{-}16a)$$

$$\pi_{\tau z} = \frac{\tau_{zr}}{g_p \cdot r_2} = \frac{1}{2} \left(\lambda - \frac{\lambda_o^2}{\lambda} \right) \qquad (4\text{-}16b)$$

The dimensionless angular velocity and the axial velocity can be found from Eq.(4-11a) and Eq.(4-11b), respectively,

$$\pi_\omega = \frac{\omega_1}{\left(\frac{g_p \cdot r_2}{K}\right)^s} = \pi_{\omega_1} - \sigma \int_{\lambda_1}^{\lambda} \frac{d\lambda}{\pi_\mu \cdot \lambda^3} \qquad (4\text{-}17a)$$

$$\pi_v = \frac{v_z}{r_2 \left(\frac{g_p \cdot r_2}{K}\right)^s} = \frac{1}{2} \int_{\lambda_1}^{\lambda} \frac{\lambda_o^2 - \lambda^2}{\pi_\mu \cdot \lambda} d\lambda \qquad (4\text{-}17b)$$

Finally, the dimensionless volumetric flowrate may be derived from Eq.(4-13c) as:

$$\pi_q = \frac{q}{\pi \cdot r_2^3 \left(\frac{g_p \cdot r_2}{K}\right)^s} = \frac{1}{2} \int_{\lambda_1}^{1} \frac{\lambda (\lambda^2 - \lambda_o^2)}{\pi_\mu} d\lambda \qquad (4\text{-}18)$$

and the volumetric flowrate may be then calculated by:

$$q = \pi \cdot r_2^3 \left(\frac{g_p \cdot r_2}{K}\right)^s \pi_q \qquad (4\text{-}19)$$

4.5. Analysis of the three independent dimensionless variables

By examining Eqs.(4-14) through (4-18), it may be found that there are three independent dimensionless variables in the helical flow system:

(i) the ratio of the inner and the outer radii, 'λ_1', which defines the relative scale of the annular helical flow;

(ii) the flow behaviour index of the power-law fluid, 'n', which defines the non-Newtonian degree of the fluid rheological behaviour;

(iii) the dimensionless group 'π_{ω_1}', which defines the magnitude of the inner tube rotary speed relative to the equivalent axial shear

rate.

Once the above dimensionless variables are known, the helical flow system will be defined in general terms.

To solve Eqs.(4-14) through (4-19), the constant σ and λ_o must be determined simultaneously first by trial-and-error numerical integrations of Eqs.(4-15a) and (4-15b) combining with Eq.(4-14). Once σ and λ_o are known, other dimensionless equations can be solved directly by performing the corresponding numerical integrations, respectively.

4.5.1. Influence of $\pi_{\omega 1}$ on various profiles

The dimensionless angular velocity of the inner cylinder, $\pi_{\omega 1}$, is an important parameter of a helical flow system because $\pi_{\omega 1}$ determines its characteristics. Generally speaking, an annular helical flow is composed of two simple flows: the axial flow and the tangential flow. When $\pi_{\omega 1} = 0$, i.e. $\omega_1 = 0$, only the axial velocity exists and the flow is purely axial which has been discussed in Chapter 2. When $\pi_{\omega 1} \neq 0$, both the axial and tangential flow exist and they combine together to develop the annular helical flow. The higher the value of $\pi_{\omega 1}$, the stronger the tangential flow relative to the axial flow. Therefore, $\pi_{\omega 1}$ may be taken as a measure of the tangential flow relative to the axial flow.

Fig.(4-2) to Fig.(4-4) illustrate the influence of $\pi_{\omega 1}$ on various profiles. Fig.(4-2) shows the apparent viscosity profiles and in this figure, significant influences of $\pi_{\omega 1}$ on the profiles may be noticed. First, as the value of $\pi_{\omega 1}$ increases, the apparent viscosity decreases, more rapidly in the central region than near the boundaries, and thus the apparent viscosity becomes more and more uniform across the annular

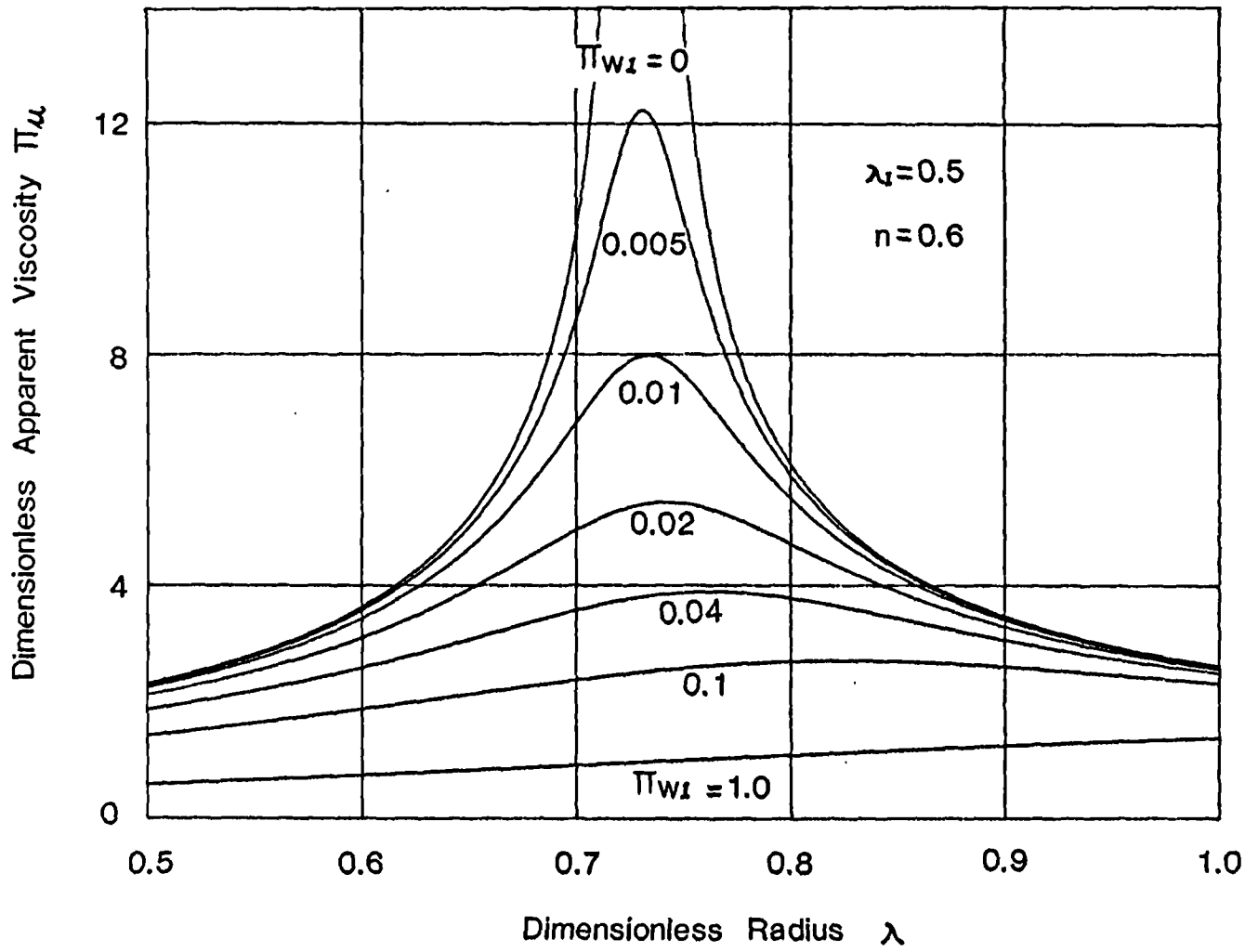

Fig.4-2 Influence of Π_{wI} on viscosity profile

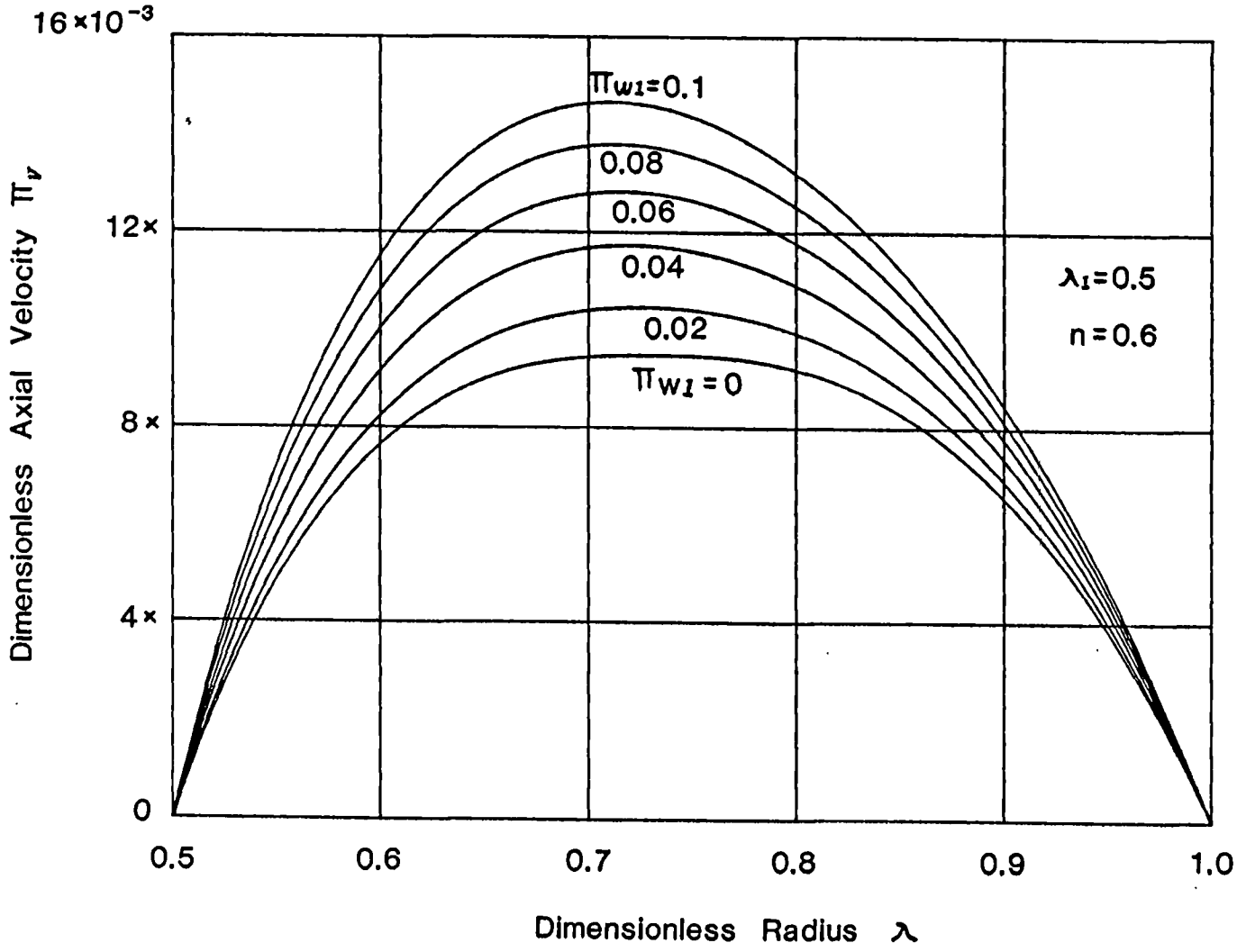

Fig.4-3 Influence of π_{w1} on axial velocity profile

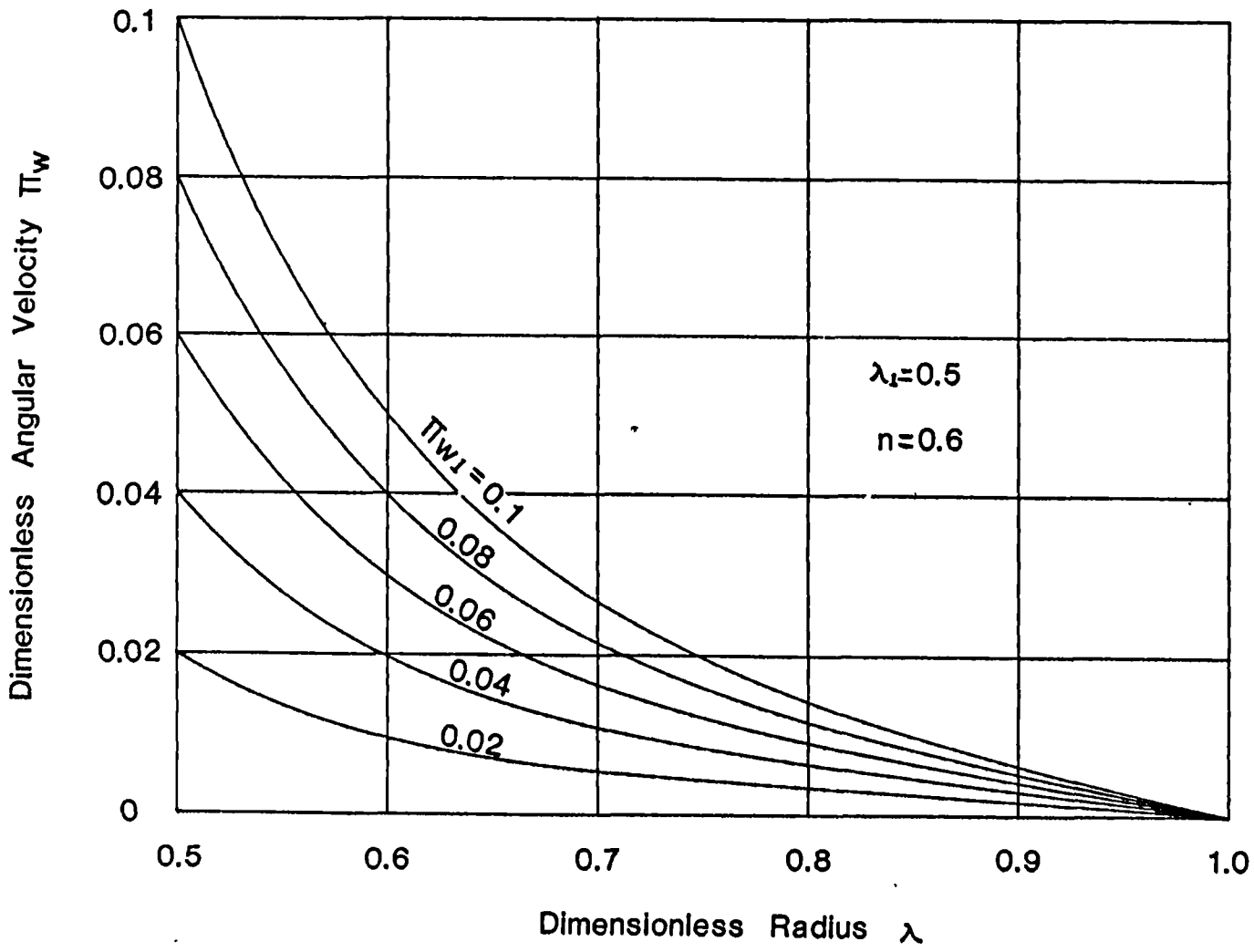

Fig.4-4 Influence of Π_{w1} on angular velocity profile

space. Particularly when $\pi_{\omega 1}$ reaches a value of about 1 for the case in Fig.(4-2), the apparent viscosity profile becomes nearly a straight line and in this situation, the apparent viscosity may be actually approximated by retaining only the first term and dropping out the second one in the brackets of Eq.(4-14). Physically this implies that the tangential flow becomes relatively strong so that the effect of the axial flow may be neglected. Another important feature is the position of the maximum apparent viscosity. When $\pi_{\omega 1} = 0$ for the case of purely annular axial flow, the radial distance of the maximum viscosity, which is infinite, coincides with the zero axial shear stress point λ_o. As $\pi_{\omega 1}$ increases from zero, the position of the maximum viscosity moves outwards while λ_o moves inwards (which may be seen in Fig.(4-3)) and when $\pi_{\omega 1}$ reaches a certain value, the maximum viscosity begin to occur on the wall of the outer tube. This is because that, as $\pi_{\omega 1}$ increases, the resultant shear rate, which is the vector sum of the tangential and the axial shear rates, becomes more and more dominated by the tangential shear rate alone.

The axial velocity profiles corresponding to different values of $\pi_{\omega 1}$ are shown in Fig.(4-3) and it is evident that the axial velocity and the angular velocity become interdependent in helical flow of power-law fluids. As $\pi_{\omega 1}$ increases, the axial velocity also increases. This should be expected because in the preceding analysis of the apparent viscosity profiles we have seen that the apparent viscosity over the entire annular space is decreased by increasing $\pi_{\omega 1}$. So the flow resistance is lower and thus the axial velocity is higher at a higher value of $\pi_{\omega 1}$. Fig.(4-4) shows the angular velocity profiles corresponding to different values of $\pi_{\omega 1}$. Of course the angular velocity increases over the entire annular space with increase of $\pi_{\omega 1}$.

4.5.2. Influence of 'n' on various profiles

It is well known that the flow behaviour index, n, is a measure of the deviation in rheological behaviour of power-law fluids from that of Newtonian fluids. For the helical flow system of power-law fluids, when n = 1, i.e. the fluids are Newtonian, the two component flows, i.e. the axial and tangential flows, are independent of each other and the resultant helical flow is only a superposition of the two component flows. When $n \neq 1$, however, the axial and tangential flow become interdependent, which has been shown in the preceding analysis. In this case the helical flow is not simply a superposition of the two simple flows. Generally, for the helical flow of power-law fluids, 'n' may be used as a measure of the interdependence between the axial flow and tangential flow.

Figs.(4-5) to (4-7) show the influences of n on various profiles. It can be seen from Fig.(4-5) that the apparent viscosity profiles are significantly different for different values of n. With increasing values of n, the shear-dependent characteristic becomes less and less pronounced and the apparent viscosity profile becomes more and more flat. When n = 1 for the case of Newtonian fluids, the apparent viscosity becomes uniform across the annulus.

Fig.(4-6) shows the axial velocity profiles for different values of n. As in the case of annular axial flow, the effect of decreasing the value of n is to flatten the axial velocity profiles. Fig.(4-7) shows the angular velocity profiles. As shown in the figure, the dimensionless angular velocity decreases with the decrease of n in all the regions other than on the boundaries. The degree of interdependence of the axial and tangential flows for different values of n will be shown in the following analysis of the axial volumetric flowrate.

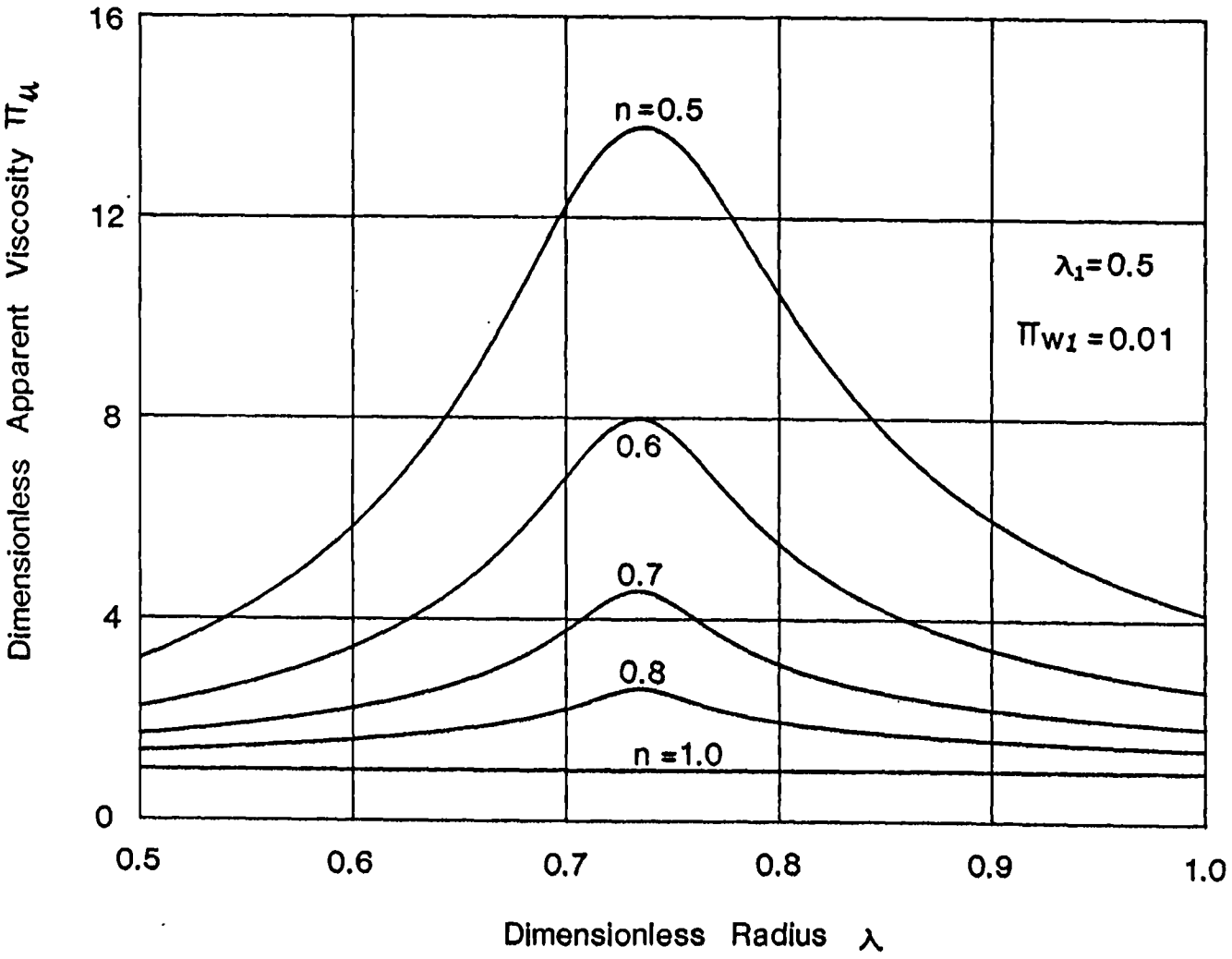

Fig.4-5 Influence of 'n' on apparent viscosity profile

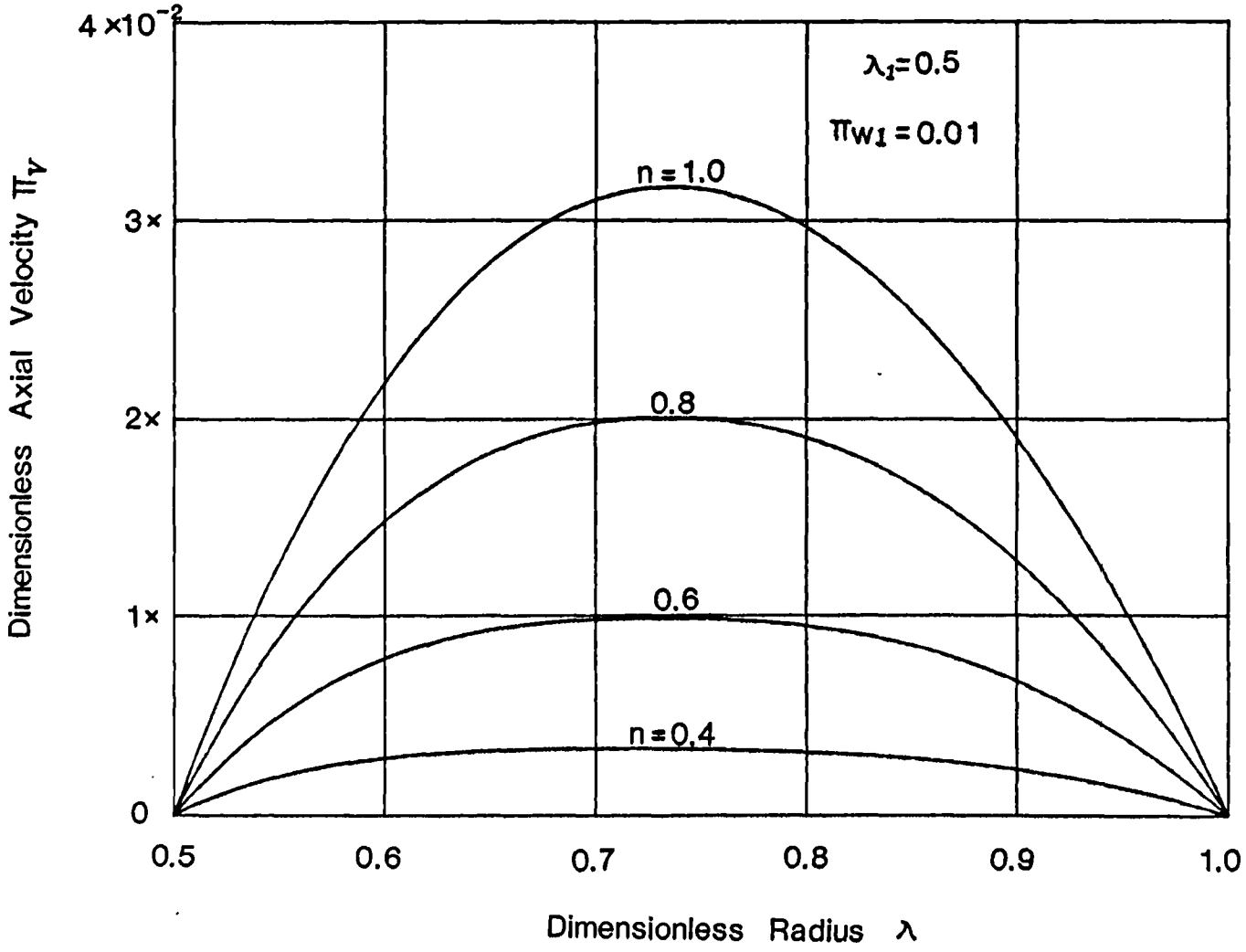

Fig.4-6 Influence of 'n' on axial velocity profile

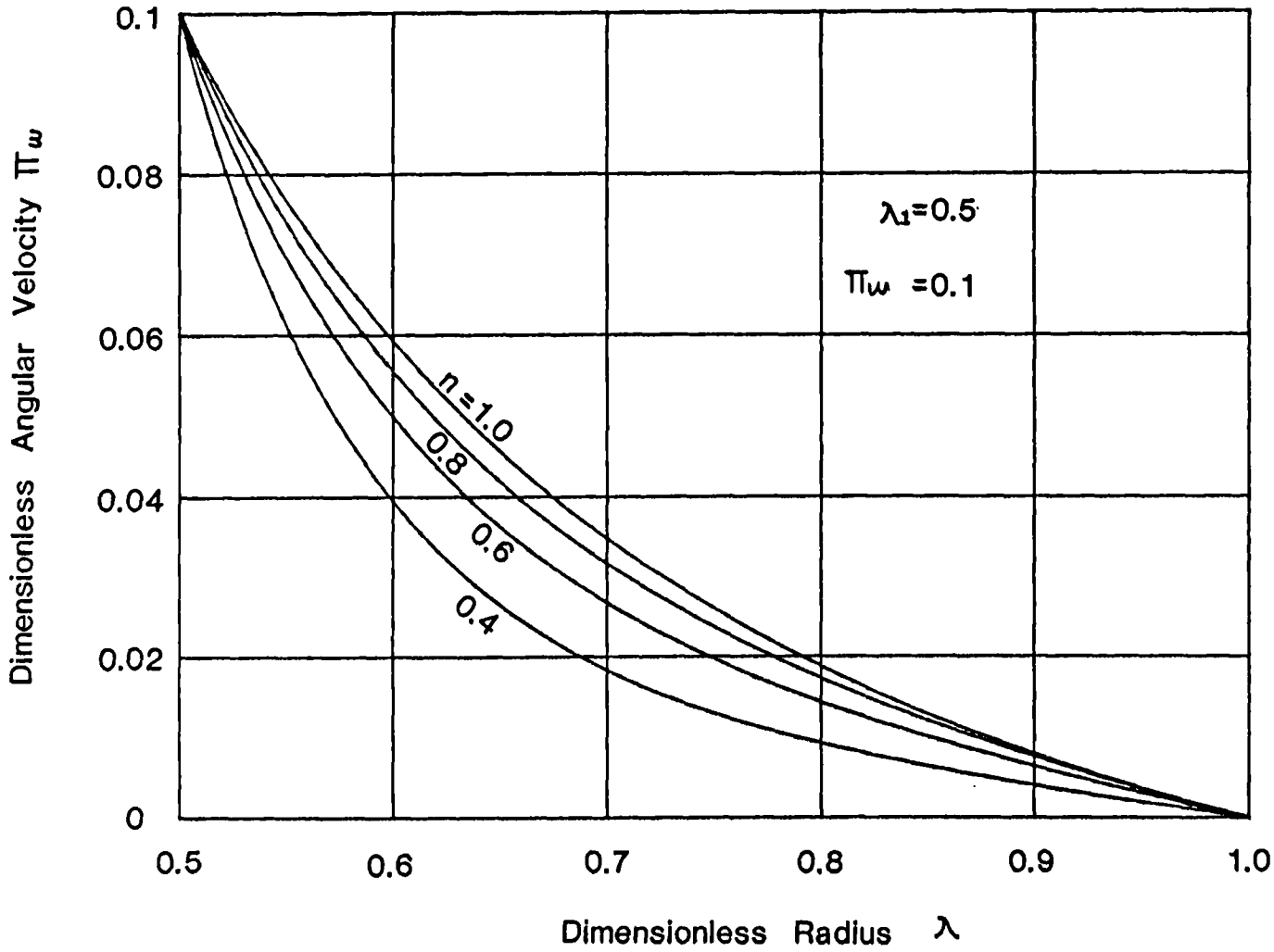

Fig.4-7 Influence of 'n' on angular velocity profile

4.5.3. Axial volumetric flowrates

Another important characteristic of the helical flow of power-law fluids is the influence of the three independent dimensionless variables on the axial volumetric flowrate. The influence of the dimensionless inner tube rotary speed $\pi_{\omega 1}$ on the axial volumetric flowrate π_q for different values of the flow behaviour index 'n' is shown in Fig.(4-8). It may be seen that, for n = 1, π_q remains the same with increase of $\pi_{\omega 1}$, showing that the axial flow is independent of the tangential flow. For the cases of n < 1, however, π_q increases with increase of $\pi_{\omega 1}$, showing that the axial flow becomes dependent on the tangential flow. In the preceding section we have shown that the apparent viscosity decreases and the axial velocity increases over the entire annular space with increase of $\pi_{\omega 1}$. So it is not surprising to see that the volumetric flowrate π_q is higher at a higher value of $\pi_{\omega 1}$.

The degree of interdependence of the axial and tangential flows with different values of the flow behaviour index n is shown in Fig.(4-9). The ratio of the dimensionless volumetric flowrate at $\pi_{\omega 1} = 0.1$, i.e. $\pi_q|_{\pi_{\omega 1}=0.1}$, to that at $\pi_{\omega 1} = 0$, i.e. $\pi_q|_{\pi_{\omega 1}=0}$, is used to show the interdependence under a constant value of λ_1. The higher the ratio, the higher the degree of interdependence. From Fig.(4-9) it may be seen that, as n decreases from the value of unity, the ratio increases, slowly at the beginning but more and more rapidly as n is getting smaller and smaller. Therefore, the value of n may be taken as a measure of the interdependence. The smaller the n value, the more interdependent between the axial flow and the tangential flow.

Fig.(4-10) shows the dimensionless volumetric flowrate π_q vs the dimensionless inner tube rotary speed $\pi_{\omega 1}$ for different values of the

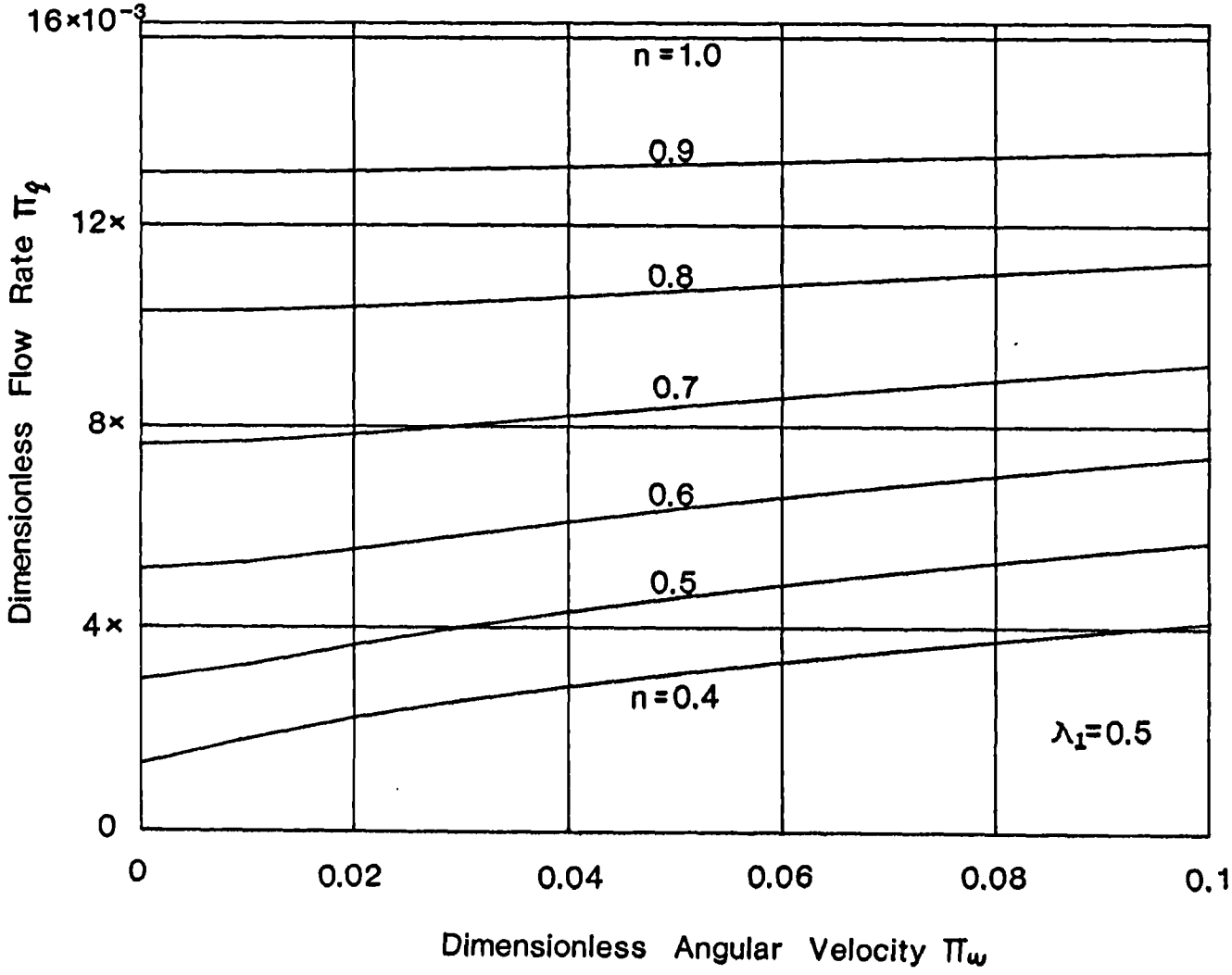

Fig.4-8 Influence of $\pi_{\omega 1}$ and 'n' on axial volumetric flowrates

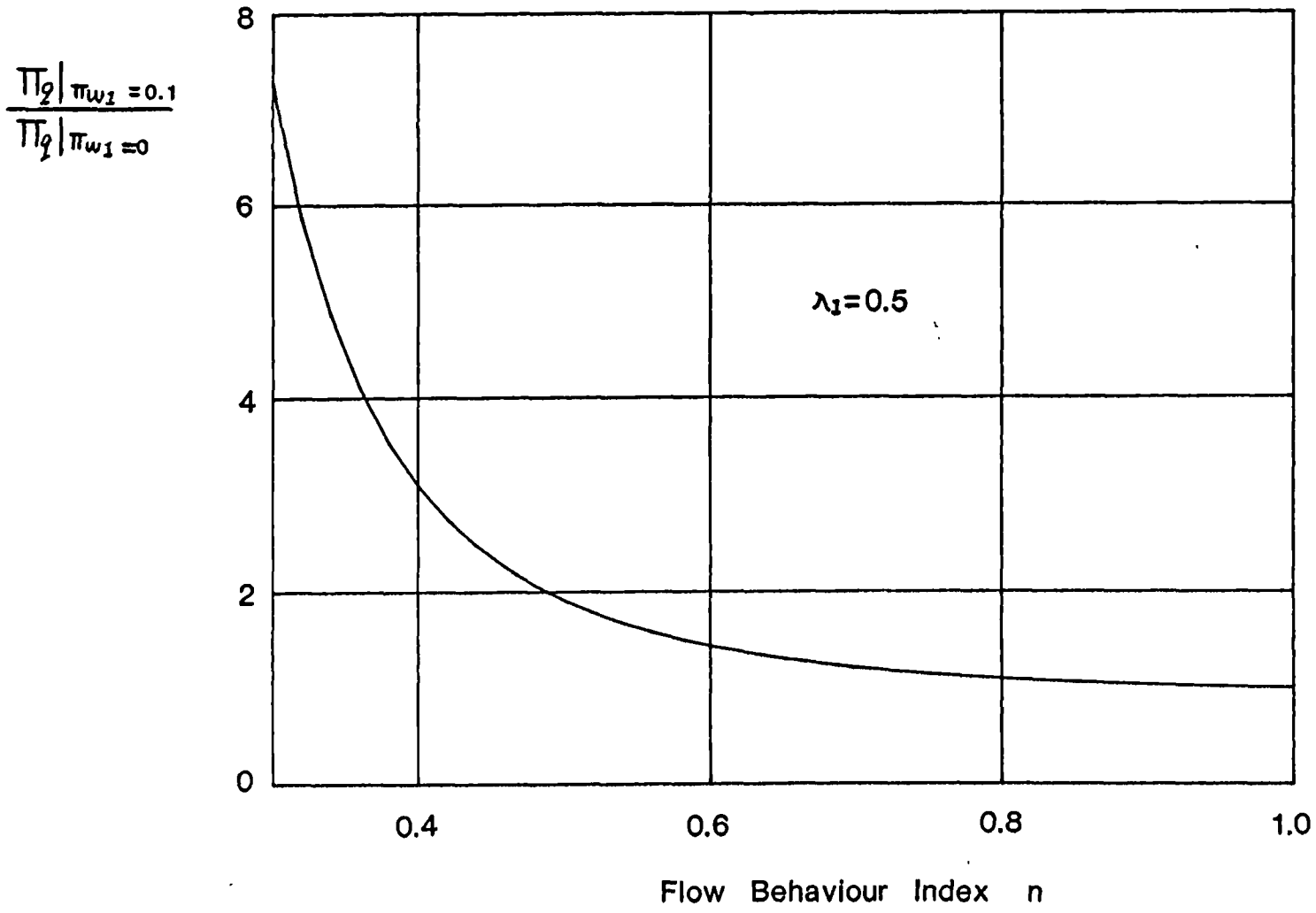

Fig.4-9 Influence of 'n' on interdependence between rotational flow and axial flow

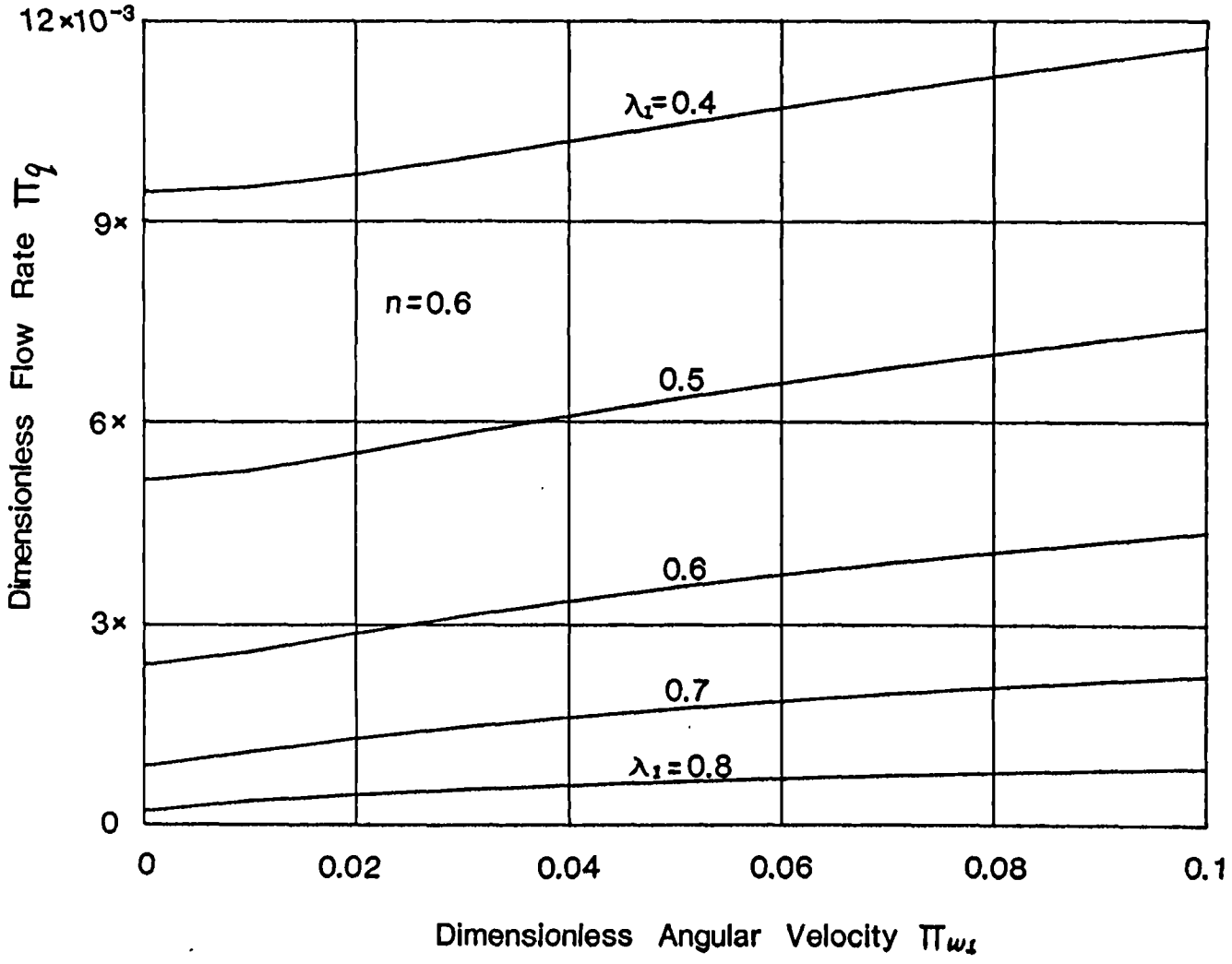

Fig.4-10 Influence of π_{w_1} and λ_1 on axial volumetric flowrates

radii ratio κ_1. It may be seen that, under a constant value of n, which is not equal to one, π_q increases with the increase of $\pi_{\omega 1}$ for all values of κ_1, but π_q has a lower value for a higher value of κ_1. This is understandable considering that the value of κ_1 is a measure of the annular scale. If we keep the radius of the outer tube constant, then an increase of κ_1 is equivalent to an increase in the radius of the inner tube, and thus to a decrease in the annular cross-section area. Therefore, the volumetric flowrate π_q decreases with increase of κ_1.

4.6. Derivation of the dimensionless equation for axial pressure gradient

In Section 4.4, we have derived the expression for the dimensionless volumetric flowrate for annular helical flow of power-law fluids. It should be noted that the present definition of the dimensionless volumetric flowrate, as shown in Eq.(4-18), is identical to those used in Chapter 2 for the concentric annular axial flow and in Chapter 3 for the eccentric annular flow of power-law fluids, i.e.

$$\pi_q = \frac{q}{\pi \cdot r_2^3 \cdot \left(\frac{g_p \cdot r_2}{K} \right)^s}$$

In the previous cases, the pressure gradient expressions have been obtained by simply reversing the above expression for g_p because the independent dimensionless variables in those cases are irrelevant to the axial volumetric flowrate or/and pressure gradient. For the present case of the annular helical flow, however, one of the independent dimensionless variables, i.e. $\pi_{\omega 1}$, according to its definition, depends on the axial pressure gradient. So the expression obtained by reversing the above expression will not be an explicit expression for the axial

pressure gradient. Therefore an iterative solution method must be used, as one shown in Walker and Al-Rawi's paper[29], in order to calculate the pressure gradient.

In this section, we will modify the dimensionless variable $\pi_{\omega 1}$ so that an explicit solution for the axial pressure gradient can be derived. Then the pressure gradient in the helical flow can be calculated without using any iterative solution method.

First, let's define the dimensionless axial pressure gradient as:

$$\pi_p = \frac{\left(\frac{g_p \cdot r_2}{K}\right)}{\left(\frac{q}{\pi \cdot r_2^3}\right)^n} \tag{4-20}$$

Based on Eq.(4-18), the expression for π_p may be obtained as:

$$\pi_p = \frac{1}{(\pi_q)^n} = \left[\frac{1}{2}\int_{\lambda_1}^{1} \frac{\lambda\,(\lambda^2 - \lambda_o^2)}{\pi_\mu}\, d\lambda\right]^{-n} \tag{4-21}$$

Next, we should eliminate g_p from the defination of $\pi_{\omega 1}$. Based on Eq.(4-19), the following relationship exists:

$$\left(\frac{g_p \cdot r_2}{K}\right)^s = \left(\frac{q}{\pi \cdot r_2^3}\right)\frac{1}{\pi_q}$$

Then we may write $\pi_{\omega 1}$ as:

$$\pi_{\omega 1} = \frac{\omega_1}{\left(\frac{g_p \cdot r_2}{K}\right)^s} = \frac{\omega_1 \cdot \pi_q}{\left(\frac{q}{\pi \cdot r_2^3}\right)}$$

Now, if we define the new dimensionless inner tube rotary speed as:

$$\pi_{\omega 1}' = \frac{\omega_1}{\left(\frac{q}{\pi \cdot r_2}\right)^3} \tag{4-22}$$

then it will not contain g_p. The relationship between $\pi_{\omega 1}$ and $\pi_{\omega 1}'$ is:

$$\pi_{\omega 1} = \pi_{\omega 1}' \cdot \pi_q \tag{4-23}$$

The physical significance of $\pi_{\omega 1}'$ is still the same as that of $\pi_{\omega 1}$, which has been explained in Section 4.4. We call $\pi_{\omega 1}'$ the modified dimensionless angular velocity of the inner tube.

If the modified dimensionless variable $\pi_{\omega 1}'$ is used to replace $\pi_{\omega 1}$ as one of the three independent dimensionless variables, the expression for the dimensionless constant σ, which is necessary for calculating π_p by using Eq.(4-21), must be modified accordingly to eliminate $\pi_{\omega 1}$ from its expression. Substituting Eq.(4-23) into Eq.(4-15a), it may be found that:

$$\sigma = \pi_{\omega 1}' \left(\frac{\pi_q}{\int_{\lambda_1}^{1} \frac{d\lambda}{\pi_\mu \cdot \lambda^3}} \right)$$

Substituting Eq.(4-18) into the above equation, the expression for σ becomes:

$$\sigma = \frac{\pi_{\omega 1}' \int_{\lambda_1}^{1} \frac{\lambda\,(\lambda^2 - \lambda_o^2)}{\pi_\mu}\, d\lambda}{2 \int_{\lambda_1}^{1} \frac{d\lambda}{\pi_\mu \cdot \lambda^3}} \tag{4-24}$$

The expression for the dimensionless constant λ_o is still the same, i.e. Eq.(4-15b).

Now, for the pressure gradient calculation, the three independent

dimensionless variables are λ_1 , n and $\pi_{\omega 1}'$ where $\pi_{\omega 1}'$ is defined by Eq.(4-22). To calculate the dimensionless axial pressure gradient, the constant σ and λ_0 must be determined by combining Eq.(4-14) and solving Eq.(4-24) and Eq.(4-15b) simultaneously. Then Eq.(4-21) is used to obtain π_p. The axial pressure gradient g_p may be calculated then by:

$$g_p = \frac{K}{r_2} \left(\frac{q}{\pi \cdot r_2^3} \right)^n \pi_p \qquad (4\text{-}25)$$

4.7. Influence of $\pi_{\omega 1}'$ on axial pressure gradient

The calculations of the axial pressure gradient with different values of $\pi_{\omega 1}'$ and n have been made and the results are shown in Fig.(4-11) to (4-13). In these figures, the axial pressure gradient has been normalised by dividing the corresponding pressure gradient under the stationary inner tube condition. It may be seen that, as $\pi_{\omega 1}'$ increases, or as the inner tube rotary speed increases, the pressure gradient decreases. This is because, as explained in Section 4.5, as the inner tube rotary speed increases, the apparent viscosity decreases and so does the flow resistance, and thus the axial pressure gradient decreases if the volumetric flowrate is held constant. Also it may be seen that, the smaller the n value, the more pronounced the reduction of the pressure gradient, and the more pronounced the interdependence between the rotational flow and the axial flow.

The influence of the dimensionless inner tube rotary speed on the axial pressure gradient for different values of the ratio of the inner and outer radii, λ_1 , is shown in Fig.(4-14). An interesting characteristic may be seen from the figure, i.e. there is a point for each value of $\pi_{\omega 1}'$ at which the pressure gradient reduction is most pronounced. This point is between $\lambda_1 = 0.5$ and 0.6 for each value of

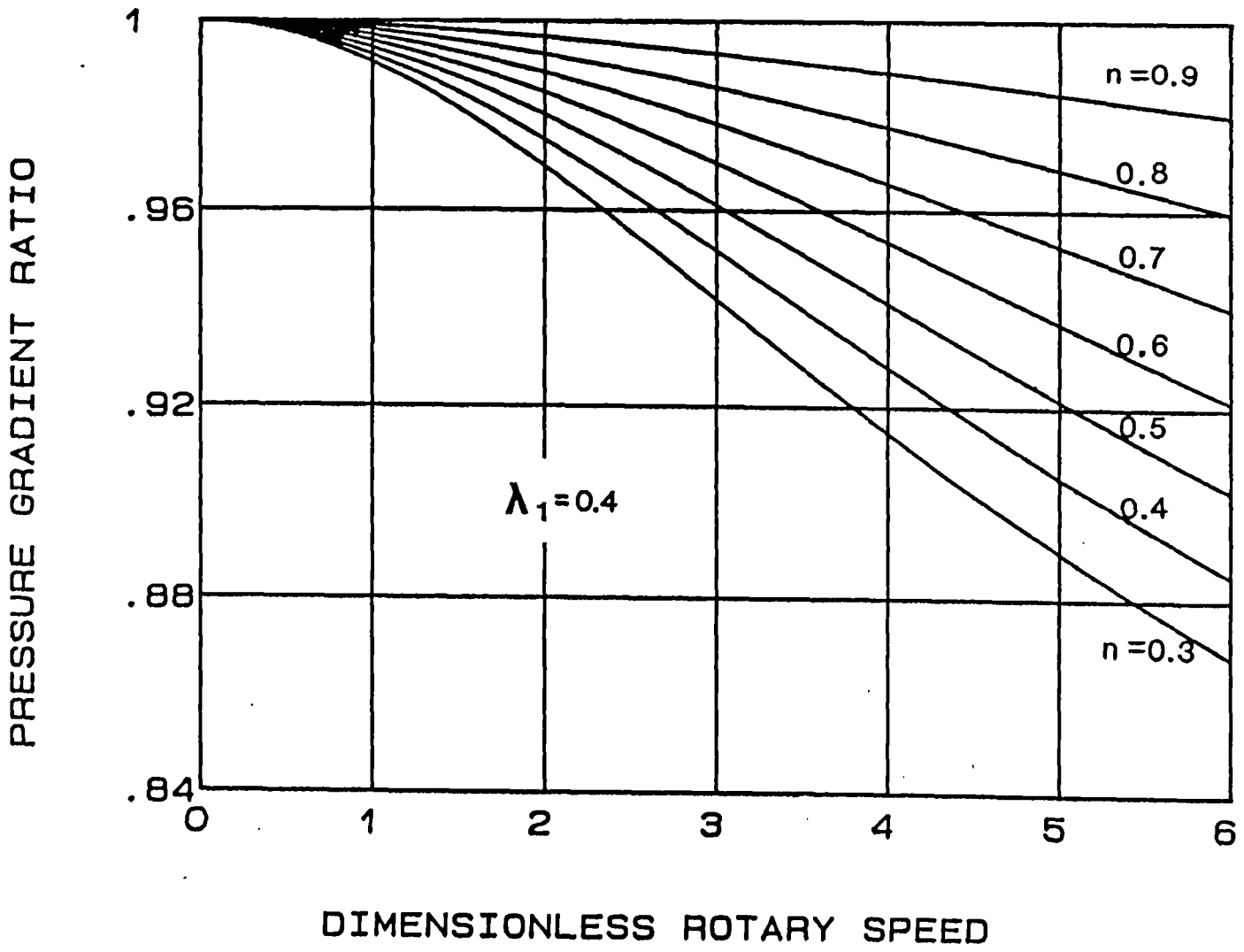

Fig.4-11 Influence of π_{wi}' and n on axial pressure gradient for $\lambda_1 = 0.4$

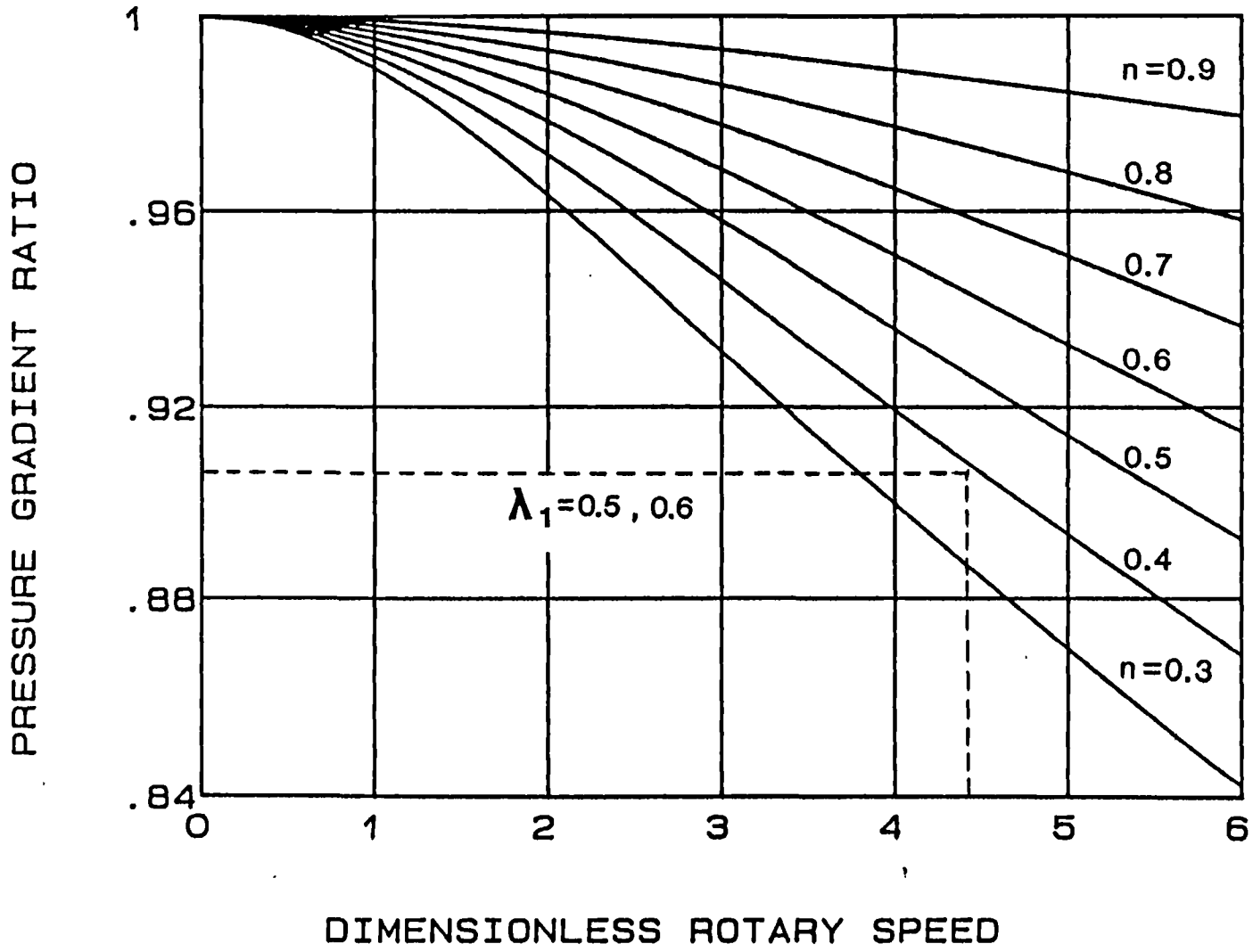

Fig.4-12 Influence of $\pi_{\omega 1}'$ and 'n' on axial pressure gradient for $\lambda_1 = 0.5, 0.6$

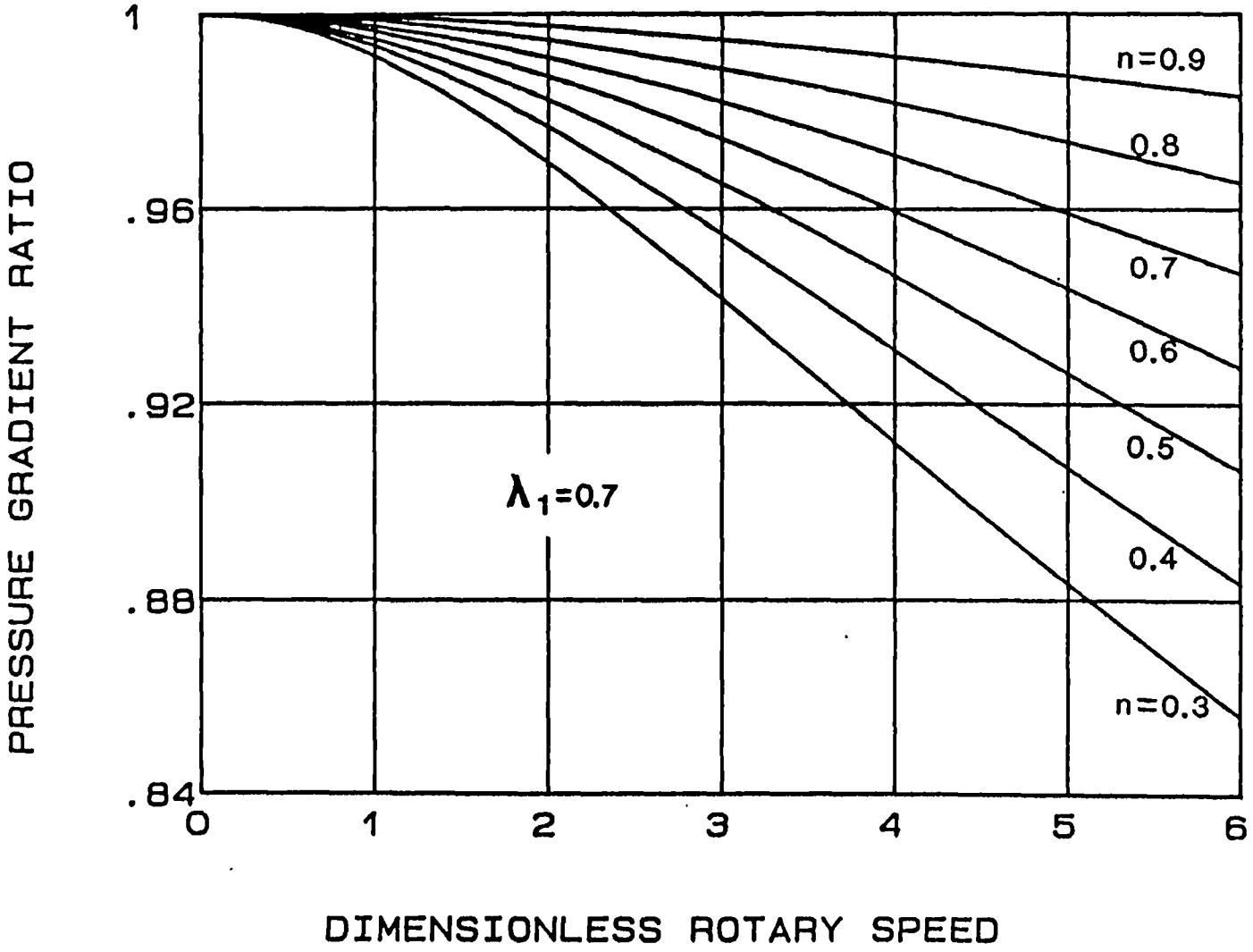

Fig.4-13 Influence of π_{w1}' and 'n' on axial pressure gradient for $\lambda_1 = 0.7$

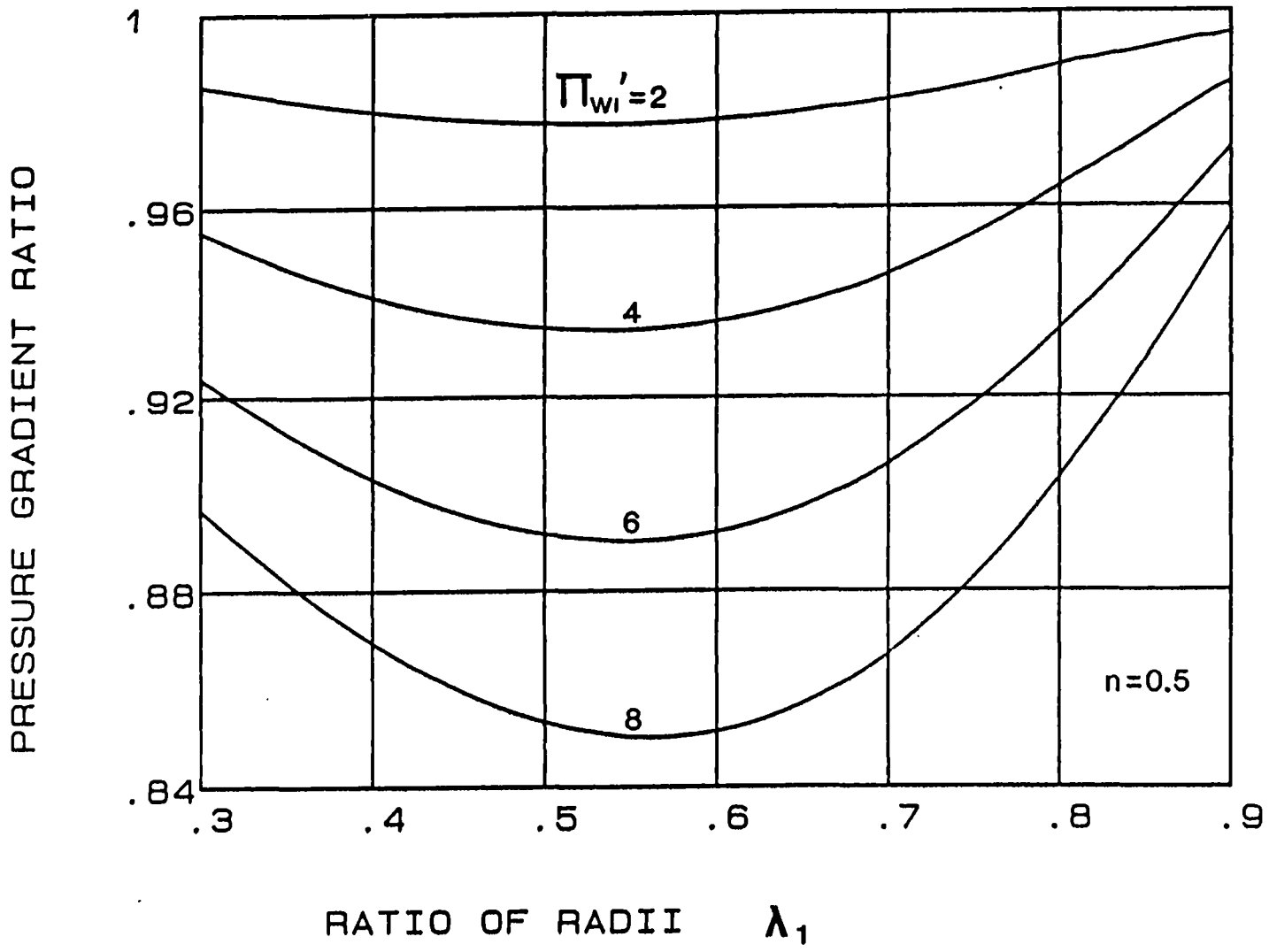

Fig.4-14 Influence of Π_{w1}' and λ_1 on axial pressure gradient

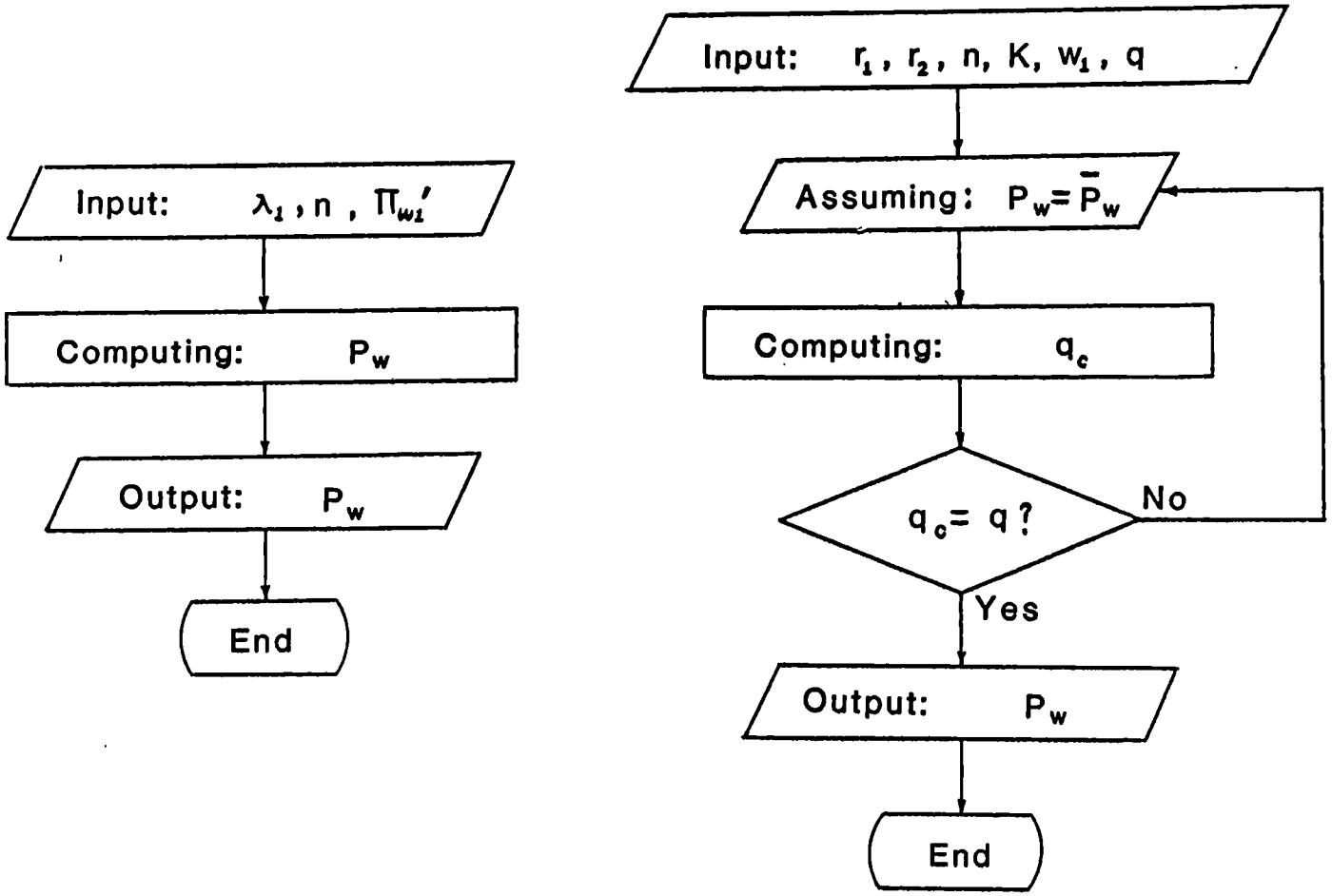

Present Method

Walker and Al-Rawi's Method

Fig.4-15 Comparison between the present and the previous methods for pressure gradient calculations

$\pi_{\omega 1}$' shown in the figure. This explains why Fig.(4-12) is shown for both the cases of λ_1 = 0.5 and 0.6.

Comparison between using the proposed method and the previous Walker and Al-Rawi's method[29] to calculate the pressure gradient for helical flow of power-law fluids has been made and is shown in Fig.(4-15). It may be seen that there are three advantages of the present new method over the previous one. Firstly, the characteristics of the pressure gradient behaviour in the helical flow system can be understood completely by analysing only three independent variables with the proposed method while with the previous one, six variables have to be analysed; secondly, in contrast to the previous method, the pressure gradient can be calculated directly without using any iterative solution method with the proposed method; and thirdly, it is only possible to use the proposed dimensionless equations in laboratories to simulate various industrial operational conditions, e.g. flow of drilling fluids through drilling annuli when the drillpipe is rotated.

4.8. Rig-site method for predicting the reduction of the annular friction pressure drop (AFPD) caused by drillpipe rotation.

During oilwell drilling operations, drilling fluids are circulated from the bottom of the hole up to the surface through the annulus between the drillpipe and the casing or wellbore. So the annular friction pressure drop (AFPD) of the circulating fluid will directly affect the dynamic pressure and thus the pressure differential between the drilling fluids and the formation at the bottom of the hole. Therefore accurate calculation of AFPD is essential to the design of the drilling hydraulics to optimize the hydraulic parameters on the drill bit, and to the design of the bottom hole dynamic pressure to contain

the formation pressure and, at the same time, minimize the chip "hold down" effect of the pressure differential on the penetration rate. Currently, the calculations of AFPD are made based on the unrealistic condition that the drillpipe (inner tube) is stationary and thus it is assumed that AFPD is not affected by the drillpipe rotation during drilling operations.

It is well-known that drilling fluids are non-Newtonian fluids and can be described by power-law model. In the previous sections, it has been shown that, when the pressure gradient or AFPD is held constant, the volumetric flowrate will be increased with rotation of the inner tube (drillpipe) because of the shear-thinning behaviour of power-law fluids. By the same token, if the volumetric flowrate is held constant, the pressure gradient or AFPD will be reduced with the inner tube (drillpipe) rotation. The later case represents the situation in the drilling annulus because during drilling operations, the volumetric flowrate of the circulating fluid depends on the output of the mud pumps and it will not be affected by drillpipe rotation. So it is AFPD which must be influenced by drillpipe rotation. Therefore, the proposed method for pressure gradient calculations in annular helical flow may be applied directly to the oilwell drilling industry to predict the reduction of AFPD caused by drillpipe (inner tube) rotation.

However, in order to eliminate lengthy calculations, a simple method has been developed in the present analysis which can be used by drilling engineers on the rig-site. The procedures will be presented in the following discussions and an example of using the rig-site method will also be given.

4.8.1. Procedures

(i) Calculate the annular friction pressure drop (AFPD) by assuming that the drillpipe is not rotated. Although the exact solution for this case is available, as discussed in Chapter 2, the following simpler solution may be used as an approximation:

$$P_o = 4^{1+n} \cdot \left(\frac{1+2n}{n} \right)^n \frac{L \cdot K}{(d_2-d_1)^{1+n}} (v_f)^n \qquad (4\text{-}26)$$

The above equation is obtained by reversing Eq.(A3-14) in Appendix (A3-2) for the pressure gradient and substituting g_p, w and h with P_f/L, $(d_2+d_1)\cdot\pi/2$ and $(d_2-d_1)/2$, respectively and then expressing q in terms of v_f. Comparison between the above equation and the exact solution has been made in the present analysis and the results are shown in Fig.(4-16). It may be seen that the error caused by using the above equation is less than 2.3% as long as $d_1/d_2 \geq 0.3$;

(ii) Calculate the dimensionless drillpipe rotary speed, $\pi_{\omega 1}'$, using Eq.(4-22);

(iii) From Figs.(4-11) to (4-13), find the pressure ratio, F_p, i.e. the ratio of the annular friction pressure drop when the drillpipe is rotated to that which occurs when the drillpipe is stationary;

(iv) The corrected (or actual) annular frictional pressure drop under the condition of a rotating drillpipe may be obtained by:

$$P_\omega = F_p \cdot P_o \qquad (4\text{-}27)$$

and the pressure reduction is:

$$\Delta P = P_o - P_\omega \qquad (4\text{-}28)$$

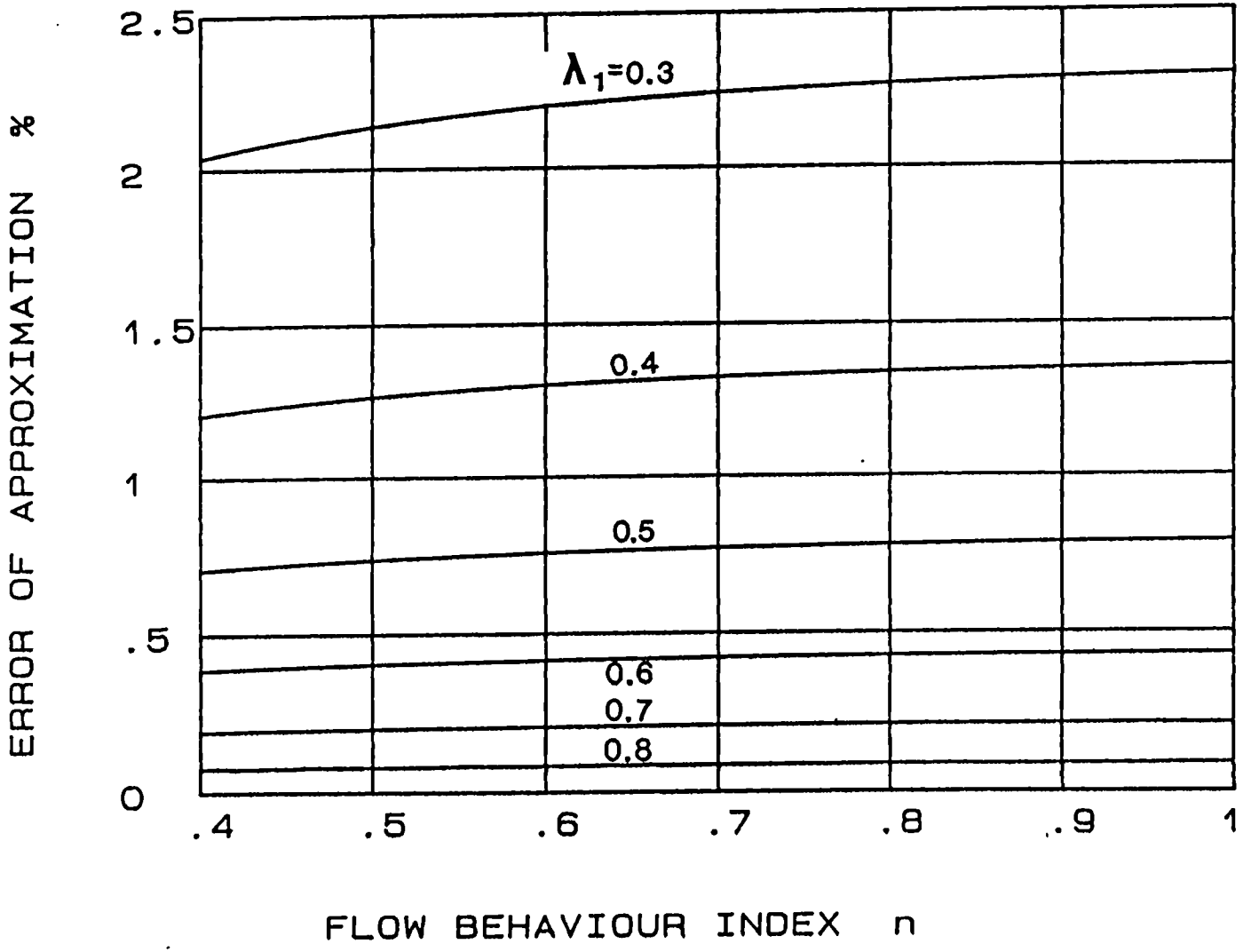

Fig.4-16 Accuracy of the constant-height slot model for approximation of pressure gradients in concentric annular flow

4.8.2. Example

a) Assume:

Drillpipe size: $d_1 = 5$ in = 12.7 cm

Casing size: $d_2 = 9\ ^5/_8$ in = 24.45 cm

Ratio: $\pi_1 = d_1/d_2 = 0.52 \simeq 0.5$

Casing setting depth: $L = 10{,}000$ ft $= 3.048 \times 10^5$ cm

Drillpipe rotary speed: $\omega_1 = 155$ rpm = 16.23 rad/sec

Drilling fluids: $K = 15$ lbf-s^n/100ft^2 = 71.82 dyne-s^n/cm^2

$n = 0.4$

Annular fluid velocity: $v_f = 120$ ft/min = 60.96 cm/sec

so the circulating rate of the drilling fluid is:

$$q = \frac{\pi}{4}(d_2^2 - d_1^2)\cdot v_f = 2.09 \times 10^4 \text{ cm}^3$$

b) Predict the reduction of AFPD inside the casing (assume the flow is laminar).

c) Solution:

(i) $$P_o = 4^{1+0.4}\cdot\left(\frac{1+2\times0.4}{0.4}\right)^{0.4} \frac{3.048\times10^5\times71.82}{(24.45-12.7)^{1+0.4}} \times 60.96^{0.4}$$

$= 4.58\times10^7$ dyne/cm^2

= 655 psi

(ii) The dimensionless drillpipe rotary speed:

$$\pi_{\omega 1}' = \frac{16.23\times\pi\times(24.45/2)^3}{2.09\times10^4} = 4.46$$

(iii) From Fig.(2), it is found that:

$$F_p = 0.905$$

(iv) The corrected annular friction pressure drop:

$$P_\omega = 0.905 \times 655 = 593 \text{ psi}$$

The pressure reduction caused by drillpipe rotation is:

$$\Delta P = 655 - 593 = 62 \text{ psi}$$

The reduction of AFPD caused by drillpipe rotation in the above example is about 10%. It may be shown that, under some drilling conditions, the value of the dimensionless drillpipe rotary speed $\pi_{\omega 1}'$ may be up to about 6 and the reduction of AFPD may be up to 15%.

4.9. Summary and conclusions

A group of dimensionless equations have been derived in the above analysis for the laminar helical flow of power-law fluids through concentric annuli and three independent dimensionless variables are identified which are:

(i) the ratio of the inner and outer radii of the annulus, $\bar{\kappa}_1$, which defines the relative scale of the annulus;

(ii) the flow behaviour index of the power-law fluid, $\bar{n}$, which defines the interdependence between the rotational flow and the axial flow in the helical flow system;

(iii) the dimensionless inner tube rotary speed, $\bar{\pi}_{\omega 1}$, which defines

the magnitude of the inner tube rotary speed, ω_1, relative to the equivalent axial shear rate developed by the axial pressure gradient.

Using the dimensionless equations, the characteristics of the annular flow can be understood by simply analysing the effect of the three independent dimensionless variables on the flow system.

In addition, an explicit expression for the pressure gradient in the annular helical flow has also been derived and procedures have been developed which can be used by drilling engineers on the rig-site to correct for the reduction of the annular friction pressure drop caused by drillpipe rotation.

CHAPTER 5.

ADDITIONAL REMARKS ON THE PRESENT STUDIES AND RECOMMENDATIONS FOR FUTURE EXTENSIONS

5.1. About "laminar" eccentric annular flow

In Chapter 3, a new method was developed to analyse the "laminar" eccentric annular flow of power-law and Bingham plastic fluids. Strictly speaking, however, eccentric annular flow can not be classified as simply "laminar" or "turbulent", as we usually do for flow through pipes or concentric annuli. This may be better understood by examining the following two phenomena which may be encountered in eccentric annuluar flow.

5.1.1. Transition from laminar to turbulent flow

Usually, the flow regime of a flowing fluid is determined by calculating its Reynolds number which may be expressed in general as:

$$N_{Re} = \frac{d \cdot v_f \cdot \rho}{\mu_e} \qquad (5\text{-}1)$$

where "d" is a geometric size parameter. For pipe flow, "d" is the pipe diameter and for other channel flows, "d" is an equivalent diameter of the channel. It has long been known that if the Reynolds number is below about 2100, the flow is laminar and the fluid elements follow streamlines. If it is above 2100, however, turbulences will be developed in the flow and therefore the flow is turbulent. From the above equation, it is obvious that the Reynolds number for the flow

system which has a larger "d" will first reach 2100 and thus the flow will first change from laminar to turbulent flow, and vice versa.

For eccentric annular flow, because of the offset of the inner tube relative to the outer tube, one side of the annulus will be enlarged and thus has a larger geometric size while the other side will be reduced and thus has a smaller geometric size. Therefore, unlike the case in pipe flow or concentric annular flow, an eccentric annular flow will not change from laminar to turbulent flow in all areas at the same time. Rather, if we gradually increase the fluid velocity, at some point turbulences will be developed first in the area which is of the maximum dimension and then they will spread towards the areas with smaller dimensions until they have reached the entire eccentric annulus. Thereafter the flow is turbulent in all areas of the eccentric annulus.

Therefore, using the term: "laminar" in Chapter 3, the author implies that the flow is laminar over the entire eccentric annulus.

5.1.2. Secondary flow

Another phenomenon which may be encountered in eccentric annular flow is that the flow may not be purely axial, as we assumed in the analyses in Chapter 3. Mitsuishi and Aoyagi[12] found in their experiments that secondary flow exists in eccentric annular flow under the low Reynolds number laminar flow conditions. However, they claimed that the secondary flow velocity was always less than 2% of the axial velocity and thus was negligible under the conditions of their experiments. They attributed the secondary flow to the viscoelastic properties of the polymer solutions used in their experiments. In the present author's opinion, the primary reason is probably the non-axisymmetry of the eccentric annular geometry. Therefore, it may well

be the case that secondary flow also exists in eccentric annular flow of inelastic fluids, though the secondary flow velocity is perhaps even weaker than in the case for elastic fluids.

5.2. Discussions on turbulent eccentric annular flow

Before this discussion, let's first examine a simple case of pipe flow. Assume that there are two separate pipes with different diameters through which the same kind of fluid is flowing. If the pressure gradients are the same in both the pipes, then we will find that the fluid velocity is higher in the larger pipe than in the smaller one, regardless of the flow regime and the rheological behaviour of the fluid. This explains why the velocity is higher in the enlarged area than in the reduced area in an eccentric annular flow, as shown in Chapter 3. Similar explanations may be also given to the volumetric flowrate and the pressure gradient behaviours in the eccentric annular flow.

Therefore, although the mathematical models obtained in Chapter 3 for laminar eccentric annular flow are not valid if the flow regime is not laminar, the general behaviour of turbulent eccentric annular flow of both Newtonian and non-Newtonian fluids should be similar to those of the corresponding laminar eccentric annular flow, i.e.

(i) the velocity is higher in the enlarged area than in the reduced area of the eccentric annulus;

(ii) with increasing eccentricity, the volumetric flowrate increases if the pressure gradient is held constant, or conversely, the pressure gradient decreases if the volumetric flowrate is held constant.

5.3. About "laminar" annular helical flow

In Chapter 4, a group of dimensionless equations were developed to describe the 'laminar' annular helical flow of power-law fluids. To avoid the possible confusion over the word "laminar", it is necessary to clarify that, by saying "laminar", the author has two implications:

(i) it is the combined flow of both the axial flow and the rotational flow that is laminar, not the axial flow or rotating flow alone;

(ii) the fluid elements follow the helical or spiral streamlines and no secondary flow or no vortices occur in the flow.

Over half a century ago, Taylor[32,33] used the cases of rotating flow of viscous liquids between two rotating tubes to study the stability problem. For the case of rotating flow developed by rotating the inner tube with the outer tube stationary, he found that when a certain critical rotary speed of the inner tube was exceeded, a kind of flow vortices, now called "Taylor votices", would emerge whose axes are located along the circumferences and these vortices rotate in alternately opposite directions. He developed a criterion, now called the "critical Taylor number", to determine the critical condition for the Taylor vortices. Later, many other investigators [34,35,36,37] also found the Taylor votices in the combined flow of the rotating and the axial flow, i.e. the annular helical flow. They tryed to correlate the influence of the axial flow on the critical Taylor number and they found that it was possible to develop a kind of correlation which could be used only under their own experimental conditions, most of which had a high radii ratio (or small annular clearance) and low axial Reynolds

number. However, the general conclusions they reached are consistent, i.e. the critical Taylor number will be increased with increasing the axial Reynolds number, or in other words, the axial flow will ease the development of the Taylor vortices.

The above investigations were conducted in Newtonian fluids. Sinevic, et.al.[38] experimentally confirmed that Taylor vortices also exist in purely rotational flow of power-law non-Newtonian fluids and concluded that the critical Taylor number in this case is very dependent on the width of the annular clearance and the flow behaviour index. Although the present author did not find any evidence in literature, it seems reasonable to assume that Taylor vortices will occur in helical flow of non-Newtonian fluids.

5.4. Recommendations for future extensions of the present studies

In this part of the thesis, the author has presented two parallel theoretical studies, i.e. on laminar eccentric annular flow and on laminar helical flow, respectively. Although parts of these studies have been substantiated indirectly by previous investigations for power-law fluids, as mentioned in the corresponding sections entitled "previous studies", more comprehensive experimental data are still necessary to confirm the results of the present new studies completely, especially for Bingham plastic fluids.

As for various cases of turbulent annular flow of non-Newtonian fluids, the situation is that, as Skelland remarked twenty years ago[2d], "there is a complete lack of experimental data on the velocity distributions and friction losses.....". This is still unfortunately true today. What is more, the words "a complete lack of experimental data" are also suitable to describe the situation in the investigations

into transitions from laminar to turbulent flow for various cases of annular flow.

There is no doubt that any further effort made to improve our current understanding of, and any experimental data related to, non-Newtonian annular flow would be valuable and should be acknowledged. However, from the standpoint of practical industrial interests, the present author would like to make the following suggestions for future extensions of the studies presented in this thesis on non-Newtonian annular flow:

(i) Investigations into turbulent non-Newtonian annular flow

The present author fully recognizes the complexity involved in these investigations. So some simple empirical or approximate methods should be used without hesitance whenever it is apparent that exact theoretical treatments would be rather formidable. These investigations should be mainly directed towards volumetric flowrate/presure gradient correlations because these are the main interests in terms of industrial applications. Also they should be conducted systematically from simple to complicated cases.

First, these investigations should be conducted in concentric annuli with the inner tube stationary. Currently, there have been several empirical methods used in industry for this case of turbulent annular flow. The introductions of these methods may be seen in references (2e, 21c, 39, 40). Further investigations may experimentally confirm or modify one of these previous methods, or alternatively develop a new empirical method based on the experimental data if none of these previous methods is found to be sufficiently accurate. Then based on these results and also on the theoretical studies presented in this part of the thesis, these investigations may be extended to the case of

turbulent annular flow in eccentric annuli and some kind of empirical method may be established to correlate the effect of the inner tube eccentricity on the volumetric flowrate/pressure gradient. In the last stage of the investigations, the effect of the inner tube rotation should be examined.

(ii) Investigations into the laminar-turbulent transitions in various cases of non-Newtonian annular flow

There have been some empirical methods currently used in industry to determine the critical condition when the transition from laminar flow to turbulent flow occurs in concentric annuli with the inner tube stationary. These methods have been referred to in references (2e, 21c, 40). Future investigations into this problem should be conducted in a similar fashion to that for turbulent annular flow, i.e. in concentric annuli first to confirm/modify one of the previous mehtods or to develop a new one, and then in eccentric annuli without inner tube rotation and lastly in concentric/eccentric annuli with inner tube rotation. It is expected that some kind of empirical method could be developed based on the experimental data for each of the above different cases.

It is well recognized that non-Newtonian annular flow is a very complicated and rather formidable problem to deal with, especially compared with flow through circular pipes. However, with advances in instrumentation technology and with introduction of more and more powerful computers, it is possible that in the near future our level of understanding on this problem may reach the same level of our current understanding on non-Newtonian flow through circular pipes, provided that increasing amount of effort will be invested to investigate this problem.

PART TWO

DRILLED CUTTINGS TRANSPORT THROUGH DRILLING ANNULI AT VARIOUS ANGLES

INTRODUCTION

In order to extract oil from beneath the earth, one must somehow breaks the rock and drill a hole miles down from the surface. This is essential and everyone can realize that. But can everyone also realize that it is equally essential to bring the broken rocks up to the surface somehow, one hundred percent up to the surface, in order to drill a "hole"?

During rotary oilwell drilling operations, one of the primary functions of the circulating fluid, i.e. the drilling fluid, is to lift the drilled cuttings up to the surface through the annular space between the drillpipe and the wellbore. This transport process is usually called the "drilled cuttings transport" and the ability of the drilling fluid to lift the drilled cuttings is called the "carrying capacity" of the drilling fluid.

Compared with transport processes of solid-liquid mixtures through pipes or open channels, which are usually encountered in civil engineering, mining engineering, chemical engineering, etc., the transport process of the drilled cuttings during drilling operations has following three unique characteristics:

i) the rheologically non-Newtonian behaviour of the transporting medium, i.e. the drilling fluids;

ii) the specific "annular" geometry of the conduit through which

the cuttings are transported;

iii) the inclination of the conduit, i.e. the hole angle, which may vary from vertical to horizontal.

In addition, there are also some other unique characteristics which may arise if the drillpipe is rotated or if the annulus is not concentric, etc. These features result in the transport of cuttings being a very complicated process.

Understanding of the cuttings transport process relies on knowledge in three areas:

i) flow characteristics of the transporting medium, the drilling fluid, through the drilling annulus;

ii) settling characteristics of the transported medium, the drilled cuttings, in the transporting medium;

iii) mechanism of the drilled cuttings transport process itself.

Obviously, without understanding in area (i) and (ii), one can hardly talk about the mechanism of the cuttings transport process.

At the beginning of rotary oil drilling, no effort was made on a scientific evaluation of the carrying capacity of the drilling fluids because excessively high circulating rates of drilling fluids were usually used during drilling operations and thus "hole cleaning" did not appear to be a problem. This pratice remained until the 1940's. Then people began to recognize that increasing the pressure drop through the bit nozzles could greatly improve the drilling efficiency and therefore jet drill bits were introduced. However, with the limited output housepower and pressure of the mud pumps, the circulating rates of drilling fluids had to be reduced in order to increase the pressure

drop across the bit. So a question began to come up: what circulating rate of the drilling fluid was really required in order to transport the drilled cuttings up to the surface and keep the hole clean ?

In 1949, Hall, et.al.[1] first reported experimental studies on the carrying capacity of drilling fluids in vertical wells and from then until the early 1980's, many other investigations were also conducted. Since the mid 1970's, as the development of the offshore oil industry and the advancement of the directional drilling technique, an increasing amount of interest began to show in the investigations into drilled cuttings transport in deviated wells. Until now, a tremendous amount of effort has been expended on investigations into cuttings transport in both the vertical and the deviated wells. However, most of the investigators limited themselves to experimental observations and were satisfied to know merely "what happened", without enough effort to know "why" and to understand the mechanism. Without good understanding of the cuttings transport process, it is not surprising to see that drilling engineers still often find themselves bewildered by the problems associated with inadequate transport of drilled cuttings during drilling operations, especially during directional drilling operations.

With the aim of improving our understanding of the drilled cuttings transport mechanism, a comprehensive theoretical and experimental investigation into the drilled cuttings transpot in the oil drilling wells at different angles has been conducted and is reported in this part of the thesis. This part consists of six chapters. Some basic concepts used in the present studies are first introduced in Chapter 6. Charter 7 presents theoretical and experimental investigations into the particle settling velocity in drilling fluids. A new model is developed in this chapter for the calculation of the particle settling velocity in power-law fluids. Chapter 8 is a comprehensive theoretical analysis of

various factors affecting cuttings transport based on both the previous and the present studies. In Chapter 9, the concept of the minimum transport velocity (MTV) is introduced and a comprehensive literature survey on relevant studies is presented. Then in Chapter 10, a comprehensive theoretical study on the minimum transport velocity (MTV) in drilling annuli is presented and general correlations for predicting the critical conditions of MTV are developed. Finally, recommendations for future continuing investigations are proposed in Chapter 11.

CHAPTER 6.

BASIC CONCEPTS

In the process of transporting drilled cuttings through the drilling annulus, the cuttings always settle vertically downwards relative to the transporting fluid because the density of cuttings is generally higher than that of the fluid. So, in order to bring the cuttings up to the surface, the annular fluid velocity must be higher than the cuttings settling velocity.

In a vertical drilling annulus, the cuttings travel to the surface at a velocity which is equal to the difference between the fluid velocity and the cuttings settling velocity. This particle's net upward velocity is usually called the "transport velocity". If the mean annular fluid velocity is used to represent the fluid velocity, the transport velocity may be then expressed as:

$$v_t = v_f - v_s \qquad (6\text{-}1)$$

To evaluate the carrying capacity of drilling fluids in vertical annuli, it is often more convenient to express the cuttings transport velocity relative to the fluid velocity. Therefore the concept of the "cuttings transport ratio" was introduced which is defined as the ratio of the transport velocity to the mean annular fluid velocity, i.e.

$$F_T = \frac{v_t}{v_f} \qquad (6\text{-}2a)$$

This concept first appeared in Sifferman, et.al.'s paper[2]. Substituting Eq.(6-1) into the above equation, the cuttings transport

ratio becomes:

$$F_T = 1 - \frac{v_s}{v_f} \qquad (6\text{-}2b)$$

From the above equation it may be seen that the cuttings transport ratio, F_T, depends on the cuttings settling velocity, v_s and the mean fluid velocity, v_f. For the zero cuttings settling velocity, $v_s = 0$, the cuttings transport velocity is equal to the mean fluid velocity, $v_t = v_f$, and thus the cuttings transport ratio is unity, $F_T = 1$. In this case, any non-zero annular fluid velocity can transport the cuttings up to the surface. As the settling velocity v_s increases, both the transport velocity v_t and the transport ratio F_T decrease. The higher the F_T value, the easier it is to transport the cuttings, and vice versa.

Based on Eq.(A6-7) in Appendix (A6-1) it may be seen that the cuttings concentration, C_s, during drilling operations is approximately inversely proportional to the cuttings transport ratio, F_T, i.e.:

$$C_s = \frac{d_2^2 \cdot v_d}{F_T \cdot (d_2^2 - d_1^2) \cdot v_f} \qquad (A6\text{-}7)$$

So the cuttings concentration decreases as the cuttings transport ratio increases, and vice versa.

Therefore the cuttings transport ratio, F_T, is an excellent measure of the carrying capacity of a drilling fluid in a vertical annulus and it has been widely used in industry for many years in design of the cuttings transport programme for vertical drilling.

For directional drilling, however, the situation is different because there is at least one section of the annulus in a directional

well which is not vertical, rather which is inclined or even horizontal. In this section of the annulus, the cuttings tend to settle downwards towards the low-side of the wellbore and may slide along or rest and form a cuttings bed there. So the cuttings transport velocity in this case is different from that defined by Eq.(6-1) and thus the cuttings transport ratio defined by Eqs.(6-2) can not be used as an indicator of the carrying capacity of the drilling fluid.

To deal with this problem, most of the previous investigators used the in-situ cuttings concentration as an alternative indicator of the carrying capacity of the drilling fluid in laboratories. However this method is quite unacceptable in industry because not only is it still impossible to predict the in-situ cuttings concentration but also the only knowledge of the in-situ cuttings concentration is not adequate to evaluate the performance of cuttings transport in the inclined section of the drilling annulus during directional drilling operations. This will be further explained in Chapter 8.

In recent years[3,4], two separate investigators have made an effort to investigate the mechanism of cuttings-bed formation in inclined annuli. They established mathematical models to predict the cuttings bed formation and the critical circulating rate or the critical mean annular fluid velocity required to transport the cuttings out of the annulus completely. Although the validity of these models are doubtful, which will be examined closely in Chapter 9, the concept is rather valuable. Based on field experience and experimental observations, there is a general consensus among drilling engineers that, as long as no cuttings bed is formed on the low-side wall of the annulus, there will be no trouble associated with the inadequate transport of drilled cuttings during directional drilling operations. Therefore, in the present author's opinion, it is the critical circulating rate or the

critical mean annular fluid velocity required to prevent the cuttings-bed formation which should be used as the guideline for hole clean and as the indicator of the carrying capacity of the drilling fluid during directional drilling. In other words, in order to clean the hole during directional drilling, the annular fluid velocity must be equal or higher than this critical velocity. If increasing one parameter will result in an increase of the critical velocity, and thus an increase of the annular fluid velocity required for hole cleaning, then the effect of increasing the parameter is to decrease the carrying capacity of drilling fluids, and vice versa. This critical mean annular fluid velocity, called the "minimum transport velocity" or MTV, will be investigated in Chapter 9 and Chapter 10.

CHAPTER 7.

CUTTINGS SETTLING VELOCITY IN DRILLING FLUIDS

The settling velocity of solid particles is one of the major factors that affects many solid-liquid transport processes. In the preceding chapter we have shown that, during vertical drilling operations, the cuttings transport performance can be evaluated by calculating the cuttings transport ratio, F_T, which is defined as:

$$F_T = \frac{v_t}{v_f} = 1 - \frac{v_s}{v_f} \qquad (6\text{-}1)$$

From the above equation it may be seen that it is essential to know the cuttings settling velocity, v_s, in addition to the mean annular fluid velocity, v_f, in order to evaluate the cuttings transport performance during vertical drilling operations. The mean annular fluid velocity, v_f, can be calculated by simply dividing the output volumetric flowrate of the mud pumps (the circulating rate) by the annular cross section area, both of which are known parameters during drilling operations. However, the settling velocity of the drilled cuttings will be affected by many unknown factors and this causes difficulty in evaluating the cuttings transport performance in vertical wells.

According to the previous investigations[5,6], in a deviated well, cuttings are transported as heterogeneous flow where a radial cuttings concentration gradient exists, like the case in solid-liquid mixture transport through circular pipes. If the fluid velocity is not high enough, a cuttings bed will be formed on the low-side wall of the wellbore. Based on previous studies on solid-liquid mixture flow [7,8,9,10], one of the most important factors that determine the

characteristics of a heterogeous flow of a solid-liquid mixture system is the settling velocity of the solid particles in the liquid. Therefore knowledge of the cuttings settling characteristics in drilling fluids is vital for understanding the cuttings transport process in drilling annuli.

In this chapter, the basic principles and previous investigations will be reviewed and then an effort will be made towards investigating into settling velocities of variously shaped particles in drilling fluids.

7.1. Basic principles

Before the discussion, it is necessary to clarify that, in the present analysis, the "settling velocity" of solid particles in a fluid will always refer to the terminal settling velocity of the solid particles relative to the surrounding fluid, no matter the fluid itself is quiescent or dynamic. In previous studies, the term "slip velocity" was sometimes used to refer to the particle settling velocity in dynamic fluids and there have been some confusions of "settling velocity" with "slip velocity".

Traditionally, the settling velocity of a solid particle has been studied in quiescent fluids based on the force balance principle. However, the results have also been used in the cases of dynamic fluids with the state of the fluid flow sometimes being taken into account. In the similar fashion, the present studies will be conducted first in quiescent fluids and then an extension to dynamic fluids will be considered afterwards.

The case of solid particles settling in a quiescent fluid may be much simplified by assuming that the particles are separated

sufficiently so as not to collide or interact with each other and that the system is under the influence of gravity only. Then the effective gravitational force causing a particle to settle can be written as:

$$F_g = V_s \cdot (\rho_s - \rho_f) \cdot g \qquad (7\text{-}1)$$

The fall of the particle in the fluid results in a resistant force, called the "fluid drag force", which may be expressed as:

$$F_D = C_D \cdot A_p \frac{\rho_f \cdot v_s^2}{2} \qquad (7\text{-}2)$$

where A_p is a projected characteristic area of the particle which depends upon the shape of the particle and its orientation during settling; C_D is the so called "drag coefficient" which depends upon the flow regime of the fluid surrounding the settling particle, the shape of the particle and also the rheological behaviour of the fluid.

After the particle has reached its terminal settling velocity, the two forces acting upon it, i.e. F_g and F_D, are in equilibrium. So from Eqs.(7-1) and (7-2), the particle settling velocity, v_s, may be obtained as:

$$v_s = \left[2 \cdot g \frac{V_s \cdot (\rho_s - \rho_f)}{A_p \cdot C_D \cdot \rho_f} \right]^{1/2} \qquad (7\text{-}3a)$$

For spherical particles, $V_s = \pi \cdot d_s^3/6$ and $A_p = \pi \cdot d_s^2/4$. Substituting these terms into Eq.(7-3a) yields:

$$v_s = \left[\frac{4}{3} g \frac{d_s \cdot (\rho_s - \rho_f)}{C_D \cdot \rho_f} \right]^{1/2} \qquad (7\text{-}3b)$$

From the above equation it may be seen that the particle settling velocity, v_s, can be calculated easily once the drag coefficient C_D is determined.

It should be remembered that Eq.(7-3a) and (7-3b) are derived solely based on the force balance principle, so they are valid for both the laminar and the turbulent settling regimes and for both Newtonian and non-Newtonian fluids.

7.2. Particle settling velocity in Newtonian fluids

Newtonian fluids refer to the fluids for which shear stress has a linear relationship with shear rate. The well-known Newton's law of friction describes this linear relationship:

$$\tau = \mu \cdot \gamma \qquad (7\text{-}4)$$

in which μ is a constsnt and is called the viscosity of the fluid.

For spherical particles settling in Newtonian fluids, dimensional analysis and experimental results indicate that the drag coefficient C_D is a unique function of the particle Reynolds number which is defined as[11a]:

$$N_{Ren} = \frac{d_s \cdot v_s \cdot \rho_f}{\mu} \qquad (7\text{-}5)$$

When N_{Ren} is less than unity, the fluid around the settling particle is in laminar motion and thus the particle is in the laminar settling regime. Neglecting the inertia effect, Stokes[11a] obtained by theoretical treatments that:

$$C_D = \frac{24}{N_{Ren}} \qquad (N_{Ren} < 1) \qquad (7\text{-}6)$$

This is the so called "Stokes' law".

When N_{Ren} is greater than about 1000, the turbulent flow around the particle will be developed and the viscous effect becomes negligible. Based on experimental results, the drag coefficient in this case approaches a constant:

$$C_D = 0.44 \qquad (N_{Ren} > 1000) \qquad (7\text{-}7)$$

This is the well known "Newton's law".

Between the laminar and the turbulent settling regimes, there is a transitional settling regime. Allen's correlation[11a] for the drag coefficient in the transitional regime is:

$$C_D = \frac{30}{N_{Ren}^{5/8}} \qquad (1 < N_{Ren} < 1000) \qquad (7\text{-}8a)$$

and Bird, et.al[12a] gave that:

$$C_D = \frac{18.5}{N_{Ren}^{3/5}} \qquad (2 < N_{Ren} < 500) \qquad (7\text{-}8b)$$

Combining Eqs.(7-3b) through (7-8), the settling velocity of spherical particles in Newtonian fluids in various settling regimes may be obtained as follows:

Stokes' law model:

$$v_s = g \frac{(\rho_s - \rho_f) \cdot d_s^2}{18 \cdot \mu} \qquad (N_{Ren} < 1) \qquad (7\text{-}9)$$

Based on Allen's correlation,

$$v_s = 0.1039 \cdot \left[g \frac{(\rho_s - \rho_f)}{\rho_f} \right]^{0.7273} \frac{d_s^{1.1818}}{(\mu/\rho_f)^{0.4545}}$$

$$(1 < N_{Ren} < 10^3) \qquad (7\text{-}10a)$$

Based on Bird, et.al.'s correlation,

$$v_s = 0.1528 \cdot \left[g \frac{(\rho_s - \rho_f)}{\rho_f} \right]^{0.7143} \frac{d_s^{1.1429}}{(\mu/\rho_f)^{0.4286}}$$

$$(2 < N_{Ren} < 500) \qquad (7\text{-}10b)$$

Newton's law model:

$$v_s = 1.74 \cdot \left[g \frac{d_s \cdot (\rho_s - \rho_f)}{\rho_f} \right]^{1/2} \qquad (N_{Ren} > 10^3) \qquad (7\text{-}11)$$

It should be remembered that the above equations are developed only for spherical particles settling in quiescent Newtonian fluids. It may be seen that the particle settling velocity in this case depends on the particle diameter and density, and the fluid viscosity and density.

7.3. Previous studies on drilled cuttings settling velocities in drilling fluids

In the preceding section we have discussed the settling velocity of solid particles in Newtonian fluids. Unfortunately, the mathematical models developed in the preceding section, i.e. Eq.(7-9) through Eq.(7-11), can not be applied directly to the case of settling

velocities of drilled cuttings in drilling fluids because:

(i) the drilling fluids are generally non-Newtonian fluids;

(ii) the drilled cuttings are generally non-spherical particles.

In this section, we will examine the methods which have been used by previous investigators to tackle the cuttings settling velocity problem.

7.3.1. Non-Newtonian nature of drilling fluids

Drilling fluids are generally non-Newtonian fluids. The rheological models commonly used by drilling engineers to approximate the non-Newtonian behaviour of drilling fluids are the power-law model, which may be expressed as[13a]:

$$\tau = -K \cdot |\gamma|^{n-1} \cdot \gamma \qquad (n \leq 1) \qquad (7\text{-}12)$$

and the Bingham plastic model, which may be expressed as:

$$\tau = \mp \tau_y - \mu_p \cdot \gamma \qquad (|\tau| \geq \tau_y) \qquad (7\text{-}13)$$

where "-" is used for $\gamma > 0$ and "+" for $\gamma < 0$.

Although only Newtonian fluids possess a property which strictly may be called the "viscosity" and all non-Newtonian fluids require two or more parameters to describe their consistency behaviour, it is often convenient to refer to an "apparent viscosity" of a non-Newtonian fluid. According to Newton's law of friction, this apparent viscosity is defined as[13a]:

$$\mu_a = \left| \frac{\tau}{\gamma} \right| \qquad (7\text{-}14)$$

For Power-law fluids, from Eq.(7-12) it may be found that:

$$\mu_a = K \cdot \left| \gamma \right|^{n-1} \qquad (7\text{-}15)$$

and for Bingham plastic fluids, it may be found from Eq.(7-13) that:

$$\mu_a = \mu_p + \left| \frac{\tau_y}{\gamma} \right| \qquad (7\text{-}16)$$

Eq.(7-15) and (7-16) indicate that the apparent viscosities of both power-law and Bingham plastic fluids are shear-dependent. Their viscosities decrease with increasing shear rates and this kind of behaviour is usually called "shear thinning".

The settling problem of drilled cuttings in drilling fluids is complicated by the non-Newtonian behaviour of the fluids, i.e. their shear-dependent viscosities. Theoretically the viscosity affecting the particle settling velocity in a non-Newtonian fluid should be that of the fluid envelop surrounding the particle and this viscosity depends on the shear rate distribution around the particle. Unfortunately it is impossible to develop a general analytical equation to describe the shear rate distribution around a settling particle, unless some approximations are introduced and the case is limited to the completely creeping motion of a spherical particle[14]. Therefore the method which has been used by previous investigators for the cuttings settling velocity in drilling fluids is to try to find an equivalent or a representative viscosity to account for the non-Newtonian nature of drilling fluids.

Chien[15] suggested that, for water-based bentonite suspensions, the Bingham plastic viscosity, μ_p, could be used as an equivalent viscosity

and for polymer type drilling fluids, the effective viscosity, according to the defination of Skelland[13b], for pipe flow of Bingham plastic fluids should be used which is expressed as:

$$\mu_e = \mu_p + \frac{\tau_y \cdot d}{6 \cdot v_f} \qquad (7\text{-}17)$$

Moore[16] suggested using the effective viscosity of power-law fluids derived for the flow between two parallel flat plates:

$$\mu_e = \frac{K \cdot (d_2 - d_1)}{12 \cdot v_f} \left[\frac{12 \cdot v_f}{(d_2 - d_1)} \frac{(2n+1)}{3 \cdot n} \right]^n \qquad (7\text{-}18)$$

Zeidler[17] adapted the apparent viscosity corresponding to the wall shear rate and wall shear stress of an annular flow. He suggested that the wall shear stress should be calculated based on the friction factor by using the method proposed by Fredrickson and Bird[18]. In laminar annular flow, the friction factor for the power-law fluids may be approximated by:

$$f = \frac{16}{N_{Re}(n, \kappa_1)} \qquad (7\text{-}19)$$

and for turbulent annular flow:

$$f = \frac{0.0791}{N_{Re}(n, \kappa_1)} \qquad (7\text{-}20)$$

where the modified Reynolds number is defined by:

$$N_{Re}(n, \kappa_1) = \frac{d_2^n \cdot v_f^{2-n} \cdot \rho_f}{K} \frac{(1 + \kappa_1)}{2^{(n-3)} \cdot (1-\kappa_1^2)^{(n+1)}} \left[\frac{n \cdot (1-\kappa_1)^{(2+s)}}{(2n+1)} I \right]^{-n} \qquad (7\text{-}21)$$

where $\kappa_1 = d_1/d_2$, $s = 1/n$ and 'I' is a function of κ_1. In Fredrickson and Bird's original paper[19], a group of curves were provided to determine the value of 'I'. However, based on the present author's analysis, the value of 'I' may be approximated for flow through drilling annuli, where $\kappa_1 \geq 0.2$, by:

$$I = 0.55 + 0.43 \cdot \kappa_1 \qquad (7\text{-}22)$$

Then, based on the defination for the friction factor, the wall shear stress may be approximated by:

$$\tau_w = f \frac{\rho_f \cdot v_f^2}{2} \qquad (7\text{-}23)$$

and, based on Eq.(12), the corresponding shear rate may be calculated by:

$$\gamma_w = \left(\frac{\tau_w}{K} \right)^{1/n} \qquad (7\text{-}24)$$

and the apparent viscosity can be then obtained by:

$$\mu_a = \frac{\tau_w}{\gamma_w} \qquad (7\text{-}25)$$

It should be noted that the equivalent viscosities proposed by the above investigators for particle settling are functions of the fluid velocity and are independent of the particle settling velocity. If one agrees that the viscosity which affects the particle settling is that of the fluid envelop surrounding the particle, as stated earlier, an argument that may be easily raised against the methods proposed above

is that the effective or apparent viscosity of annular or pipe flow represents only the equivalent fluid viscosity corresponding to a particular position in the flow and can not describe the behaviour of the fluid surrounding the settling particles. Particularly one should notice that, if the fluid velocity approaches zero, i.e. the fluid is stagnant, both the effective and the apparent viscosity for annular or pipe flow will approach infinity and the settling velocity would be zero. This is obviously not true.

Later Zeidler[20] proposed another equivalent viscosity which was defined as the viscosity that a Newtonian fluid would have in order to yield the same settling velocity as that of the particle settling in a non-Newtonian fluid. Based on experimental results, he developed an empirical equation for the equivalent shear rate surrounding a settling particle. This equation takes the form of:

$$\gamma_{eq} = \frac{v_s}{d_{sde}} \frac{1-n}{2} \left(\frac{d_{sde}}{d_{si}}\right)^{[(n+5)\cdot(1.1-0.98\cdot(1-n^2)^{0.5})]} \qquad (7\text{-}26)$$

where d_{sde} and d_{si} are two characteristic dimensions of the particle defined by Zeidler[20]. Then the equivalent viscosity is calculated by:

$$\mu_{eq} = K\cdot(\gamma_{eq})^{n-1} \qquad (7\text{-}27)$$

Walker and Mayes[21] developed an empirical relation for determining the shear stress caused by a circular disk in flatwise settling. The relation is given by:

$$\tau_s = 68.95\cdot[h_s\cdot(\rho_s - \rho_f)]^{1/2} \qquad (7\text{-}28)$$

The corresponding shear rate, γ_s, is determined by a smooth plot of Fann viscometer dial readings against shear rates. The apparent viscosity, μ_a, is then calculated by:

$$\mu_a = \frac{\tau_s}{\gamma_s} \qquad (7-29)$$

It should be pointed out that, in contrast to the previous methods, the equivalent viscosity determined by the Zeidler's second method[20] or the Walker and Mayes' method[21] depends only upon the particle settling velocity and is independent of the fluid velocity. So the particle settling velocity derived based on the equivalent viscosity determined by Eq.(7-27) or (7-29) is also independent of the fluid velocity.

It is interesting to know that a similar method to Zeidler's second one[20] and Walker and Mayes one[21] was also used by investigators for proppant particle settling velcoities in fracturing fluids. Novotny[22] suggested using the simple formula v_s/d_s to calculate the effective shear rate on a settling proppant particle. Daneshy [23] suggested using $3(v_s/d_s)$. However, it should be noted that proppant particles are small and closely sized, compared with drilled cuttings. So proppant particles usually settle in the laminar settling regime while drilled cuttings may settle in any of the laminar, transitional and turbulent settling regimes.

7.3.2. Shape irregularity of drilled cuttings

In addition to the non-Newtonian behaviour of drilling fluids, the drilled cuttings settling velocity problem is also complicated by the shape irregularity of the drilled cuttings.

In the previous studies, an equivalent characteristic dimension was usually used to characterise the cuttings size and also the shape. Then the settling velocity of the drilled cuttings would be calcualted based on this characteristic dimension, regardless of the shape of the cuttings.

The most commonly used characteristic dimension is probably the volume equivalent diameter which is defined as the diameter of a sphere whose volume is equal to that of the particle concerned, i.e.:

$$d_{sv} = \left(\frac{6 \cdot V_s}{\pi} \right)^{1/3} \qquad (7\text{-}30)$$

This volume equivalent diameter first appeared in Hall, et.al.'s paper [1] for the cuttings settling velocity. By using d_{sv}, any shaped particle is treated as a sphere and the settling velocity of the particle is calculated based on the diameter of this equivalent sphere.

There is also another characteristic dimension which is called the "hydraulic diameter" and was introduced for drilled cuttings by Walker and Mayes[21]. The hydraulic diameter of a particle is defined as four times the ratio of the projected cross-section area to the corresponding perimeter of the particle, i.e.:

$$d_{sh} = \frac{4 \cdot A_{sp}}{L_{sp}} \qquad (7\text{-}31)$$

Although the above two characteristic dimensions of non-spherical particles have been widely used in the oil drilling industry, especially the first one, it must be pointed out that it is not enough to characterise both the size and the shape of a non-spherical particle by only one parameter in order to calculate its settling velocity.

Wadell[24] showed in as early as 1934 that, by using the volume equivalent diameter as a characteristic size of a particle, the settling velocity of the particle in Newtonian fluids would be a function of both the volume equivalent diameter and the particle's sphericity which is defined as:

$$\Psi = \frac{\text{Surface area of a sphere of volume equal to that of the particle}}{\text{Surface area of the particle}} \qquad (7\text{-}32)$$

Because a sphere has the minimum possible surface area of any shaped particle of the same volume, the value of sphericity is always less than or equal to 1. For a spherical particle, $\Psi = 1$; the greater the difference between the particle's shape and a spherical shape, the smaller the value of Ψ. According to Wadell[24], if the volume of a particle remains constant, the smaller the value of Ψ, the larger the fluid drag force on the particle during settling and thus the smaller the settling velocity of the particle. Therefore, while the volume equivalent diameter is used as the characteristic dimension of a non-spherical particle, the sphericity of the particle should be used at the same time to evaluate the particle's shape effect on its settling velocity.

Unfortunately, the sphericity as a measurement of a particle's shape has not yet been introduced into cuttings settling velocity calculations in the drilling industry, though it is sometimes used as a qualitative indicator. This is largely due to the complexity involved in evaluating the sphericity of irregular shaped cuttings.

Table 7-1: Previous models for cuttings settling velocity

(In Consistent Units)

Flow Regime	Cuttings' Shape & Orientation	Settling Velocity Models v_s =
Pigott (1941)[36]		
Lam.	Spheres	$= \frac{g.(\rho_s - \rho_f).d_s^2}{18\ \mu}$
	Disk Flatwise	$= \frac{g.(\rho_s - \rho_f).d_{sd}^2}{46.3\ \mu}$
Tur.	Spheres	$= 1.58\ [\ \frac{g\ (\rho_s - \rho_f)\ d_s}{\rho_f}\ ]^{1/2}$
	Disks Flatwise	$= 0.61\ [\ \frac{g\ (\rho_s - \rho_f)\ d_{sd}}{\rho_f}\ ]^{1/2}$
Hall, *et.al.*(1950)[1]		
Lam.	Spheres	$= \frac{d_s^2\ (\rho_s - \rho_f)\ g - 6\ d_s\ \tau_y}{18\ \mu_{eq}}$
	Disks	$= \frac{3\pi\ h_s\ d_{sd}\ (\rho_s-\rho_f)g - 6\pi\ \tau_y(d_{sd}+2h_s)}{64\ \mu_{eq}}$
Tur.	Spheres & Disks	$= \frac{\mu_{eq}\ N_{Res}}{\rho_f\ d_{sv}}$ $\quad N_{Res} = f(\ C_D\ N_{Res}^2)$

Table 7-1: Cont.-I

Williams and Bruce (1951)[31]		
Tur.	Spheres	$= \frac{v_e}{1 + \frac{d_s}{d}}$	$v_e = 1.74 \left[\frac{g(\rho_s-\rho_f)d_s}{\rho_f}\right]^{\frac{1}{2}}$
	Disk Flatwise		$v_e = 1.35 \left[\frac{g(\rho_s-\rho_f)h_s}{\rho_f}\right]^{\frac{1}{2}}$
	Disk Edgewise		$v_e = 1.80 \left[\frac{g(\rho_s-\rho_f)\ h_s}{\rho_f}\right]^{\frac{1}{2}}$
Zeidler (1972)[17]			
Lam.	con.= 0.049 m = 0.782	$= \text{con.}\left(\frac{4}{3}g\right)^{m} \frac{\rho_f^{m-1}\ (\rho_s-\rho_f)^{m}\ d_s^{3m-1}}{\mu_{eq}^{2m-1}}$
Tran.	con.= 0.172 m = 0.612	
Tur.	con.= 0.441 m = 0.516	
Chien (1970)[15]			
Tur.		$= \left[\frac{4}{3} g \frac{(\rho_s-\rho_f)\ d_s}{1.72\ \rho_f}\right]^{1/2}$
Moore (1974)[16]			
Lam.		$= \frac{g\ (\rho_f-\rho_f)\ d_s^{2}}{30\ \mu_{eq}}$
Tran.		$= 0.154 \frac{d_s[g(\rho_s-\rho_f)]^{2/3}}{(\rho_f\ \mu_{eq})^{1/3}}$
Tur.		$= \left[\frac{4}{3} g \frac{(\rho_s-\rho_f)\ d_s}{1.5\ \rho_f}\right]^{1/2}$

Table 7-1: Cont.-II

Zeidler (1974) See Reference 20		
Walker and Mayes (1975)[21]		
Lam. & Tran.	Disks	$= 0.048\ \tau_s \left[\frac{d_{sh}\ \gamma_s}{\rho_f^{1/2}} \right]^{1/2}$ and $\tau_s = 68.59 \left[h_s\ (2.49 - \rho_f \right]^{1/2}$
Tur.		$= 41.8 \left[\frac{h_s\ (\rho_s - \rho_f)}{\rho_f} \right]^{1/2}$
EXLOG (1983)[I-40] Solve the following quadratic equations for v_s		
	Spheres	$3v_s(40\mu + \rho_f\ v_s\ d_s) = 4g\ d_s^2\ (\rho_s - \rho_f)$
	Disks Flatwise	$v_s(40\mu + \rho_f\ v_s\ d_s) = 2g\ h_s\ d_s(\rho_s - \rho_f)$

7.3.3. Previous models for cuttings settling velocities

In the preceding two sections, we discussed that, in order to investigate the cuttings settling velocity problem, the previous investigators used an equivalent viscosity to account for the non-Newtonian behaviour of drilling fluids and used a characteristic dimension to account for the shape irregularity of drilled cuttings. Then the case of the settling velocity of drilled cuttings in drilling fluids was converted to the case of the settling velocity of spherical particles in Newtonian fluids. Using this approach, they developed various methematical models for calculating settling velocities of drilled cuttings in drilling fluids. Table (7-1) has listed the mathematical models proposed by the previous investigators.

It should be mentioned that, by using one of the methods discussed in the section 7.3.1 to characterise the non-Newtonian nature of drilling fluids, the previous investigators developed their cuttings settling velocity models without making any distinction between in stagnant and dynamic fluids. Therefore, some previous models [15,16,17] for cuttings settling velocities are functions of the fluid velocity while some[20,21] are independent of the fluid velocity.

7.4. Theoretical and experimental studies on settling velocities of variously shaped particles in power-law fluids

In the preceding discussion of the previous investigations on the settling velocity of drilled cuttings in drilling fluids, we analysed various methods used by the previous investigators for the non-Newtonian behaviour of drilling fluids and for the shape irregularity of drilled cuttings. From the analysis we identified problems with these previous

methods. The objective of this section is to use a different approach to develop a generalised settling velocity model for variously shaped particles based on a generalised particle Reynolds number for power-law fluids.

7.4.1. Drag coefficient correlations for spherical particles

In order to derive the drag coefficient correlations for spherical particles settling in power-law fluids, dimensional analysis has been performed which is shown in Appendix (A7-1). The result shows that the drag coefficient is a function of not only the generalised particle Reynolds number but also the flow behaviour index of the power-law fluids. The generalised particle Reynolds number for power-law fluids is defined as:

$$N_{Rep} = \frac{d_s^{n} \cdot v_s^{(2-n)} \cdot \rho_f}{K} \qquad (7\text{-}33)$$

It should be noticed that, for Newtonian fluids, $n = 1$ and $K = \mu$, the above equation returns to Eq.(7-5). Therefore, Eq.(7-5) may be treated as a special case of Eq.(7-33) for $n = 1$.

An interesting point may be found if we express Eq.(7-33) in the form as follows:

$$N_{Rep} = \frac{d_s \cdot v_s \cdot \rho_f}{K \cdot \left(\frac{v_s}{d_s}\right)^{(n-1)}} \qquad (7\text{-}33a)$$

Comparing the above expression with Eq.(7-5) it may be found that the term on the denominator of the above expression may be considered as the equivalent viscosity of the power-law fluids around a settling

particle. Based on Eq.(7-15), this equivalent viscosity corresponds to a shear rate of v_s/d_s, as suggested by Novotny[22], which depends upon the particle settling velocity and the particle size.

In fact, the present approach of describing the non-Newtonian behaviour of power-law fluids has been used in previous studies on the particle settling velocity in laminar creeping settling regime in power-law fluids. According to these studies, the drag coefficient correlation may be expressed as[13c]:

$$C_D = \frac{24}{N_{Rep}} X \qquad (N_{Rep} < 0.1) \qquad (7-34)$$

where X is constant and its value depends upon the flow behaviour index 'n'. The lower and upper bounds of the value of X have been evaluated by Wasserman and Slattery[25].

Examining Eq.(7-34) and also Eqs.(7-6) through (7-8), it may be found that a generalised form of the drag coefficient correlation for spherical particles and for both Newtonian and power-law fluids in all settling regimes may be written as:

$$C_D = \frac{a}{N_{Rep}^{\ b}} \qquad (7-35)$$

where the constants "a" and "b" are functions of both the fluid flow regime around the particle and the flow behaviour index of power-law fluids.

7.4.2. Drag coefficient correlations for non-spherical particles

In section 7.3.2, it has been shown that, for non-spherical particles, the volume equivalent diameter together with the sphericity

of the particles should be used to describe the effects of the size and the shape of the particles on their settling velocities. Unfortunately, the practical application of the sphericity concept in the drilling industry has been hindered by the difficulty in calculating the sphericities of irregular shaped cuttings. However, if the drilled cuttings are characterised either as disks or rectangular plates in addition to spheres, the sphericity equation, i.e. Eq.(7-32) may be greatly simplified. For disks:

$$\Psi = \frac{2.621 \cdot F_{hb}^{2/3}}{1 + 2 \cdot F_{hb}} \qquad (7\text{-}36)$$

where $F_{hb} = h_s/d_{sd}$, i.e. the ratio of the thickness to the diameter of the disk. For rectangular plates:

$$\Psi = \frac{2.418 \cdot F_{hb}^{2/3}}{1 + 2 \cdot F_{hb}} \qquad (7\text{-}37)$$

where $F_{hb} = h_s/b_{eq}$, i.e. the ratio of the thickness to the equivalent width of the rectangular plate. The derivation of the above two equations is given in Appendix (A7-2). By using the above equation, as long as the ratio of the thickness to the width of the cuttings is estimated, the sphericity of the cuttings can be calculated easily.

In order to accommodate the particle's shape effect on the settling velocity, the drag coefficient correlation, i.e. Eq.(7-35), may be modified for non-spherical particles as:

$$C_D' = F_s \cdot C_D = F_s \frac{a}{N_{Rep}^{b}} \qquad (7\text{-}38)$$

where F_s is the shape factor which depends upon the particle's

sphericity and the particle settling regime. Using the above equation, the particle Reynolds number N_{Rep} is calculated based on the volume equivalent diameter d_{sv}, which is defined by Eq.(7-30). The values of the constants a, b and F_s in the above equation must be determined experimentally.

7.4.3. New model for settling velocities of variously shaped particles in power-law fluids

Combining Eq.(7-3b) with Eq.(7-33) and Eq.(7-38), the mathematical model for settling velocities of variously shaped particles in power-law fluids can be derived as:

$$v_s = \left[\frac{4}{3} g \frac{(\rho_s - \rho_f) \cdot d_s^{(1+b \cdot n)}}{a \cdot F_s \cdot K^b \cdot \rho_f^{(1-b)}} \right]^{\frac{1}{[2-b \cdot (2-n)]}} \quad . \quad (7\text{-}39)$$

Where d_s is the diameter of a sphere or the volume equivalent diameter of a non-spherical particle defined by Eq.(7-30). One should notice that, for Newtonian fluids and spherical particles, n = 1, K = μ and F_s = 1. When a = 24 and b = 1, Eq.(7-39) becomes identical to Eq.(7-9) which is Stokes' law model. If a = 0.44 and b = 0, Eq.(7-39) returns to Eq.(7-11) as Newton's law model. Therefore the commonly used particle settling velocity models for Newtonian fluids and spherical particles, i.e. Eqs.(7-9) through (7-11), may be considered as the special cases of Eq.(7-39).

7.4.4. Experiment Description

In order to determine the values of the constants a, b and F_s, in

Eq.(7-39), an extensive experimental programme has been carried out in stagnant power-law fluids. A detailed description of the experiment is given below.

Settling Columns

The experimental setups were two columns, one was a clear perspex column, 88 mm ID and 2000 mm long, and another was a glass cylinder, 60 mm ID and 450 mm long. In order to ensure that the columns are long enough to establish the terminal settling velocity of the particles, a theoretical analysis has been performed to analyse the distance required by a particle after entering the fluid and before reaching its terminal settling velocity. The results confirmed the validity of the two columns. This analysis is presented in detail in Appendix (A7-3). In addition, a fluorescent light was placed, when necessary, behind the columns during the tests to help observe the particle's movement in the fluids.

Testing Fluids

Two types of fluids were selected as testing fluids, one was Shell Tellus Oil 68 as a Newtonian fluid and the other was water-based carboxymethyl cellulose (low viscosity CMC and high viscosity CMC) and Xanthum gum biopolymer (XC) solutions to provide power-law-type fluids. Through pilot tests, the concentrations of CMC, XC were selected so that proper distributions of the values of n and K could be obtained during the tests. The fluids were mixed at 20°C with a SILVERSON mixer at 6000 rpm. The rheological properties were measured with two viscometers, namely a FANN 35SA to provide the data under high shear rate condition

TABLE (7-2): Physical and rheological properties of the fluids used in the particle settling velocity experiments

	Concentration g/L	Tem. °C	ρ_s g/cm^3	n	K Pa.s^n	γ^* sec^{-1}
CMC	LO.VIS.CMC-35 HI.VIS.CMC-3	19.5	1.015	0.798	0.194	5-1021
CMC+XC	HI.VIS.CMC-6 XC-1	21	1.002	0.627	0.1696	5-1021
CMC+XC	HI.VIS.CMC-10 XC-1	18.5	1.003	0.597	0.4579	5-1021
CMC-XC	HI.VIS.CMC-8 XC-3	21.3	1.003	0.449	0.7688	5-1021
Shell Tellus Oil - 68		20	0.88	1.000	0.1653	

* These are shear rate ranges within which n and K were determined.

TABLE (7-3): Physical properties and dimensions of the particles used in the particle settling velocity experiments

Materials	Density g/cm^3	Shape	Dimension mm	Sphericity
Bauxite Proppant	3.71	Sphere	0.3*	1.00
Intermediate Proppant	3.22	Sphere	0.4-0.75*	1.00
Sands	2.63	Well Rounded	1.2-2.2*	1.00
Glass Beads	2.63	Sphere	4-6	1.00
Marbles	2.47	Sphere	15.5-25.1	1.00
Steel Balls	7.75	Sphere	3.17-6.34	1.00
Aluminium	2.70	Disk	6.4x2.1 9.7x3.1	0.75 0.75
Aluminium	2.70	Rectangle	5.9x4.1x2.1 10x8x2.1	0.73 0.62
Plastic	2.28	Disk	6.4x2.2 9.6x3.2	0.76 0.76

* These values are based on screen analysis.

(170-1021 1/sec) and a HAAKE-MVIIP VT181 to provide the low shear rate data (5-159 1/sec). The two viscometers were calibrated with standard oil. The fluid densities were determined with a density bottle whose volume was calibrated with water at 20°C (see Appendix (A7-4)). The properties of the fluids are shown in Table (7-2).

Testing Particles

A wide range of solid particles were used, proppant with diameters of 0.3-0.75 mm, well rounded sand particles with diameters of 1.2-2.2 mm (based on the sieve analysis) to simulate approximately spherical drilled cuttings, and glass beads/steel balls to provide the drag coefficient values in a wide range of particle Reynolds numbers. In addition, a variety of disks and rectangular plates of plastic and aluminium in composition were also used to simulate non-spherical drilled cuttings. These particles were painted with different colours on their edges and faces to ease identification of their orientation during settling. The densities of the particles were determined with a density bottle and the method has been described in Appendix (A7-4). Table (7-3) shows the sizes and properties of the particles.

Settling Velocity Measuring System

A video camera and a video tape recorder were assembled to record the movement of the particles during settling in the columns. In addition, a BBC computer clock with an accuracy of 1% per second was incorported with the video system so that the time and the corresponding position of a particle settling in the column could be recorded simultaneously for calculating its velocity. When the settling

velocity was below about 10 mm/sec, a stop watch was used.

Testing Procedures

The polymer fluids were prepared and poured into the column around 16 hours before starting the test to release of entrapped air bubbles and stablize the rheological properties of the fluid. Proppants and sands were dropped into the columns from the top in a cluster and the particles settling midway were traced to measure the settling velocity. Other particles were dropped into the columns one by one and for disks and rectangular plates, their orientation during settling was visually observed and recorded. For the same particle in the same fluid, about four to eight data were obtained to ensure repeatability and accuracy. Test results showed that the variation of the data for sands was within 10% and for other particles within 5%. For polymer fluids, the perspex column was used and the settling velocity of a particle was measured after its free fall of about 600 mm. For convenience, the glass cylinder was used for the tests in oil and around 150 mm was allowed to let the particle reach its terminal settling velocity. Based on the theoretical analysis, which is shown in Appendix (A7-3), only about 60 mm is required within an accuracy of 1% for a steel ball with a diameter of 6.34 mm settling in the oil. To check this analysis, the velocities in two sections of the cylinder after 150 mm settling were measured and the result confirmed that the 150 mm allowed was adequate. The rheological properties were measured before and after each test and the averages were used for the study.

Wall-Effect Correction

Because the fluids were confined in the cylinders in the present experiment, the projected area of a settling particle decreased the effective cross-section area of the cylinder, requiring the fluid to move around the particle with a greater velocity than if the fluid were infinite in extent. This will increase the drag force of the particle and decrease its terminal settling velocity. This effect is usually called the "wall-effect" and it must be corrected before the experimental data of the particle settling velocity can be used for analysis of the drag coefficient. In this study, the following two simple empirical equations[26] were selected to take into account the wall effect. For the laminar settling regime:

$$F_W = 1 - (d_S/d)^{2.25} \qquad (7\text{-}40a)$$

and for the turbulent settling regime:

$$F_W = 1 - (d_S/d)^{1.5} \qquad (7\text{-}40b)$$

The wall-free settling velocity can then be calculated by:

$$v_S(\text{corrected}) = v_S(\text{measured})/F_W \qquad (7\text{-}41)$$

7.4.5. Experimental results

The experimental data of the settling velocities for both the spherical and non-spherical particles have been listed in Table (7-4). For spherical particles, by regressional analysis, the values of the constants "a" and "b" defined in Eq.(7-35) were obtained which are

TABLE (7-4): Experimental data of the settling velocities of variously shaped particles in power-law fluids

Particle Size [mm]	Particle Density [g/cm^{-3}]	OIL ρ_f=0.88 [g/cm^{-3}] μ =1.653	CMC =1.015 n=0.798 K=1.940	CMC+XC =1.002 =0.627 =1.696	CMC+XC =1.003 =0.597 =4.579	CMC+XC =1.003 0.449 =7.688
		Settling Velocities v_s [cm/sec]				
Particle Material: Proppant			Shape: spherical			
0.3	3.71	0.19	0.23	0.28	0.07	
0.4	3.22	0.18	0.28	0.35	0.09	
0.65	....	0.33	0.46	0.54	0.13	
0.8	....	0.46	0.61	0.75	0.2	
Particle Material: Sands			Shape: Roundish			
1.2	2.63	0.68	1.13	1.65	0.47	0.11
1.5	...	1.21	1.64	2.81	0.66	0.28
1.8	....	1.97	2.21	4.49	1.14	0.43
2.2	....	2.27	2.64	5.31	1.41	0.64
Particle Material: Glass Beads			Shape: Spherical			
4.0	2.63	7.06	9.31	20.38	7.82	5.11
6.0	....	13.0	16.8	31.25	15.7	13.7
15.5	2.47		53.5		60.1	67.5
Particle Material: Steel			Shape: Spherical			
3.17	7.75	17.05	25.8	57.74	30.2	32.3
3.97	....		34.9	76.56	41.9	47.8
5.0	....		46.2		60.0	66.2
6.34	....		66.5		77.0	105

TABLE (7-4): Continue ···

Particle Size [mm]	Particle Density [g/cm^{-3}]		CMC ρ_f=1.015 n=0.798 K=1.940	CMC+XC =1.002 =0.627 =1.696	CMC+XC =1.003 =0.597 =4.579	CMC+XC =1.003 0.449 =7.688
			Settling Velocities v_s [cm/sec]			
Particle Material: Plastic			Shape: Disk			
6.4x2.2	2.28		7.95/U	12.66/F	7.23/E	3.73/E
9.6x3.2	....		13.1/F	21.21/F	11.1/F	12.5/E
Particle Material: Aluminium			Shape: Disk			
6.4x2.1	2.7		10.1/U	17.6/F	10.1/U	9.15/E
9.7x3.1	....		17.6/F	28.85	16.6/F	14.9/F
Particle Material: Aluminium			Shape: Rectangular			
5.9x4.1x2.1	2.7		8.67/U	15.67/F	10.1/U	6.23/E
10x8.0x2.1	....		12.1/F	20.27/F	10.4/F	13.7/U

Note: 1) The values for fluid rheological properties are in c.g.s units

2) E — Edgewise F — Flatwise U — Unstable

3) Settling velocities shown here are the average values of 4 - 8 data points.

TABLE (7-5): Drag coefficient correlations for spherical particles in the laminar settling regime

FLUID	n	$C_D = \frac{a}{(N_{Rep})^b}$	N_{Rep}	DATA POINTS	AVERAGE ERROR %
OIL	1.00	$C_D = \frac{32.1}{N_{Rep}^{0.888}}$	0.003-3	11	14.87
CMC	0.8	$C_D = \frac{32.75}{N_{Rep}^{0.824}}$	0.006-4	9	12.60
CMC-XC	0.63	$C_D = \frac{33.24}{N_{Rep}^{0.878}}$	0.01-3	8	15.7
	0.60	$C_D = \frac{33.63}{N_{Rep}^{0.936}}$	0.001-3	8	12.96
	0.45	$C_D = \frac{35.9}{N_{Rep}^{0.989}}$	0.002-1	5	4.10

TABLE (7-6): Drag coefficient correlations for spherical particles in the transitional settling regime

FLUID	n	$C_D = \frac{a}{(N_{Rep})^b}$	N_{Rep}	DATA POINTS	AVERA. ERROR %
CMC	0.8	$C_D = \frac{23.83}{N_{Rep}^{0.731}}$	3-100	7	2.87
CMC+XC	0.6-0.63	$C_D = \frac{27.07}{N_{Rep}^{0.803}}$	2-130	13	6.84
	0.45	$C_D = \frac{32.18}{N_{Rep}^{0.847}}$	1-150	7	5.46

shown in Table (7-5) and (7-6) for the laminar and transitional settling regimes, respectively. Based on the experimental results, the following equations can be used to approximate the values of "a" and "b" for various values of 'n' and under different settling regimes:

$$a = 39.8 - 9 \cdot n$$
$$b = 1.2 - 0.47 \cdot n \qquad (N_{Rep} < 5 \ , \ n > 0.45) \qquad (7\text{-}42)$$

$$a = 42.9 - 23.9 \cdot n$$
$$b = 1 - 0.33 \cdot n \qquad (1 < N_{Rep} < 200) \qquad (7\text{-}43)$$

Because of the difficulty in tracing the particles with the video camera when they settle too fast, only limited data for particle settling velocity in the turbulent settling regime have been obtained. These data showed that the drag coefficient in the turbulent settling regime becomes basically a constant and the value of this constant depends on the flow behaviour index n. However, the present author suggests using the following approximations in the absence of more detailed and reliable data:

$$a = 0.35$$
$$b = 0 \qquad (N_{Rep} > 200) \qquad (7\text{-}44)$$

Based on the experimental data for non-spherical particles, the shape factor, F_s, can be approximated by following empirical equations:

$$F_s = 1.5 - 0.5 \cdot \psi \qquad (N_{Rep} < 1) \qquad (7\text{-}45)$$

$$F_s = 2.6 - 1.6 \cdot \psi \qquad (N_{Rep} > 1) \qquad (7\text{-}46)$$

in which the sphericity ψ can be calculated for disks and rectangular plates using Eqs.(7-36) and (7-37), respectively. For spherical particles, $\psi = 1$ and $F_s = 1$.

More detailed presentation and analysis of the experimental results may be found in reference (27).

7.4.6. Particle Settling Velocity in Dynamic Fluids

The present experiment has been conducted only in stagnant fluids. In dynamic fluids, because there is a fluid velocity profile across the flow channel, i.e. from zero on the boundary to a maximum value in the middle, the position of the particle during settling must be recorded continuously in addition to allow measuring of the particle's velocity in the experiment. Then the fluid velocity distribution surrounding the particle during settling may be taken into account and the particle settling velocity be calculated correctly. Unfortunately this work has not been done so far because of the difficulty in determining the particle's position during settling in dynamic fluids.

There have always been some arguments regarding the difference between the particle settling velocity in stagnant fluids and that in dynamic fluids. Some investigators[28,29] claimed, based on their experimental results, that the particle settling velocity was basically independent of the fluid velocity. But some investigators[22,30] argued that a particle in a shear-thinning fluid should settle faster when the fluid is dynamic than when it is stagnant because of the additional shear rate imposed by the fluid motion.

In the present author's opinion, when fluid is in laminar flow, the shear rate distribution around a settling particle should be mainly dominated by the particle's motion relative to the fluid and the

influence of the fluid motion itself may be negligible. However if the fluid motion is turbulent, the turbulences and the eddies may well penetrate into the zone near the particle surface even when the particle's velocity relative to the fluid is low. So the influence of the fluid motion on the shear-rate distribution around the particle may not be negligible in this case.

The present author intuitively speculates that the influence of the fluid motion on the shear rate distribution around a settling particle may depend upon the ratio of the Reynolds number of the fluid flow to the particle Reynolds number, i.e.

$$F_{Re} = \frac{N_{Re}}{N_{Rep}} \qquad (7-47)$$

When the value of F_{Re} is relatively small, the influence of the fluid motion on the particle's settling velocity is negligible. The degree of the influence of the fluid motion increases with increasing the value of F_{Re}, and there is a limit to the F_{Re} value beyond which the influence of the fluid motion becomes important while the effect of the particle's velocity relative to the fluid becomes negligible.

However, before this problem has been fully investigated, it is suggested that, if a non-Newtonian fluid is in laminar motion, the equivalent viscosity for a particle settling in the fluid should be determined based on the relative velocity between the particle and the fluid, i.e. based on the particle settling velocity. In this case, the particle settling velocity model developed in the present study, i.e. Eq.(7-39), may be used directly in dynamic fluids. If the fluid is in turbulent flow, the fluid surrounding the particle should be also considered as in turbulent flow and the particle should be considered as settling in the turbulent settling regime, regardless of the particle's

velocity relative to the fluid. In this case, by setting $a = 0.35$ and $b = 0$, Eq.(7-39) may be used to approximate the particle settling velocity in turbulent fluid flow.

CHAPTER 8.

FACTORS AFFECTING CUTTINGS TRANSPORT DURING OILWELL DRILLING — THEORETICAL ANALYSIS AND LITERATURE REVIEW

In the first part of the thesis, theoretical studies on the non-Newtonian annular flow was performed and as the result, we now have a fairly good, though not complete, understanding of the characteristics of drilling fluid flow through drilling annuli. Then in the preceding chapter, we investigated drilled cuttings settling velocities in drilling fluids. With this fundamental knowledge in hand, we are going to examine drilled cuttings transport process itself in this chapter.

Numerous variables can be named which affect cuttings transport during drilling operations. Some of the variables can be specified in the drilling programme design and controlled during drilling operations while some other variables can not be specified and controlled. Instead, when cuttings transport occurs to be a problem during drilling operations because of the effects of those uncontrollable variables, the controllable variables must be adjusted to ensure hole cleaning. The controllable variables include annular fluid velocities, fluid flow regimes, rheological properties and densities of drilling fluids, hole angles, drillpipe rotary speeds, cuttings concentrations (drilling penetration rate) and the annular size (sometimes). The uncontrollable variables include the cuttings sizes and densities, the annular size (sometimes) and annular geometry, etc.

The above named variables are only the most relevant controllable and uncontrollable variables and certainly there are some other variables which also affect cuttings transport. However, if the effects of all the variables were to be studied, the work would be rather formidable and also unnecessary. Therefore, from the practical

standpoint, investigations into cuttings transport have been conducted in the past towards understanding those most relevant and important variables.

In this chapter, the effects of above named most relevant variables on cuttings transport will be examined individually based on both the previous and the present theoretical studies and the experimental results.

8.1. Annular fluid velocity

The annular fluid velocity is usually evaluated in terms of its average velocity, v_f, which is equal to the circulating rate divided by the annular cross-setion area, though there is a velocity profile across the annulus. This parameter has long been recognized as the most important factor affecting cuttings transport in both vertical and inclined annuli.

In vertical annuli, we have shown in Chapter 6 that the carrying capacity of drilling fluids may be evaluated by using an indicator called the "cuttings transport ratio" which is defined as:

$$F_T = 1 - \frac{v_s}{v_f} \qquad (6\text{-}2b)$$

The higher the value of F_T, the better the cuttings transport performance. We have also shown that both the cuttings transport velocity, v_t, and the cuttings transport ratio, F_T, increase with increase of the annular fluid velocity, v_f. In fact, this may be shown mathematically from the derivative of Eq.(6-2b):

$$\frac{dF_T}{dv_f} = \frac{v_s}{v_f^2} > 0 \qquad (8\text{-}1)$$

Therefore there is no doubt that increasing the annular fluid velocity is advantageous to cuttings transport. However, taking the second derivative of Eq.(6-2b) yields:

$$\frac{d^2F_T}{dv_f^2} = \frac{-2 \cdot v_s}{v_f^3} < 0 \qquad (8\text{-}2)$$

So mathematically the rate of increase of the cuttings transport ratio, F_T, will decrease with increase of the annular fluid velocity, v_f. Fig.(8-1) qualitatively illustrates the increase of the cuttings transport ratio with increase of annular fluid velocity in vertical annuli.

Sifferman, et.al.[2] reported based on experimental results that the cuttings transport ratio increased with increase of the annular fluid velocity but began to level out or increased more slowly in the velocity range of 100 to 200 ft/min.

For field operations, the requirement for lifting cuttings to the surface determines a minimum allowable fluid velocity (say 100 ft/min, depending upon the particular situation), and this minimum velocity is determined mainly based on the cuttings settling velocity. On the other hand, the hole condition often dictates that the annular fluid velocity must be below some upper limit beyond which sloughing and wash-out would occur and an enlarged hole result (though it is only a speculation). Also a higher fluid velocity will result in a higher annular pressure loss, thus higher differential pressure on the bottom of the hole and this will reduce the drilling rate. Therefore the drilling hydraulic programme is often designed so that the annular fluid velocity is in

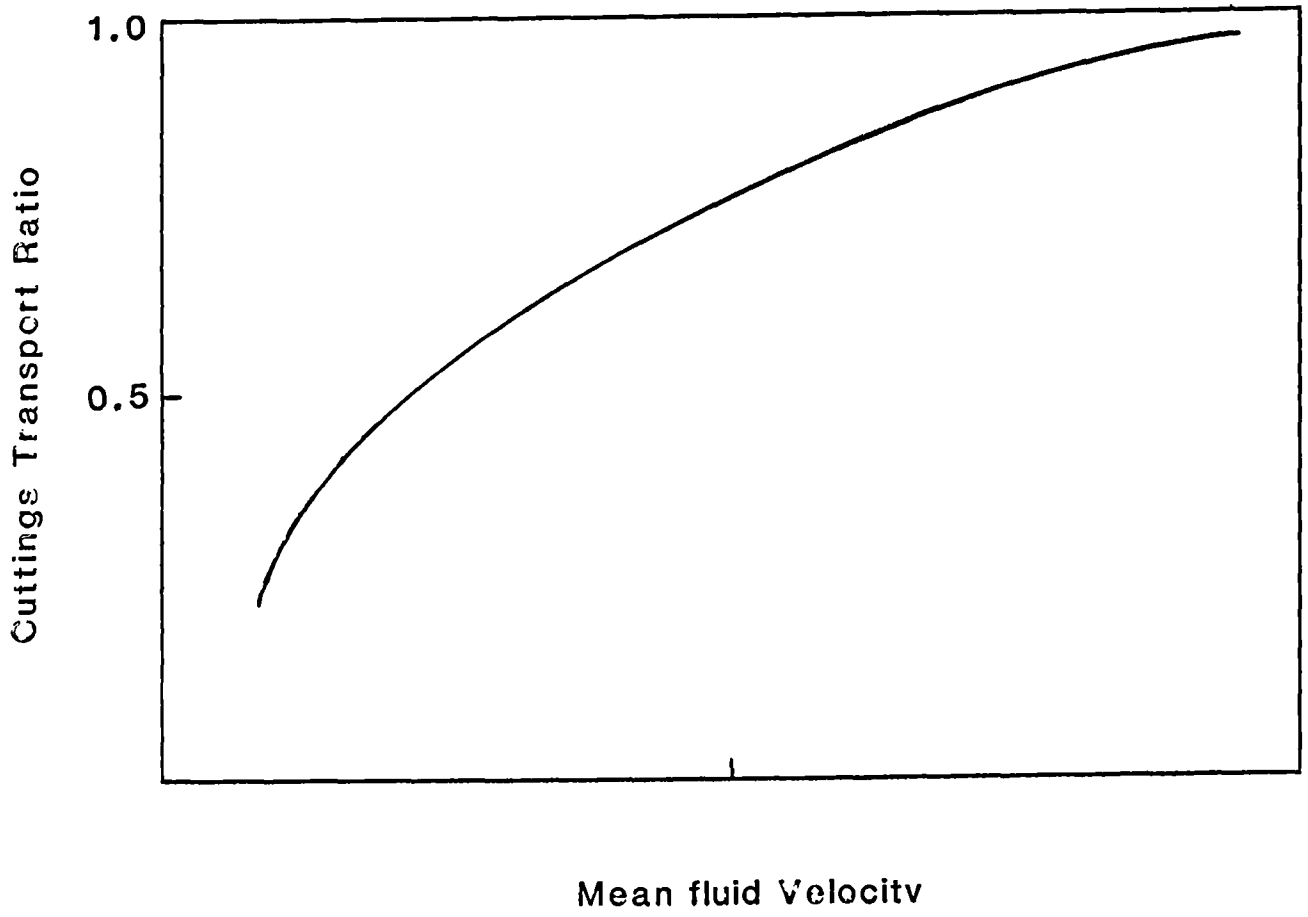

Fig.8-1 Increase of the cuttings transport ratio with increase of the annular fluid velocity

the region between the lower and upper limits and at the same time one of the bit hydraulic parameters (say horsepower or impact force) can be maximised and the most efficient operation achieved.

For the minimum annular fluid velocity, Williams and Bruce[31] suggested 100 to 125 ft/min if turbulent flow could be maintained. Hopkin[32] suggested 20 to 30 ft/min during hard rock drilling and up to 200 ft/min during very fast upper-hole drilling, in excess of the maximum settling velocity of the cuttings.

In inclined annuli, the cuttings tend to settle out and form a cuttings-bed on the low-side wall of the wellbore and the concomitant reduction in annular flow area leads to a higher effective fluid velocity, as reported by Tomren, et.al.[5]. In this case the cuttings transport ratio can not be used as an indicator of the cuttings transport performance.

Tomren, et.al.[5] reported based on their experimental results that higher fluid velocity gave more effective hole cleanning at all hole angles, regardless of the fluid viscosities and flow regimes. Based on their experimental results, it may be seen that the annular fluid velocity required to keep the hole clean in an inclined annulus is generally higher than that in the corresponding vertical annulus.

It should be noted that, although a large amount of experimental work [33,5,6,39,4] has been conducted on cuttings transport in inclined annuli, very limited effort[3,4] has been made to investigate the minimum fluid velocity which is required in order to keep an inclined annulus clean. So far, there is still no reliable knowledge on design of cuttings transport for hole cleanning during directional drilling. The investigations conducted by the present author will be presented in Chapter 9 and Chapter 10.

8.2. Annular flow regime

It has long been known that two distinct types of flow, i.e. laminar and turbulent flow, are encountered in the movement of fluid elements and between them there is a region of transitional flow. The determination of the annular flow regime may be accomplished by calculating the Reynolds number which may be defined as:

$$N_{Re} = \frac{d_{eq} \cdot v_f \cdot \rho_f}{\mu_e} \qquad (8\text{-}3)$$

Laminar flow is generally thought to occur below a N_{Re} value of about 2100 and turbulent flow above 2100. The distributions of the local velocities in the two types of flow are distinctively different. In laminar flow, the fluid elements follow the streamlines and there is a parabolic velocity profile across the flow. As one goes from the walls of an annular space into its hydraulic centre, the fluid velocity will increase from zero to a maximum value. In turbulent flow, however, the fluid elements move in countless eddies and swirls and the "time mean values" of the local velocities are almost constant throughout its cross-section compared with those in laminar flow. The difference in nature of these different types of flow will affect the carrying capacity of drilling fluids.

Williams and Bruce[31] stated that, in laminar flow, cuttings would be turned against walls and slide down alone the walls for a distance because of the fluid velocity difference from the walls to the central part of the flow. They referred to this phenomenon as the "torque effect". They concluded that turbulent flow was advantageous over the laminar flow from the standpoint of removing cuttings.

Because of the existence of the velocity profile across the annular

space in laminar flow, Zeidler[17] thought that the concept of the transport velocity, v_t, which is based on the mean annular fluid velocity, could not adequately predict the removal and transport of cuttings in laminar flow.

Hopkin[32] observed in his experiments that the cuttings might tend to be kept in the central higher velocity region in laminar flow for some reason, e.g. the centrifugal force developed on the cuttings by the drillpipe rotation.

Tomren, et.al.[5] and Okrajni and Azar[6] observed that cuttings transport performance in deviated wells would be improved in turbulent flow.

Based upon the above studies, a conclusion may be drawn that turbulent annular flow has an advantage over laminar flow in cuttings transport in both the vertical and inclined drilling annuli, though the results of these studies are not completely consistent. The improvement of cuttings transport under turbulent flow may be attributed to:

i) the flattened fluid velocity profile, thus higher fluid velocity in the near-wall region and smaller "torque effect";

ii) the destructive action of the countless eddies and swirls in turbulent flow on the cuttings bed in inclined annuli.

On the other hand, it should be mentioned that the effect of the hydraulic action of annular flow on wellbore stability should not be ignored. It is generally thought that sloughing and wash-out of the wellbore may take place more likely in turbulent flow than in laminar flow because the fluid velocity is higher near the wellbore in turbulent flow. Although there is hardly any evidence for this speculation, caution should be exercised should turbulent flow be designed for

better cuttings transport performance in a drilling programme.

8.3. Viscosities of drilling fluids

In a vertical annulus, the way in which the fluid viscosity affects cuttings transport depends totally upon how it affects the cuttings settling velocity, provided the annular flow regime remains the same. Generally speaking, the resistant force to settling of cuttings, i.e. the fluid drag force, increases with an increase in viscosity, so the cuttings settling velocity decreases as the fluid viscosity increases. Therefore high viscosity should be advantageous in transporting cuttings. In the laminar settling regime, the cuttings settling velocity is inversely proportional to the fluid viscosity. As the fluid flow regime around settling cuttings changes from laminar to turbulent, the rate of decrease in settling velocity with increasing viscosity decreases, and in turbulent settling, the viscosity effect can be almost neglected. Therefore it may be expected that the viscosity effect on cuttings transport is more pronounced in laminar settling than in turbulent settling.

Sifferman, et.al.[2] reported the increased cuttings transport ratio with increase of viscosity.

Hussaini and Azar[34] concluded that apparent viscosity, yield point and initial gel strength had a significant effect on cuttings transport at low and medium annular fluid velocities, but had no effect at high velocities. They also claimed that increasing the ratio of yield strength to plastic viscosity increased the carrying capacity of the drilling fluids.

Tomren, et.al.[5] concluded that, within a particular flow regime, fluids with higher viscosities gave better cuttings transport.

However, they also claimed that, low viscosity fluids in turbulent flow performed just as well as high viscosity fluids in laminar flow.

Hopkin[32] reported a different conclusion: the cuttings settling velocity was found to be approximatelly constant up to a funnel viscosity of about 90 sec/qt or to a yield value of 15 $lb/100ft^2$. Only increasing the funnel viscosity or yield value above these values would effect a significant reduction in the particle settling velocity.

Williams and Bruce[31] reported that high-viscosity, high-gel fluids returned a larger percentage of the large cuttings. However they also reported that, for small and medium sized cuttings, low-viscosity, low-gel fluids transported the cuttings to the surface more rapidly and also brought up larger percentages of the cuttings than did the high-viscosity, high-gel fluids, espeacially for the medium sized cuttings. They concluded that low-viscosity and low-gel strength were advantageous in removing cuttings, which is in contradition with the conclusions drawn by other investigators and what is theoretically expected. The possible explanation is that the low-viscosity, low-gel fluids used in their experiments were in the turbulent flow regime while the high-viscosity, high-gel fluids were in the laminar flow regime. As they reported, when the flow was laminar, most cuttings were easily turned on edge and forced to the walls where the local fluid velocity was much lower than the average fluid velocity. So these cuttings may lodge in the hole, as claimed by Prokop[35].

From the above studies it may be seen that the conclusions drawn based on the experiments in vertical annuli are generally consistent with what have been expected theoretically, though there are some contradictions. Also it may be seen that the fluid viscosity effect on the cuttings settling velocity or on cuttings transport is closely related to the fluid flow regime. However one point must be clarified:

the cuttings settling regime and the annular flow regime are two different concepts. It is the fluid flow regime around settling cuttings, i.e. the cuttings settling regime, not the annular flow regime, that changes the viscosity effect on the cuttings settling velocity. This clarification is necessary because there are cases where the annular fluid flow is laminar but the cuttings in the fluid are in turbulent settling and thus the viscosity effect is that under the turbulent settling regime. Most of the previous investigators failed to state this point explicitly in their papers.

In inclined annuli, the situation will be different because the way in which the fluid viscosity affects cuttings transport does not depends upon how it affects the cuttings settling velocity, but mainly depends upon how it affects the annular flow regime. Theoretically it is expected that, if the annular flow regime (laminar or turbulent) can be maintained, then the higher viscosity fluid will give better cuttings transport but the effect should be small; however if the annular flow regime changes with change of the fluid viscosity, the cuttings transport may be affected appreciably.

In inclined annuli, Tomren, et.al.[5] reported that, within a particular regime, fluids with higher viscosity gave better cuttings transport. Okrajni and Azar[6] reported that, under the laminar flow regime, the viscosity effect was slight or even negligible for high-angle wells. Under the turbulent flow regime, they reported that the cuttings transport was generally not affected by the mud rheological properties. Note that the conclusions drawn by Tomren, et.al.[5] and by Okrajni and Azar[6] are not consistent in terms of the viscosity effect in the turbulent annular flow regime.

8.4. Densities of drilling fluids and cuttings

In drilling annuli, settling of cuttings in drilling fluids is due to the effective gravitational force acting on the cuttings, whose magnitude depends upon the density difference between the cuttings and the fluid. Decreasing the density difference $(\rho_s - \rho_f)$ will decrease the effective gravitational force, thus decrease the settling velocity of the cuttings and increase the carrying capacity of the drilling fluid. Therefore it is obvious that higher density drilling fluids are advantageous in removing cuttings.

Williams and Bruce[31], Hopkin[32] and Sifferman, et.al.[2] concluded from their experimental results that increasing the density of a drilling fluid would result in an increase in its carrying capacity, but Sifferman, et.al.[2] further stated that the effect was less pronounced at higher fluid velocities.

However, for field operations, the use of higher density drilling fluids to clean the hole is normally impractical, unless the density is required to contain the formation pressure.

8.5. Size and shape of drilled cuttings

Both the gravitational force and the drag force acting on a settling particle in liquid will increase with increase in the particle's size but the net effect is that of increasing the gravitational force. Therefore, in vertical annuli, it is obvious that increasing in cuttings size will increase the cuttings settling velocity and thus decrease the cuttings transport ratio.

The experimental results of Williams and Bruce[31], Sifferman, et.al.[2] and Walker and Mayes[21] showed the effect of decreasing the

carrying capacity with increasing the cuttings size in vertical annuli.

In inclined annuli, the effect of the cuttings size on cuttings transport should be similar to that in vertical annuli, though there is still no experimental evidence to support this speculation.

As for cuttings shape, in the preceding chapter we have shown that the shape effect on the cuttings settling velocity may be evaluated by using a parameter called the "sphericity" of the cuttings, Ψ. For spherical cuttings, $\Psi = 1$. The more non-spherical the cuttings, the smaller the value of Ψ, the higher the fluid drag force to cuttings settling and accordingly the lower the cuttings settling velocity in drilling fluids. Therefore it is easier to transport non-spherical cuttings than spherical ones in vertical annuli, provided the volume equivalent diameters of the cuttings remain the same.

In inclined annuli, the situation will be different because the cuttings tend to settle out and form a cuttings-bed on the low-side wall of the annulus. It is yet to be investigated how the cuttings shape will affect transport of those cuttings in the cuttings-bed.

In addition to the size and shape, cuttings orientation during settling also affects cuttings settling velocity, and accordingly affects the carrying capacity of drilling fluids in vertical annuli.

Pigott[36] and Hall, et.al.[1] thought that cuttings tended to be carried up in the position of greatest resistance to the flow past it, i.e. the broadside to the flow, so the settling velocity was lowered.

Williams and Bruce[31] reported that, in laminar annular flow, disks with thickness to diameter ratios ranging from 0.3 to about 0.8 usually were transported flatwise and would turn on edge if the ratios were less than 0.3 or greater than 0.8. The cuttings with the ratios less than 0.3 were difficult to remove from the wellbore.

Tomren, et.al.[5] reported that, in laminar annular flow, the

cuttings near the annular outer-wall travelled edgewise while those at the centre travelled flatwise, and in turbulent annular flow, cuttings orientation appeared to be random with most of the cuttings travelling flatwise and distributed away from the outer-wall.

Walker and Mayes[21] reported that, in stagnant fluids, flat fall always occured above a particle Reynolds number of 13 and edge fall occured predominantly below 3.5 and unstable fall occured in the range of 2.5 to 10.

According to the experiments conducted by the present author in stagnant fluids, the orientation of a non-spherical particle during settling is independedt of its orientation when entering the fluid. The orientation during settling is that which would offer the greatest possible resistance to its settling. When the generalised particle Reynolds number N_{Rep} is above about 10, a plate-like particle settles flatwise and would turn on edge if N_{Rep} falls below about 1. In the range of $1 < N_{Rep} < 10$, unstable settling results and no preferred orientation can be noted. A detailed drag force analysis with different settling orientations has also been performed by the present author which may be seen in the reference (27).

8.6. Drillpipe rotation

When the drillpipe is rotated, a tangential component of the fluid velocity will be induced and annular helical flow be developed in the drilling annulus. The detailed analysis of annular helical flow for power-law fluids has been performed in Chapter 4. Theoretically the introduction of the tangential component of the fluid velocity due to the drillpipe ratation in a drilling annulus may influence the cuttings behaviour in the following two respects:

(i) in vertical annuli, the cuttings will be transported in a spiral or helical path, instead of in a straight upward path in the case of no drillpipe rotation, thus a centrifugal force will be induced which will push the cuttings outwards across the annulus. As different axial fluid velocities, which are responsible for transporting cuttings, exist across the annulus, local cuttings transport velocities will be affected by cuttings outward movement;

(ii) the drillpipe rotation may sometimes induce some additional turbulences and this may also affect the cuttings behaviour in the annulus. Particularly in high-angle wells where a cuttings-bed has been formed on the low-side wall of the wellbore, these additional turbulences may provide some mechanical destructive action on the cuttings-bed and help to remove these cuttings out of the cuttings-bed.

All of the experimental results obtained by previous investagtors [1,2,5,6,17,31,32,37] showed increased cuttings transport with pipe rotation, though only a minor effect was reported by some of them.

Williams and Bruce[31] thought that in the laminar annular flow, the centrifugal force induced by pipe rotation would throw the cuttings into the higher velocity region which exists in the central portion of the annulus and thus prevent the cuttings from slipping down along the wall of the drill pipe. But they claimed that the effect was not so pronounced for fluids in turbulent flow.

Thomas, et.al.[37] reported an increased average cuttings rise velocity with increasing drill pipe rotary speed and this phenomenon was more pronounced at a lower annular fluid velocity and appeared to be negligible at a higher fluid velocity. They further stated that there was a threshold value beyond which further increase in rotary speed seemed to have no effect on the cuttings rise velocity. They claimed

that this threshold rotary speed was about 20 rpm based on their experiment. If this is true, then the effect of the pipe rotation on cuttings transport during normal drilling operations, where the rotary speed is usually much higher, would be negligible. This may be explained by considering that if the rotary speed is too high, the induced centrifugal force may be so strong that the cuttings may be thrown outwards, past the central higher velocity region and into the lower velocity region near the outer-wall where the cuttings may slide down along the outer-wall, as they would do near the central pipe-wall.

In inclined annuli, Tomren, et.al.[5] thought that the effect of the centrifugal force to swirl the cuttings into the central higher velocity region in the annulus was minimized by the stronger tendency of the cuttings to settle through the fluid and form a cuttings-bed on the low-side of the wellbore. They claimed only a slight effect of the pipe rotation on cuttings transport in an inclined annulus.

Okrajni and Azar[6] reported that an increase in rotary speed provided better cuttings transport and this effect was more pronounced at higher hole angles.

8.7. Drillpipe/hole eccentricity

Usually the drillpipe is positioned eccentrically relative to the wellbore, particularly in deviated wells where the drillpipe has a strong tendency to offset towards the low-side wall of the wellbore because of the gravity effect. The change of the pipe position in the wellbore will result in the different fluid velocity profile across the annulus and this will affect cuttings transport. Based on the theoretical studies performed by the present author[38] and other investigators(see Chapter 3), in an eccentric annulus, the fluid

velocity will be reduced in the reduced area while it will be increased in the enlarged area. This relative change in fluid velocity depends upon the drillpipe/hole eccentricity. The greater the eccentricity, the greater the relative reduction of the velocity in the reduced area and greater the relative increase of the velocity in the enlarged area.

In vertical drilling annuli, Sifferman, et.al.[2] showed a slightly better cuttings transport in an eccentric annulus but Thomas, et.al.[37] reported that there was no definite trend regarding the effect of the pipe/hole eccentricity.

Tomren, et.al.[5] reported that, in vertical annuli, cuttings behaviour was nearly the same for all eccentricities. The only difference was that there was noticeable reduction in cuttings velocities in the reduced area of the annuli. But since a corresponding increase in cuttings velocities occurred in the enlarged area, the effects appeared to cancel out with each other.

In inclined annuli, Tomren, et.al.[5] reported that the cuttings bulid-up was lowest when the pipe was concentric with the wellbore. Okrajni and Azar[6] reported that higher annular cuttings concentration was observed when the pipe was positioned eccentrically, especially for high-angle wells under the laminar annular flow.

Based on the theoretical analysis performed by the present author[38], in a deviated well, since the drillpipe has a strong tendency to offset towards the low-side wall of the wellbore due to the gravity effect, the fluid velocity in this low-side region will be reduced, or say , be lower than in other regions, in the eccentric annulus. At the same time, since the gravity effect will also cause the cuttings to be transported through the annulus in the low-side region, it may be concluded that the drillpipe offset towards the low-side wall of the wellbore will reduce the cuttings transport velocity and

accordingly reduce the carrying capacity of drilling fluids.

8.8. Cuttings concentration (drilling rate)

Various particle settling velocity models, e.g. Stokes' law and Newton's law models (see Chapter 7), are generally developed based on the assumption that the particle concentration in the fluid is sufficiently low and thus the particles are sufficiently separated in the fluid so as not to collide or interact with each other. However this is not true under most circumstances and some hydrodynamic interference and collisions between the particles will occur as the particles settle through the fluid. As a result, the settling velocity will be normally lower than that calculated from the settling velocity models. Govier and Aziz[11b] have given an extensive discussion on this problem and on various correlations to account for the effect of the particles concentration on the settling velocity.

For cuttings transport, based on experimental results of Sifferman, et.al.[2], there is no consistent trend for the effect of the cuttings feed concentration on cuttings transport. But they claimed that certainly the effect was minor in the range of 0 to 6% by volume. This is probably because the effect of the cuttings concentration is normally over-shadowed by other more important factors.

For drilling operations, many investigators suggested that the cuttings concentration in the annulus should be maintained below a certain limit beyond which down-hole troubles like stuck pipe, high torque and drag, etc. may result. Pigott[36] suggested in as early as 1941 that this limit should be about 5% by volume and this has been commonly accepted in practice for vertical drilling. However, Iyoho[33] thought that a limit of 5% by volume was too conservative, especially

in inclined annuli where concentrations several times higher could be expected in drilling operations.

The equation for calculating the cuttings concentration in vertical drilling annuli has been derived and given in Appendix (A6-1).

In inclined annuli, as the cuttings transport ratio can not be used as a criterion of the cuttings transport performance, some investigators [5,6,39] used the in-situ cuttings concentration instead, as an alternative cuttings transport indicator. In the present author's opinion, this method is not acceptable for field applications because of the following reasons:

(i) there is no reliable method to predict the cuttings concentration in the inclined section of the annulus for directional drilling operations;

(ii) merely using the in-situ cuttings concentration is not adequate to indicate the cuttings transport performance in inclined annuli because this parameter does not take into account the cuttings size effect, which is rather important. This may be better understood by considering the following case. Assume there are two inclined annuli both of which have the same cuttings concentration. But in one annulus cuttings are larger in size and in the other cuttings are smaller. Then it is possible that the annulus with larger cuttings may have a cuttings bed formed on the low-side wall and thus may result in some problems during drilling operations while in the annulus with smaller cuttings, no cuttings-bed is formed and all the cuttings can be transported smoothly out of the hole without any trouble.

In the following two chapters, we will investigate what criterion should be used to indicate the cuttings transport performance in

inclined annuli.

8.9. Hole angle

Unlike the case of a vertical drilling annulus, the axis of an inclined annulus is not in the same direction as the gravity force. So there is always a tendency of the cuttings to settle vertically downwards and towards the low-side wall in a inclined annulus as being transported with the flow of drilling fluids. If we take the axis of the annulus as the z-axis in a cylindrical coordinate system, then there are two components of the cuttings velocity if the drillpipe is not rotated, one is the axial component and another the radial component. The cuttings are transported up to surface with a rate which equals the axial component velocity while the radial component causes the cuttings to move towards the low-side wall of the wellbore. If the fluid force generated by the flow is not strong enough to keep the cuttings in suspension, the cuttings will settle on the low-side wall, accumulate and form a cuttings-bed there. This is a potentially dangeous situation during drilling operations and may result in serious troubles such as stuck drillpipe, high torque and drag, etc. Since the radial component of the cuttings velocity increases with increase of the hole angle from vertical, it may be speculated that cuttings transport will be worsened at a higher hole angle.

As advances of the directional drilling technique and the development of the offshore oil industry since the 1970's, more and more attention has been attracted towards investigations of cuttings transport in deviated wells. Several experimental studies [5,6,39,4] have been reported so far. Based on these experiments, the major characteristics of cuttings transport in inclined annuli have been

Table 8-1: The major characteristics of cuttings transport in inclined drilling annuli[5,6]

Hole Angle ϕ	V_f ft/sec	Characteristics
$\phi \leq 10^\circ$	1 - 4	Similar to, but slightly worse than that in vertical annuli. No cuttings bed was formed.
$10^\circ \leq \phi \leq 30^\circ$	≤ 2	Unstable bed. Bed height $< \frac{1}{8}$ in
	≤ 3	Transported mostly along the low-side wall of the annulus in clusters or slugs.
	3 - 4	Transported smoothly along the low-side wall with a radial concentration gradient as heterogeneous flow.
$30^\circ \leq \phi \leq 60$	≤ 3	Bed was formed and slide downward along the low-side wall by gravity against the flow.
	3 - 4	Bed was unstable and broken in places, cuttings were transported in slugs.
$60^\circ \leq \phi \leq 90^\circ$	1 - 4	Bed was formed but did not slide downward even when circulation was stopped.

summarised in Table (8-1).

Special attention should be given to the situations where the hole angles are in the range of 35 to 55 degrees, which are referred to as the "critical angles". According to the experimental results[5,6], when the hole angle is between 35 to 55 degrees, not only the cuttings bed will be formed, but also it will slid downwards along the wall by gravity if the annular fluid velocity is not high enough. Obviously this sliding-down phenomenon depends on the friction coefficient between the cuttings and the wall of the wellbore under the "wet" condition. This "wet" friction coefficient is affected by many factors including the smoothness of the surfaces of the wellbore and the cuttings, the shape of the cuttings and the properties of the drilling fluid, etc. Because all the previous experiments were conducted under the different conditions from those in the field operations regarding these respects, it is hard to say whether this phenomenon will actually happen and what is the critical hole angle in inclined drilling annuli.

CHAPTER 9.

MINIMUM TRANSPORT VELOCITY IN INCLINED DRILLING ANNULI — CONCEPT AND LITERATURE REVIEW

As discussed in the preceding chapter, the major concern regarding cuttings transport in inclined drilling annuli is the formation of cuttings-bed on the low-side wall of the hole as this may result in serious trouble such as stuck drillpipe, high torque and drag, etc. during drilling operations. Although a large amount of effort [33,5,6,39,3,4] has been expended during the past ten years towards the investigations into cuttings transport in directional drilling wells, there are still no reliable method to determining what circulating rates of drilling fluids are required for hole cleaning and there is considerable lack of understanding regarding what fluid properties are favourable for cuttings transport during directional drilling. The present chapter and Chapter 10 will be dedicated to the investigations into the problems of cuttings bed formation in inclined drilling annuli.

According to the previous experimental results[5,6], in an inclined annulus where a cuttings-bed has been formed, a pseudo-equilibrium state exists between the cutting-bed and the free cuttings in the flow stream. Under a given low circulation rate, at the beginning, the cuttings will be gradually accumulated on the low-side wall of the hole and form a stationary "cuttings bed" there until a certain height of the cuttings bed has been formed and thus the cross-section area for the flow been reduced so that the fluid velocity becomes high enough to keep those cuttings not in the bed in suspension, or actually until the rate of build-up of the bed is equal to the rate of bed erosion. Then,

increasing the circulation rate will reduce the thickness of the cuttings bed. If the circulation rate is continuously increased, a critical point will be reached at which the cuttings bed will start to move or disappear and all the cuttings will be transport up to the surface. Obviously, it is this critical circulation rate which is required in order to clean an inclined annulus. Therefore the minimum transport velocity (MTV) for hole cleaning during directional drilling is defined by the present author as the mean annular fluid velocity corresponding to this critical circulation rate.

For many industrial engineering operations, the minimum transport velocity (MTV) is not a new concept. In fact, similar problems have been under investigations for many decades in many engineering operations related to trasnsport of solid-liquid mixtures through pipelines and transport of sediment grains in open channels. However, in the petroleum drilling industry, it is only several years ago that pepole began to realize the importance of MTV for directional drilling programme design. So far, two investigations[3,4] have been conducted and reported on the correlations of MTV for cuttings transport in highly deviated wells and these correlations were developed based on the correlations and the principles used for solid-liquid mixture flow through circular pipes.

In the present chapter, we will begin our discussion with a general review of the basic characteristics of solid-liquid mixture flow through pipelines. Then, previous investigations and various correlations of MTV will be examined individually for transport of solid-liquid mixtures through pipelines, transport of sediment grains in open channels and transport of drilled cuttings in highly deviated wells.

9.1. Characteristics of solid-liquid mixture flow through pipelines

Transport of solid-liquid mixtures through pipelines has been practiced for a long time in civil engineering, mining engineering, mechanical engineering, chemical engineering, etc. The earliest industrial solid-liquid pipeline may date back to 1884[40]. Though only water is usually used as the carrying liquid, the transported solids may be sands or gravels in dredging and similar operations, coal or ores in mining operations, or chemical materials, etc. The transport distance may be as long as over several hundred miles and the pipelines may be up to 18 inches in diameter[11c]. Although this process obviously gives a wet product, the advantages are considerable, for example, ease of installation, operation and maintenance.

The general behaviour of the solid-liquid mixtures flowing in pipelines has been subjected to investigations since the turn of the century[41]. However, it is only within the last four decades, during which a tremendous amount of theoretical and experimental works was conducted, that our understanding of the process has gradually reached a satisfactory level from the standpoint of engineering applications. In this section, we will have a general review of the characteristics of solid-liquid mixture flow through pipelines based on the previous investigations.

9.1.1. General picture

The description of the general behaviour of solid-liquid mixtures is complicated by a number of factors not present in the case of a single liquid phase system. As Govier and Aziz discussed[11d], these factors include:

i) The flow of solid-liquid mixtures may not be characterised merely as laminar or turbulent. The relative quantities and the distributions of the phases must be considered;

ii) Because of the difference in densities between solids and liquids, the distributions of these two phases and their velocities in horizontal or inclined flow may not be symmetrical about the flow axis;

iii) In most cases, solids and liquids move at different mean velocities and thus the in-situ concentrations are not the same as the concentrations at which they are introduced or removed from the system.

Consequently, no general equations can be derived to cover all aspects of solid-liquid mixture flow. However, a general picture of solid-liquid mixture flow may be discribed by considering a case of a sand-water mixture system which flows in a horizontal pipeline and has a solid size and concentration similar to those used in hydraulic transport.

At a relatively low flowrate, the mixture velocity is insufficient relative to the sand settling velocity to maintain the sands in suspension. So the sands will settle out and form a bed on the bottom of the pipe, reducing the cross-section area through which the flow can take place and increasing the mixture velocity in the available space. This continues until an equilibrium state is reached at which the mixture velocity is high enough to maintain the remaining sands in suspension while a stationary and continuous bed of sands exists on the bottom of the pipe. If the flowrate is gradually increased, the thickness of the bed will be gradually reduced and more and more sands come into suspension until the situation emerges where the whole bed begins to move along the bottom of the pipe. The sands in the

immediate vicinity of the bottom of the pipe slide or roll forward whereas the sands on the top of the moving bed move forward by jump or saltation on the bed surface. Eventually, when the flowrate is sufficiently high, the bed will disappear and all the sands will be transported in suspension. There is, however, a vertical concentration gradient across the pipe and most of the sands travel in the lower half of the pipe. Further increasing the flowrate, the sands will be transported in a practically homogeneous suspension.

9.1.2. Flow pattern classification

Based on the above description, flow of solid-liquid mixtures may be generally classified as: [11C,40]:

a. Homogeneous flow pattern

This flow pattern refers to the flow of mixtures in which the flowrate is high enough to keep the solid particles in symmetrical suspension about the axis of the pipe, or in other words, the particles are distributed homogeneously across the pipe;

b. Heterogeneous flow pattern

Because of the difference in densities, solid particles have a tendency to settle out of the liquid and this causes a distortion of the solid concentration profile with more solid particles being contained in the lower than in the upper half of the pipe. More strictly speaking, the heterogeneous flow pattern refers to the flow of the mixtures in which the particles are suspended asymmetrically about the axis of the

pipe and a vertical solid concentration gradient exists across the pipe;

c. Moving bed flow pattern

When the gravitational force causing particles to settle is stronger than the force which lifts them, the particles tend to accumulate on the bottom of the pipe in the form of seperated 'dunes' or a continuous moving bed. The dunes or the bed moves along the pipe at a lower velocity than that of the liquid and the particles are caused to roll and tumble forward by the shear force exerted on them by the liquid flow;

d. Stationary bed flow pattern

If the flowrate is further decreased, thus decreasing the force which drives or lifts the particles, the particles may settle on the bottom of the pipe and rest there to form a stationary and continuous bed with the uppermost particles tumbling over one another. Further decreasing the mixture velocity, the bed will be continuously built up and eventually, the blockage of the pipe occurs.

9.1.3. Particle size classification

The particle size is one of the most important factors that determines the flow behaviour or the flow pattern of a solid-liquid system. According to previous investigators [42,7,43,44,40,11C,45], the behaviour of solid particles such as sand or powered coal in water flowing in horizontal pipes may be generally classified in terms of

particle sizes (or diameters) as follows:

i) Ultra-fine particles, say 30 microns or smaller, are usually transported as homogeneous mixtures, that is, pattern (a) described previously;

ii) Fine particles, about 30 to 100 microns, can no longer be suspended homogeneously but still in a fully suspended state. So there is a particle concentration gradient across the pipe due to the gravity effect. This corresponds to the flow pattern (b);

iii) Medium-sized particles, say 100-1000 microns, may be sometimes transported in a fully suspended state if the mixture velocities are high and the turbulent fluctuations are strong, or may be transported with a moving deposit on the bottom of the pipe. This corresponds to a transitional flow pattern between the flow pattern (b) and (c);

iv) Coarse particles, in the range of 10^3-10^4 microns, are seldom fully suspended under the commonly used velocities in hydraulic transport and usually transported in the moving bed or stationary bed flow pattern. The particles move by succesive jumps or saltations on the bottom of the pipe;

v) Ultra-coarse particles, those greater than 10^4 microns, may not be suspended at any normal mixture velocities in hydraulic transport and only be transported in the moving or stationary bed pattern.

It must be pointed out that the above classification of the flow behaviour of the mixtures based on the particles size are far from complete and the size divisions are very much arbitrary. The flow behaviour of a solid-liquid mixture also depends on many other factors. Furthermore, in most cases, the solid particles consist of not a single size but a considerably wide range of sizes which may cover two or

three size divisions. However, in a general way, the above classification may give some idea of how a solid-liquid system might behave and provide a basis for comparing one system with another if their solid or liquid phases are different.

Based on the above classification, the ultra-fine and fine particles are usually transported in the fully suspended state and are not likely to form a deposit under the usual hydraulic transport conditions. Bearing in mind that our purpose in this chapter is to study the mechanism of bed formation, our attention hereafter will be focussed on the particles larger than 100 microns in diameter.

9.1.4. Pressure gradient behaviour

Another important characteristic of solid-liquid mixtures in horizontal pipes is their pressure gradient behaviour. Measurements of the presure gradient of solid-water mixtures in horizontal pipes were first made and reported in 1906 by Blatch[41] and later by many other investigators [42,46,7,43,47,48,49]. Based on these investigations, the typical pressure gradient behaviour of a solid-water mixture flowing in a horizontal pipe can be represented by a group of log-log curves of the pressure gradient vs the mean mixture velocity as shown in Fig.(9-1).

Firstly, we may see that mixture pressure gradients are greater than that of water, and as the solid concentration increases, the pressure gradient increases. Secondly, unlike a straight line for water, there is a minimum pressure gradient point on each curve corresponding to a non-zero solid concentration and both increasing or decreasing the mean mixture velocity from this point will increase the pressure gradient. Blatch[41] explained that a large amount of sand was dragged along the bottom of the pipe at a very low velocity while practically clear

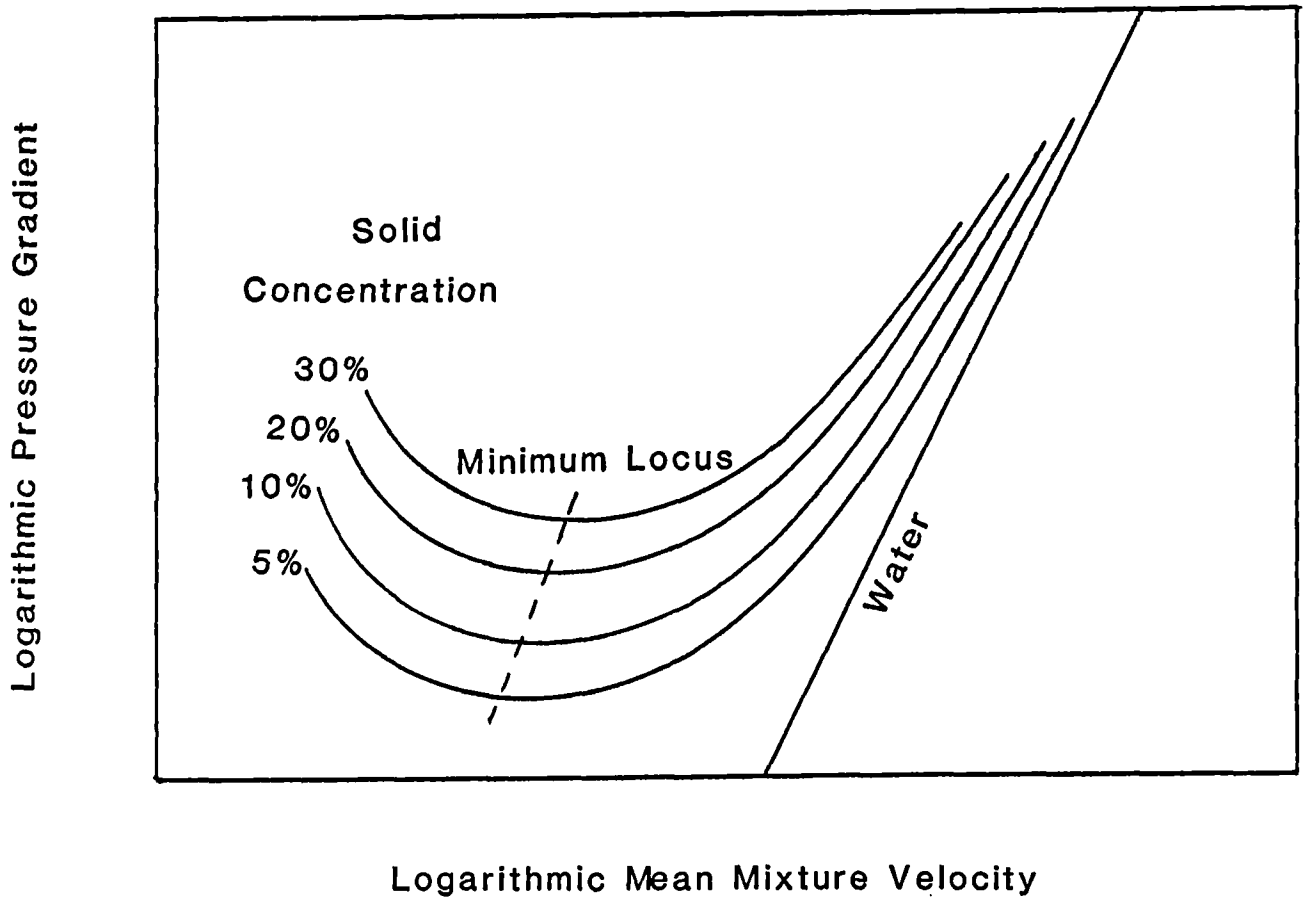

Fig.9-1 Pressure gradient behaviour in solid-liquid mixture transport through horizontal pipes

water flows in the upper part of the cross-section, and that the cause of the higher pressure gradient is due to the dragging of the sands along the bottom of the pipe and to the small cross-section area available for the flow of water. This behaviour may be classified as the moving or stationary bed pattern, i.e. the flow pattern (c) or (d). At high velocities, all the sands are carried in suspension throughout the cross-section area and the cause of the higher pressure gradient is due to the higher mixture velocity or to the higher friction resistance of the mixture flow. This corresponds to the asymmetric or symmetric suspension pattern, i.e. the pattern (b) or (a). If the mixture velocity is continuously increased, the mixture pressure gradient will continuously increased and approach the pressure gradient of water.

It is interesting to note that, as many investigators [42,7,47,48,40,11c,45] recognized, the mixture velocity at the point of the minimum pressure gradient corresponds to the critical mixture velocity below which the solids would begin to deposit on the bottom of the pipe. Therefore, it can be easily deduced that this critical mixture velocity, from both the viewpoints of safty and economics, is the optimum transport velocity for a solid-liquid mixture system.

9.2. Minimum transport velocity (MTV) in pipelines — Correlations and principles

As discussed in the preceding section, the optimum transport velocity of a solid-liquid system is the critical mixture velocity below which the solids deposit on the bottom of the pipe, and this velocity coincides with that at which the minimum pressure gradient occurs. This critical velocity is usually called the "minimum transport velocity" (MTV) or "critical deposit velocity".

It should be noted that the concept of the minimum transport velocity (MTV) refers only to the solid-liquid system with closely sized particles. For a system with a wide particle size range, this concept should be applied to an arbitrarily selected narrow fraction of the particle size range and in this situation, MTV of the system corresponds to a range of velocities, instead of a single value, for the whole range of particle sizes.

The necessity of undertaking research on MTV has long been recognized. Since the first attempt was made and reported by Durand and Condolios[42] in 1952, many other theoretical and experimental studies have been carried out and various correlations have been developed. In this section, a review and discussion of these correlations will be presented.

9.2.1. Principles of various correlations

a. Durand and Condolios' correlation (1952) [42]

The first extensive experiment on MTV was conducted and reported by Durand and Condolios. The solid particles used in the experiment include sands, coal, gravels and pebbles with uniform sizes. The sizes of the particles varied from 20 microns up to 100 mm and the diameters of the pipes used ranged from 40 to 700 mm (1.5 to 27$^1/_2$ in.). In attempting to correlate the experimental data, they assumed that MTV was proportional to the square root of the pipe diameter 'd' and the specific weight of the particles. Then they proposed that MTV could be correlated by the following formula:

$$\frac{v_{mt}}{[2 \cdot g \cdot d \cdot (m - 1)]^{1/2}} = F_{mt} \qquad (9\text{-}1)$$

where $m = \rho_s/\rho_f$, v_{mt} is the minimum transport velocity and F_{mt} is a dimensionless constant for a given system but varies from system to system as a function of the particle size and concentration. Based on the experimental results, they concluded that, for particles less than 1 mm in diameter, the particle size and concentration tended to increase the value of F_{mt} but for particles above 1 mm in diameter, the particle size and concentration had practically no further influence on F_{mt} , in other words, v_{mt} became independent of particle size and concentration above the particle size of 1 mm. They gave a value of 1.34 for F_{mt} for particles above 1 mm in diameter.

b. Worster's correlation (1952) [46]

Worster employed the approach used in sediment transport through open channels to investigate the problem of MTV for solid-liquid mixture transport through pipelines. He assumed that the force acting on a particle by the fluid flow should be in the form:

$$F_p = C_p \cdot d_s^2 \cdot \rho_f \cdot v_p^2 \qquad (9\text{-}2)$$

where C_p is a force coefficient and v_p is the fluid velocity near the particle. He used the friction velocity v_* to replace v_p to represent the velocity near the particle on the bottom of the pipe and, using the boundary flow theory, he developed a general correlation for the beginning of the particle's movement which takes the form:

$$\frac{v_{*mt}^2}{g \cdot d_s \cdot (m - 1)} = f\left(\frac{d_s \cdot v_{*mt} \cdot \rho_f}{\mu} \right) \qquad (9\text{-}3)$$

where v_{*mt} is the friction velocity corresponding to the critical

condition of MTV and the term in the parenthesis on the right-hand side is, what Worster called, the Reynolds number of the boundary roughness. According to Worster, if the value of this term is less than 50, the boundary flow is laminar or transitional; if the value is greater than 50, the turbulent boundary flow occurs and in this case, Eq.(9-3) may be written as:

$$\frac{v_{*mt}^2}{g \cdot d_s \cdot (m - 1)} = \text{const.} \qquad (9\text{-}4)$$

In the present author's opinion, Worster's correlation is an improvement over Durand and Condolios' correlation[42] considering the following two respects:

(i) As water usually flows under the turbulent regime in pipelines, the Newton's law model for particle settling velocities, i.e. Eq.(7-11), may be combined into Eq.(9-3), and then the equation may be written as:

$$\frac{v_{*mt}}{v_s} = f'\left(\frac{d_s \cdot v_{*mt} \cdot \rho_f}{\mu} \right) \qquad (9\text{-}5)$$

If v_{*mt} is taken as a measure of the particle's lift-off tendency and v_s is taken as a measure of the particle's settling tendency, the above equation states that the critical condition for MTV is governed by the ratio of these two velocities and this ratio is a function of the Reynolds number for boundary flow;

(ii) When the equation:

$$v_{*mt} = \left(\frac{\tau_{wmt}}{\rho_f} \right)^{1/2} \qquad (9\text{-}6)$$

is substituted into Eq.(9-3), it becomes:

$$\frac{\tau_{wmt}}{g \cdot d_s \cdot (\rho_s - \rho_f)} = f'\left(\frac{d_s \cdot v_{*mt} \cdot \rho_f}{\mu} \right) \qquad (9\text{-}7)$$

and this equation is of the same form as that of the well-known Shields' relation[50] for the critical condition of the sediment grain movement in open channel flow (which will be discussed in detail in the next section). Therefore, Worster's correlation, i.e. Eq.(9-3), unifies the condition for MTV in pipelines and that for the beginning of sediment transport.

Unfortunately, Worster did not use the experimental data to fit in Eq.(9-3) and establish this equation as a mathematical model for MTV.

c. Newitt, et.al.'s correlation (1955)[7]

Based on experimental data, Newitt, et.al. proposed three different equations for the transitional velocities between the flow patterns. The first one corresponds to the transtional velocity from homogeneous to heterogeneous suspension flow, i.e. from the flow pattern (a) to (b), and this transitional velocity is calculated by:

$$v_1 = \text{const.} \left(2 \cdot g \cdot d \frac{v_s}{v_1} \right)^{1/2} \qquad (9\text{-}8)$$

The second equation is for the transitional velocity from the heterogeneous suspension to the moving bed flow pattern, i.e. from the flow pattern (b) to (c), which takes the form of:

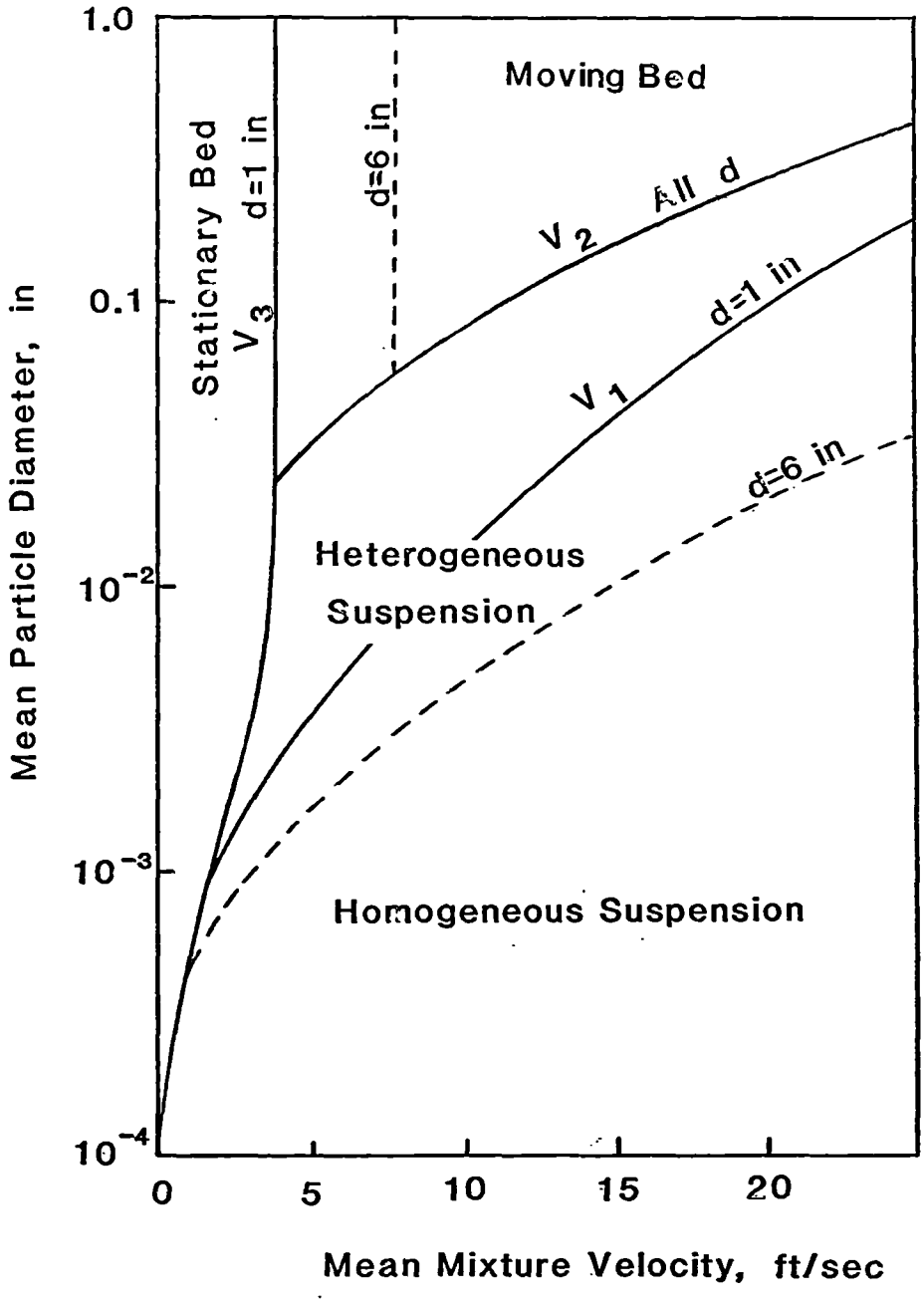

Fig.9-2 Flow patern map for solid-liquid mixture transport through pipelines (after Newitt, et.al.)

$$v_2 = 17 \cdot v_s \qquad (9\text{-}9)$$

The third equation is for the transtional velocity from the moving bed to stationary bed flow pattern, i.e. from the flow pattern (c) to (d). They proposed Durand and Condolios' correlation, i.e. Eq.(9-1), for this transitional velocity, i.e. $v_3 = v_{mt}$. Newitt, et.al. also developed a simple flow pattern map which is shown in Fig.(9-2).

d. Spells' correlation (1955) [8]

Spells correlated some published data and proposed the following equation for MTV:

$$\frac{v_{mt}}{[g \cdot d_s \cdot (m - 1)]^{1/2}} = 0.0251 \cdot \left(\frac{d \cdot v_{mt} \cdot \rho_m}{\mu} \right)^{0.3875} \qquad (9\text{-}10)$$

This equation is based on data basically taken from sand-water mixtures and with particle diameters between 0.056 and 0.84 mm.

When the Newton's law model for particle settling velocities is combined into the above equation, it becomes:

$$\frac{v_{mt}}{v_s} = 0.0144 \cdot \left(\frac{d \cdot v_{mt} \cdot \rho_m}{\mu} \right)^{0.3875} \qquad (9\text{-}11)$$

Comparing the above equation with Worster's correlation of Eq.(9-5) it may be found that there is a similarity between these two equations, i.e. the critical condition for MTV is governed by the ratio of a characteristic fluid velocity to the particle settling velocity and this ratio is a function of a flow Reynolds number. However, in the present correlation, the mean fluid velocity is used, instead of the friction velocity v_{*mt} in Eq.(9-5) of Worster's correlation.

For mixed sized particles, Spells reasoned that it was the coarser particles which should be expected to be of greatest significance in determining MTV for the system. He suggested using the particle diameter d_{85} which corresponds to the value at which 85% of the particles by weight are smaller.

e. Hughmark's correlation (1961) [44]

Hughmark, also based on the published data, proposed the following correlation:

$$\frac{v_{mt}}{(g \cdot d)^{1/2}} = f[C_s \cdot (m - 1) \cdot F_{mt}] \qquad (9\text{-}12)$$

where F_{mt} is a constant. Hughmark gave $F_{mt} = 1$ for particles with diameters ranging from 0.37 to 2 mm. He claimed that the left-hand side of the above equation may be taken as the square root of the Froude number which is the ratio of the fluid dynamic force to the gravity force. However, it should be noted that the pipe diameter 'd' is used in this term instead of the particle diameter 'd_s'. So this Froude number does not represent the ratio of the forces acting opon the particles. Therefore, the significance of the Froude number in Eq.(9-12) is doubtful.

f. Sinclair's correlation (1962) [51]

Sinclair carried out an extensive experiment with sand-water and coal-water mixtures and with particles ranging from 0.03 to 2 mm in diameter. By performing dimensional analysis, he proposed the following correlation for MTV:

$$\frac{v_{mt}^2}{g \cdot d_s \cdot (m-1)^{0.8}} = C_1 \cdot \left(\frac{d_s}{d}\right)^{C_2} \qquad (9\text{-}13)$$

Where C_1 and C_2 are constants and should be evaluated based on the experimental data. Sinclair employed the boundary layer theory to interpret his experimental results and found that, $C_1 = 650$ and $C_2 = 0$ for $d_s/d < 0.001$ under which a particle is wholly immersed in the laminar viscous sublayer; $C_1 = 0.19$ and $C_2 = -2$ for $d_s/d > 0.05$ under which the particles project into the turbulent region; and for the small range of d_s/d between 0.01 and 0.04, $C_1 = 3.4$ and $C_2 = -1$.

As Sinclair claimed, the left-hand side of the above equation may be considered as a modified Froude number. Eq.(9-13) implys that, for a given system, or say, for a given value of d_s/d, the critical condition for MTV is dependent upon the modified Froude number.

For mixed sized particles, Sinclair used d_{85} as a representative particle diameter for the same reason as stated by Spells[8].

g. Thomas' correlation (1962) [9,10]

The most comprehensive study on MTV for solid-liquid mixture transport in pipes is, in the present author's opinion, that reported by Thomas. He carried out experiments with 1.045 inch pipe and with glass beads of 0.078 and 0.31 mm in diameter. To develope his correlation, Thomas first analysed various forces possibly acting upon a single particle resting on the bottom of the pipe for the limiting case of infinite dilution, or say nearly zero concentration, and concluded that the only two forces that would effect the lift of the particles off the bottom were:

i) the gravitational force;

ii) Bernoulli forces caused by the mean velocity distribution across the particle and by the instantaneous turbulent velocity fluctuations.

Then he reasoned that if the particle settling velocity v_s was taken as a measure of the gravitational force and the friction velocity v_{*o} was taken as a measure of the fluid lifting force acting upon the particle, the ratio of these two terms, v_s/v_{*o}, could be considered as one of the primary factors in the MTV correlation. Based on the theory of turbulence and dimensional analysis, Thomas proposed that the minimum transport condition for the limiting case of infinite dilution could be expressed in the form:

$$\frac{v_s}{v_{*o}} = C \left[\left(\frac{d_s \cdot v_{*o} \cdot \rho_f}{\mu}\right)^{C_1} \cdot \left(\frac{d \cdot v_{*o} \cdot \rho_f}{\mu}\right)^{C_2} \cdot (m-1)^{C_3} \right]$$

or

$$\frac{v_s}{v_{*o}} = C \left[N_{Reb}^{C_1} \cdot N_{Re}^{C_2} \cdot (m-1)^{C_3} \right] \qquad (9\text{-}14)$$

where v_{*o} is the friction velocity under the critical minimum transport velocity condition for the limiting case of infinite dilution; N_{Reb} is, according to Thomas' interpretation, the particle Reynolds number and N_{Re} is the pipe Reynolds number. From the analysis of the experimental data, he obtained that $C = 4.9$, $C_1 = 1$, $C_2 = -0.6$ and $C_3 = 0.23$.

For the system with a certain solid concentration, Thomas found that the concentration dependence of the minimum transport condition could be correlated by:

$$\frac{v_{*c}}{v_{*o}} = 1 + 2.8 \cdot C_s \cdot \left(\frac{v_s}{v_{*o}}\right)^{1/3} \qquad (9\text{-}15)$$

where v_{*c} is the critical friction velocity corresponding to the minimum transport velocity condition for the system with solid concentration of C_s.

The present author would like to mention that the term N_{Reb} in Eq.(9-14), which also appears in Worster's correlation[46] of Eq.(9-3), may be also interpreted as the "particle-boundary layer Reynolds number" in addition to the particle Reynolds number as Thomas interpreted. According to the theories of turbulent boundary layer and sediment transport [50,52], for a particle resting on the bottom of the pipe, the value of N_{Reb} is proportional to the ratio between the particle size and the thickness of the viscous sublayer, and thus it reflects the degree to which the particle projects into the turbulent zone of the boundary layer. Nevertheless, from the theoretical point of view, Eq.(9-14), is probably the most extensive correlation for MTV considering the following respects:

i) If the term N_{Re} and $(m - 1)$ are neglected and the Newton's law model for particle settling velocities, i.e. Eq.(7-11), is substituted for v_s, Eq.(9-14) may be then written as:

$$\frac{v_{*o}^2}{g \cdot d_s \cdot (m - 1)} = f\,(N_{Reb}) \qquad (9\text{-}16)$$

which is of the same form as Worster's correlation, i.e. Eq.(9-3), and with the well-known Shields' relation[50] for the beginning of sediment transport;

ii) The term N_{Re} may be considered as a pipe flow Reynolds number

which determines the characteristics of pipe flows and particularly, the turbulent degree of the flow which is often considered as the basic criterion of asymmetric suspension in solid-water mixture flows;

iii) The term (m - 1) reflects the influence of the inertia force due to the density difference between particles and the liquid. As long as the particle's motion is not uniform, some inertia influence should be expected.

For mixed sized particles, Thomas claimed that MTV could be correlated by using Eq.(9-14), provided the mean particle diameter was used.

h. Condolios and Chapus' correlation (1963) [47]

Condolios and Chapus conducted tests using sand materials with mixed sizes ranging from 0.4 to 2.04 mm. They found that, when sands began to settle down on the bottom of the pipe and form a sand-bed, the bed thickness and the true mixture velocity above the bed would adjust themselves in such a way that:

$$\frac{v_e}{(4 \cdot g \cdot R_h)^{1/2}} = F_{mt} \qquad (9\text{-}17)$$

where F_{mt} is a function of sand concentrations and sizes; R_h and v_e are the hydraulic radius and the mean fluid velocity, respectively, of the free-flow section above the bed. When the thickness of the bed is very small or approaches to zero, R_h approaches to d/4 and then v_e becomes the critical velocity when the bed disappears, or say, v_e becomes v_{mt}. Therefore, the correlation for MTV may be written as:

$$\frac{v_{mt}}{(g \cdot d)^{1/2}} = F_{mt}' \qquad (9\text{-}18)$$

Condolios and Chapus obtained an experimental curve of F_{mt} vs the sand concentrations and based on this curve, F_{mt} is in the range of about 1.4 to 2.3 corresponding to sand concentrations from 1% to 18%.

i. Zandi and Govatos' correlation (1967) [53]

Zandi and Govatos proposed a flow pattern index or regime index, as they called, to indicate the transitions between the flow patterns. This index is of the form:

$$N_Z = \frac{v_m^2 \cdot C_D^{1/2}}{C_s \cdot g \cdot d \cdot (m - 1)} \qquad (9\text{-}19)$$

After inspecting the data published by other investigators, they claimed that a value of 40 for the flow pattern index could be taken as the upper limit of the transition from saltation to heterogeneous flow, i.e. the minimum transport condition may be expressed as:

$$40 = \frac{v_{mt}^2 \cdot C_D^{1/2}}{C_s \cdot g \cdot d \cdot (m - 1)} \qquad (9\text{-}20)$$

j. Babcock's Correlation (1968) [48]

Babcock developed an equation for the pressure gradient in a solid-liquid mixture flow based on his own and other published experimental data. Then, he differentiated the equation in terms of the mixture velocity to find the locus of the minima, the result is:

$$10 = \frac{v_{mt}^{2} \cdot C_D^{1/2}}{C_s \cdot g \cdot d \cdot (m - 1)} \qquad (9\text{-}21)$$

Because the locus of the minima corresponds to the condition for MTV, as discussed previously, the above equation can be used as a correlation of MTV. In fact, the above equation is of the same form as Zandi and Govatos' flow pattern index[53] but suggests a transition value of 10 rather than 40.

k. Wicks' correlation (1968) [54]

Wicks conducted tests in 1 and 6 inch pipes with sand materials ranging from 0.044 to 0.35 mm in size. He used water, oil and kerosene, respectively, as carrying liquids to study the fluid viscosity effect. Wicks analysed various forces acting on the particles lying on the surface of the sand-bed and concluded that there are four kinds of forces which are responsible for the particles' motion on the bed surface. These forces are gravity force, buoyant force, lift force and drag force. Based on the moment balance principle, Wicks developed a criterion for incipient particle motion on the bed surface and finally reached a general correlation for MTV as:

$$\frac{\rho_f^{3} \cdot d_s \cdot v_m^{4}}{g \cdot (\rho_s - \rho_f) \cdot \mu} = C_1 \cdot \Gamma^{C_2} \qquad (9\text{-}22)$$

where

$$\Gamma = \left(\frac{d_s}{d} \right)^{2/3} \cdot \left(\frac{d \cdot v_m \cdot \rho_f}{\mu} \right)$$

Based on the experimental data, Wicks obtained that $C_1 = 0.1$, $C_2 = 3$

for $\Gamma < 40$ and $C_1 = 100$, $C_2 = 1.5$ for $\Gamma > 400$.

l. Wasp, et.al.'s correlation (1970) [45]

Wasp, et.al.[45] evaluated Durand and condolios' correlation[42] using extensive published data and concluded that their correlation only gave good predictions for the data obtained under their own experimental conditions. Wasp, et.al. proposed that an equation in the form of:

$$\frac{v_{mt}}{2 \cdot g \cdot d \cdot (m-1)^{1/2} \cdot \left(\frac{d_s}{d}\right)^{1/6}} = F_{mt} \qquad (9\text{-}23)$$

could be a possible correlation for all the data they evaluated. The value of F_{mt} they gave is around 1.87.

m. Wilson's correlation (1974) [55,56]

Wilson[55] developed a MTV correlation, called the "bed-slip" model, based on the concept that the bed of particles will begin to slip when the driving force produced by the fluid flow or the pressure gradient exceeds the mechanical friction between the bed particles and the pipe wall. The final form of his correlation may be expressed in the functional form as:

$$\left(\frac{f}{2 \cdot f_s \cdot C_b}\right) \cdot \left[\frac{v_{mt}^2}{2 \cdot g \cdot d \cdot (m-1)}\right] = f\left(\frac{f_i}{f}, d_s, C_s\right) \qquad (9\text{-}24)$$

where C_b is the volumetric fraction of solids in the bed; f_s is the friction coefficient between the solids and the pipe; f_i is the interface friction coefficient and f is the fluid flow friction factor.

Based on the above correlation, Wilson[56] later developed a nomogram method to determine the minimum transport velocity for sand-water mixtures.

n. Hanks and Sloan's correlation (1981) [57]

The most complicated correlation of MTV for solid-liquid mixture flows in pipes is probably that reported by Hanks and Sloan. They analysed the radially directed forces acting on a suspended particle in a horizontal turbulent pipe flow and wrote the force balance equation as:

$$V_s \cdot (\rho_s - \rho_f) \cdot g - F_L = 0$$

where F_L is the total lift force. According to their theoretical considerations, F_L consists of a Bernoulli lift force, a turbulent lift force and a Magnus lift force which arises from particle spin effects. They further made use of the turbulent flow theory and developed a correlation for MTV in the form of a first-order, non-linear differential equation. In general, their correlation may be expressed in an implicit funtional form as:

$$f(C_1, C_2, C_3, C_4, C_5, v_{mt}, d_s, d, \rho_s/\rho_f, \mu) = 0 \qquad (9\text{-}25)$$

where C_1 ... C_5 are five coefficients in the differential equation. Then, based on the previously published data, they evaluated the values of these coefficients by using a numerical optimization technique.

Although Hanks and Sloan claimed that their model was an improvement on the previous ones, both qualitatively and quantitatively, the applicability of their model is doubtful when one realises that the

value of one of the five coefficients was chosen arbitrarily and the values of the other four would be definitely different if they were evaluated based on different sets of experimental data.

o. Roco and Shook's Method (1985) [58]

The most recent study of MTV in pipes is probably that reported by Roco and Shook. They studied the shapes of the distribution curves of particle velocities and concentrations, which were drawn based on two differential equations developed earlier by themselves. When they compared these curves with other published MTV correlations, they found that the minimum transport condition could be identified by the inflection point on the particle velocity distribution curve in the vicinity of the pipe bottom. Practically speaking, however, this approach does not give a new correlation for MTV, though providing some useful information on the characteristics of the mixture flows.

9.2.2. Discussions

Comparisons of using different correlations to calculate MTV have been made by several previous investigators [51,54,49,57] and it has been found that the predictions using different correlations are quite different, one prediction may be up to several times higher/lower than the other. Examining the experimental results reported by the previous investigators, it may also be found that the data are all rather scattered, even when the set of data is obtained under the same experimental conditions. In the present author's opinion, the scatter of the experimental data and the disparity between different MTV correlations may be attributed to the following reasons:

i) Considerable confusion exists as to the precise defination of the term "minimum transport velocity". Depending upon the individual preference, MTV may be defined as the transitional velocity between the stationary bed and the moving bed flow patterns, or between rolling and saltation of particles, or between saltation of particles and asymmetric suspension;

ii) Even when MTV is precisely defined theoretically, there is some degree of uncertainty during experiments as to decide exactly when the critical condition for MTV occurs. In the previous investigations, this critical condition was usually decided based on visual observations or by locating the locus of the minima on the curves of the pressure gradients vs the mixture velocities. Although some instruments[59,60] were developed during late the 1970's, which were claimed to be useful in deciding the critical condition for MTV, the present author did not find further evidence in literature for their effectiveness.

iii) From the previous discussions it may be seen that, depending upon the individual preference, different principles have been used by different investigators and not surprisingly, the MTV correlations will be different from one to another;

iv) In terms of pipe diameters, particle sizes and concentrations, and liquid viscosities, different systems of solid-liquid mixtures were used by different investigators in their experiments and, based on the experimental results obtained from different systems, the MTV correlations will also be different.

Therefore, much work remines to be done before MTV can be predicted with good accuracy for solid-liquid mixture flow in pipelines. However, as Govier and Aziz[11c] remarked, "from the various correlations and

particularly if care is taken to select those based on data similar to a proposed application, a reasonable estimate of v_{mt} (MTV) should be possible."

9.3. Transport of sediment particles in open channels

Other investigations relevant to the minimum transport condition in drilling annuli are those on initiation of sediment transport in open channels. Particularly, the Shields' relation for the critical condition of initiation of sediment transport, as mentioned in the previous sections, is of importance. Although a large amount of work has been conducted after Shields' experiment, the Shields' relation is still in the leading position concerning the correlations of initiation of sediment transport [50,61,62].

In this section, we will discuss the basic principles for initiation of sediment transport and the Shields' relation.

9.3.1. Basic principles

Sediment transport refers to the movement of granular materials or sediment grains in an open channel under the action of the forces generated by flow of water or air. For the simplest case, consider that the uniform sized sediment grains rest on the bottom of an open channel and water flows through the channel over the sediment grains. At low velocities, the fluid forces are not strong enough to move the grains downstream. As the water velocity, and therefore the fluid forces, are slowly increased, there comes a critical point where the grains begin to move downstream with the flow, then sediment transport has begun. This is so called "initiation of sediment transport".

A great deal of attention has been paid to the determination of the critical threshold for initiation of sediment transport since it is an important practical parameter in civil engineering schemes such as canals, irrigation channels, etc. Before examining the investigations of this critical threshold, let us look at the various forces acting upon a single grain lying on the surface of the sediment in a channel as shown in Fig.(9-3).

Assuming that the sediment is cohesionless, then the forces are of two opposed kinds: the submerged weight of the grain, F_g, which tends to hold the grain in place, and the fluid lift force, F_L, and drag force, F_D, which tend to lift, roll or slide the grain out of its position in the bed. The two different types of fluid forces, F_L and F_D, combine to produce a resultant which acts downstream. This resultant force may move the grain by lifting it over the grains surrounding it or by rotating the grain about some "pivot". In the later case, which has generally been considered to be more important for sediment transport, the balance is between the components of fluid forces acting upwards in the direction of "easiest movement" and the component of gravity acting downwards in the opposite direction. In considering the condition for the beginning of sediment movement, we must first determine the positions of the points at which the forces act and then balance the moments of the forces about the "pivot".

However, despite the intuitive attraction of using the "moments of the forces" approach, it has been proved impossible to determine theoretically the condition of the beginning of sediment movement because of too many variables involved. Firstly, the direction of the easiest movement varies greatly from grain to grain, depending upon the local packing and the degree of the "exposure" of the grain to the flow; secondly, the fluid forces also vary greatly from grain to grain, being

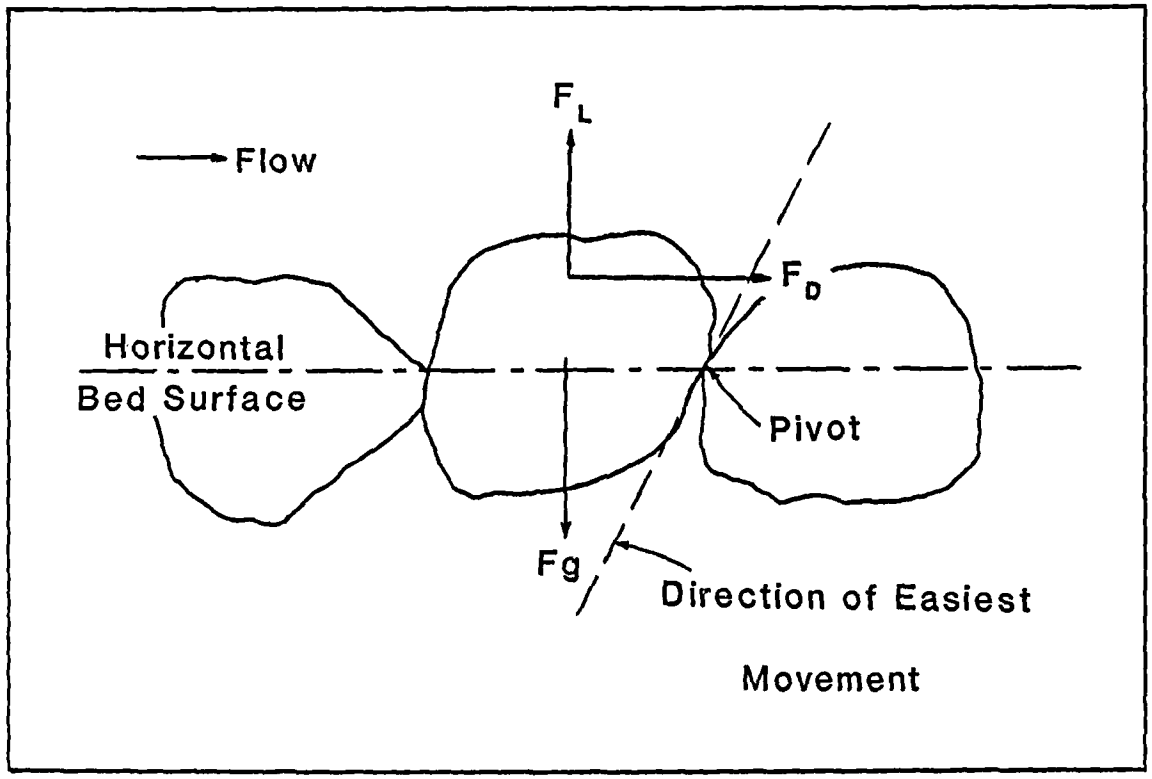

Fig.9-3 Forces acting upon a particle resting on the surface of the sediment in open channel flow

strongest for the most exposed grains, and furthermore the fluid forces fluctuate with time, even for a "steady flow". Therefore the critical condition for the initiation of sediment movement must be determined experimentally.

9.3.2. Shields' relation [50]

Based on the preceding discussion, the critical condition for initiation of sediment transport is dependent upon the diameter and the submerged specific weight of the grains, the density and the viscosity of the fluid, and the critical shear stress scting on the surface of the grain bed. Thus, we may write that:

$$f[\, d_s,\ g(\rho_s-\rho_f),\ \rho_f,\ \mu,\ \tau_c\,] = 0 \qquad (9\text{-}26)$$

Using dimensional analysis, the number of the variables can be reduced to only two:

$$f\left[\frac{\tau_c}{g\cdot(\rho_s-\rho_f)\cdot d_s},\ \frac{d_s\cdot\tau_c^{1/2}\cdot\rho_f^{1/2}}{\mu}\right] = 0 \qquad (9\text{-}27)$$

Substituting the shear velocity $v_* = (\tau_c/\rho_f)^{1/2}$ into the above function, it becomes:

$$f\left[\frac{\tau_c}{g\cdot(\rho_s-\rho_f)\cdot d_s},\ \frac{d_s\cdot v_*\cdot\rho_f}{\mu}\right] = 0$$

or

$$\frac{\tau_c}{g\cdot(\rho_s-\rho_f)\cdot d_s} = f'\left(\frac{d_s\cdot v_*\cdot\rho_f}{\mu}\right) \qquad (9\text{-}28)$$

The above relation is the so called "Shields' relation". The term on the left-hand side is generally referred to as the "Shields' Beta (β)" which may be interpreted as the ratio of the fluid shear force to the gravity force. The term on the right-hand side is usually called the "grain size Reynolds number" or "boundary Reynolds number", N_{Reb}, which may be interpreted as being proportional to the ratio between the grain size and the thickness of the viscous sublayer, and therefore its value indicates the degree to which the grains project into the turbulent zone of the boundary layer.

Based on experimental data, Shields obtained a curve of Shields' Beta, β, vs the grain size Reynolds number, N_{Reb}, which is shown in Fig.(9-4). This curve is usually called the Shields' diagram". After Shields, many other similar experiments were also conducted. Because of the difficulty in deciding exactly when the critical threshold is reached, considerable scatter of the experimental data was shown, as in the case for solid-liquid mixture flow in pipes discussed in the preceding section.

From the Shields' diagram, it may be seen that the Shields' Beta, β, generally decreases as the grain size Reynolds number increases. When N_{Reb} is below about one, β is nearly inversely proportional to N_{Reb}, i.e.

$$\beta = \frac{\text{constant}}{N_{Reb}}$$

or

$$\frac{\tau_c}{g\cdot(\rho_s-\rho_f)\cdot d_s} = \frac{\text{constant}}{\left(\frac{d_s\cdot v_*\cdot \rho_f}{\mu}\right)} \qquad (9\text{-}29)$$

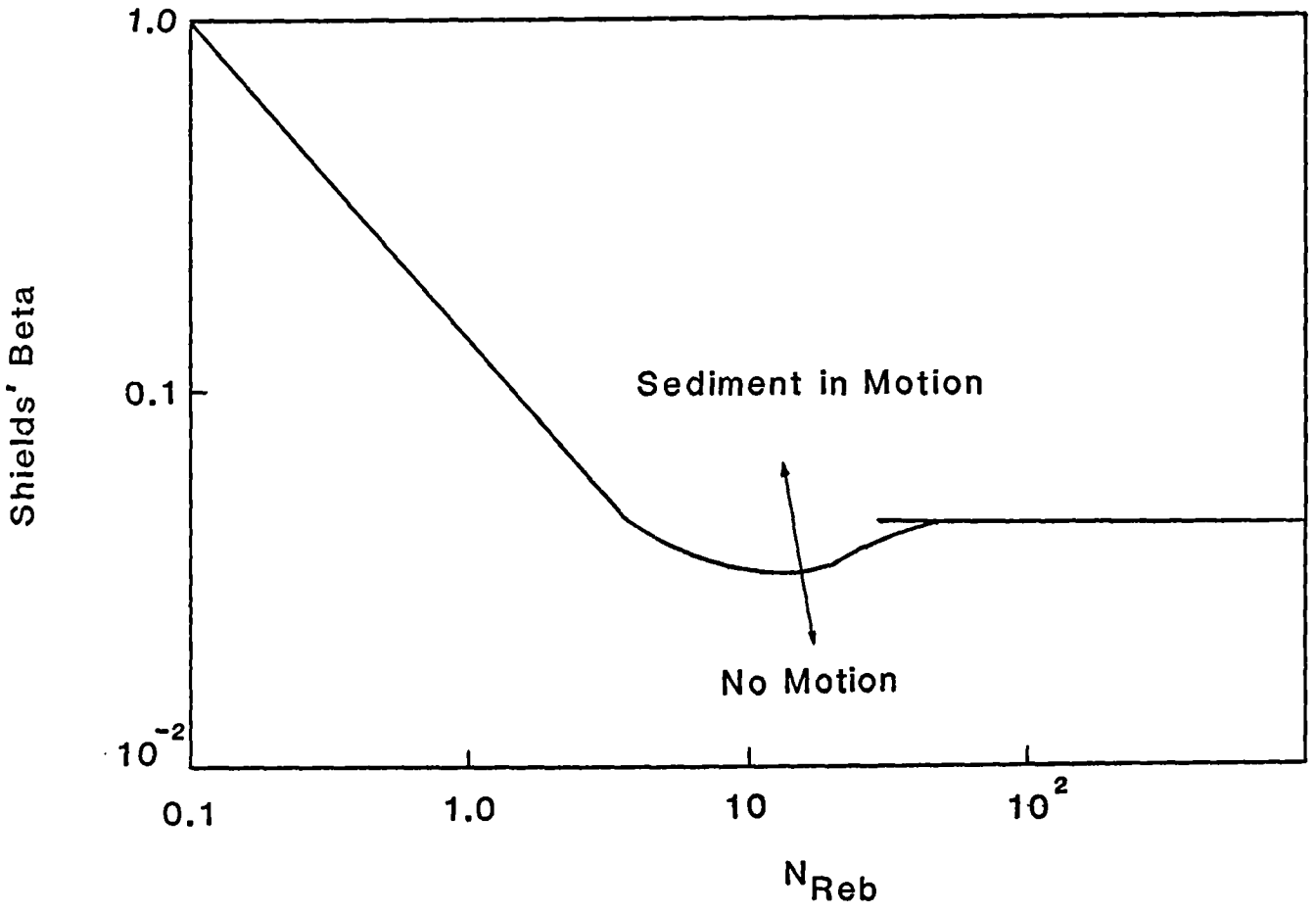

Fig.9-4 Shields' diagram for sediment transport

According to Yalin[50], when N_{Reb} is beyond about 70, β may be approximated by a constant:

$$\beta = 0.05$$

or

$$\tau_c = 0.05 \cdot g \cdot (\rho_s - \rho_f) \cdot d_s \qquad (9\text{-}30)$$

9.4. Previous MTV correlations for cuttings transport in deviated wells

The investigations into the minimum transport velocity (MTV) in drilling annuli were only started several years ago, though the problem has been identified for at least ten years[33]. Two numerical models have been developed by different investigators who claimed that their models can be used to determine the minimum fluid velocity required for deviated hole cleanning. In this section, we will have a detailed analysis of the foundations and applicabilities of these models.

a. Gavignet and Sobey's correlation (1986) [3]

Gavignet and Sobey made the first theoretical attempt to develop a correlation of MTV for cuttings transport in deviated wells. Based on the so called "two layer model", they established an overall momentum balance equation for an annular flow where a cuttings-bed with a certain height has been formed on the low-side wall. This momentum balance equation takes the form:

$$A_c \cdot \tau_f \cdot S_f + A_a \cdot \tau_i \cdot S_i = A_f \cdot \tau_c \cdot S_c \qquad (9\text{-}31)$$

where A_a, A_f and A_c represent the cross-section area of the total annulus, the fluid flow section and the cuttings bed section, respectively; S_f, S_c and S_i represent the perimeters of the fluid flow section, the cuttings bed section and the interfacial surface, respectively; τ_f, τ_c and τ_i represent the wall shear stresses of the fluid flow section, the cuttings bed section and the interfacial surface, respectively.

In order to obtain various wall shear stresses in Eq.(9-31), Gavignet and Sobey made several assumptions which lack foundations:

(i) The wall shear stress in the fluid flow section above the cuttings bed may be defined as:

$$\tau_f = \frac{1}{2} f_f \cdot \rho_f \cdot v_f^2 \qquad (9\text{-}32)$$

where f_f is the fluid friction factor which, they assumed, may be calculated by:

$$f_f = 16/N_{Re} \qquad (9\text{-}33)$$

in the laminar flow regime, and by:

$$f_f = [4 \cdot \log(N_{Re} \cdot f_f^{1/2}) - 0.4]^{-2} \qquad (9\text{-}34)$$

in the turbulent flow regime. It must be pointed out that the above two equations are actually the friction factor correlations for Newtonian pipe flow[52b] and they can not be used for a non-Newtonian annular flow where a cuttings bed has been formed on the low-side wall;

(ii) Gavignet and Sobey reasoned that the cuttings wall shear stress τ_c comes from two contributions: one is due to the fluid friction and

the other is due to the sliding friction of the cuttings in the bed. Thus they assumed that the cuttings wall shear stress may be expressed as:

$$\tau_c = \frac{1}{2} f_c \cdot \rho_c \cdot v_c^2 + f_s \cdot (\rho_s - \rho_f) \cdot g \cdot C_s \cdot \sin(\Phi) \qquad (9\text{-}35)$$

where f_c is the friction factor for the fluid in the cuttings bed and f_s is a sliding friction factor for the cuttings bed, v_c is the cuttings bed moving velocity and Φ is the hole angle.

It must be pointed out that the above expression is an unreasonable and undefined equation because: (1) Gavignet and Sobey did not state clearly how to define and calculate f_c, and they would be wrong if they assumed that f_c could be calculated by using Eq.(9-33) and (9-34); (2) v_c, according to the authors, is the "velocity of cuttings layer". Again they did not state clearly how to define and obtain this velocity. According to previous experiments in annuli and in pipes (as discussed previously), the particles forming a bed will not move at the same velocity, rather, the particles on the top surface of the bed will move forward by jumps or saltations while the particles on the bottom of the bed will slide or roll forward, or may be stationary if the bed is too thick; (3) even if the assumption that τ_c comes from two contributions is reasonable, the two contributions are not necessarily distributed in the way as suggested in Eq.(9-35).

(iii) For interfacial shear stress, Gavignet and Sobey assumed that:

$$\tau_i = \frac{1}{2} f_i \cdot \rho_f \cdot (v_f - v_c) \cdot \left| v_f - v_c \right| \qquad (9\text{-}36)$$

where f_i is the interfacial friction factor which, they assumed without presenting derivation, may be calculated by:

$$f_i = \frac{2}{[4.06 \cdot \log(d_{eq}/d_s) + 3.36]^2} \qquad (9\text{-}37)$$

where d_{eq} is the hydraulic diameter of the annulus and d_s is the cuttings diameter.

Based on the above discussion, it may be seen that, even if Eq.(9-31) can be used to describe the momentum balance in a drilling annulus where a cuttings bed has formed (about which the present author is not convinced), the methods proposed by Gavignet and Sobey for predicting the bed thickness based on Eq.(9-31) is still unacceptable. Although they claimed that their model matched the data reported by Iyoho[33], it should be understood that fitting a model to a set of experimental data and then comparing the model with the same set of data does not mean that the model can predict other data obtained under different conditions.

b. Martin, et.al.'s correlation (1987) [4]

Martin, et.al. developed a correlation which, they claimed, could be used to predict the "minimum average fluid velocity" for ensuring a certain cuttings "recovery percentage". Although the present author can not comprehend the physical significance of the concept, the "minimum average fluid velocity", as defined by Martin, et.al., will be presently assumed to be similar to the minimum transport velocity (MTV) defined by the present author and other previous investigators in solid-liquid mixture flows.

Martin, et.al. gave the following correlation without presenting any theoretical consideration:

$$\frac{v_{mt}}{[g \cdot d \cdot (m-1)]^{1/2}} = C \left(\frac{d \cdot v_{mt} \cdot \rho_f}{\mu} \right)^{-1/2} \qquad (9\text{-}38)$$

where C is a coefficient which is a function of hole angle Φ and the fluid viscosity μ, according to Martin, et.al. They expressed the final form of the above equation as:

$$v_{mt} = \left\{ C \frac{[(\rho_s - \rho_f) \cdot g \cdot \mu]^{1/2}}{\rho_f} \right\}^{2/3} \qquad (9\text{-}39)$$

They claimed that, based on their experimental data, a relation of:

$$C = f(\Phi, \mu) \qquad (9\text{-}40)$$

has been developed which was included in their computer programme.

There are several points which the present author would like to mention:

(i) Martin, et.al.'s correlation does not include two important parameters, i.e. the annular and the cuttings sizes. Although a parameter "d", which is the inside diameter of a pipe, does appear on both sides of Eq.(9-38), they actually cancel each other and thus the correlation is independent of "d", which may be seen in Eq.(9-39);

(ii) According to Eq.(9-39), increasing fluid viscosity will increase the value of the "minimum average fluid velocity", or say, decrease the carrying capacity of drilling fluids, which is in contradiction with the experimental results[5,6] and with the correlations proposed for solid-liquid mixture flows[7,8,54]. In addition, Martin, et.al. used the Newtonian viscosity in their correlation and did not state what equivalent viscosity should be used

to cope with the non-Newtonian nature of drilling fluids;

(iii) Martin, et.al. used the concept of "recovery rate" in percentage repeatedly in their paper as a measure of the hole clean. This is misleading if one considers that, if we drill 1000 ft and want to make a 1000 ft hole, 100% of the drilled cuttings must be transported up to surface, not any less.

CHAPTER 10.

MINIMUM TRANSPORT VELOCITY IN INCLINED DRILLING ANNULI — THEORETICAL ANALYSIS AND GENERAL CORRELATIONS

A general review of the investigations has been given in the preceding chapter on the minimum transport velocity (MTV) in solid-liquid mixture transport through horizontal pipelines and on initiation of sediment movement in open channels. In addition, two MTV models developed by the previous investigators for cuttings transport in deviated wells have also been analysed and it has been shown that these models are unacceptable from both the theoretical and the practical points of view.

In this chapter, we will systematically investigate the critical conditions of MTV for cuttings transport in inclined drilling annuli and based on the basic principles, which have been used in the MTV correlations for solid-liquid mixture flow through pipelines and open channels, general correlations of MTV for cuttings transport in drilling annuli at various angles will be established.

10.1. Characteristics of MTV in inclined drilling annuli

It is obvious that there is a general similarity in critical MTV conditions for any solid-liquid transport processes, i.e. they all refer to the critical conditions for the beginning of the movement of the deposited solid particles under the action of the liquid flow. However, for the cuttings transport process through inclined drilling annuli, the following specific characteristics must be recognized:

i) Non-Newtonian nature of transporting liquid

Unlike the cases of solid-liquid flow through pipelines or open channels, where the transporting media are Newtonian fluids and generally water, the drilled cuttings are transported by circulating drilling fluids which are generally non-Newtonian in rheological behaviour. Therefore, the correlations for the dynamic action of drilling fluid flow on the transported cuttings must be different from those for Newtonian fluids;

ii) Fluid flow regime

Within the velocity range usually encountered in solid-water mixture transport through pipelines, water always flows in the turbulent flow regime because of its low viscosity. For example, in a 5 cm (2 in) pipe, the flow of water becomes turbulent once the average velocity exceeds about 5 cm/s, which is much lower than the velocities usually used in solid-liquid mixture transport through pipelines. In drilling annuli, however, both laminar and turbulent flow regimes may occur because equivalent viscosities of drilling fluids are usually much higher than that of water. Therefore, the mechanism of cuttings transport must be investigated under both the laminar and the turbulent flow regimes;

iii) Conduit geometry — concentric/eccentric annuli

Unlike solid-liquid transport in circular pipes or sediment transport in open channels, the cuttings are transported through an annular space between the drillpipe and the casing or wellbore, which may be concentric or eccentric, and thus the flow, which is responsible for transporting cuttings, may be axial if the drillpipe is stationary or may be helical if the drillpipe is rotated;

iv) Inclination of the drilling annuli

Another complexity of cuttings transport is that the axis of the annular space may be in any inclination angle between vertical and horizontal. Based on previous investigations[5,6], it is expected that the annular inclination is an important factor which affects the characteristics of cuttings transport and the condition for MTV in drilling annuli.

10.2. Initiation of cuttings movement over the cuttings-bed

In this section, we will examine the mechanism of initiation of the cuttings movement over the cuttings bed by analysing various forces acting on the surface of the cuttings-bed and establishing the critical conditions for initiation of the cuttings movement.

10.2.1. Forces acting on a cutting resting on the low-side wall of an inclined annulus

Let us start the present investigations into MTV for cuttings transport by considering various forces acting on a single cutting lying on the low-side wall of an inclined wellbore. Bearing in mind that the purpose is to predict the critical condition for transport of all the cuttings forming the cuttings-bed up to surface with the flow of drilling fluids, the following assumptions are reasonable and also necessary in the present force analysis:

i) A cuttings-bed composed of a single-layer of cuttings exists on the low-side wall of the annulus;

ii) The bed is formed loosely so that the interactions between the cuttings are negligible;

iii) The surfaces of the cuttings and the annular wall are cohesionless.

Then, based on the above assumptions, the forces affecting initiation of the movement of a cutting in the bed are of two kinds: those tending to hold the cutting in place — the submerged weight of the cutting, and those tending to lift, roll or slide the cutting out of its position — the lift force and the drag force generated by the fluid flow. These forces have been illustrated in Fig.(10-1), in which, the surface of the annular wall has been imagined to be a plane since the diameters of cuttings are small in comparison with the diameter of the wellbore. The mathematical expressions for each of these forces may be obtained as follows:

i) Gravity force F_g

This force acts vertically downwards through the centre of the cutting and is equal to the submerged weight of the cutting in the drilling fluid:

$$F_g = V_s \cdot (\rho_s - \rho_f) \cdot g \qquad (10\text{-}1)$$

ii) Drag force F_D

This force is due to the fluid viscous drag, acting mainly on the upper exposed surface of the cutting and through some point above the centre of the cutting. It acts in the same direction with the flow and parallel to the surface of the annular wall. The general form of the drag force may be expressed as:

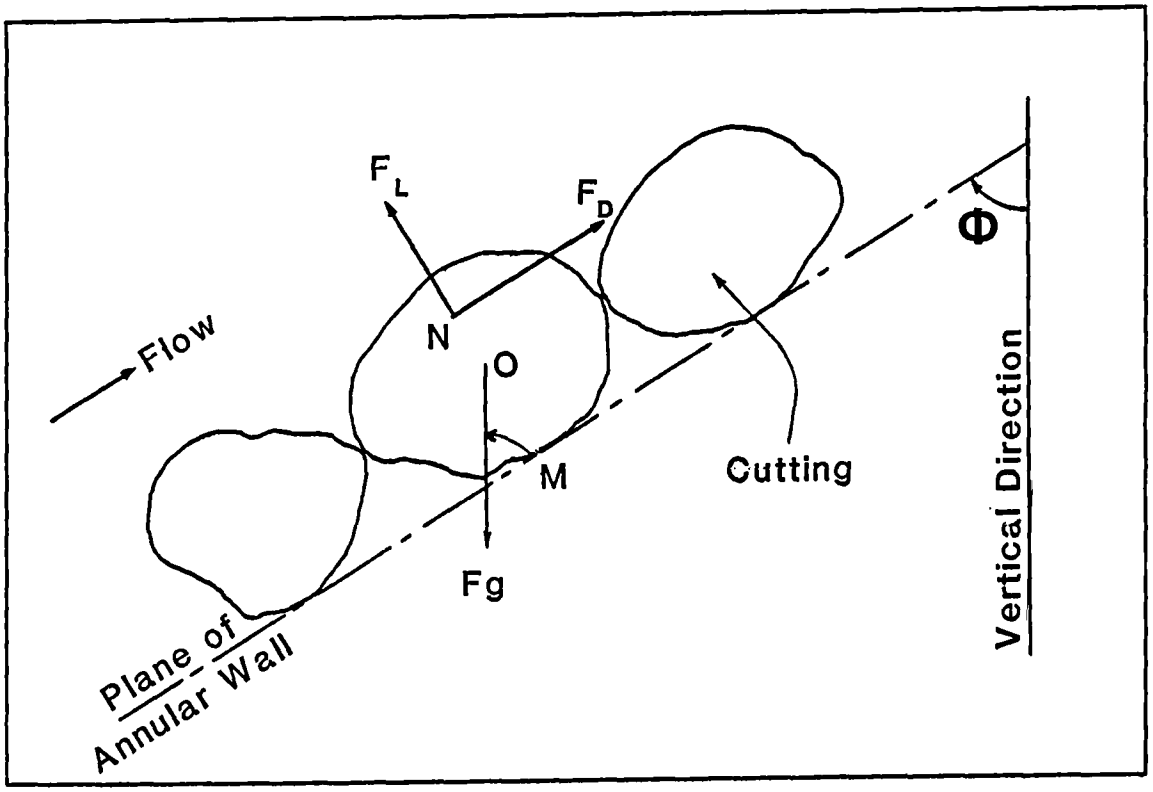

Fig.10-1 Forces acting on a cutting resting on the low-side wall of an inclined annulus in annular flow

$$F_D = C_D \cdot A_e \frac{\rho_f \cdot v_p^2}{2} \qquad (10\text{-}2)$$

where A_e is the projected area of the upper exposed portion of the particle and v_p is the representative velocity of the fluid in the vicinity of the cutting.

iii) Lift force F_L

This force arises because of two reasons. First is the asymmetric distribution of the time-mean fluid velocity around the cutting. Since fluid velocities are higher over the top of the cutting than underneath it, there is also an asymmetric pressure distribution around the cutting with higher pressure on the lower surface than on the upper surface. So a net upward lift force exists on the cutting. Second is the instantaneous turbulent velocity fluctuations. When the flow of the fluid is turbulent, the instantaneous fluid velocity normal to the flow direction may exist. The lift force F_L is the resultant of the above two forces and generally may also be expressed in the form:

$$F_L = C_L \cdot A_L \frac{\rho_f \cdot v_p^2}{2} \qquad (10\text{-}3)$$

where A_L is the projected area of the particle in the direction normal to the flow.

10.2.2. Initiation of cuttings movement

The cuttings originally resting on the surface of the annular wall may start to move under the action of the fluid flow. The ways in which the cuttings start to move may be of two kinds, namely rolling or sliding and lift-off.

i) Rolling or Sliding

Under the action of the fluid drag force, the cuttings may roll or slide along the surface of the annular wall in the direction of the flow and thus the cuttings may be transported in the moving-bed flow pattern. Summarising the forces shown in Fig.(10-1) in the direction of the flow, it may be found that the condition for a cutting to roll on the surface is:

$$\overline{NM}\cdot F_D - \overline{OM}\cdot F_g\cdot\cos(\Phi) \geq 0$$

or

$$\overline{NM}\cdot C_D\cdot A_e \frac{\rho_f\cdot v_p^2}{2} - \overline{OM}\cdot V_s\cdot(\rho_s-\rho_f)\cdot g\cdot\cos(\Phi) \geq 0 \qquad (10\text{-}4)$$

If the surface of the annular wall is smooth and the cutting is not well roundish, the rolling of the cutting may be accompanied by sliding on the surface.

ii) Lift-off

If the fluid lift force is strong enough, the cuttings may be lifted off the surface of the annular wall and move forward within the flow stream. Then the fluid velocity distribution around the cuttings will become symmetric and the lift force be reduced or vanish if the flow is laminar. Thus the cutting may settle back on the surface and then the lift force will be increased and the cutting be lifted off again. The continuous repeat of this process will result in the continuous cutting's jumping and tumbling forwawrd along the flow stream on the surface of the annular wall. If the flow is turbulent and the lift

force generated by the velocity fluctuation in the direction normal to the flow is strong enough to keep the cuttings in the flow stream, the cuttings will be transported in suspension. Referring to Fig.(10-1), the condition for a cutting to be lifted off may be written as:

$$F_L - F_g \cdot \sin(\Phi) \geq 0$$

or

$$C_L \cdot A_L \frac{\rho_f \cdot v_p^2}{2} - V_s \cdot (\rho_s - \rho_f) \cdot g \cdot \sin(\Phi) \geq 0 \qquad (10\text{-}5)$$

Now, two critical conditions for initiation of cuttings movement have been established. Although these equations are not complicated in form, it is unfortunately impossible to solve them by theoretical treatments because of the too many unknown coefficients involved. However, from the preceding discussion, the mechanism of initiation of cuttings movement and the principal affecting factors have been made clear.

10.3. The set of the independent variables affecting MTV

Based on the preceding force analysis, it is not difficult to identify the variables affecting the critical condition for MTV in an inclined annulus. In this section, these variables will be discussed separately as the parameters defining the various components of a solid-liquid system flowing in an inclined drilling annulus.

i) Fluids

In section 7.3.1 of chapter 7, we have discussed that drilling

fluids are usually characterised as either power-law fluids or Bingham plastic fluids. The rheological behaviour of these non-Newtonian fluids are defined by two parameters. For power-law fluids, they are the consistency index 'K' and the flow behaviour index 'n'. For Bingham plastic fluids, they are the plastic viscosity 'μ_p' and the yield stress 'τ_y'. However it is often more convenient to use a single parameter, called the "apparent viscosity", to describe the rheological behaviour of the fluids under a particular shear rate. In this way, the problem associated with that shear rate may be treated with the same method used for Newtonian fluids.

In inclined drilling annuli, the critical condition for MTV is only relevant to the particles' movement in the vicinity of the low-side wall of the annulus. Thus MTV should be affected by the properties of the fluid in the same region. Therefore, it is reasonable to employ the apparent viscosity 'μ_a' at the low-side outer-wall of the annulus to describe the fluid rheological behaviour, instead of using two parameters. Then, there are two independent variables which define the properties of the fluid in the vicinity of the low-side annular wall. The two variables are:

$$\rho_f \ , \ \mu_a$$

where ρ_f is the density of the fluid. Based on the above discussion, the apparent viscosity μ_a is defined as:

$$\mu_a = \frac{\tau_w}{\gamma_w} \qquad (10\text{-}6)$$

where τ_w and γ_w are the shear stress and the shear rate, respectively, at the low-side outer-wall of the annulus.

ii) Cuttings

The case can be much simplified by first considering uniformly sized, roundish particles and with a fixed concentration in the fluid. To define this kind of granular material, only two parameters are required, i.e.

ρ_s , d_s

Like many other granular materials, drilled cuttings are usually not uniform in size and not roundish in shape. So a representative size of drilled cuttings should be used, like d_{ss} used by Spell[8] and Sinclair[51] or the mean particle size used by Durand and condolios[42] and Thomas[10] for the mixed sized granular materials. In the present studies, it is intended that the cuttings size distribution, shape and concentration effects will be investigated using an experimental method and a representative size of the cuttings will be selected and a correction factor will be introduced for the shape and concentration effects based on the experimental results.

iii) Annular size and geometry

Theoretically, three parameters are required to define the size and geometry of an annular space: the inner and outer diameters, and the eccentricity of the annulus. However, because MTV is only related to the low-side region of the annulus and the diameters of the annulus are much larger than those of cuttings, the equivalent width of the annulus at the lowest position, b_{ea}, will be adopted to describe the annular size and geometry:

b_{ea}

In this way, the number of necessary parameters to define the annular size and geometry is reduced to only one and this will greatly simplify the general correlations to be established for MTV without losing too much accuracy.

iv) Gravitational constant and hole angle

As particles settle in a fluid under the action of the gravitational force, the gravitational constant 'g' must be included. Considering that the settling of the particles is due to the density difference between the particles and the fluid, the parameter describing the gravitational effect may be written as:

$g \cdot (\rho_s - \rho_f)$

However, for simplicity, the above parameter may be incorporated with the hole angle "Φ" to give a single parameter which affects the cuttings movement on the low-side wall of an inclined annulus. From the preceding force analysis it may be seen that, if the direction of the reference coordinate system is defined based on the direction of the annular axis, then the fluid drag force and the lift force acting upon a cutting on the low-side wall of the annulus are always parallel and normal to the annular axis, respectively, and both their magnitudes and directions are independent of the hole angle. The only force whose direction relative to the annular axis is affected by the hole angle is the gravitational force. Based on the force analysis, the component of the gravitational resistant force to a particle's rolling or sliding on the annular wall is:

$$g \cdot (\rho_s - \rho_f) \cdot \cos(\Phi)$$

and the resistant component to the particle's lift-off from the annular wall is:

$$g \cdot (\rho_s - \rho_f) \cdot \sin(\Phi)$$

Therefore, different parameters should be used for the gravitational and hole angle effects, depending upon the conditions for the particles to roll or slide along, or to lift-off the annular wall.

v) Fluid Flow

In the present analysis, it is assumed that the drillpipe is not rotated and the annular flow is purely axial, though the effect of drillpipe rotation can be investigated using an experimental method. Intuitively, the mean annular fluid velocity would be chosen as a parameter describing the dynamic condition of the annular axial flow. However, the condition of MTV is only relevant to the dynamic condition of the flow in the lower region of the annular space and near the outer wall while the mean annular fluid velocity can not describe adequately the dynamic condition at this specific region. Therefore a local dynamic parameter corresponding to the region where the cuttings-bed is formed should be used to describe the dynamic condition of the flow. For this purpose, the shear stress τ_w on the outer wall at the lowest position may be selected as the local dynamic parameter because it is a direct indication of the fluid forces acting on the particles lying on the surface of the cuttings-bed. However, a relationship is often used in fluid mechanics which relates the wall shear stress with a another

parameter, called the friction velocity 'v_*' in the form:

$$v_* = \left(\frac{\tau_w}{\rho_f} \right)^{1/2} \qquad (10\text{-}7)$$

and this parameter has the dimension of velocity. Therefore, for convenience, the friction velocity v_* is chosen as the parameter describing the dynamic condition around the cuttings resting on the low-side annular wall. Once the flow system is given, the mean annular fluid velocity, i.e. MTV, can be calculated based on v_*.

Now, a total of seven independent variables have been identified for a given critical condition of MTV in an inclined drilling annulus. It should be mentioned that some other factors may also affect MTV, e.g. the surface conditions of the wellbore. Firstly, the cohesionless of the surface has been assumed in the present study but realistically this may not be true when the surface of the wellbore is covered with the mud filter cake; secondly, the smoothness of the surface may also affect the initiation of the particles' rolling and sliding movement. These factors may be corrected by a correction factor based on some special laboratory tests or field tests, provided the tests are feasible.

Based on the above analysis, in an inclined drilling annulus, the critical condition for initiation of particles' rolling movement is defined by the following fuction:

$$f\,[\rho_f\ ,\ \mu_a\ ,\ \rho_s\ ,\ d_s\ ,\ b_{ea}\ ,\ g\cdot(\rho_s-\rho_f)\cdot\cos(\Phi)\ ,\ v_{*mt}] = 0 \qquad (10\text{-}8)$$

and the critical condition for particles' lift-off from the low-side annular wall is defined by:

$$f'[\rho_f\ ,\ \mu_a\ ,\ \rho_s\ ,\ d_s\ ,\ b_{ea}\ ,\ g\cdot(\rho_s-\rho_f)\cdot\sin(\Phi)\ ,\ v_{*mt}] = 0 \qquad (10\text{-}9)$$

where v_{*mt} represents the minimum transport friction velocity when the critical MTV condition is achieved.

10.4. Derivation of the dimensionless groups

In this section, dimensional analysis technique will be used to derive the general functions which define the critical conditions of MTV.

If the parameters d_s, v_{*mt}, ρ_f in Eq.(10-8) and (10-9) are taken as the three basic quantities, based on dimensional analysis which has been shown in Appendix (A10-1), four dimensionless groups can be obtained for each of Eq.(10-8) and (10-9), i.e.

$$\Pi_1 = \frac{v_{*mt}^2}{d_s\cdot g\cdot(\frac{\rho_s-\rho_f}{\rho_f})\cdot\cos(\Phi)} \qquad \text{for Eq.(10-8)} \qquad (A10\text{-}4)$$

$$\Pi_1' = \frac{v_{*mt}^2}{d_s\cdot g\cdot(\frac{\rho_s-\rho_f}{\rho_f})\cdot\sin(\Phi)} \qquad \text{for Eq.(10-9)} \qquad (A10\text{-}9)$$

$$\Pi_2 = \frac{d_s\cdot v_{*mt}\cdot\rho_f}{\mu_a} \qquad (A10\text{-}5)$$

$$\Pi_3 = \frac{d_s}{b_{ea}} \qquad (A10\text{-}6)$$

$$\Pi_4 = \frac{\rho_f}{\rho_s} \qquad (A10\text{-}7)$$

Therefore, the critical condition for MTV are determined, repectively, by:

$$f (\Pi_1 , \Pi_2 , \Pi_3 , \Pi_4) = 0 \qquad (10\text{-}10)$$

for initiation of particles' rolling movement, and by:

$$f'(\Pi_1' , \Pi_2 , \Pi_3 , \Pi_4) = 0 \qquad (10\text{-}11)$$

for initiation of particles' lift-off movement.

10.5. Analysis of the dimensionless groups

In order to achieve a clear idea of the significance of each of the above dimensionless groups, it is necessary to analyse each of them individually.

i) Dimensionless group Π_1 and Π_1'

The dimensionless groups Π_1 and Π_1' are the only groups in which the gravitational factor $g\cdot(\rho_s-\rho_f)$ is present. Substituting Eq.(10-7) into Π_1 and Π_1', it may be found that:

$$\Pi_1 = \frac{\tau_{wmt}}{d_s\cdot g\cdot(\rho_s-\rho_f)\cdot\cos(\Phi)} \qquad (A10\text{-}4)$$

$$\Pi_1' = \frac{\tau_{wmt}}{d_s\cdot g\cdot(\rho_s-\rho_f)\cdot\sin(\Phi)} \qquad (A10\text{-}10)$$

It is obvious that Π_1 and Π_1' are actually the ratios of the fluid dynamic force to the effective gravitational force. In fact, both Π_1 and Π_1' may be considered as the modified particle Froude number which

is significant as long as the gravitational force is important. From the previous force analysis it has been shown that the gravitational force is the only force which acts against initiation of the particles' movement and holds the particles in cuttings bed. Therefore, it is expected that the dimensionless groups Π_1 or Π_1' will be the most important parameter dominating the corresponding critical condition of MTV in inclined annuli.

ii) Dimensionless group Π_2

Generally speaking, the dimensionless group Π_2 is a Reynolds number which represents the ratio of an inertia force to a viscous force acting on particles lying on the surface of the low-side wall of an inclined annulus. This may be better understood if we express Π_2 in the form:

$$\Pi_2 = \frac{d_s^2 \cdot \rho_f \cdot v_{*mt}^2}{\mu_a \cdot d_s \cdot v_{*mt}}$$

where the numerator represents an inertia force and the denominator represents a viscous force.

In addition, when the flow is turbulent, the dimensionless group π_2 may be interpretered in a different way. According to the turbulent boundary layer theory, the dimensionless factor:

$$\frac{y \cdot v_* \cdot \rho_f}{\mu} \qquad (10\text{-}12)$$

characterises the nature of flow near a solid boundary, where y represents the distance from the point considered to the solid boundary. The nature of the boundary layers are defined by the values of this dimensionless factor as follows[s2a]:

$$0 < \frac{y \cdot v_* \cdot \rho_f}{\mu} < 5 \qquad \text{Viscous Sublayer} \qquad (10\text{-}13a)$$

$$5 < \frac{y \cdot v_* \cdot \rho_f}{\mu} < 70 \qquad \text{Buffer Layer} \qquad (10\text{-}13b)$$

$$\frac{y \cdot v_* \cdot \rho_f}{\mu} > 70 \qquad \text{Turbulent Zone} \qquad (10\text{-}13c)$$

Inverting the above equations for y, the corresponding thicknesses of the boundary layers can be determined. In Appendix (A10-2), calculations are made for some cases of Newtonian fluids with viscosities roughly equivalent to those of drilling fluids in order to have some ideas of the boundary layer thicknesses relative to the sizes of drilled cuttings in drilling annuli.

It is interesting to note that the dimensionless group Π_2 is of the same form as the expression (10-12). However, instead of containning a characteristic distance 'y', the dimensionless group Π_2 contains a particle diameter 'd_s'. Therefore, when a particle is lying on the outer wall of the annulus, the value of Π_2 reflects the degree to which the particle projects into the buffer layer or turbulent zone. In other words, the value of the dimensionless group Π_2 is proportional to the ratio of the particle diameter to the thickness of the viscous sublayer. Referring to the theory of sediment transport[50], the dimensionless group Π_2 is referred to here as the "particle-boundary layer Reynolds number", as mentioned in Section 9.2.1.g. Thus the particle-boundary layer Reynolds number is defined as:

$$N_{Reb} = \frac{d_s \cdot v_{*mt} \cdot \rho_f}{\mu_a} \qquad (10\text{-}14)$$

As shown in the Shields' relation of Eq.(9-28), the above equation is also an important factor affecting the critical condition for MTV.

In fact, if only the first two dimensionless groups Π_1 and Π_2 are considered and the parameter of hole angle is ignored, Eq.(10-10) and (10-11) would be in the same form as the Shields' relation.

iii) Dimensionless group Π_3

The dimensionless group Π_3 reflects the influence of the particle size relative to the size of the annular clearance. The existance of solid particles on the surface of the annular wall will interfere the distributions of the shear stress and velocity across the annulus, and thus interfere with the fluid forces acting on the cuttings lying on the annular wall. The degree of this interference may be correlated by the dimensionless group Π_3.

iv) Dimensionless group Π_4

The dimensionless group Π_4 reflects the influence of the cuttings density 'ρ_S' relative to the fluid density. As the motion of cuttings is not uniform when they start to move, the influence of the inertia force and thus the cuttings density should be expected. However, as the variation of the cuttings density relative to the density of the drilling fluids is generally small during drilling operations, the value of the dimensionless group Π_4 remains nearly a constant, so the influence of Π_4 on the critical condition of MTV may be negligible.

10.6. General correlations for the critical conditions of MTV

Based on the above discussions, when the influence of the dimensionless group π_4 is neglected, Eq.(10-10) and (10-11) become, respectively,

$$f(\Pi_1, \Pi_2, \Pi_3) = 0 \qquad (10\text{-}15)$$

$$f'(\Pi_1', \Pi_2, \Pi_3) = 0 \qquad (10\text{-}16)$$

According to the Rayleigh method for dimensional analysis[63], Eq.(10-15) and (10-16) may be written as:

$$\Pi_1 = m_1 \cdot \Pi_2^{m_2} \cdot \Pi_3^{m_3}$$

$$\Pi_1' = n_1 \cdot \Pi_2^{n_2} \cdot \Pi_3^{n_3}$$

i.e. for initiation of cuttings' rolling movement:

$$\frac{v_{*mt}^2}{d_s \cdot g \cdot (\frac{\rho_s - \rho_f}{\rho_f}) \cdot \cos(\Phi)} = m_1 \cdot (\frac{d_s \cdot v_{*mt} \cdot \rho_f}{\mu})^{m_2} \cdot (\frac{d_s}{b_{ea}})^{m_3} \qquad (10\text{-}17)$$

and for initiation of cuttings' lift-off:

$$\frac{v_{*mt}^2}{d_s \cdot g \cdot (\frac{\rho_s - \rho_f}{\rho_f}) \cdot \sin(\Phi)} = n_1 \cdot (\frac{d_s \cdot v_{*mt} \cdot \rho_f}{\mu_a})^{n_2} \cdot (\frac{d_s}{b_{ea}})^{n_3} \qquad (10\text{-}18)$$

where m_1, m_2, m_3 and n_1, n_2, n_3 are the coefficients which should be evaluated based on experimental data.

It should be mentioned that some other factors which have not been considered in the above equations should be corrected based on the experimental results by modifying the coefficients m_1 and n_1, respectively. These factors include the shape, size distribution and concentration of the cuttings, the drillpipe rotation and the surface condition of the wellbore, etc.

Examining Eq.(10-17) will reveal that, when the hole angle is

horizontal, i.e. $\Phi = 90°$, initiation of the cuttings' rolling movement will be achieved with any non-zero fluid velocity and this obviously is not true. The reason is that Eq.(10-17) is developed for roundish or spherical particles on a plane surface, so any non-zero fluid drag force F_D will initiate particles' rolling if the surface is horizontal. However, if the particles are not perfectly roundish and the surface of the wellbore supports the particles not with a single point but with a fraction of its surface, then a certain magnitude of the fluid drag force will be required before the particles start to move in the way of sliding forward instead of rolling. In this situation, referring to Fig.(10-1), the total resistant force to the cutting's sliding movement on the annular wall is the sum of the component of the gravitational force in the direction of the flow and the friction force generated between the cutting and the annular wall. Therefore the independent parameter defining the effect of the gravitional force and the hole angle, as discussed in Section 10.3.iv, should be modified as:

$$g\cdot(\rho_s - \rho_f)\cdot[\cos(\Phi) + f_s\cdot\sin(\Phi)]$$

where f_s is the friction coefficient between the cuttings and the annular wall under the "wet" condition. The value of the wet friction coefficient f_s under laboratory experimental conditions may be estimated by conducting a simple test which is explained in Appendix (A10-3). Then Eq.(10-17) shoud be modified to yield:

$$\frac{v_{*mt}^{\,2}}{d_s\cdot g\cdot\left(\frac{\rho_s-\rho_f}{\rho_f}\right)\cdot[\cos(\Phi)+f_s\cdot\sin(\Phi)]} = m_1\cdot\left(\frac{d_s\cdot v_{*mt}\cdot\rho_f}{\mu_a}\right)^{m_2}\cdot\left(\frac{d_s}{b_{ea}}\right)^{m_3} \qquad (10\text{-}19)$$

This is the general correlation for initiation of cuttings' sliding

movement.

It should be noted that, during the derivation of Eq.(10-18) and (10-19), no assumption has been made on the rheological behaviour of the fluid. Therefore, they are valid for power-law, Bingham plastic and any other inelastic, time-independent fluids.

10.7. Discussions

10.7.1. Final forms of the general correlations

In the preceding section, the general MTV correlations have been established. In order to describe the dynamic condition of the annular flow and the rheological properties of the fluid in the vicinity of the low-side outer wall of the annulus, where the cuttings-bed is formed, the friction velocity $v*$ or $v*_{mt}$ and the local apparent viscosity μ_a corresponding to that position have been used in the general correlations. For drilling engineering applications, however, the more familiar and convenient parameters are the mean annular fluid velocity v_f or v_{mt} and the parameters corresponding to the type of the fluids, i.e. K, 'n' for power-law fluids and μ_p, τ_y for Bingham plastic fluids. Therefore, the transformation from $v*$ and μ_a to v_f and K, n or μ_p, τ_y are inevitable when Eq.(10-18) and Eq.(10-19) are used in drilling programme design.

In Eq.(10-7) it is shown that:

$$v_* = \left(\frac{\tau_w}{\rho_f} \right)^{1/2} \qquad (10\text{-}7)$$

and Eq.(10-6) shows that:

$$\mu_a = \frac{\tau_w}{\gamma_w} \qquad (10\text{-}6)$$

Although the power-law model and the Bingham plastic model are only valid when the flow is laminar, it is assumed in the present analysis that they can be applied to describe the rheological behaviour of drilling fluids in the viscous sublayer or in the vicinity of the annular outer wall if the annular flow is turbulent. For power-law fluids, combining the above equation with Eq.(7-12) it may be found that:

$$\mu_a = K^s \cdot \tau_w^{1-s} \qquad (10\text{-}20)$$

where $s = 1/n$. For Bingham plastic fluids, combining Eq.(10-6) with Eq.(7-13) yields:

$$\mu_a = \frac{\tau_w \cdot \mu_p}{\tau_w - \tau_y} \qquad (10\text{-}21)$$

From Eq.(10-7), (10-20) and (10-21) it may be seen that, when the fluid properties are known, both $v*$ and μ_a can be calculated from the shear stress τ_w on the low-side wall of the annulus.

In the first part of the thesis, the calculations of the wall shear stress have been discussed for some cases of the non-Newtonian annular flow. However, more effort is still required to investigate the problem before we can predict the wall shear stress for other cases of the non-Newtonian annular flow, which are also encountered during drilling operations.

When the general correlations have been numerically established, i.e. the values of m_1, m_2, m_3 and n_1, n_2, n_3 in Eqs.(10-19) and (10-18) have been obtained based on experimental data, it is not difficult to

express the resulting MTV models in terms of:

$$v_{mt} = f(\Phi\ ,\ d_s\ ,\ \rho_s,\ d_1\ ,\ d_2\ ,\ e\ ,\ \rho_f,\ K,\ n) \qquad (10\text{-}22)$$

for power-law fluids, and

$$v_{mt} = f(\Phi\ ,\ d_s\ ,\ \rho_s,\ d_1\ ,\ d_2\ ,\ e\ ,\ \rho_f,\ \mu_p\ ,\ \tau_y) \qquad (10\text{-}23)$$

for Bingham plastic fluids. The above equations are the desired final forms of the general correlations shown in Eq.(10-18) and (10-19).

10.7.2. Effect of hole angle on MTV

In the general correlations developed in the previous sections, the hole angle has been combined together with the effective gravitational force to form a single parameter based on the force analysis. This is the most important distinction between the present correlations and those in solid-liquid mixture transport through pipelines and in sediment transport through open channels.

Based on the present general correlations, the effect of the hole angle Φ on initiation of cuttings movement can be analysed according to its influence on the value of MTV or v_{*mt}. From Eq.(10-18) it may be seen that, if other parameters are known and kept constant, $\sin(\Phi)$, and thus v_{*mt}, have the miximum values when $\Phi = 90$. The value of v_{*mt} decreases with a decrease in Φ and when $\Phi = 0$, the value of v_{*mt} becomes zero. Therefore, initiation of cuttings lift-off movement is most difficult when the annulus is horizontal; as the hole angle decreases, it becomes more and more easier and if the annulus is vertical, no cuttings-bed will be formed under any non-zero fluid velocity, which is consistent with the real situations encountered during vertical

drilling operations.

The effect of the hole angle Φ on initiation of cuttings sliding or rolling movement may be analysed in the similar way based on Eq.(10-19). However, because of the involvement of the friction between the cuttings and the annular wall during sliding movement, the analysis is not so straight forward. Generally speaking, $v*_{mt}$ has the maximum value when Φ is nearly zero and has the minimum when Φ is nearly 90 . In other words, the higher the hole angle, the easier the initiation of cuttings sliding or rolling movement.

Based on the above analysis it may be concluded that, in high angle wells, the cuttings are easier to be transported in sliding or rolling movement, or say in the moving bed flow pattern, while in low angle wells, the cuttings are more likely to be transported in suspension. Therefore, Eq.(10-18) and (10-19) will generally give two different values of $v*_{mt}$ under the same condition. However, if both kinds of the cuttings movement can be accepted as the means of cuttings transport during drilling operations, the smaller one among the two different values of $v*_{mt}$ should be considered as the minimum transport friction velocity.

At this point it should be added that, the cuttings sliding or rolling movement can only be accepted as a means of cuttings transport when the sliding or rolling velocity has exceeded a mimimum allowable value, though the word "initiation" is still used. This minimum acceptable value should be determined based on experimental results and the requirement of cuttings transport during drilling operations.

10.7.3. Criterion for evaluating cuttings transport in inclined drilling annuli

In Chapter 6 and Chapter 8 we have discussed that the cuttings transport ratio is an excellent measure of the cuttings transport performance in vertical wells. In this section it will be shown that the minimum transport velocity (MTV) can be used as an indicator for cuttings transport in non-vertical wells.

In the previous sections, the general correlations for MTV have been developed based on two basic ways of initiating cuttings transport, i.e. the sliding or rolling movement which results in the transportation of the cuttings in the moving bed flow pattern, and the lift-off movement which results in the transportation of the cuttings in suspension or saltation. It is assumed throughout the derivation of these correlations that when the annular fluid velocity is equal to or greater than MTV, no cuttings-bed will be formed, or if it does, it is only a layer of moving cuttings, on the low-side wall of the annulus and all the cuttings can be transported out of the hole and thus no troubles associated with insufficient cuttings transport will be encountered during drilling operations. Therefore, it is MTV that should be used as the minimum annular fluid velocity for hole cleaning in directional drilling.

In addition, when the general correlations have been numerically established as the mathematical models, i.e. in the forms of Eq.(10-22) and (10-23), they can be used to evaluate the effects of various parameters on cuttings transport performance in non-vertical drilling wells. For example, if an increase of parameter "A" will result in an increase of MTV value, and thus an increase of the minimum annular velocity for hole cleaning, then the effect of increasing parameter

"A" is to decrease the cuttings transport performance, and vice versa. Therefore, the mathematical models derived from the present general correlations based on the experimental results can be used as the guidelines for designing various parameters for hole cleaning during directional drilling operations.

CHAPTER 11.

SUMMARY OF THE PRESENT STUDIES AND RECOMMENDATIONS FOR FUTURE WORKS

11.1. Settling velocities of variously shaped particles in non-Newtonian fluids

11.1.1. In power-law fluids

In Chapter 7, a new method was used to investigate the problem of settling velocities of variously shaped particles in power-law fluids. The main distinctions of this method from the previous ones are:

i) the generalised particle Reynolds number was used to account for the non-Newtonian nature of power-law fluids;

ii) The shape factor was incorporated into the sphericity of non-spherical particles to correlate the particle's shape effect on their settling velocities.

The experiments on settling velocities of variously shaped particles were conducted in stagnant water-based polymer solutions, which can be characterised as power-law model fluids. As a result, a new model was developed for calculations of settling velocities of variously shaped particles in power-law fluids. Based on the theoretical analysis, suggestions on using the new model in dynamic fluids were made.

To complete the above studies, further experimental investigations in the following aspects are required:

i) More extensive experimental data on particle settling velocities in the turbulent settling regime are required. During the present experiments, it was observed that the particle drag coefficient in turbulent settling regime became basically a constant and the value of the constant depends upon the flow behaviour index. However, because it was difficult to trace the high settling velocity particles with the available video equipment, only limited data were obtained during the experiments and approximations of the drag coefficients were proposed.

ii) experimental data on particle settling velocities in dynamic fluids are required. In the present studies, the present author intuitively proposed a correlation method for the influence of fluid motion on the particle's settling velocities. However, this problem can only be understood after extensive experimental investigations. To conduct the experiment on particle settling velocities in dynamic fluids, the following measurements must be made simultaneously:

a) The particle velocities;

b) The fluid velocities surrounding the settling particles.

At present, the measurement on (a) can be achieved without much difficulty. The problem is how to make the measurement on (b). If the fluid velocity profile is known, two alternative methods may be used, i.e. either to trace and record the particle's position continuously during its settling, or in some way, to control the trajectory of the particle's settling without interfering significantly with its settling.

11.1.2. In Bingham plastic fluids

During the time in which the investigations into the particle settling velocities in power-law fluids were conducted, a parallel theoretical study on the same problem in Bingham plastic fluids was also performed. Unfortunately, it was found out later that similar theoretical studies and experiments had been conducted and reported in 1967 by Ansley and Smith[64]. They developed a modified particle Reynolds number, which they called the "dynamic parameter", and successfully correlated the drag coefficient data obtained in stagnant Bingham plastic fluids with different yield stresses onto a single line. It seemed to the present author that the results of their investigations into the drag coefficient correlation were excellent. With the equipment available to the present author, it was impossible to carry on further from Ansley and Smith's investigations and therefore the plan for further investigations was cancelled.

As we know, drilling fluids may be characterised either as power-law fluids or Bingham plastic fluids. Although there is a general consensus that the power-law model is more accurate under most circumstances, there are many cases in which the Bingham plastic model must be used to characterise the "yield stress" characteristic of drilling fluids, especially of those with high concentration bentonite. Therefore, it is necessary to investigate the problem of particle settling velocities in Bingham plastic fluids in order to achieve a complete understanding of cuttings settling characteristics in drilling fluids.

When the necessary equipment is available, the present author suggests carrying on with Ansley and Smith's investigations in the following two aspects:

i) Develop a correlation method to account for the particle's shape effect on its settling velocity in stagnant Bingham plastic fluids. Although it may be assumed that the method used for power-law fluids is applicable to Bingham plastic fluids as well, it relies on the experimental results to confirm the speculation and numerically develop the correlation;

ii) Experimentally investigate the problem in dynamic Bingham plastic fluids to understand the effect of the fluid motion on the particle settling velocities. The present author fully recognizes the complexities of the problem because the fluids with a yield stress are often time-dependent and the time-dependent characteristic itself is a problem lacking understanding. However, based on experimental data, particularly if the experiments are conducted under similar conditions with those in drilling annuli, it is possible to develop some empirical correlations which are accurate enough for practical applications.

11.2. Experimental investigation on MTV

Based on the extensive theoretical studies on various correlations of the minimum transport velocities (MTV) in solid-liquid mixture flow through pipelines, on initiation of sediment transport through open channels and on the previous correlations of MTV for cuttings transport in deviated wells, two parallel general correlations of the minimum transport velocity for cuttings transport in drilling annuli at various angles have been developed and presented in Chapter 10. One correlation is developed for initiation of cuttings' sliding or rolling movement and the other for initiation of cuttings' lift-off movement. These models combine the principles used in solid-liquid mixture transport through pipelines with those used in sediment transport through open channels.

When these correlations are numerically established, they can serve as criteria to evaluate and correlate the effects of various parameters on cuttings transport during directional drilling.

To numerically establish the MTV models and study the other factors which also affect cuttings transport in inclined annuli but have not been studied so far, it is envisaged that the future investigations may be conducted in the following four stages:

i) The experiments should be carried out first using uniformly sized granular materials to simulate drilled cuttings and using water-based polymer solutions to simulate drilling fluids. The uniformly sized granular materials allow us to measure MTV data most accurately without involving the effects of particle's shape and size distribution while the water-based polymer solutions are transparent which allow us to determine the critical minimum transport condition with visual observations, and thus without having to rely on some kind of instrument which has not been identified. At the beginning of this stage, the criteria for determining the critical conditions for the beginning of cuttings' sliding or rolling movement and lift-off movement must be studied based on the characteristics of the physical process of the cuttings transport. These criteria will be then used to determine the critical conditions of MTV and the values of the coefficients in the MTV correlations, i.e. Eqs.(10-18) and (10-19), can be obtained based on the experimental data.

ii) After the numerical models have been developed, other factors which have not been considered yet should be experimentally investigated for more realistic drilling conditions. These factors include the shape, the size distribution and the concentration of the cuttings, the drillpipe rotation and the surface condition of the wellbore. Based

on the experimental data, the coefficients m_1 and n_1 in the corresponding models should be modified to accommodate these effects.

iii) Experiments in oil-based fluids should be conducted in this stage of the investigation to study the effect of the fluid-type, provided some kind of instrument has been identified which can help us to determine the critical condition for MTV without visual observations. Theoretically speaking, water-based fluids and oil-based fluids are unlikely to behave differently in terms of their effects on MTV conditions, as long as their rheological behaviours are identical. However, as oil-based muds are more and more commonly used for directional drilling, it is worth while to experimentally confirm this speculation and, if necessary, to make some modifications on the coefficients of the MTV models, and most of all, to give more confidence to the people who are going to use these models during directional drilling with oil-based drilling fluids.

iv) Based on the above experiments, the final forms of the MTV models can be developed, and if necessary, simplified to eliminate some factors which are not so important. Then these models should be transfered onto computers for field applications.

Appendix (A3-1): Summary of the bipolar coordinate method for eccentric annular flow of power-law fluids

a) Coordinate transformation

The bipolar coordinate system consists of two series of orthogonal circles. Fig.(A3-1) illustrates the bipolar coordinate system together with the familiar rectangular coordinate system. The transformation from the rectangular to the bipolar coordinate system represents a conformal mapping which is defined by[22]:

$$\Psi = \ln\left(\frac{a + Q}{a - Q}\right) = 2\cdot\tanh^{-1}\left(\frac{Q}{a}\right) \qquad \text{(A3-1a)}$$

or

$$Q = a\cdot\tanh\left(\frac{\Psi}{2}\right) \qquad \text{(A3-1b)}$$

where Ψ and Q are two complex numbers defined by:

$$\Psi = \xi + i\eta \qquad \text{(A3-2a)}$$

$$Q = x + iy \qquad \text{(A3-2b)}$$

and 'a' is a constant such that all the η circles of the bipolar coordinates pass through the points $(\pm a, 0)$ in the corresponding rectangular coordinate system.

Based on Eqs.(A3-1) and Eqs.(A3-2), the relation between the rectangular coordinates, x and y, and the bipolar coordinates, ξ and η, can be found as follows:

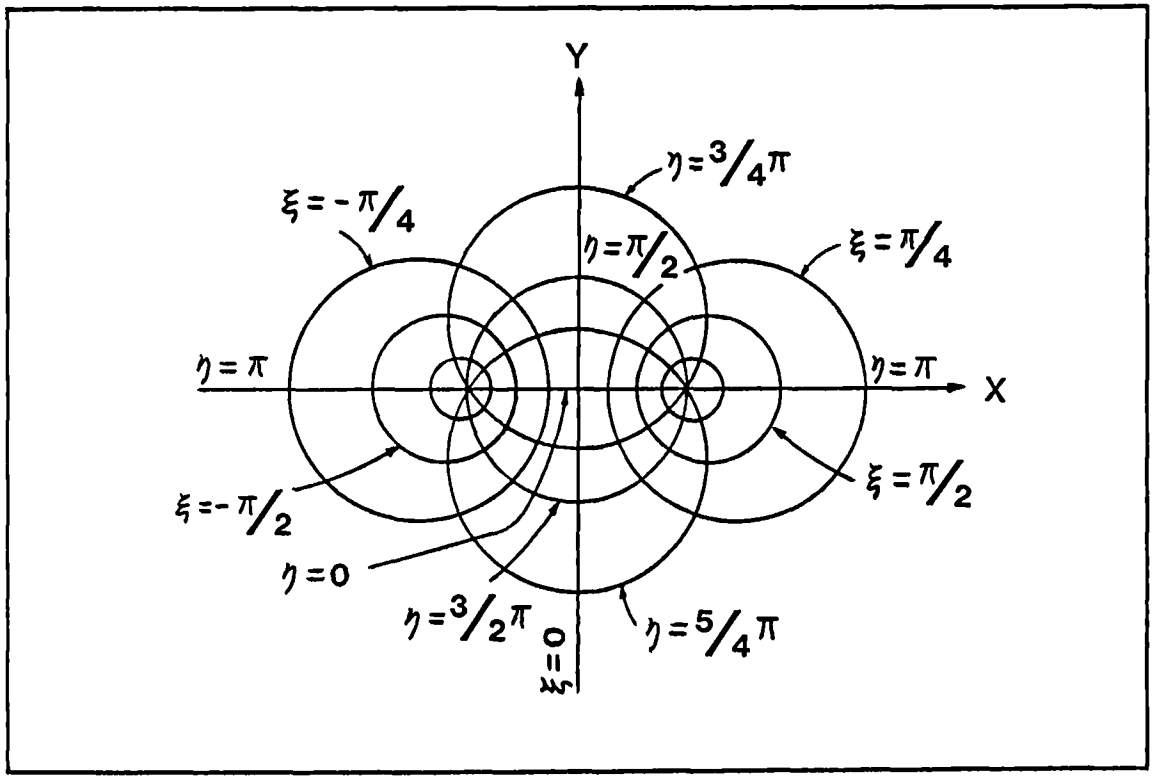

Fig.A3-1 Bipolar coordinates and rectangular coordinates

$$x = \frac{a \cdot \sinh(\xi)}{\cosh(\xi) + \cos(\eta)} \qquad \text{(A3-3a)}$$

$$y = \frac{a \cdot \sin(\eta)}{\cosh(\xi) + \cos(\eta)} \qquad \text{(A3-3b)}$$

Consider the eccentric annulaus formed by $\xi = \xi_1$ and ξ_2 as shown in Fig.(A3-2). The circle $\xi = \xi_1$ represents the inner tube and the circle $\xi = \xi_2$ represents the outer tube. Then any point within the eccentric annulus can be described by ξ from ξ_1 to ξ_2 and by η from 0 to 2π. Based on the geometric consideration and the coordinate transformation, the following relationships may be found:

$$\xi_1 = \cosh^{-1}\left(\frac{1 - \lambda_1^2 - E^2}{2 \cdot E \cdot \lambda_1}\right) \qquad \text{(A3-4a)}$$

$$\xi_2 = \cosh^{-1}\left(\frac{1 - \lambda_1^2 + E^2}{2 \cdot E}\right) \qquad \text{(A3-4b)}$$

$$a = r_1 \cdot \sinh(\xi_1) = r_2 \cdot \sinh(\xi_2) \qquad \text{(A3-5)}$$

where the dimensionless eccentricity $E = e/r_2$.

It can be seen that through the coordinate transformation, the eccentric annulus is mapped onto a rectangular region bounded by $\xi = \xi_1$ and ξ_2 and by $\eta = 0$ and 2π.

b) **Procedures of using the bipolar coordinate method to calculate volumetric flowrates in eccentric annular flow of power-law fluids**

(i) write the equation of motion for eccentric annular flow in the rectangular coordinate system in terms of the shear stress components:

$$\frac{\partial \tau_{zx}}{\partial x} + \frac{\partial \tau_{zy}}{\partial y} = g_p \qquad \text{(A3-6)}$$

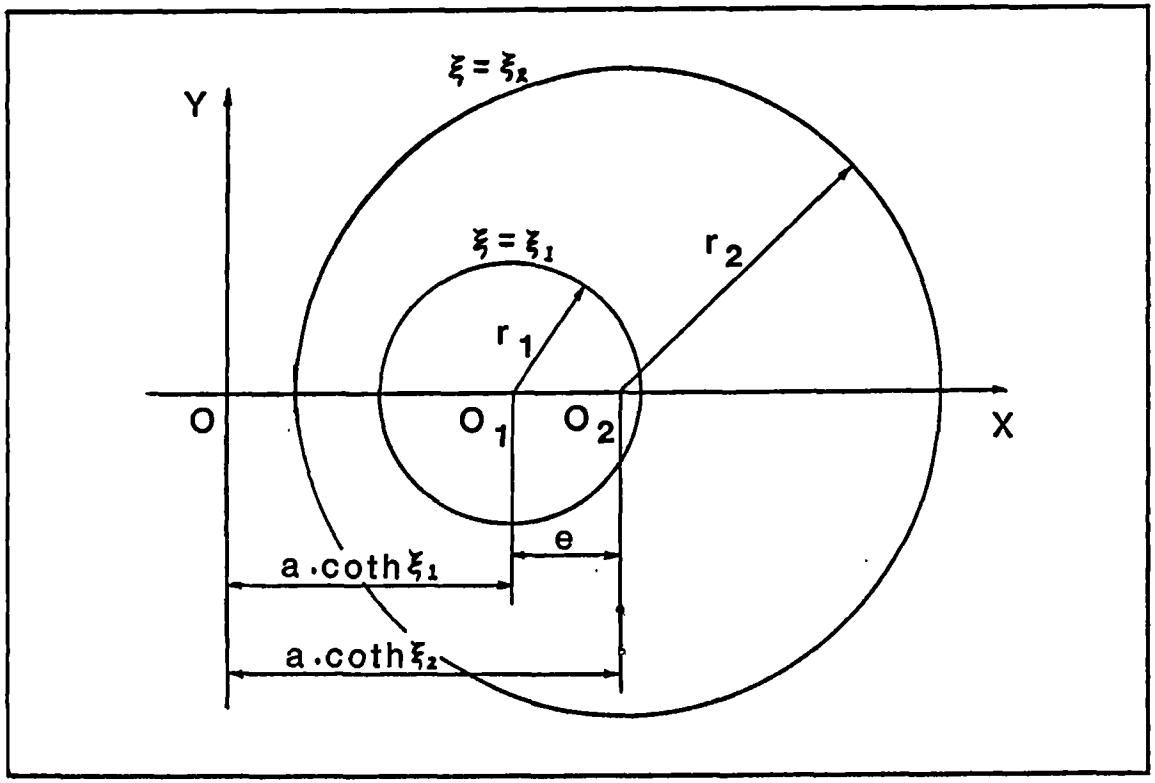

Fig.A3-2 Eccentric annulus defined by bipolar coordinates

(ii) Transform the above equation from the rectangular to bipolar coordinate system. After some tedious treatments, we may arrive at:

$$\frac{\cosh(\xi) + \cos(\eta)}{a} \left(\frac{\partial \tau_{z\xi}}{\partial \xi} + \frac{\partial \tau_{z\eta}}{\partial \eta} \right) - \frac{\sinh(\xi)}{a} \tau_{z\xi} + \frac{\sin(\eta)}{a} \tau_{z\eta} = g_p \qquad \text{(A3-7)}$$

(iii) express the above equation in terms of velocity gradients. For non-Newtonian fluids, the shear stress $\tau_{z\xi}$ and $\tau_{z\eta}$ in bipolar coordinate system may be expressed as:

$$\tau_{z\xi} = - \mu_a \frac{\cosh(\xi) + \cos(\eta)}{a} \frac{\partial v_z}{\partial \xi} \qquad \text{(A3-8a)}$$

$$\tau_{z\eta} = - \mu_a \frac{\cosh(\xi) + \cos(\eta)}{a} \frac{\partial v_z}{\partial \eta} \qquad \text{(A3-8b)}$$

where μ_a is the apparent viscosity of the non-Newtonian fluids defined by Eq.(1-6) in Chapter 1. For the eccentric annular flow of power-law fluids, μ_a may be expressed in the bipolar coordinate system as:

$$\mu_a = K \left\{ \frac{\cosh(\xi) + \cos(\eta)}{a} \left[\left(\frac{\partial v_z}{\partial \xi} \right)^2 + \left(\frac{\partial v_z}{\partial \eta} \right)^2 \right]^{1/2} \right\}^{n-1} \qquad \text{(A3-9)}$$

Substituting Eqs.(A3-8) into Eq.(A3-7) and simplifying, we may finally arrive at:

$$\frac{\partial}{\partial \xi} \left(\mu_a \frac{\partial v_z}{\partial \xi} \right) + \frac{\partial}{\partial \eta} \left(\mu_a \frac{\partial v_z}{\partial \eta} \right) = - g_p \left[\frac{a}{\cosh(\xi) + \cos(\eta)} \right]^2 \qquad \text{(A3-10)}$$

The above equation is a non-linear second order differential equation.

(iv) solve the differential equation for velocities over the rectangular region bounded by $\xi = \xi_1$ and ξ_2 and by $\eta = 0$ and 2π.

(v) calculate the volumetric flowrate by collecting the velocities over the rectangular region using the formula:

$$q = 2 \cdot r_2^2 \cdot \int_0^{\pi} \int_{\xi_1}^{\xi_2} \left[\frac{\sinh(\xi_2)}{\cosh(\xi) + \cos(\eta)} \right]^2 v_z \, d\xi \, d\eta \qquad \text{(A3-11)}$$

Appendix (A3-2): Derivation of the slot model for eccentric annular flow of power-law fluids

For the laminar flow of power-law fluids between two parallel flat plates with the width 'w' and separated by a distance 'h', the expressions for the shear stress, velocity profiles and the volumetric flowrate are, respectively,[2c,21]

$$\tau_{zy} = y \cdot g_p \qquad \text{(A3-12)}$$

$$v_z = \frac{n}{1+n} \left(\frac{g_p}{K} \right)^s \left[\left(\frac{h}{2} \right)^{\left(\frac{1+n}{n}\right)} - y^{\left(\frac{1+n}{n}\right)} \right] \qquad \text{(A3-13)}$$

$$q = \frac{2 \cdot w \cdot n}{1+2 \cdot n} \left(\frac{g_p}{K} \right)^s \left(\frac{h}{2} \right)^{\left(\frac{1+2n}{n}\right)} \qquad \text{(A3-14)}$$

The idea of the slot model is that an eccentric annulus may be treated as a slot with a variable height. A slot equivalent of an eccentric annulus is shown in Fig.(A3-3). Iyoho and Azar[18] found that the equivalent slot height may be calculated by:

$$h_e = r_2 \cdot \{ \left[1 - (E \cdot \sin\theta)^2 \right]^{1/2} + E \cdot \cos\theta - \kappa_1 \} \qquad \text{(A3-15)}$$

Using the cylindrical coordinate system, the r-coordinate of the eccentric annulus is calculated by:

$$r = r_1 + \frac{h_e}{2} + y \qquad \text{(A3-16a)}$$

Expressing the above equation for y gives:

$$y = r - \left(r_1 + \frac{h_e}{2} \right) \qquad \text{(A3-16b)}$$

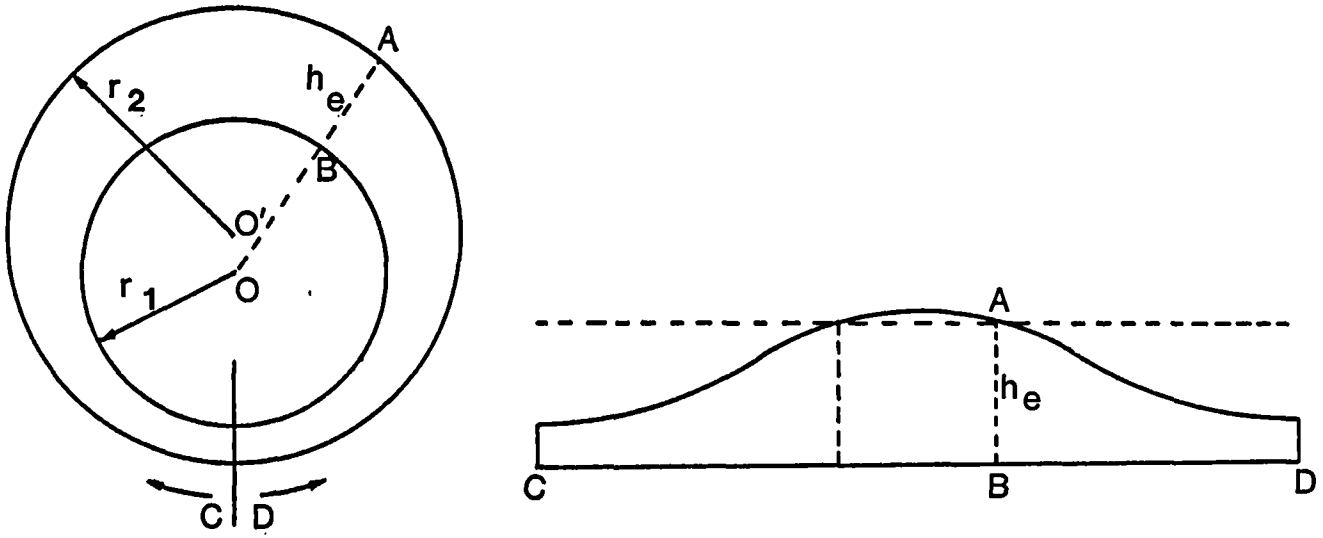

ECCENTRIC ANNUIUS

EQUIVALENT SLOT

Fig.A3-3 Slot equivalent of an eccentric annulus

Substituting (A3-16b) into Eqs.(A3-12) and (A3-13) for y, the shear stress and the velocity profiles for the eccentric annular flow are obtained as:

$$\tau_{zr} = g_p \cdot [\, r - (r_1 + \frac{h_e}{2}) \,] \qquad \text{(A3-17)}$$

$$v_z = \frac{n}{1+n} \left(\frac{g_p}{K} \right)^s \{ \left(\frac{h_e}{2} \right)^{(\frac{1+n}{n})} - [\, r - (r_1 + \frac{h_e}{2})]^{(\frac{1+n}{n})} \} \qquad \text{(A3-18)}$$

For the volumetric flowrate, Tosun[19] argued that the flow area of the slot should be equal to the flow area of the eccentric annulus such that:

$$\pi(r_2^2 - r_1^2) = \Psi \int_0^{2\pi} \int_{-h_e/2}^{h_e/2} dy\, d\theta = \Psi \int_2^{2\pi} h_e\, d\theta \qquad \text{(A3-19)}$$

where Ψ is the area correction factor which can be obtained by substituting Eq.(A3-15) into the above equation and integrating:

$$\Psi = \frac{\pi \cdot r_2}{2} \left[\frac{1 - \lambda_1^2}{2 \cdot \Phi - \pi \cdot \lambda_1} \right] \qquad \text{(A3-20)}$$

in which Φ is an integral defined by:

$$\Phi = \int_0^{\pi/2} [\, 1 - (E \cdot \sin\theta)^2 \,]^{1/2} d\theta \qquad \text{(A3-21)}$$

Then the volumetric flowrate can be calculated by:

$$q = \Psi \int_0^{2\pi} \int_{-h_e/2}^{h_e/2} v_z\, dy\, d\theta \qquad \text{(A3-22)}$$

Integrating the above equation yields:

$$q = \pi \cdot r_2^3 \cdot \left(\frac{g_p \cdot r_2}{K} \right)^s \pi_q^e \qquad \text{(A3-23)}$$

where the dimensionless volumetric flowrate is calculated by:

$$\pi_q^e = \left(\frac{1}{2} \right)^{\frac{1+n}{n}} \frac{n}{1 + 2 \cdot n} \left[\frac{1 - \lambda_1^2}{2 \cdot \Phi - \pi \cdot \lambda_1} \right] \int_0^{\pi} \left(\frac{h_e}{r_2} \right)^{\left(\frac{1+2n}{n}\right)} d\theta \qquad \text{(A3-24)}$$

Eq.(A3-23) and Eq.(A3-24) are the final solutions given by Uner, et.al.[20].

APPENDIX (A6-1): Calculation of the cuttings concentration in vertical drilling annuli

Based on Eq.(6-1), the cuttings transport velocity v_t may be expressed as:

$$v_t = \frac{q_s}{A_a \cdot C_s} \qquad (A6\text{-}1)$$

The annular fluid velocity may be expressed as:

$$v_f = \frac{q_f}{A_a \cdot (1 - C_s)} \qquad (A6\text{-}2)$$

where A_a is the annular cross-section area, q_s is the cuttings volume generated in unit time, q_f is the circulating rate of drilling fluids and C_s is the cuttings concentration by volume.

Based on Eqs.(A6-1) and (A6-2), the cuttings transport ratio may be written as:

$$F_T = \frac{v_t}{v_f} = \frac{(1 - C_s) \cdot q_s}{C_s \cdot q_f} \qquad (A6\text{-}3)$$

Expressing the above equation for C_s yields:

$$C_s = \frac{q_s}{q_s + F_T \cdot q_f} \qquad (A6\text{-}4)$$

where the quantities q_s and q_f may be calculated, respectively, by:

$$q_s = \frac{\pi}{4} d_2^{\,2} \cdot v_d$$

$$q_f = \frac{\pi}{4} (d_2^{\,2} - d_1^{\,2}) \cdot v_f$$

where v_d is the drilling rate. So Eq.(A6-4) may be written as:

$$C_s = \frac{d_2^2 \cdot v_d}{d_2^2 \cdot v_d + F_T \cdot (d_2^2 - d_1^2) \cdot v_f} \qquad (A6\text{-}5)$$

Because q_s is usually much smaller than $F_T \cdot q_f$, Eqs.(A6-4) and (A6-5) may be approximated by the following equations, respectively:

$$C_s = \frac{q_s}{F_T \cdot q_f} \qquad (A6\text{-}6)$$

$$C_s = \frac{d_2^2 \cdot v_d}{F_T \cdot (d_2^2 - d_1^2) \cdot v_f} \qquad (A6\text{-}7)$$

Example:

Assuming: $d_2 = 12\text{-}1/4" = 31.12$ cm

$v_d = 100$ ft/hr $= 0.8467$ cm/sec

$q_f = 650$ gal/min $= 41.01 \times 10^3$ cm^3/sec

Then:

$$q_s = \frac{\pi}{4} d_2^2 \cdot v_d = 0.644 \times 10^3 \text{ cm}^3/\text{sec}$$

If we let $F_T = 0.5$, then from the approximate equation, i.e. Eq.(A6-6):

$$C_s = \frac{q_s}{F_T \cdot q_f} = 0.0314 = 3.14\ \%$$

by using the exact equation, i.e. Eq.(A6-4):

$$C_s \simeq \frac{q_s}{q_s + F_T \cdot q_f} = 0.0309 = 3.09\ \%$$

The difference between the exact and the approximate equations is only 0.05 %.

APPENDIX (A7-1): Dimensional analysis of C_D for power-Law fluids

In power-law fluids, the fluid drag force acting on a settling particle may be expressed in the functional form as:

$$F_D = f(v_s, d_s, \rho_f, K, n) \qquad (A7-1)$$

The dimensions of each term in the above equation are:

$[F_D] = LT^{-2}M$ $\quad [K] = L^{-1}T^{n-2}M$ $\quad$ n - dimensionless

$[v_s] = LT^{-1}$ $\quad [d_s] = L$ $\quad [\rho_f] = L^{-3}M$

There are totally six independent variables. If we choose v_s, d_s and ρf as three basic quantities, according to Buckingham Π-theorem for dimensional analysis, Eq.(A7-1) may be written as:

$$f'(\Pi_1 , \Pi_2 , \Pi_3) = 0 \qquad (A7-2)$$

where

$$\Pi_1 = v_s^{x1} \cdot d_s^{y1} \cdot \rho_f^{z1} \cdot F_D^{m1} \qquad (A7-3a)$$

$$\Pi_2 = v_s^{x2} \cdot d_s^{y2} \cdot \rho_f^{z2} \cdot K^{m2} \qquad (A7-3b)$$

$$\Pi_3 = v_s^{x3} \cdot d_s^{y3} \cdot \rho_f^{z3} \cdot n^{m3} \qquad (A7-3c)$$

For the dimensionless group Π_1, equating the like exponents yields:

$$\begin{aligned} L:&\quad 0 = x_1 + y_1 - 3\cdot z_1 + m_1 \\ T:&\quad 0 = -x_1 - 2\cdot m_1 \\ M:&\quad 0 = z_1 + m_1 \end{aligned} \tag{A7-4}$$

Assuming $m_1 = 1$ and solving the matrix (A7-4) yields:

$$x_1 = -2 \ , \ y_1 = -2 \ , \ z_1 = -1$$

Therefore, the dimensionless group Π_1 may be expressed as

$$\Pi_1 = \frac{F_D}{v_s^{\,2}\cdot d_s^{\,2}\cdot \rho_f} \tag{A7-5}$$

Similarly, we may find $x_2 = 2-n$, $y_2 = n$, $z_2 = 1$ and $m_2 = 1$ for the dimensionless group Π_2, and $x_3 = y_3 = z_3 = 0$ and $m_3 = 1$ for Π_3. So the Eq.(A7-2) becomes:

$$f'\left(\frac{F_D}{d_s^{\,2}\cdot \rho_f \cdot v_s^{\,2}} , \frac{v_s^{\,(2-n)}\cdot d_s^{\,n}\cdot \rho_f}{K} , n \right) = 0$$

or

$$\frac{F_D}{A_{sp}\cdot(\rho_f \cdot v_s^{\,2})/2} = f''(N_{Rep} , n) \tag{A7-6}$$

where N_{Rep} is the generalised particle Reynolds number for power-law fluids and is defined as:

$$N_{Rep} = \frac{v_s^{\,(2-n)}\cdot d_s^{\,n}\cdot \rho_f}{K} \tag{A7-7}$$

According to the defination of the drag coefficient in Eq.(7-2), it may be found that:

$$C_D = \frac{F_D}{A_{sp} \cdot (\rho_f \cdot v_s^2)/2} = f''(N_{Rep} , n) \qquad (A7\text{-}8)$$

Hence the drag coefficient C_D for power-law fluids is a funtion of both the generalised particle Reynolds number N_{Rep} and the flow behaviour index n.

APPENDIX (A7-2): Derivation of the sphericity equations for disks and rectangular plates

The diamater of the volume equivalent sphere of a non-spherical particle is:

$$d_{sv} = \left(\frac{6 \cdot V_s}{\pi} \right)^{1/3} \qquad \text{(A7-9)}$$

So the surface area of the volume equivalent sphere is:

$$A_{sphere} = \pi \cdot d_{sv}^2 = \pi \cdot \left(\frac{6 \cdot V_s}{\pi} \right)^{2/3} \qquad \text{(A7-10)}$$

For plate-like particles, the surface area may be expressed as:

$$A_{plate} = 2 \cdot A_{sf} + A_{se} \qquad \text{(A7-11)}$$

where A_{sf} is the one side face-area and A_{se} is the total edge-area of the particle. Based on the defination of sphericity in Eq.(7-32), the sphericity of a plate-like particle may be written as:

$$\psi = \frac{A_{sphere}}{A_{plate}} = \frac{\pi \cdot \left(\frac{6 \cdot V_s}{\pi} \right)^{2/3}}{2 \cdot A_{sf} + A_{se}} \qquad \text{(A7-12)}$$

Case a: Disks

For disks, assume $F_{hb} = h_s/d_{sd}$, then:

$$V_s = \frac{\pi}{4} F_{hb} \cdot d_{sd}^3 \qquad A_{sf} = \frac{\pi}{4} d_{sd}^2 \qquad A_{se} = \pi \cdot F_{hb} \cdot d_{sd}^2$$

Substituting these terms into Eq.(A7-12) yields:

$$\psi = \frac{2.621 \cdot (F_{hb})^{2/3}}{1 + 2 \cdot F_{hb}} \qquad \text{(A7-13)}$$

Case b: Rectangular Plates

Assuming that a rectangular plate may be approximately replaced by an equivalent square plate which has the same volume and the same thickness, then the equivalent width of the square plate is:

$$b_{eq} = (b_{s1} \cdot b_{s2})^{1/2} \qquad \text{(A7-14)}$$

If we assume that $F_{hb} = h_s/b_{eq}$, then:

$$V_s = F_{hb} \cdot (b_{eq})^3 \qquad A_{sf} = (b_{eq})^2 \qquad A_{se} = 4 \cdot F_{hb} \cdot (b_{eq})^2$$

Substituting these terms into Eq.(A7-12) yields:

$$\psi = \frac{2.418 \cdot (F_{hb})^{2/3}}{1 + 2 \cdot F_{hb}} \qquad \text{(A7-15)}$$

APPENDIX (A7-3): Distance required by a particle before reaching its terminal settling velocity

Equation of motion

When a particle starts to settle from rest in a fluid under the action of gravity, the forces acting on the particle are not in equilibrium, i.e. $F_g \neq F_D$, which are defined in Eqs.(7-1) and (7-2), respectively. So the particle will accelerate until a maximum velovity is reached. Then the forces F_g and F_D become equal in magnitude and hereafter the particle will settle relative to the fluid with a uniform velocity and this velocity is the so called "terminal settling velocity".

If we denote v(t) for the particle velocity at time "t" during its accelerating period, then the equation of motion for the particle may be expressed as:

$$V_s \cdot \rho_s \frac{dv(t)}{dt} = F_g - F_D \qquad \text{(A7-16a)}$$

i.e.

$$V_s \cdot \rho_s \cdot \frac{dv(t)}{dt} = V_s \cdot (\rho_s - \rho_f) \cdot g - C_D \cdot A_p \frac{\rho_f \cdot v(t)^2}{2}$$

or

$$\frac{dv(t)}{dt} = \frac{(\rho_s - \rho_f) \cdot g}{\rho_s} - \frac{A_p \cdot \rho_f}{V_s \cdot \rho_s} \frac{C_D \cdot v(t)^2}{2} \qquad \text{(A7-16b)}$$

It should be noted that the drag coefficient C_D is also a function of the particle velocity, v(t). In Newtonian fluids, based on

Eq.(7-35) and (7-5), C_D may be expressed as:

$$C_D = \frac{C}{v(t)^m} \qquad \text{(A7-17)}$$

where C and "m" are constants and are equivalent to "a" and "b" in Eq.(7-35). Combining Eq.(A7-16b) with Eq.(A7-17) yields:

$$\frac{dv(t)}{dt} = P - Q \cdot v(t)^{m'} \qquad \text{(A7-18)}$$

where, $P = \frac{(\rho_s - \rho_f) \cdot g}{\rho_s}$, $Q = \frac{C \cdot A_p \cdot \rho_f}{2 \cdot V_s \cdot \rho_s}$ and $m' = 2 - m$.

Based on Eqs.(7-6) through (7-8), it may be seen that the value of "m" in Eq.(A7-17) is between 0 and 1. So $1 \leq m' \leq 2$ in Eq.(A7-18). Now let's evaluate two extreme cases when $m' = 1$ and $m' = 2$ which correspond to the cases of the laminar and turbulent settling regimes, respectively.

Case a: $m' = 1$ ($m = 1$)

In this case, the particle velocity at time 't' can be obtained by integrating Eq.(A7-18):

$$P - Q \cdot v(t) = C_1 \cdot e^{-Q \cdot t}$$

Where C_1 is a constant of integration. Applying the initial condition that $v(t) = v_o$ at time $t = 0$, we have $C_1 = P - Q \cdot v_o$. So the above equation may be written as:

$$v(t) = \frac{P}{Q} + \left(v_o - \frac{P}{Q} \right) \cdot e^{-Q \cdot t} \qquad \text{(A7-19)}$$

The settling distance during the period between t = 0 and t can be found by integrating Eq.(A7-19):

$$S(t) = \frac{P}{Q}\,t + \frac{1}{Q}\left(v_o - \frac{P}{Q}\right)\cdot\left(1 - e^{-Q\cdot t}\right) \qquad \text{(A7-20)}$$

Case b: m'= 2 (m = 0)

In a similar way, integrating Eq.(A7-18) yields:

$$v(t) = \left(\frac{P}{Q}\right)^{1/2} \cdot\left\{\frac{e^{[2\cdot(Z\cdot t + W)]} - 1}{e^{[2\cdot(Z\cdot t + W)]} + 1}\right\}$$

$$= \left(\frac{P}{Q}\right)^{1/2} \cdot \tanh(Z\cdot t + W) \qquad \text{(A7-21)}$$

$$S(t) = \frac{1}{Q}\ln\left[\frac{e^{(Z\cdot t + W)} + e^{-(Z\cdot t + W)}}{2}\right]$$

$$= \frac{1}{Q}\ln[\cosh(Z\cdot t + W)] \qquad \text{(A7-22)}$$

where $Z = (P\cdot Q)^{1/2}$ and

$$W = \frac{1}{2}\ln\left(\frac{\sqrt{P} + \sqrt{Q}\cdot v_o}{\sqrt{P} - \sqrt{Q}\cdot v_o}\right)$$

Analysis

Now the settling distance required by a particle before reaching its terminal settling velocity can be evaluated by analyzing Eq (A7-19) through (A7-22). For m = 1 or m' = 1, from Eq.(A7-19) we may obtain that:

$$\lim_{t \to \infty} v(t) = \frac{P}{Q} = \frac{2\cdot V_s\cdot(\rho_s - \rho_f)\cdot g}{C\cdot A_p\cdot\rho_f} \qquad \text{(A7-23)}$$

In this case, Based on Eq.(A7-17), $C = \frac{24 \cdot \mu}{d_s \cdot \rho_f}$, and Eq.(A7-23) corresponds to Stokes law model i.e. Eq.(7-9) for the laminar settling regime. Similarly, for the turbulent settling regime, m = 0 and m'= 2, from Eq (A7-21) we may obtain that:

$$\lim_{t \to \infty} v(t) = \left(\frac{P}{Q}\right)^{1/2} = \left[\frac{2 \cdot V_s \cdot (\rho_s - \rho_f) \cdot g}{C \cdot A_p \cdot \rho_f} \right]^{1/2} \qquad \text{(A7-24)}$$

In this case, C = 0.44 and Eq.(A7-24) is the Newton's law model, i.e. Eq.(7-11). According to Eqs.(A7-23) and (A7-24), theoretically a particle will not reach its terminal settling velocity until the time approaches infinity. Therefore approximations must be introduced for practical calculations.

Let's assume that the particle settling velocity calculated from the standard correlations, v_s, is the terminal settling velocity. When the ratio of v(t) and v_s is 'α', which is nearly but less than 1, we assume the particle has reached its terminal settling velocity. The corresponding time period t_α can be obtained by solving Eqs.(A7-19) and (A7-21).

In the laminar settling regime, m = 1 and m' = 1, from Eq.(A7-23) it may be seen that $v_s = P/Q$. Expressing P/Q as v_s, $v(t)/v_s$ as 'α' and 't' as t_α in Eq.(A7-19) and solving for t_α, we may find:

$$t_\alpha = \frac{1}{Q} \ln\left(\frac{1 - v_o/v_s}{1-\alpha}\right) \qquad \text{(A7-25)}$$

Similarly, in the turbulent settling regime, m = 0 and m' = 2. From Eq.(A7-24) it may be find that $v_s = (P/Q)^{1/2}$. Expressing $(P/Q)^{1/2}$ as v_s, $v(t)/v_s$ as 'α' and 't' as t_α in Eq.(A7-21) and solving for t_α, we

may find:

$$t_\alpha = \frac{\frac{1}{2}\ln(\frac{1+\alpha}{1-\alpha}) - W}{Q \cdot v_s} \qquad \text{(A7-26)}$$

The corresponding distance can be then calculated easily by substituting t_α for 't' into Eq.(A7-20) for laminar settling or into Eq.(A7-22) for turbulent settling.

Example:

Steel ball: $d_s = 0.634$ cm

$\rho_s = 7.75$ g/cm^3

Oil: $\rho_f = 0.88$ g/cm^3

$\mu = 1.653$ dyne-sec/cm^2

Then from Eq (A7-18), we have $P = 869.6$ cm/sec^2. Based on Bird, et.al's correlation, i.e. Eq.(7-10b), $v_s = 41.21$ cm/sec and $N_{Ren} = 13.9$. So the particle settles in the transitional settling regime.

Now, let's estimate the possible minimum/maximum time and distance required by this particle before it reaches its terminal settling velocity based on the above analysis by assuming that it settles in the laminar/turbulent settling regime.

For simplicity, we assume the initial particle velocity $v_o = 0$ and thus $W = 0$ in Eq.(A7-22) and Eq.(A7-26). This assumption is conservative considering that, if $0 < v_o < v_s$, then $0 < v_o/v_s < 1$ and $W > 0$, so from Eqs.(A7-25) and (A7-26), it may be seen that the time required to reach the terminal settling velocity would be shorter.

For the case of $m = 1$ and $m' = 1$, $Q = P/v_s = 21.1$. For the case of $m = 0$ and $m' = 2$, $Q = P/v_s^2 = 0.5121$. For different values of 'α', the table below lists the corresponding time period t_α and the distance $S(t)$.

Cases	α	0.95	0.96	0.97	0.98	0.99
m=1	t_α (sec)	0.141	0.152	0.165	0.184	0.217
m'=1	S(t) (cm)	3.96	4.37	4.90	5.67	6.99
m=0	t_α (sec)	0.087	0.092	0.099	0.109	0.125
m'=2	S(t) (cm)	2.27	2.49	2.76	3.15	3.82

APPENDIX (A7-4): Method for determining solid particle densities with a density bottle

Facilities:

One density bottle and one balancer.

Calibration of the Capacity of the Density Bottle

1. Dry and weigh the density bottle, obtain W_b;
2. Fill the density bottle with water and weigh, obtain W_{b+w};
3. Calculate the weight of the water in the bottle,

   $W_w = W_{b+w} - W_b$
4. Check the density of water at the ambient temperture, obtain ρ_w;
5. Calculate the volume of the water in the bottle,

   $V_w = W_w / \rho_w$
6. The capacity of the bottle is equal to the volume of the water in the bottle,

   $C_b = V_w$

Determination of the Density of Solid Particles

1. Wash and dry the solid particles;
2. Weigh a small amount of solid particles (about 1/2 C_b in volume) and obtain W_s;
3. Put the particles into the bottle and fill the bottle with water, weigh the mixture and obtain W_m;
4. Calculate the volume of the particles,

$$V_s = C_b - V_w = C_b - \frac{W_w}{\rho_w} = C_b - \frac{(W_m - W_s)}{\rho_w}$$

5. Calculate the density of the particles,

$$\rho_s = \frac{W_s}{V_s}$$

Symbols:

C = Capacity of the density bottle

V = Volume

W = Weight

Subscripts:

b = Bottle

m = Mixture of solid and water

s = Solid

w = Water

\+ = "and"

APPENDIX (A10-1): Dimensional analysis for the critical conditions of MTV in inclined drilling annuli

The critical conditions for the cuttings' rolloing or sliding and the lift-off movements on the low-side wall of an inclined annulus are defined, respectively, by following functions:

$$f[\ \rho_f\ ,\ \mu_a\ ,\ \rho_s\ ,\ d_s\ ,\ b_{ea}\ ,\ g(\rho_s - \rho_f)\cdot\cos(\Phi)\ ,\ v_{*mt}] = 0 \qquad (10\text{-}7)$$

$$f[\ \rho_f\ ,\ \mu_a\ ,\ \rho_s\ ,\ d_s\ ,\ b_{ea}\ ,\ g(\rho_s - \rho_f)\cdot\sin(\Phi)\ ,\ v_{*mt}] = 0 \qquad (10\text{-}8)$$

The above functions are of the exactly same form except the terms of the gravitational components, one containning $\cos(\Phi)$ and the other containning $\sin(\Phi)$. Because $\cos(\Phi)$ and $\sin(\Phi)$ are dimensionless, only the dimensional analysis for the first function, i.e. Eq.(10-7), will be given here while the same procedures may be followed for Eq.(10-8).

The dimensions of each term in Eq.(10-7) are as follows:

$$[\rho_f] = [\rho_s] = L^{-3}\cdot M \qquad [d_s] = [b_{ea}] = L$$

$$[v_{*mt}] = L\cdot T^{-1} \qquad [\mu_a] = L^{-1}\cdot T^{-1}\cdot M$$

$$[g\cdot(\rho_s - \rho_f)\cdot\cos(\Phi)] = L^{-2}\cdot T^{-2}\cdot M$$

There are totally seven independent variables. If d_s , v_{*mt} and ρ_f are taken as the three basic quantities, according to the Buckingham Pi theorem, Eq.(10-7) may be written as:

$$f(\Pi_1\ ,\ \Pi_2\ ,\ \Pi_3\ ,\ \Pi_4) = 0 \qquad (A10\text{-}1)$$

where the dimensionless grougs in the above equation may be expressed

as:

$$\Pi_1 = d_s^{x1} \cdot v_{*mt}^{y1} \cdot \rho_f^{z1} \cdot [g \cdot (\rho_s - \rho_f) \cdot \cos(\Phi)]^{m1}$$

$$\Pi_2 = d_s^{x2} \cdot v_{*mt}^{y2} \cdot \rho_f^{z2} \cdot \mu_a^{m2}$$

$$\Pi_3 = d_s^{x3} \cdot v_{*mt}^{y3} \cdot \rho_f^{z3} \cdot b_{ea}^{m3} \qquad \text{(A10-2)}$$

$$\Pi_4 = d_s^{x4} \cdot v_{*mt}^{y4} \cdot \rho_f^{z4} \cdot \rho_s^{m4}$$

For the dimensionless group Π_1, equating the like exponents, we may obtain:

$$\begin{aligned} &L: \quad 0 = x_1 + y_1 - 3 \cdot z_1 - 2 \cdot m_1 \\ &T: \quad 0 = 0 - y_1 - 0 - 2 \cdot m_1 \qquad \text{(A10-3)} \\ &M: \quad 0 = 0 + 0 + z_1 + m_1 \end{aligned}$$

Assuming $m_1 = -1$ and solving the matrix (A10-3) yields $x_1 = -1$, $y_1 = 2$ and $z_1 = 1$. Then the dimensionless group Π_1 becomes:

$$\Pi_1 = \frac{\rho_f \cdot v_{*mt}^2}{d_s \cdot g \cdot (\rho_s - \rho_f) \cdot \cos(\Phi)}$$

or

$$\Pi_1 = \frac{v_{*mt}^2}{d_s \cdot g \cdot (\frac{\rho_s - \rho_f}{\rho_f}) \cdot \cos(\Phi)} \qquad \text{(A10-4)}$$

Similarly, we may obtain that $x_2 = 1$, $y_2 = 1$ and $z_2 = 1$ for $m_2 = -1$, $x_3 = 1$, $y_3 = z_3 = 0$ for $m_3 = -1$ and $x_4 = y_4 = 0$, $z_4 = 1$ for

$m_4 = -1$. Then the expressions for the dimensionless groups Π_2 , Π_3 and Π_4 are, respectively,

$$\Pi_2 = \frac{d_s \cdot v_{*mt} \cdot \rho_f}{\mu_a} \tag{A10-5}$$

$$\Pi_3 = \frac{d_s}{b_{ea}} \tag{A10-6}$$

$$\Pi_4 = \frac{\rho_f}{\rho_s} \tag{A10-7}$$

Similarly, we may express Eq.(10-8) as:

$$f(\Pi_1' , \Pi_2 , \Pi_3 , \Pi_4) = 0 \tag{A10-8}$$

where the dimensionless group Π_1' may be obtained as:

$$\Pi_1' = \frac{v_{*mt}^2}{d_s \cdot g \cdot (\frac{\rho_s - \rho_f}{\rho_f}) \cdot \sin(\Phi)} \tag{A10-9}$$

Other three dimensionless groups for Eq.(A10-8) are exactly same as those in Eq.(A10-5) through (A10-7).

APPENDIX (A10-2): Estimation of boundary layer thicknesses in turbulent pipe flow of Newtonian fluids[52a]

Example: pipe diameter: $d = 6$ [cm]

mean flow velocity: $v_f = 100$ [cm/sec]

Case 1: Newtonian fluids (water)

$\mu = 1$ [cp] $= 0.01$ [dyne-sec/cm^2]

$\rho_f = 1$ [g/cm^3]

Then, the pipe flow Reynolds number is:

$$N_{Re} = \frac{d \cdot v_f \cdot \rho_f}{\mu} = \frac{6 \times 100 \times 1}{0.01} = 6 \times 10^4$$

which is greater than 2100, the flow is turbulent. The friction factor is:

$$f = \frac{0.0791}{(N_{Re})^{1/4}} = \frac{0.0791}{(6 \times 10^4)^{1/4}} = 50.54 \times 10^{-4}$$

The shear stress on the pipe wall is:

$$\tau_w = f \frac{\rho_f \cdot v_f^2}{2} = 50.54 \times 10^{-4} \times \frac{1 \times 100^2}{2} = 25.27 \text{ [dyne/cm}^2\text{]}$$

The friction velocity is:

$$v_* = \left(\frac{\tau_w}{\rho_f}\right)^{1/2} = \left(\frac{25.27}{1}\right)^{1/2} = 5.027 \text{ [cm/sec]}$$

Then the thicknesses of the boundary layers are calculated as follows:

$$\delta_{viscous} = 5 \frac{\mu}{v_* \cdot \rho_f} = 5 \times \frac{0.01}{5.027 \times 1} = 0.01 \text{ [cm]}$$

$$\delta_{buffer} = 70 \frac{\mu}{v_* \cdot \rho_f} = 70 \times \frac{0.01}{5.027 \times 1} = 0.14 \text{ [cm]}$$

Case 2: Newtonian fluids

$\mu = 20$ [cp] $= 0.2$ [dyne-sec/cm^2]

$\rho_f = 1$ [g/cm^3]

Then the pipe flow Reynolds number is:

$$N_{Re} = \frac{6 \times 100 \times 1}{0.2} = 3 \times 10^3$$

which is also greater than 2100, the flow is turbulent.

$$f = \frac{0.0791}{(3 \times 10^3)^{1/4}} = 106.9 \times 10^{-4}$$

$$\tau_w = 106.9 \times 10^{-4} \times \frac{1 \times 100^2}{2} = 53.45 \text{ [dyne/cm}^2\text{]}$$

$$v_* = \left(\frac{53.45}{1}\right)^{1/2} = 7.311 \text{ [cm/sec]}$$

Then the thicknesses are:

$$\delta_{viscous} = 5 \times \frac{0.2}{7.311 \times 1} = 0.14 \text{ [cm]}$$

$$\delta_{buffer} = 70 \times \frac{0.2}{7.311 \times 1} = 1.91 \text{ [cm]}$$

Conclusions:

Based on the above calculations, except the cases of extremely low viscosity fluids and thus very high Reynolds numbers (water in the above calculations), the thicknesses of the viscous sublayer and the buffer layer are of the same order as the size of drilled cuttings, which are usually a few millimeters in their equivalent diameters.

In drilling annuli, the equivalent viscosities of the drilling fluids are roughly of the same order with the Newtonian fluid in Case 2 of the above calculations. So Case 2 may be taken as a representative example for the situation in drilling annuli. Because the viscous stress predominates in the viscous sublayer and is of the same order with the Reynolds stress in the buffer layer, the viscosity effect may not be negligible for initiation of the cuttings movement in the vicinity of the annular wall even the annular flow is turbulent.

On the other hand, other respects of the viscosity effect should be considered. Comparing Case 1 and Case 2 we may see that, increasing the viscosity will increase the viscous sublayer and at the same time decrease the Reynolds number. So increasing the viscosity may increase the fluid dray force and thus increase the fluid flow ability to initiate a cuttings rolling or sliding movement. At the same time, if the flow is turbulent, increasing viscosity may also reduce the normal Reynolds stress or instantaneous normal velocity in the turbulent flow and accordingly reduce the fluid dispersing force or reduce the ability of the fluid flow to keep the cuttings in suspension. What is the net effect will depend upon the particular situation.

APPENDIX (A10-3): Test procedures for the friction coefficient between the cuttings and the annular wall

Facilities:

1) An annular (or pipe) circulating loop. The outer pipe of the annulus is transparent so that the cuttings movement inside the annulus can be visually observed. The annulus can be set at any angle between the horizontal and the vertical positions;
2) (Simulated) drilling fluids;
3) (Simulated) drilled cuttings.

Test procedures:

1) Set the annulus in the horizontal position;
2) Circulating the cuttings with the fluid through the annulus until a thin (a single layer of) cuttings-bed has been formed on the low-side wall of the annulus. Then stop circulating.
3) Slowly raise one end of the annulus from the horizontal position until the cuttings-bed starts to slide down towards the low-side end of the annulus;
4) Measure the inclination angle of the annulus and obtain Φ_c.
5) The firction coefficient between the annular wall and the cuttings are determined by the following formula:

$$f_s = \frac{1}{\tan(\Phi_c)} \qquad \text{(A10-10)}$$

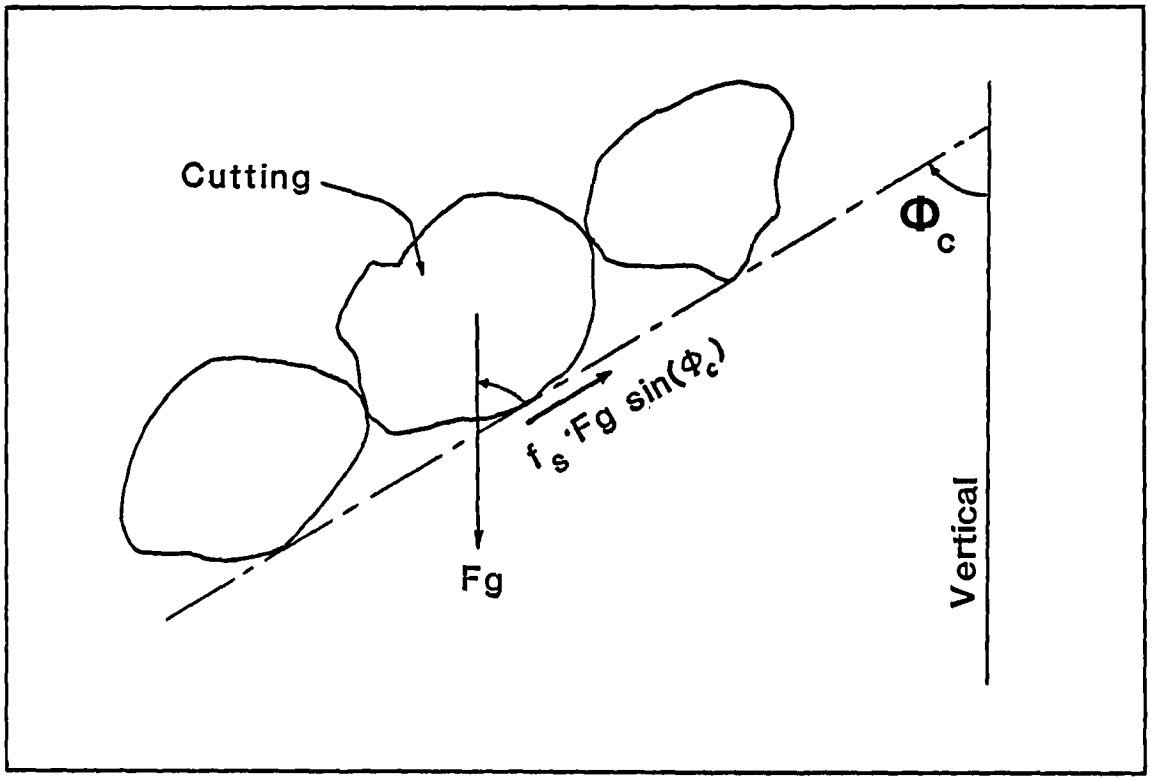

Fig. A-10-1 Critical angle for cuttings sliding-down when circulation is stopped

Principles:

When the cuttings are resting on the surface of an inclined annular wall, they have a tendency to slide down towards the low-side end of the annulus because of the action of the gravitational force in the direction towards the low-side end and parallel to the surface (hereafter we call "sliding force"). However, there is a friction force generated between the cuttings and the wall which acts against the sliding-down tendency of the cuttings. The magnitudes of both the forces depend upon the inclination angle of the annulus. When the annulus is in the horizontal position, the friction force is maximum and the sliding force is zero. If one side of the annulus is raised gradually, the friction force will be decreasing and the sliding force be increasing in magnitudes until a critical inclination angle, Φ_c, is reached at which the magnitude of the friction force is equal to that of the sliding force. Further raising the annulus will cause the cuttings to slide down towards the low-side end of the annulus.

Referring to Fig.(A10-1), a force balance equation may be written for the critical condition at Φ_c at which the friction force is equal to the sliding force:

$$f_s \cdot F_g \cdot \sin(\Phi_c) - F_g \cdot \cos(\Phi_c) = 0 \qquad \text{(A10-11)}$$

Simplifying the above equation yields:

$$f_s \cdot \sin(\Phi_c) - \cos(\Phi_c) = 0 \qquad \text{(A10-12)}$$

Solving the above equation gives Eq.(A10-10).

REFERENCES

PART ONE

1. Schlichting, H.: Boundary layer theory, McGraw-Hill Book Company, New York, Sixth Ed.(1968), (a) p.80-82 and p.500-504; (b) p.80-81
2. Skelland, A.H.P.: Non-Newtonian flow and heat transfer, John Wiley & Sons, Inc., New York(1967), (a) p.2-12; (b) p.112-115; (c) p.79-80, 110-111, 119-120; (d) p.234; (e) p.224-225
3. Bird, R.B., Stewart, W.E., and Lightfoot, E.N.: Transport phenomena, John Wiley & Sons, Inc., New York(1960), (a) p.101-103; (b) p.85
4. Fredrickson, A.G., and Bird, R.B.: "non-Newtonian flow in annuli," Ind. and Eng. Chem., Vol.50, No.3, March 1958, p.347-352
5. Tiu, C. and Bhattacharyya, S.: "Developing and fully developed velocity profiles for inelastic power-law fluids in an annulus," A.I.Ch.E.J., Vol.20, No.6, Nov. 1974, p.1140-1144
6. Hanks, R.W. and Larsen, K.M.: "The flow of power-law non-Newtonian fluids in concentric annulus," Ind. Eng. Chem. Fundam., Vol.18, No.1, 1979, p.33-35
7. Laird, W.M.: "Slurry and suspension transport, Basic flow studies on Bingham plastic fluids," Ind. and Eng. Chem., Vol.49, No.1, Jan. 1957, p.138-141
8. Yuan, S.W.: Foundations of fluid mechanics, Prentice-Hall International, Inc., London(1970), (a) p.115; (b) p.269-274
9. Dryden, H.L., Murnaghan, F.P. and Bateman, H.: Hydrodynamics, Dover Publications, Inc., U.S.A.(1956), p.198

10. Heyda, J.F.: "A green's function solution for the case of laminar incompressible flow between non-concentric circular cylinders," J. of the Franklin Institute, Vol.267, No.1, Jan. 1959, p.25-34

11. Redberger, P.J., and Charles, M.E.: "Axial laminar flow in a circular pipe containing a fixed eccentric core," Canadian J. of Chem. Eng., Aug. 1962, p.148-151

12. Mitsuishi, N., and Aoyagi, Y.: "Non-Newtonian fluid flow in an eccentric annulus," J. of Chem. Eng. of Japan, Vol.6, No.5, 1973, p.402-408

13. Guckes, T.L.: "Laminar flow of non-Newtonian fluids in an eccentric annulus," Paper 74-Pet-57, presented at ASME Petr. Mech. Eng. Conf., Dallas, Sept. 15-18, 1974

14. Snyder, W.T., and Goldstein, G.A.: "An analysis of fully developed laminar flow in an eccentric annulus," A.I.Ch.E.J., Vol.11, No.3, May 1965, p.462-467

15. Jonsson, V.K., and Sparrow, E.M.: "Results of laminar flow analysis and turbulent flow experiments for eccentric annular ducts," A.I.Ch.E.J., Vol.11, No.6, Nov. 1965, p.1143-1145

16. Tao, L.N. and Donovan, W.F.: "Through-flow in concentric and eccentric annuli of fine clearence with and without relative motion of the boundaries," ASME Trans., Vol.77, 1955, p.1291-1299

17. Vaughn, R.D.: "Axial laminar flow of non-Newtonian fluids in narrow eccentric annuli," SPEJ, Dec. 1965, p.277-280

18. Iyoho, A.W., and Azar, J.J.: "An accurate slot-flow model for non-Newtonian fluid flow through eccentric annuli," SPEJ, Oct. 1981, p.565-572

19. Tosun, I.: "Axial laminar flow in an eccentric annulus: an approximate solution," A.I.Ch.E.J., Vol.30, No.5, Sept. 1984, p.877-878

20. Uner, D. Ozgen, C. and Tosun, I.: "Flow od a power-law fluid in an eccentric annulus," Paper SPE17002, 1987

21. Bouryoyne Jr, A.T., et.al.: Applied dilling engineering, SPE textbook series, Vol.2, Society of petroleum engineers, Richardson, TX(1986), (a) p.141-143; (b) 477-483; (c) p.144-154

22. Morse, P.M. and Feshback, H.: Methods of theoretical physics, Vol.II, McGraw-Hill Book Company, Inc., New York(1953), p.1210-1211

23 Rivlin, R.S.: "Solution of some problems in the exact theory of visco-elasticity," J. Rational Mech. Anal., Vol.5, No.1., 1956, p.179-187

24 Coleman, B.D., and Noll, W.: "Helical flow of general fluids," J. of Applied Physics, Vol.30, No.10, 1959, p.1508-1512.

25 Fredrickson, A.G.: "Helical flow of an annular mass of viscoelastic fluid," Chem. Eng. Science., Vol.11, No.4, 1960, p.252-259

26 Savins, J.G., and Wallick, G.G.: "Viscosity profiles, discharge rates, pressures, and torques for a rheological complex fluid in a helical flow," A.I.Ch.E.J., Vol.12, No.2, March 1966, p.357-363

27 Dierckes, A.C., and Schowater, W.R.: "Helical flow of non-Newtonian polyisobutylene solution," Ind. and Eng. Chem. Fundam., Vol.5, No.2, May 1966, p.263-271

28 Rea, D.R., and Schowater, W.R.: "Velocity profiles of a non-Newtonian fluid in helical flow," Trans., Soc. of Rheology, Vol.11, 1967, p.125-143

29 Walker, R.E. and Al-Rawi, O.: "Helical flow of bentonite slurries," Paper SPE3108 presented at 45th SPE Annual Fall Meeting, Houston, Oct. 4-7, 1970

30 Xisheng, L., and Yinghu, Z.: "An analysis of properties of laminar flow flied of power-law fluid in annular space," Paper SPE14870,

present at the SPE International Meeting, Beijing, 1986

31 Tanner, R.I.: "Observations on the use of Oldroyd-type equations of state for viscoelastic liquids," Chem. Eng. Science, Vol.19, 1964, p.349-355

32 Taylor, G.I.: "Stability of a vicous liquid contained between two rotating cylinders," Phil. Trans. of the Royal Society, Series A, Vol.223(1923), p.289-343

33 Taylor, G.I.: "Fluid friction between rotating cylinders," Proc. of the Royal Society of London, Series A, Vol.157(1936), p.546-578

34 Snyder, H.A.: "Experiments on the stability of spiral flow at low axial Reynolds numbers," Proc. of the Royal Society of London, Series A, Vol.265(1961), p.198-214

35 Schwarz, K.W., Springett, B.E. and Donnelly, R.J.: "Modes of instability in spiral flow between rotating cylinders," J. of Fluid Mech., Vol.20(1964), p.281-289

36 Chung, K.C. and Astill, K.N.: "Hydrodynamic instability of viscous flow between rotating coaxial cylinders with fully developed axial flow," J. Fluid Mech., Vol.81(1977), p.641-655

37 Gu, Z.H., and Fahidy, T.Z.: "Visualization of flow patterns in axial flow between horizontal coaxial rotating cylinders," Canadian. J. of Chem. Eng., Vol.63, Feb. 1985, p.14-21

38 Sinevic, V., Kuboi, R. and Nienow, A.W.: "Power numbers, Taylor numbers and Taylor vortices in viscous Newtonian and non-Newtonian fluids," Chem. Eng. Science, Vol.41, No.11, 1986, p.2915-2923

39 Fredrickson, A.G., and Bird, R.B.: Correspondence entitled "Friction factors for axial non-Newtonian annular flow," Ind. and Eng. Chem., Vol.50, No.10, Oct. 1958, p.1599-1600

40 EXLOG: Theory and applications of drillling fluid hydraulics, DReidel Publishing Company, U.S.A.(1985), p.103-106

PART TWO

1. Hall, H.N., Thompson, H., and Nuss, F.: "Ability of drilling mud to lift bit cuttings," Petroleum Trans., AIME, Vol.189, 1950, p.35-46
2. Sifferman, T.R., et.al.: "Cuttings transport in full-scale vertical annuli," JPT, Nov. 1974, p.1295-1302
3. Gavignet, A.A. and Sobey, I.J.: "A model for the transport of cuttings in highly deviated wells," paper SPE15417 presented at the 61st Annual Technical Conference and Exhibition, New Orleans, Oct. 5-8, 1986
4. Martin, M., et.al.: "Transport of cuttings in directional wells," paper SPE/IADC16083 presented at the SPE/IADC Drilling Conference, New Orleans, March 15-18, 1987
5. Tomren, P.H., et.al.: "An experimental study of cuttings transport in directional wells," SPE Drilling Eng., Feb. 1986, p.43-56
6. Okrajni, S.S., and Azar, J.J.: "The effects of mud rheology on annular hole cleaning in directional wells," SPE Drilling Eng., Aug. 1986, p.297-308
7. Newitt, D.M., et.al.: "Hydraulic converying of solids in horizontal pipes," Trans. Instn. Chem. Engrs., Vol.33, 1955, p.93-110
8. Spells, K.E.: "Correlations for use in transport of aqueous suspensions of fine solids through pipes," Trans. Instn. Chem. Engrs. Vol.33, 1955, p.79-84
9. Thomas, D.G.: "Transport characteristics of suspensions — Part 2: Minimum Transport velocity for flocculated suspensions in horizontal pipes," A.I.Ch.E.J., Vol.7, No.3, Sept. 1961, p.423-430
10. Thomas, D.G.: "Transport characteristics of suspensions, Part 6: Minimum transport velocity for large particle size suspensions

in round horizontal pipes," A.I.Ch.E.J., Vol.8, No.3, July 1962, p.373-378

11. Govier, G.W., and Aziz, K.: The flow of complex mixture in pipes, Van Nostrand Reinhold Company, New York(1972), (a) p.4-6; (b) p.13-19; (c) p.617-657; (d) p.290-291
12. Bird, R.B., et.al.: Transport phenomena, John Wiley & Sons, Inc., New York(1960), (a) p.190-194;
13. Skelland, A.H.P.: Non-Newtonian flow and heat transfer, John Wiley & Sons, Inc., New York(1967), (a) p.2-12; (b) p.74 (c) p.143-144
14. Acharya, A., et.al.: "Flow of inelastic and viscoelastic fluids past a sphere, I. drag coefficient in creeping and boundary-layer flows," Rheol. Acta., Vol.15, 1976, p.454-470
15. Chien, S.F.: "Laminar flow pressure loss and flow pattern transition of Bingham plastics in pipes and annuli," Int. J. Rock Mech. Min. Sci., Vol.7, 1970, p.339-356
16. Moore, P.L.: Drilling practices manual, Petroleum Publishing Co., First Ed.(1974), p.228-239
17. Zeidler, H.U.: "An experimental analysis of the transport of drilled particles," SPEJ, Feb. 1972, p.39-48
18. Fredrickson, A.G. and Bird, R.B.: Correspondence entitled "Friction factors for axial non-Newtonian annular flow," Ind. and Eng. Chem., Vol.50, No.10, Oct. 1958, p.1599-1600
19. Fredrickson, A.G., and Bird, R.B.: "non-Newtonian flow in annuli," Ind. and Eng. Chem., Vol.50, No.3, March 1958, p.347-352
20. Zeidler, H.U.: "Fluid and drilled particle dynamics related to drilling mud carrying capacity," Ph.D. dissertation, U. of Tulsa, Tulsa, Oklahoma, 1974

21. Walker, R.E., and Mayes, T.M.: "Design of muds for carrying capacity," JPT, July 1975, p.893-900

22. Novotny, E.J.: "Proppant transport," Paper SPE 6813, presented at 52th SPE annual fall meeting, Denver, Oct. 9-12, 1977

23. Daneshy, A.A.: "Numerical solution of sand transport in hydraulic fracturing," JPT, Jan., 1978, p.132-140

24. Wadell, H.: "The coefficient of resistance as a function of Reynolds number for solids of various shapes," J. of Franklin Institute, April, 1934, p.459-490

25. Wasserman, M.L., and Slattery, J.C.: "Upper and lower bounds on the drag coefficient of a sphere in a power-model fluid," A.I.Ch.E.J., Vol.10, No.3, May 1964, p.383-388

26. Brown, G.G., and associates: Unit operations, John Wiley & Sons, Inc., New York(1950), p.79

27. Peden, J.M. and Luo, Y.: "Settling velocity of variously shaped particles in drilling and fracturing fluids," SPE Drilling Eng., Dec 1987, p.337-343, also paper SPE16243 (1986)

28. Shah, S.N.: "Proppant settling correlations for non-Newtonian fluids under static and dynamic conditions," SPEJ, April 1982, p.164-170

29. Sample, K.J., and Bourgoyne, A.T.: "An experimental evalution of correlations used for predicting cuttings slip velocity," Paper SPE6645, presented at 52th SPE annual fall meeting, Denver, Oct. 9-12, 1977

30. Clark, P.E., and Quadir, J.A.: "Prop. Transport in hydraulic fractures: a critical review of particle settling velocity equations," Paper SPE/DOE9866, presented at the SPE/DOE low permeability symposium, Denver, May 27-29, 1981.

31. Williams, C.E., and Bruce, G.H.: "Carrying capacity of drilling muds," Petroleum Trans. AIME, Vol.192, 1951, p.111-120

32. Hopkin, E.A.: "Factors affecting cuttings removal during rotary drilling," JPT, June 1967, p.307-314

33. Iyoho, A.W.: "Drilled-cuttings transport by non-Newtonian drilling fluids through inclined, eccentric annuli," Ph.D thesis in Petroleum Eng., 1980, The University of Tulsa, Tulsa, Oklahoma, U.S.A.

34. Hussaini, S.M., and Azar, J.J.: "Experimental study of drilled cuttings transport using common drilling muds," SPEJ, Feb. 1983, p.11-20

35. Prokop, C.L.: the discussion of the paper presented by Hall, H.N., et.al., Petroleum Trans, AIME, Vol.189, 1950, p.46

36. Pigott, R.J.S.: "Mud flow in drilling," Oil and Gas J., May 22, 1941, p.62-64

37. Thomas, R.P., et.al.: "Drill pipe eccentricity effect on drilled cuttings behaviour," JPT, Sept. 1982, Vol.34, No.9, p.1929-1937

38. Luo, Y. and Peden, J.M.: "Flow of Drilling fluids through eccentric annuli," paper SPE16692 presented at the 62nd Annual Technical Conference and Exhibition, Dallas, Sept.27-30, 1987, Revised version to be published in SPE Drilling Eng. Journal

39. Becker, T.E. and Azar, J.J.: "Mud weight and hole-geometry effects on cuttings transport while drilling directionally," paper SPE14711

40. Zandi, I.: "Hydraulic Transport of Bulky Materials," Advances in Solid-liquid flow in pipes and its applications, Edited by Zandi, I., Pergamon Press Ltd., Oxford(1971), p.1-34

41. Miss Blatch, Discussion: Water Filtration at Washington D.C., American Sci. of Civil Engrs, Tanns., Vol.57, Dec. 1906, p.400-408

42. Durand, R. and Condolios, E.: "The hydraulic transport of coal and solid materials in pipes," Proc. of a colloquium on the hydraulic transport of coal held by the National Coal Board in London on Nov. 5-6, 1952, Published by the National Coal Board, London, 1953, p.39-52

43. Smith, R.A.: "Experience on the flow of sand-water slurries in horizontal pipes," Trans. Instn. Chem. Engrs., Vol.33, 1955, p.85-92

44. Hughmark, G.A.: "Aqueous transport of settling slurries," Ind. Eng. Chem., Vol.53, No.5, May 1961, p.389-390

45. Wasp, E.J. et.al.: Solid-liquid Flow; Slurry pipeline transport, Trans., Technical Publications (1975-1977), Vol.1, No.4, 1977, p.61-98

46. Worster, R.C.: "The hydraulic transport of solids," Proc. of a Colloquium on the Hydraulic Transport of Coal held by the National Coal Board in London, Nov. 5-6, 1952

47. Condolios, E. and Chapus, E.E.: "Designing solid-handling pipelines," Chem. Eng., July 8, 1963, p.131-138

48. Babcock, H.A., "Heterogeneous flow of heterogeneous solids," Int. Suposium Advances in Solids-Liquid Flow in Pipes and Its Applications, Philadelphia, March 1968

49. Hayden, J.W. and Stelson, T.E.: "Hydraulic conveyance of solids in pipes," Advances in solid-liquid flow in pipes and its applications , Edited by Zandi, I., Pergamon Press Ltd., Oxford(1971), p.149-163

50. Yalin, M.S., Mechanics of sediment transport, Pergaman Press Ltd., Oxford(1972), p.74-110

51. Sinclair, C.G.: "The limit-deposit velocity of heterogeneous suspensions," Symposium proceedings on Interactions Between Fluids and Particles, London, 1962, p.78-86

52. Yuan, S.W.: Foundations of fluid mechanics, Prentice-Hall International, Inc., London(1970), (a) p.357-396; (b) p.268, p.383-384

53. Zandi, I. and Govatos, G.: "Heterogeneous flow of solids in pipelines," Journal of the Hydraulic Division, Proc. of the American Society of Civil Engrs., Vol.93, No.HY3, May 1967, p.145-159

54. Wicks, M.: "Transport of solids at low concentration in horizontal pipes," Advances in solid-liquid flow in pipes and its applications, Edited by Zandi, I., Pergamon Press Ltd., Oxford (1971), p.149-163

55. Wilson, K.C.: "Coordinates for the limit of deposition in pipeline flow," Proc. of 3rd Int. Conf. on the Hydraulic Transport of Solids in Pipes, Golden, Colorado, May 15-17, 1974, p.E1.1–E1.13

56. Wilson, K.C.: "Deposition-limit nomograms for particles of various densities in pipeline flow," Paper A1 presented at 6th Int. Conf. of the Hydraulic Transport of Solids in Pipes, Sept. 26-28, 1979

57. Hanks, K.W., and Sloan, D.G.: "A rheology-based correlation for minimum deposition velocity," Proc. of 6th Slurry Transport Association Conf., Las Vegas, March 1981, p.107-120

58. Roco, M.C. and Shook, C.A.: "Critical deposit velocity in slurry flow," A.I.Ch.E.J., Vol.31, No.8, Aug.1985, p.1401-1404

59. Ercolani, D. and Ferrini, F.: "Electric and thermic probes for measuring the limit deposit velocity," Proc. of 6th Int. Conf. on the Hydraulic Transport of Solids in Pipes, Canterbury, U.K., Sept. 26-28, 1979, p.27-42

60. Kazanskij, I.B.: "Criticcal velocity of depositions for fine slurries - New results," Proc. of 6th Int. Conf. on the Hydraulic Transport of Solids in Pipes, Canterbury, U.K.,

Sept. 26-28, 1979, p.43-56

61. Middleton, G.V. and Southard, J.B.: Mechanics of sediment movement, SEPM short course No.3, Binghamton, 1977, p.6.1-6.50

62. Leeder, M.R.: Sedimentology, George Allen & Unwin Ltd., London(1982), p.67-75

63. Granger, R.A.: Fluid mechanics, CBS College Publishing, New York (1985), p.375-377

64. Ansley, R.W. and Smith, T.N.: "Motion of spherical particles in a Bingham plastic," A.I.Ch.E.J., Vol.13, No.6, Nov. 1967, p.1193-1196